# Higher order thalamic nuclei facilitate the generalisation and maintenance of Spike and Wave Discharges in a genetic model of Absence Epilepsy

A thesis submitted to Cardiff University
in partial fulfilment for the
degree of Doctor of Philosophy
by
Zoe Serena Atherton MSci

School of Biosciences, Cardiff University, May 2021

# Summary

Spike and wave discharges (SWD), generated by the cortico-thalamo-cortical (CTC) network, are pathological, large amplitude oscillations and the hallmark of absence seizures. SWD begin in an initiation network in both humans and animal models, including the genetics absence epilepsy rats from Strasbourg (GAERS), where it is in the primary somatosensory cortex (S1). The mechanisms of how SWD rapidly spread across the brain is unknown. This thesis investigates mechanisms beyond the principal CTC network, i.e. in higher-order thalamic (HO) nuclei to explore their role in the generalisation of SWD in freely moving GAERS. Their diffuse connectivity, altered synaptic anatomy in GAERS and known interactions with the initiation network, make these nuclei serious potential candidates.

Firstly, HO nuclei and cortical local field potentials revealed a novel feature of cortical SWD: synchrony in cortical regions far from S1 (such as primary visual cortex, V1) become transiently unsynchronised with the SWD, i.e. there are short breaks in SWD (named SWD-breaks). Additionally, SWD can occur in S1 only or in S1 and the neighbouring primary motor cortex (M1), but not elsewhere. These spontaneous events provided a unique insight since they represent unsuccessful maintenance and generalisation of SWD.

Afterwards, the relevance of CTC relationships was verified by local inhibition of HO nuclei with muscimol. This increased the delay of SWD propagation and occurrence of SWD-breaks. Finally, neural dynamics of HO nuclei single units revealed three groups of putative excitatory neurons. All groups exhibited a switch from tonic to burst firing before onset of SWD, but they responded differently during V1 SWD-breaks and unsuccessfully generalised SWD.

The results of these experiments converge on two main conclusions: that trans-thalamic cortical communication is utilised in the initial propagation of SWD and also has an active role in maintaining cortical synchrony throughout the paroxysmal activity.

# Collaborations

The implantations and data collection in Chapter 5 were performed together with Dr. Gábor Kozák, Tamás Földi in the laboratory of Antal Berényi and with Péter Sere in the laboratory of Magor Lörincz in the department of physiology at the University of Szeged, Hungary.

# Acknowledgements

I wish to thank the people that have been great support throughout my Ph.D. journey.

First and foremost, I thank my supervisor, Vincenzo Crunelli. Every conversation with him has been uplifting and motivating. His hard-work and passion for neuroscience is admirable and I greatly appreciate everything he has done to challenge and support me.

I would like to thank Magor Lörincz for welcoming me to his lab at the University of Szeged. It was a fantastic experience during which time I experienced scientific and personal growth, and for that I will always be grateful.

To Francis Delicata and Tatiana Morais for their kindness, authenticity, and willingness to help with any problem, at any time. It has been a pleasure to work with these people.

To my close friends for making my time in Cardiff and Szeged truly exceptional, I feel very lucky to have connected with such intelligent and generous people.

Finally, I thank my family, their faith in my capabilities has kept me positive. A particular thank-you to my mother for always being there to listen and help me maintain a wider perspective.

# Abbreviations

aCSF – artificial cerebrospinal fluid

AI – Acceleration index

AMPA – α-amino-3-hydroxy-5-methyl-4-isoxazolepropionic acid

AMPAR – α-amino-3-hydroxy-5-methyl-4-isoxazolepropionic acid receptor

AP – Anterior-Posterior

APT – Anterior pretectal nucleus

AS - Absence seizures

BL – Baseline

CAE – Childhood absence epilepsy

CL – Central lateral thalamic nuclei

CM – Centromedial thalamic nuclei

CT – Cortico-thalamic

CTC – Cortico-thalamic-cortical

DV – Dorso-Lateral

EEG – Electroencephalography

EIB – Electrode interface board

EPSP – Excitatory post-synaptic potential

ETX – Ethosuximide

FO – First order

GABA - Gamma amino-butyric acid

$GABA_AR$ – GABA subunit-a receptors

$GABA_BR$- GABA subunit-b receptors

GAERS – Genetic Absence Epilepsy Rats from Strasbourg

GAT-1 - GABA transporter 1

GHB - Gamma-Hydroxybutyrate

HCN - Hyperpolarization and Cyclic Nucleotide-activated

HO – Higher order

Ih – HCN current

IL – Intralaminar nuclei

IPSP – Inhibitory post-synaptic potential

ISI – Inter-spike interval

$I_T$ - T-current

JAE – Juvenile absence epilepsy

LB – Low bursting

LFP – Local field potential
LP – Lateral posterior group
LTS - Low-threshold calcium spike
M1 – Motor cortex
M2 - Secondary motor cortex
ML – Medio-Lateral
MRI – Magnetic resonance imaging
NEC – Non-epileptic control
NMDA – N-methyl-d-aspartate
NMDAR – N-methyl-d-aspartate receptor
NRT – Nucleus reticularis thalami
P – Post natal day
PB – Persistent bursting
PC – Paracentral nuclei
PF – Parafascicular nuclei
PFA – Paraformaldehyde
PO – Posterior thalamic group
POc/Pot – Caudal/triangular PO
POm – Rostral PO
PPC – Pairwise phase consistency
PTZ – Pentylenetetrazole
PV – Parvalbumin
S1 – Somatosensory cortex
SEM – Standard error of the mean
SWC - Spike and Wave Complex
SWD – Spike and Wave Discharges
TB – Transient bursting
TC – Thalamo-cortical
V1 – Primary visual cortex
VB – Ventrobasal thalamus
VDCC – Voltage-dependent calcium channels
VEP – Visual evoked potential
WAG/Rjj – Wistar albino Glaxo rats from Rijswijk
ZI – Zona incerta

*Note to the reader – All figures and section references are hyperlinked and can be accessed with a left click. The reader can then move back and forward with Alt+left and Alt+right, respectively.*

# Contents

# Chapter 1: Introduction

## 1.1 Epilepsy

Epilepsy is a very serious yet common neurological disorder, affecting an estimated 50 million people worldwide (de Boer et al. 2008). A positive diagnosis is made when a patient has at least 2 unprovoked seizures more than 24 hours apart (Fisher et al. 2014). A seizure is defined as “a transient occurrence of signs and/or symptoms due to abnormal excessive or synchronous neuronal activity in the brain” (Fisher et al. 2017). The broadness of this statement appropriately reflects the diversity of seizure and epilepsy types.

The International League Against Epilepsy established a classification of epilepsies, a necessary step for the affected population, from patients, through to clinicians and researchers. Seizures are classified as either focal, generalised or unknown onset. Briefly, focal seizures have a defined location of onset, the epileptic focus, which may or may not spread to both hemispheres. Conversely, generalised seizures affect both hemispheres of the brain from seizure onset (Berg et al. 2010). Seizure types are more refined based on awareness of the individual during a seizure and what kind of motor symptoms they present. This enables the clinician to determine the type of epilepsy and syndrome the patient has, considering the aetiology, and then provide appropriate therapeutic interventions.

### 1.1.1 Absence epilepsy

The behavioural manifestation of absence seizures (AS) is a brief (~10 seconds) and reversible cessation of ongoing behaviour which is sometimes replaced with facial and eye automatisms. This occurs with a lapse in consciousness while patients often stare blankly and are unresponsive to environmental cues (Panayiotopoulos et al. 1989). The severity of this absence is variable within and between patients, Studies which have been shown to correlate with various features of AS such as duration and power of the seizure oscillation in frontal regions (Mirsky and Buren 1965; Browne et al. 1974; Vuilleumier et al. 2000).

Concurrent to these clinical symptoms, major changes occur in the electroencephalogram (EEG). Normal brain activity is abruptly replaced by large amplitude, synchronous and generalized 2.5-4 Hz waves generated by cortico-

thalamo-cortical (CTC) networks *(Figure 1.1).* These ictal oscillations are called Spike and Wave Discharges (SWD) (Panayiotopoulos et al. 1989).

AS, formerly known as 'petit mal', are observed in various idiopathic, generalised epilepsies and syndromes. Dravet and Lennox-gasteaux are two syndromes in which focal seizures, EEG abnormalities and cognitive dysfunctions are present in addition to AS (Dravet 2011). Due to the different types of pharmaco-resistant seizures present in these syndromes, the treatment is complex and often unsuccessful, however, recent work has shown promising improvements with an oral cannabidiol solution (Chen et al. 2019; Lazaridis et al. 2019).

Other epilepsies that show AS are Childhood Absence Epilepsy (CAE) and Juvenile Absence Epilepsy (JAE). Aptly named, the average age of onset is 4 and 15 years, respectively. In both epilepsies, the seizures of approximately 60% of patients remit by the end of adolescence and adulthood (Crunelli and Leresche 2002; Trinka et al. 2004). Tonic-clonic seizures occur in almost all JAE patients but rarely in the CAE population, in which AS are usually the sole seizure type present. Despite the good remission rate the impact of CAE remains evident in other facets of life, as CAE is co-morbid with social and learning difficulties as well as neuropsychiatric disorders (Caplan et al. 2008) including anxiety and depression (Caplan et al. 2005; Vega et al. 2011). Moreover, approximately 30% of CAE patients are refractory to monotherapy with current first-choice treatments including ethosuximide (ETX), valproate and lamotrigine (Glauser et al. 2013), each with unwanted side-effects. The need for more effective treatments is clear and improving our understanding of epileptogenic and ictogenic mechanisms of AS will make this goal more achievable.

Magnetic resonance imaging (MRI) and electrophysiology studies of human patients have shown AS to begin in frontal-parietal areas, i.e. the cortical initiation network, before spreading across the whole brain (Westmijse et al. 2009; Benuzzi et al. 2012; Tenney et al. 2013). Changes in blood oxygen dependent signal occurred in the cortical initiation network more than 10 seconds prior to clinical and EEG identification of seizure onset (Bai et al. 2010). Additionally, synchrony between nodes in the frontal-parietal network were detected in the minute preceding SWD (Tangwiriyasakul et al. 2018). The presence of a cortical initiation network is one similarity between human patients and animal models *(Figure 1.2).*

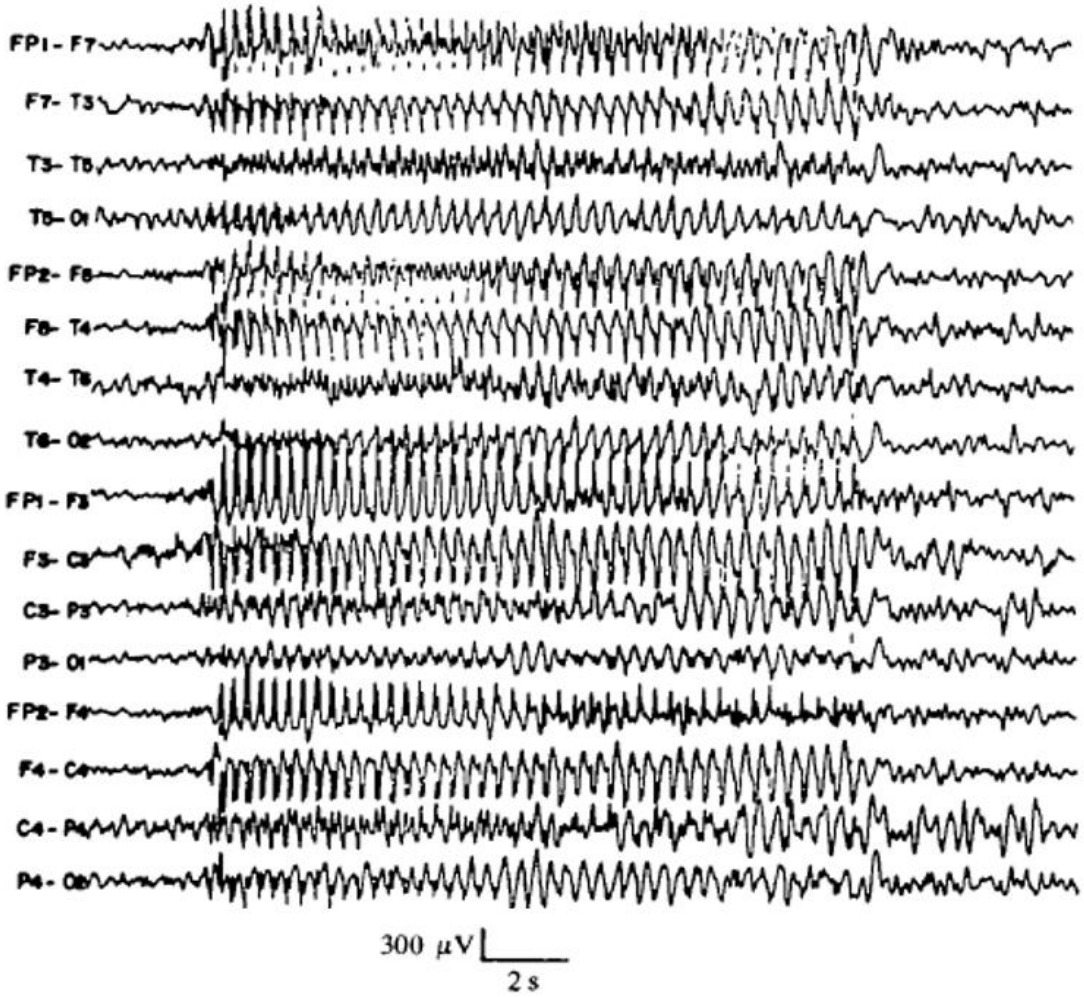


***Figure 1.1. Example of an absence seizure in a patient with childhood absence epilepsy.***

*Recordings were made across the entire cortex and the spike and wave discharge can be observed in all channels as it is a generalised form of epilepsy. [taken from Panayiotopoulos et al., 1989].*

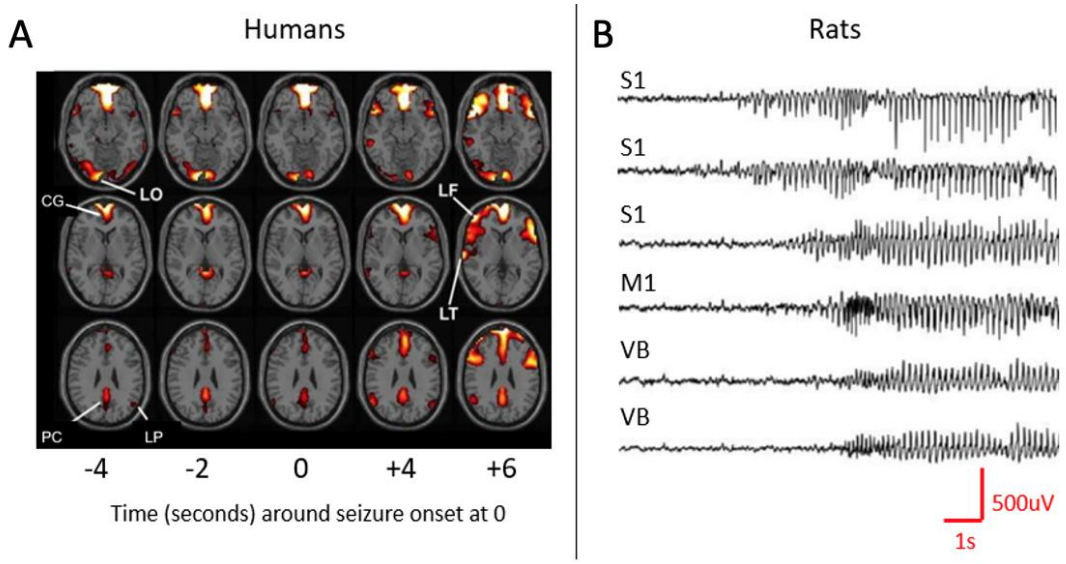


***Figure 1.2. A cortical initiation network of AS occurs across species.***

*A functional MRI (fMRI) study showed blood oxygen level dependent signal changes many seconds before seizure onset (**A**) in various brain regions, e.g. cingulate cortex (CG), lateral parietal (LP) and occipital (LO) and the precuneus (PC). After seizure onset other areas such as the lateral frontal (LF) and temporal (LT) cortex show fMRI increases. Multi-site local field potential recording (**B**) where a spike and wave discharge was first observed in the somatosensory cortex (S1), before spreading to the motor cortex (M1) and to the ventrobasal thalamus (VB). [Taken from Bai et al., 2010 (**A**) and Polack et al., 2007 (**B**) ] .*

## 1.2 The CTC network

Most sensory information is relayed through the thalamus (Jones 1985), which together with the cortex is involved in an array of functions from perceptual processing to higher order cognitive functions (Saalmann and Kastner 2011). These structures are reciprocally and often topographically connected allowing for the amplification of oscillations across the whole brain (Deschênes et al. 1998). These features facilitate the transition to and maintenance of sleep when sleep spindles and slow wave oscillations are generated by the CTC network (Crunelli et al. 2018). On the other hand, these characteristics give the network the powerful ability to disrupt the normal function of the brain, generating the pathological SWD.

Activity in CTC network is sufficient to produce and sustain SWD (Tancredi et al. 2000) and is formed from 3 neuronal components, glutamatergic TC neurons, cortico-thalamic (CT) neurons and GABA-ergic NRT neurons (Crunelli and Leresche 2002).

### 1.2.1 Thalamo-cortical nuclei

Nuclei of the dorsal thalamus can be categorised into first order (FO) and higher order (HO) nuclei. This is dependent upon the source of afferent inputs *(*Figure 1.4*)* that primarily generates excitatory activity within the nucleus, called the 'driver' input or 'Class 1' input. Other inputs are termed 'modulatory', or 'Class 2', and can change the gain of the activity and adjust transmission (Sherman and Guillery 1998). FO nuclei receive driver inputs from ascending pathways, relaying sensory information to specific cortical fields. On the other hand, the driver inputs for HO nuclei are predominantly cortical, these nuclei then project diffusely to various cortical and sub-cortical regions (Bickford 2016).

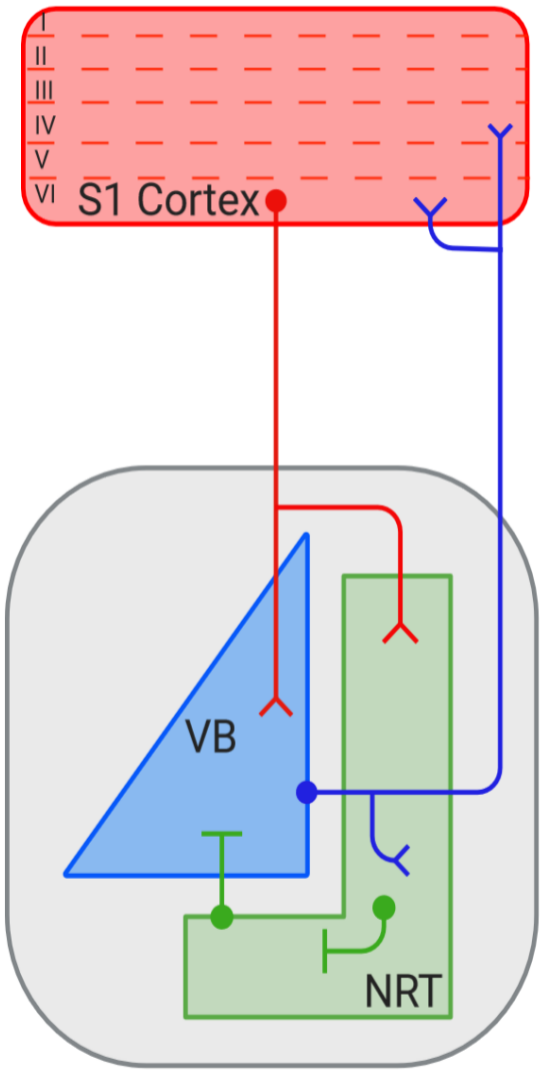


***Figure 1.3. The principal cortico-thalamo-cortical (CTC) network***.

*The CTC network has 3 principal components, the cortex, first order nuclei such as the ventrobasal (VB) thalamus and the inhibitory nucleus reticularis thalami (NRT). VB neurons relay sensory information to the cortex and activate NRT cells generating an inhibitory feedback loop. Modulatory input from cortical layer VI projects to the VB and NRT, generating an additional inhibitory feedforward loop. Excitatory inputs and inhibitory synapses are indicated by lines terminating in a '<' and a '|', respectively. Figure created with BioRender.com*

The TC neurons of FO nuclei are considered part of the principle-CTC network. Most rodent studies have investigated the ventrobasal (VB) thalamus, the topographic FO nucleus of the primary somatosensory cortex (S1) (Waite 1973), the region where SWD first occur in GAERS (Polack et al. 2007) and the WAG/Rjj (Meeren et al. 2002). In rodents, a vast majority (96-99%) of neurons of the VB are glutamatergic (Jones 1985). Inputs to the FO nuclei from sensory nuclei, such as trigeminal nucleus are relayed to layer IV and to a lesser extent layer VI of S1, via strong Class 1 synapses (Bickford 2016).

### 1.2.2 Nucleus reticularis thalamic nuclei

TC neurons also project onto the NRT, often referred to as the 'pacemaker of the thalamus' (Fuentealba and Steriade 2005). The NRT consists purely of GABAergic neurons that form a capsule lateral to nuclei of the dorsal thalamus. The NRT neurons make synapses on virtually all ipsilateral thalamic nuclei and many contralateral nuclei via the intra-thalamic commissural fibre system (Hazrati et al. 1995). TC projection to the NRT therefore generates a feed-back inhibition loop, which can strictly regulate the firing of TC neurons and this interaction can generate or contribute to many physiological oscillations, such as sleep spindles (Bazhenov et al. 2000).

Feedforward inhibition from the NRT to TC neurons also occurs, as axon collaterals from cortical layer VI form glutamatergic synapses at the NRT. This route of inhibition also influences the activity and timing of TC neuron firing and has been suggested to be involved in the genesis of SWD (McCafferty et al. 2018).

Parvalbumin, somatostatin and calbindin expressing inhibitory neurons are differentially expressed throughout the NRT, which effect the activity of NRT and network influence (Clemente-Perez et al. 2017). Within the somatosensory region of the NRT, FO nuclei predominantly synapse on the centre of the NRT, where neurons are rich in calbindin and have a higher tendency to burst (details of burst firing explained in section 1.3.1). In contrast, HO nuclei projects to the outer regions of the NRT which express somatostatin and often fail to fire bursts of action potentials or fire weak bursts with few action potentials. Finally, parvalbumin was found across all cells and thus can be used as a marker for the NRT as a whole (Martinez-Garcia et al. 2020).

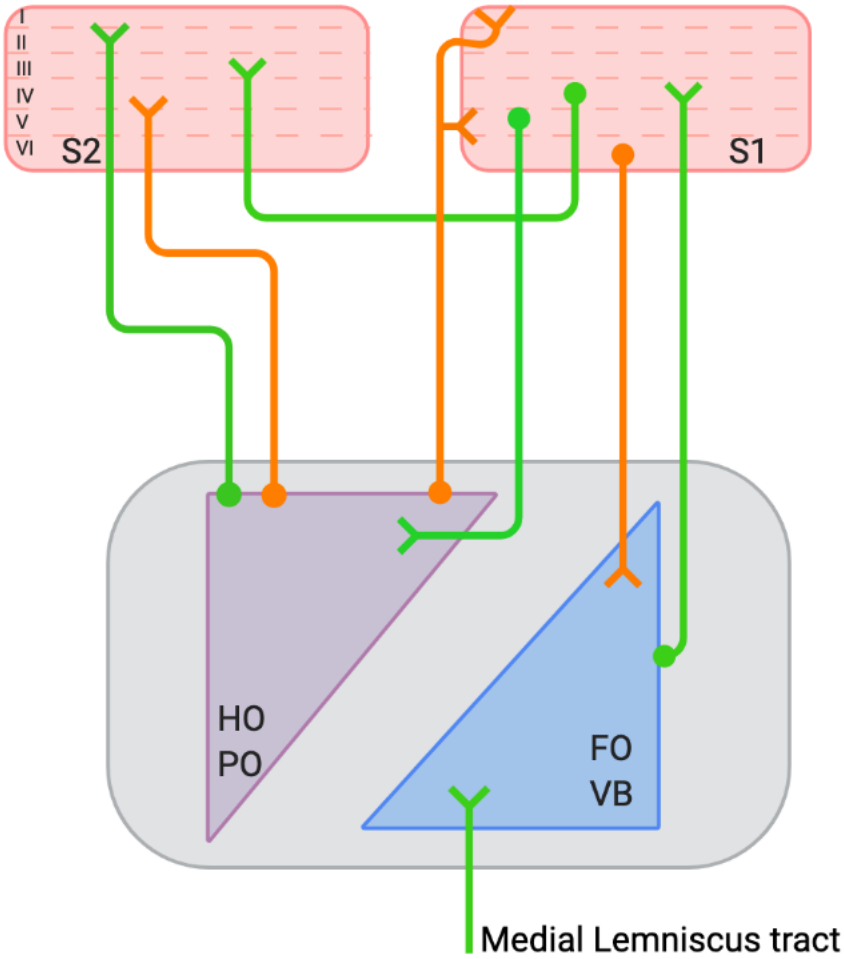


***Figure 1.4. Schematic of FO and HO nuclei and the difference in their driver and modulatory connections.***

*Network connectivity between primary (S1) and secondary somatosensory cortex (S2) and their topographic first order (FO) nuclei, e.g. ventrobasal thalamus (VB), and higher-order (HO) nuclei, e.g. posterior lateral nucleus (PO) to demonstrate differences in connectivity and type of synapse, whether class 1 (green) or class 2 (orange). Note: VB Class 1 input is from ascending sensory information whereas HO Class 1 input is from cortical layer V. PO efferents vary in their output, with both Class 1 and Class 2 synapses in the cortex, with the former usually only occurring in higher-order cortical regions. VB has only Class 1 synapses with S1. Figure created with BioRender.com*

Intra-NRT connections are present in the form of gap-junctions. Gap-junctions allow action potentials and subthreshold activity to become synchronised across cells. Two major anatomical patterns of gap junctions have been determined; coupled neuronal groups within functional lobules of the NRT in addition to groups spanning the whole axis of the NRT, traversing many functional sections that project to both FO and HO nuclei (Lee et al. 2014). Gap junctions facilitate rhythmicity of the NRT output and ultimately, in the CTC network (Deleuze and Huguenard 2006).

There is mixed evidence regarding the existence of $GABA_A$ chemical synapses (Yen et al. 1985; Sun et al. 2012; Hou et al. 2016), but such potential intra NRT axo-dendritic or dendro-dendritic synapses have been shown to have a dampening effect on activity and synchronisation (Shu and McCormick 2002). Increasing intra-NRT inhibition, a compensatory response in $\alpha$3 KO mice, was protective against pharmacologically induced seizures (Schofield et al. 2009), which demonstrates that inhibitory responses of NRT neurons could be a protective mechanism against abnormal synchronous activity such AS.

### 1.2.3 Cortical neurons

After TC neurons relay to cortical layer IV, information flows through the canonical cortical circuit, i.e. first to layers II/III, where neurons with long lateral and dorsal projecting axons reside. This morphology aids information flow to adjacent cortical regions and to layers V/VI (Di Lazzaro et al. 2016). Neurons with cell bodies in layer VI project to and modulate the activity of FO nuclei. This completes one reciprocal loop of the CTC network that enables bidirectional excitation to occur between the cortex and FO nuclei during AS (McCafferty et al. 2018).

TC neurons also project to layer VI, but the effect of this is less known (Lee and Sherman 2008). It may prime pyramidal neurons ready for the relay of sensory information via the classical columnar route (M. Oberlaender, SfN abstract: 392.01, 2018). Alternatively, this route could aid information transfer to other cortical columns and subcortical regions. Finally, CT neurons also synapse onto the NRT, the effect of which was explained in the previous section.

## 1.3 Neuronal firing in the CTC network

The ion channel composition of a neuron makes a fundamental contribution to how it responds to an input and thus subsequently influences overall network activity and synchrony. Neurons of the thalamus and some cortical interneurons harbour an interesting ion channel, the T-type calcium channel, endowing them with unique cellular and network properties (Jahnsen H and Llinás R 1984).

### 1.3.1 Tonic vs burst firing

T-type calcium channels enable neurons to fire action potentials in two different patterns, either tonically, or in a burst, depending upon the prevailing membrane potential of the cell (Tscherter et al. 2011).

The majority of T-type calcium channels are closed at resting membrane potential (approximately -60mV) (Perez-Reyes 2003), and thus the density of activated T-type calcium channels is low. During this period neurons fire tonically, generating action potentials in the classical manner, i.e. opening of voltage gated sodium channels following a suprathreshold stimulus. Tonic firing is dominant in wakeful states (Sherman, 2001) and the linear input-output they generate is useful for encoding features of stimuli faithfully.

The nature of the more complex burst firing is unleashed when the cell becomes hyperpolarised (to > ~-70mV) for at least 50-100ms as this deinactivates T-type calcium channels. Sub threshold inputs can now activate these low-threshold channels generating an inward T-current ($I_T$), forming the low-threshold calcium spike (LTS). Upon the crest of this transient wave many sodium channel driven action potentials can emerge at a high frequency, collectively forming a burst *(Figure 1.5A)* (Deschênes and Steriade 1982).

Firing barrages of action potentials can facilitate oscillogenesis, such as sleep delta waves in thalamic neurons during non-Rapid Eye Movement sleep (Tsoukatos et al. 1997) and spindle oscillations (Wang et al. 1995). Although it is tempting to assume the burst firing state is the main driver of AS, reductions in both tonic and burst firing have been shown to reduce AS (Kim et al. 2001; David et al. 2018; McCafferty et al. 2018) and thus, debate continues about the importance of burst over tonic firing in thalamic areas (Huguenard 2019).

### 1.3.2 Burst firing in the thalamus

The burst firing of TC and NRT neurons are both driven by T-type calcium channels, but their properties are very different *(Figure 1.5D).* The burst style of a cell is dependent upon what isoform of T-type channel it expresses, of which there are three; Cav3.1, Cav3.2 and Cav3.3 (Perez-Reyes 2003). Naturally, each subunit has different biophysical properties which affect the current of individual channels and resulting LTS (Huguenard 1996; Tscherter et al. 2011).

Cav3.1 and Cav3.2 both have faster activation and deactivation kinetics than Cav3.3 at the same voltage (Klöckner et al. 1999). This results in a LTS with a delayed maximal amplitude when generated by the Cav3.3 subunit as the channels take longer to open and thus the maximal current is delayed, whereas the former subunits generate a transient LTS with maximal amplitude at the beginning as the channels open quickly *(Figure 1.5C)*.

The amplitude to the LTS is positively correlated to the number of spikes a cell can fire (Tscherter et al. 2011). Cav3.1 is the dominant sub-type found in TC neurons (Talley et al. 1999) and therefore they fire bursts with action potentials at the highest frequency at the beginning of the burst. On the other hand, Cav3.2 and Cav3.3 are found in NRT neurons (Talley et al. 1999), therefore bursts in these neurons gradually increase in spike frequency until maximal amplitude is achieved, after which, they gradually decrease in frequency *(Figure 1.5D)* (Huguenard 1996; Tscherter et al. 2011).

The bursting properties of FO thalamic neurons are fairly uniform, with parameters such as number of spikes per burst and latency to burst being consistent within nuclei. On the other hand, burst properties of HO thalamic neurons are much more varied within and between nuclei (Desai and Varela 2021), which may reflect different subpopulations of neurons even within individual nuclei. Additionally, during active, wake conditions, HO nuclei burst more than FO nuclei (Ramcharan et al. 2005), which indicates intrinsic differences in excitability. Indeed, studies have already grouped different HO nuclei neurons based on based on their latency to fire and on the number of LTS a cell is able to generate after stimulation (Li et al. 2003; Wei et al. 2011) and computational evidence suggested that Cav3.2 density is higher in the distal dendrites HO neurons which can generate multiple LTS (Wei et al. 2011). As HCN channels

facilitate rhythmic burst firing it is also possible that these channels are differentially expressed but this has not yet been researched.

### 1.3.3 Burst firing in the cortex

T-type calcium channel expression occurs across cortical layers and have been shown to contribute to the propagation of excitation from distal dendrites to more proximal zones and contribute also to long-term potentiation (Uebele et al. 2009). Additionally, there are many types of cortical interneurons which can fire bursts of action potentials such as multipolar bursting cells and vasointestinal peptide expressing interneurons. However, only one of these groups, the low threshold spiking interneurons utilises T-type calcium channels. These cells are a group of somatostatin expressing interneurons, predominantly formed of the Martinotti cells in deep cortical layers which fire a burst of action potentials following inhibition (Tremblay et al. 2016). These cells are electrically coupled and project within layer V and to layer I. They are sensitive to pyramidal neuron activity and can be activated by a single pyramidal neuron. Therefore, these interneurons can exert control on other pyramidal neurons and contribute to protection of over excitation (Goldberg et al. 2004; Hayut et al. 2011).

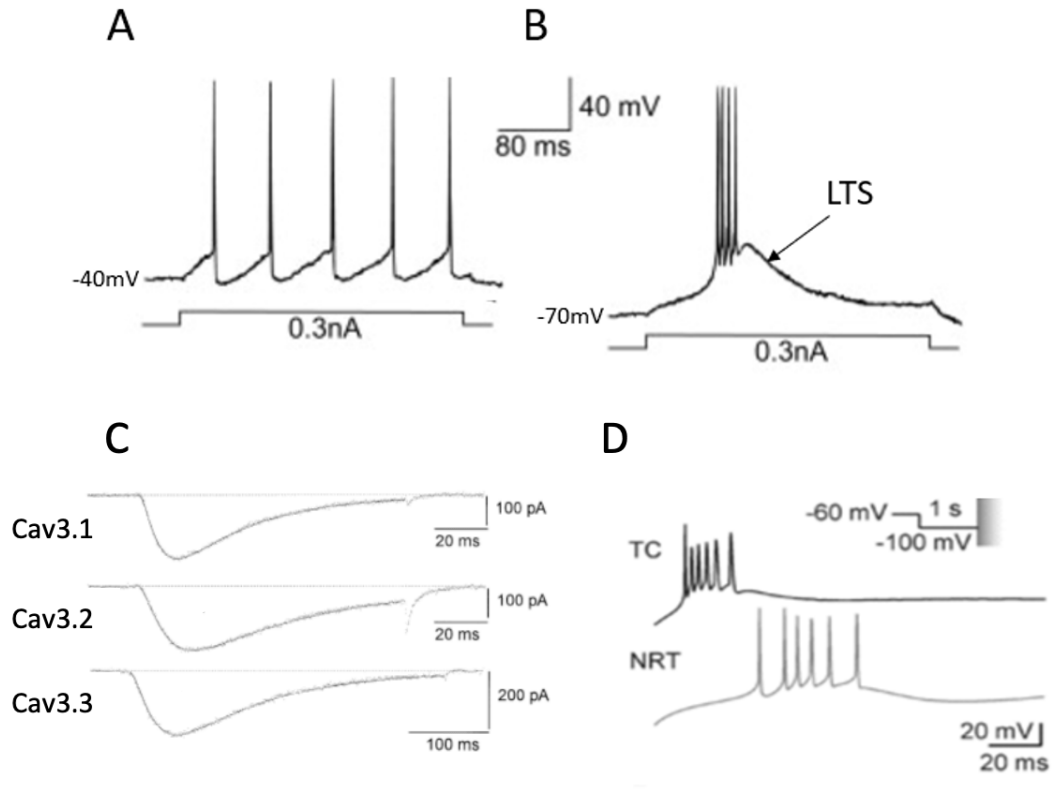


***Figure 1.5. Tonic and burst firing in the thalamus.***

*Thalamic cells can produce action potentials tonically (**A**) or in bursts (**B**) (same scalebar for both plots), from the same stimulus (here 0.3nA step), depending on whether the membrane potential is relatively depolarised (-40mV, **A**), or relatively hyperpolarised (-70mV, **B**). Burst firing relies on the slow-rising, long-lasting low threshold calcium spike (LTS, labelled in **B**), as detailed in the text. Different t-type calcium channel subunit currents (**C**), demonstrating the longer activation of Cav3.3. Traces illustrating different burst patterns in TC and NRT neurons in response to injection of artificial $I_T$ following hyperpolarisation (**D**). [Taken from Sherman, 2001 (**A** and **B**), Klöckner et al., 2008 (**C**) Tscherter et al., 2011 (**D**)].*

## 1.4 Genetics and animal models of AS

Epilepsies such as CAE are caused by genetics, however, there is not a single genetic alteration that leads to AS. Therefore the inheritance pattern is not predictable and a large range of concordance rates are reported in the literature (Crunelli and Leresche 2002). There are multiple studies assessing the genetics of various populations of childhood absence epilepsy, and other generalised epilepsy patients, that express SWD. Tested populations with AS express many, and often different, mutations (Wallace et al. 2001; Chen et al. 2003; Heron et al. 2004) which demonstrates that the origin of AS is polygenic.

The genetic diversity of the human population that express AS is reflected by the numerous animal models that can be both mono or polygenic. For an animal model to be considered so, SWD must occur in conjunction with a cessation of voluntary movements. Additionally, the seizures must be reduced after treatment of ETX. The model used in this thesis is the Genetic Absence Epilepsy Rats from Strasbourg (GAERS), and thus, it is discussed in more detail.

### 1.4.1 Genetic Absence Epilepsy Rats from Strasbourg

The polygenic GAERS model is one of the most extensively studied models in the field. This rat strain was derived by inbreeding from a small population of Wistar rats that had spontaneous AS (Vergnes et al. 1986). In parallel, rats of the same population that did not show the phenotype were inbred, establishing a control strain of these animals called the 'non-epileptic control' (NEC) rats (Danober et al. 1998).

One hundred percent of the GAERS population have AS by approximately post-natal day (P) 90 with SWD occurring at 7-11 Hz, higher than the 3 Hz SWD observed in humans. SWD are first observed in S1, where hyperexcitable neurons in layers V and VI are thought to initiate the seizure (Polack et al. 2007).

Like in the human condition, there is a developmental component, which for GAERS is separated into 3 stages. At ~P18, GAERS enter stage 1, where the first abnormal 5.5 Hz EEG oscillations can be observed, however, they lack a spike component. At P25, a harmonic frequency is evident and the 5.5 Hz oscillations have short SWD or single Spike and Wave Complexes (SWCs) embedded within them. Finally, beyond P90, all GAERS will be in stage 3 with clear SWD in the EEG with two dominant

frequencies of 7 Hz and 15 Hz (Jarre et al. 2017). In contrast to humans, the seizures in GAERS do not remit with age.

Whole gene sequencing demonstrated the complexity of mutations harboured in the GAERS model, with 1.12 million single nucleotide variants and 354 copy number variants specific to the strain (Casillas-Espinosa et al. 2017). Within these, a well-researched mutation is a single nucleotide missense arginine to proline substitution on the *CACNA1H* gene which codes for the voltage-gated $Ca_V3.2$ T-type calcium channel. This mutation results in a number of changes, including quicker recovery from inactivation of the T-type calcium current (Powell et al. 2009) and increased expression of these channels at the membrane (Proft et al. 2017), that together contribute to a gain of function. Multiple variations of a *CACNA1H* gene mutation, which codes for the voltage-gated $Ca_V3.2$ T-type calcium channel, has been found in a Chinese CAE population (Chen et al. 2003), however, a different study failed to replicate the majority these variations and link them to a specific epileptic phenotype (Heron et al. 2004).

Stargazin, a transmembrane α-amino-3-hydroxy-5-methyl-4-isoxazolepropionic acid (AMPA) receptor regulatory protein which modulates surface expression and conductance of AMPA receptors (AMPARs), is increased in GAERS (Powell et al. 2008). This mutation is the likely cause of the increase in AMPA receptor proteins observed in S1 of GAERS (Kennard et al. 2011), which could be contributing to the hyperexcitability of this region where SWD originate (Polack et al. 2007). Such mutation hasn't been reported in the human population. To my knowledge, this mutation hasn't been reported in the human population.

## 1.4.2 Other genetic models

### *1.4.2.1 Wistar albino Glaxo rats from Rijswijk*

Another well-established polygenic rat model is the Wistar albino Glaxo rats from Rijswijk (WAG/Rjj) that was developed from Wistar rats at the Glaxo Laboratories of London. This model develops 7-9 Hz SWD at around 3 months which increase in number and duration with age. Alike the GAERS, seizures do not remit with age and are often accompanied by facial myoclonic jerks, vibrassa twitching and sometimes head tilting (Coenen and Van Luijtelaar 2003).

#### *1.4.2.2 Stargazer and other monogenic mouse models*

The Stargazer mouse has a single, recessive mutation on chromosome 15. This mutation results in the insertion of a transposon on the *CACNG2* gene, which decreases its expression (Chang et al. 2009). *CACNG2* encodes for Stargazin which as aforementioned is an AMPAR auxiliary protein involved in receptor trafficking (Letts 2005) but can also form the $\gamma 2$ subunit of neuronal voltage-dependent calcium channels (VDCC) (Letts et al. 1998).

These mice show altered function of T-type calcium channels of TC neurons (Zhang et al. 2002) and have hyperexcitable NRT neurons due to an increase in N-methyl-d-aspartate receptor (NMDAR) function (Lacey et al. 2012), which can lead to epileptic activity (Steriade 2005; Huguenard and McCormick 2007). In addition to 6-8 Hz SWD, these mice have an ataxic phenotype (Noebels et al., 1990) which has been attributed to a fault in AMPA trafficking in the cerebellum.

Other mouse models with various mutations exist but have been studied relatively less than those aforementioned. The Tottering and Lethargic mouse models also have mutations in calcium channels, in the $\alpha 1$a and $\beta 4$ subunits, respectively. The former of these mutations has been found in a patients with AS (Jouvenceau et al. 2001) . The AS in these models are short, only $\sim 1$ second (Caddick et al. 1999), which can cause difficulties in experimental scenarios and are therefore used less often. Other mutations include Gria4 -/- knock-out model, which prevents generation of GluR4 subunit of AMPA receptors (Beyer et al. 2008) which caused reduced feedforward inhibition of NRT to TC (Paz et al. 2011). Finally, the R43Q knock-in model mouse that results in mutations in $\gamma 2$ subunit of $GABA_A$ receptors ($GABA_AR$) alike an Australian family with febrile seizures and absence epilepsy (Petrou and Reid 2012). Other $GABA_AR$ $\gamma 2$, and also $\beta 3$ subunit mutations exist in the human population (Wallace et al. 2001; Marini et al. 2003; Tanaka et al. 2008), however these alterations are not tissue or cell specific and thus the cellular pathway to AS remains unknown.

### 1.4.3 Pharmacological models

Pharmacological models of AS also occur, the most common being the Gamma-Hydroxybutyrate (GHB) and pentylenetetrazole (PTZ) model. PTZ is a $GABA_AR$ antagonist that induces non-convulsive and convulsive seizures at low (20-30mg/kg) and high doses (>40mg/kg), respectively (Ono et al. 1990; Kliouéva et al. 2001). PTZ

has a similar IC50 for $GABA_A$Rs with varying $\alpha, \beta$ and $\gamma$ subunit composition (Huang et al. 2001) and it has been shown to reduce tonic $GABA_A$R inhibition in rat dentate granule cells. The effect of PTZ in the thalamus is unknown, where tonic $GABA_A$R inhibition is increased in several animal models of AS (Cope et al. 2009).

GHB is a weak $GABA_B$R agonist that elicits SWD in a variety of animals, including humans, albeit, at varying frequencies. Different doses of GHB result in distinct behavioural and EEG changes. At relatively low doses, drowsiness can be observed. At slightly higher doses an absence seizure-like phenotype is evident, which can be either intermittent or continuous. However, they can be contaminated with slow delta waves due to the light hypnotic effect of GHB in this dose range. High dose application results in stronger hypnosis (Venzi et al. 2015).

The variety of animal models reflects the diversity of causes in the human population and indicates that many mechanisms can generate AS. As this work will delve into the generalisation of AS, which is relatively unknown, it is important to use a model that is well studied, with well-known network dynamics. As the GAERS fulfils these criteria it was selected for the work described in this thesis.

## 1.5 The CTC network in AS

SWD are generated from rhythmic excitation and inhibition of the CTC network. The spike component of the ongoing SWD is associated with a high frequency discharge of action potentials from cortical neurons, whereas the wave component is characterised by their hyperpolarisation (Steriade et al. 1998). Cortical and thalamic neurons become hyperpolarised at onset of AS, which is sustained throughout the seizure and rhythmic depolarisations are superimposed on this 'hyperpolarised envelope' (Pinault et al. 1998; Polack et al. 2007). In thalamic neurons, de-inactivated T-type calcium channels generate a LTS which cause NRT neurons to fire high frequency bursts at every cycle when recorded in neurolept anaesthetized GAERS (Slaght et al. 2002), but such time-locked activity was less frequent when recorded in freely moving GAERS (McCafferty et al. 2018). TC neurons also burst, but less frequently than NRT neurons (Pinault et al. 1998). Intracellular recordings provided invaluable insight to the activity in cortical and thalamic neurons during SWD, however, the cause of the initial shift to paroxysmal oscillations has been debated for a long time.

### 1.5.1 Early theories

The search for the key elements of ictogenesis within the CTC network has been ongoing for several decades. In 1954, a 'centrecephalic' theory was developed (Penfield and Jasper 1954), highlighting the midline thalamus (i.e. nucleus reuniens and paraventricular) as a potential key initiator of AS after 3 Hz stimulation to this area could generate global 3 Hz oscillations in the cat (Jasper and Droogleever Fortuyn 1947). However, not long after, attention shifted to the cortex when it emerged that PTZ injections into an artery supplying the cortex could generate SWD but not when injected to an artery supplying the thalamus (Gloor 1968). As knowledge evolved, the cortico-reticular theory was developed which recognised the essential roles of both the cortex and thalamus but theorised the NRT had a pacemaker role.

Prince and Farrel (1969) showed that following the application of high doses of intramuscularly injected penicillin, protocols that should induce spindle waves instead induced SWD, indicating a common mechanism between the two. However, this effect relied on cortical neurons being exposed to penicillin as intrathalamic or decorticated preparations resulted in a 3 Hz oscillation but not the full spike and wave pattern (Avoli and Gloor 1982).

### 1.5.2 The cortical initiation theory

Although absence epilepsy is categorised as generalised, Meeren et al. (2002) empirically showed, using non-linear association analysis on high density electrophysiological recordings in WAG/Rjj rats, that AS have a confined starting location and then spreads rapidly across the cortex and to the thalamus. These findings have been confirmed in the GAERS and both strains have their initiation site in the primary somatosensory cortex (S1) (Meeren et al. 2002; Polack et al. 2007), specifically in deep layers of the upper lip region (Polack et al. 2007). The cortical initiation theory does not dispute the importance of the thalamus. Although SWD can be generated in isolated cortical preparations (Steriade and Contreras 1998), when SWD were observed only in the cortex of a freely moving animal a clear behavioural arrest was not observed (Polack et al. 2007). However, this observation could be confounded by the short nature of these events.

Numerous studies have since reinforced the existence of a cortical initiation network, identifying unique properties of the area (i.e. S1 of rats) that makes it susceptible to abnormal activity. Within S1 of both the GAERS and WAG/Rjj models, deep layers of

the cortex are hyperexcitable when compared to non-epileptic control animals and other cortical regions within animal (D'Antuono et al. 2006; Polack et al. 2007; Polack et al. 2009).

Anatomical differences can contribute to these observations of increased excitability. Unique features of GAERS S1 neuronal morphology have not been identified (Polack et al. 2007), however in the WAG/Rjj model, there was an increase in dendritic length and arborization of pyramidal neurons in S1 vs other cortical regions (Karpova et al. 2005). Physiological factors such as alterations in ion channels will also affect responsiveness of neurons to changing membrane potentials. Studies in the WAG/Rjj show that alongside altered morphology, neurons in deep layers exhibit a late N-methyl-d-aspartate (NMDA) mediated excitatory post-synaptic potential (EPSP) more often than in NEC, suggesting an altered functionality or receptor number (D'Antuono et al. 2006). Finally, stimulation treatments for AS were effective when only targeting the cortical initiation network (van Heukelum et al. 2016) and the current gold standard treatment for AS, ETX, was most effective when supplied to S1 upper lip region vs neighbouring S1 regions and M1 (Manning et al. 2004).

The complex interplay between the cortical initiation network and the thalamus during SWD has recently been uncovered via simultaneous high-density electrophysiology in S1 and thalamus (McCafferty et al. 2018). The authors reported, through various cross-correlation analyses, a predominant feed-forward inhibition from the cortex via the NRT, to TC neurons *(Figure 1.7)***.** Additionally, they showed the presence of ictal bidirectional excitation between TC and cortical neurons.

With complex spike sorting analysis, tonic and burst firing was delineated and a tonic to burst switch was observed in thalamic neurons *(Figure 1.8)*. In NRT neurons, this switch begun before seizure onset with total firing declining from -3s, demonstrating that seizure onset is not an abrupt process. The burst firing of NRT neurons steeply increased 500ms prior to the seizure and pharmacological block of T-Type calcium channels in the NRT decreased the time spent in seizures by more than 50%. Such an effect was not observed after disruption of TC bursts, which were predominantly silent during SWD after feedforward inhibition from NRT (McCafferty et al., 2018). These results were common to the GAERS and GHB model of AS. However, animal models exist with reduced functionality of the cortical – NRT synapse (Paz et al. 2011) responsible for this feedforward inhibition, demonstrating that there are multiple potential routes to the abnormal synchrony observed in this network during AS.

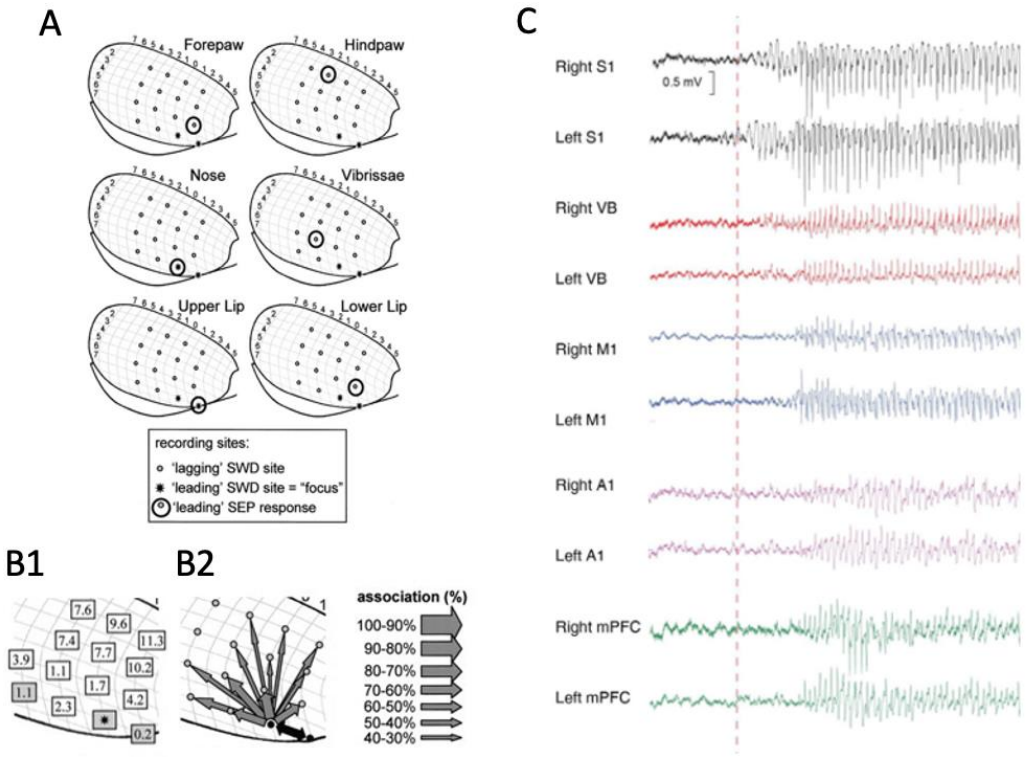


***Figure 1.6. The cortical initiation network is in the somatosensory cortex (S1) of 2 genetic models of absence epilepsy.***

*Cortical grids were placed over the right hemisphere of a WAG/Rjj rat to record SWD and the leading site was consistently found in S1, particularly in regions representing facial areas (**A**). Nearby cortical regions consistently lagged this site and the duration of the lag, shown in ms, was linearly correlated with electrode distance (**B1**). Additionally, non-linear association analysis shows associations between the cortical focal site and nearby areas, the arrow direction shows that the initiation site was consistently leading all nearby areas (**B2**). A cortical initiation network is clearly observed in freely-moving GAERS as determined by multi-site LFP recordings (**C**). Many SWC cycles can be observed in S1 before other cortical regions, i.e. the motor cortex (M1), auditory cortex (A1) and medial prefrontal cortex (mPFC) and the ventrobasal thalamus (VB). [Taken from Meeren et al., 2002 (**A** and **B**) and McCafferty et al., 2018 (**C**)].*

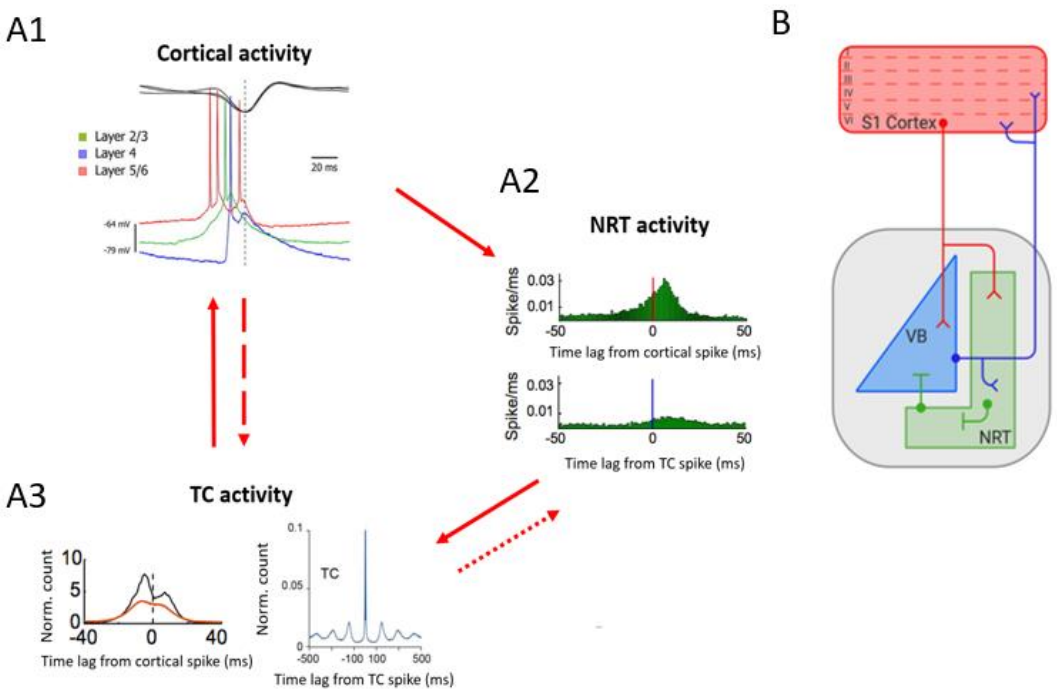


***Figure 1.7. Schematic of SWC generation based on single cell data.***

*Ictal interactions (**A**) in the CTC network (**B**) are demonstrated by key findings from single cell data (**A**). Solid, dashed and dotted red arrows indicate stronger to weaker communication during SWD. Cortical neurons in deep layers fire before those in superficial layers relative to SWC-spikes (**A1**). This activity is projected to the NRT and generates action potentials in this nucleus, more robustly than feed-back TC input, as observed by increased probability of NRT firing after a cortical spike vs TC spike (**A2**). Feedforward inhibition to TC neurons reduces their activity but makes it more synchronous (autocorrelogram, right **A3**), this activity results in bidirectional excitation with the cortex (cross- correlogram, left **A3**). [Taken from Polack et al., 2007 (**A1**) and McCafferty et al, 2018 (**A2, A3**)].*

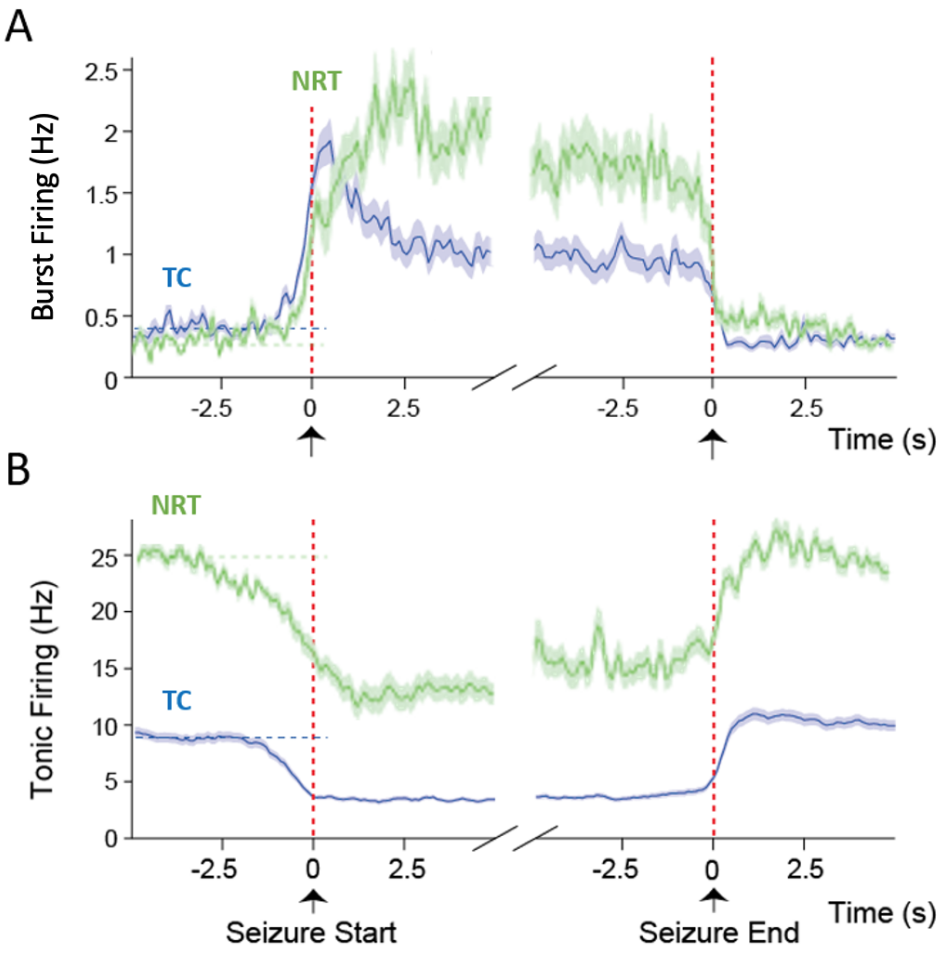


***Figure 1.8. Neural firing dynamics of VB TC and NRT neurons around seizure onset and offset.***

*Plots show the burst (**A**) and tonic (**B**) firing dynamics of NRT (green) and TC (blue) neurons at seizure onset and offset (0s in left and right panels, indicated by dotted red line). Note, tonic NRT and TC activity start to decline before onset which coincides with a shift to burst firing in both thalamic types, which return to baseline after seizure offset [Adapted from (McCafferty et al., 2018)].*

Although the cortex is where the initial SWCs are generated, thalamic alterations will significantly impact AS. For example, in VB neurons of GAERS there was an enhanced Hyperpolarization and Cyclic Nucleotide-activated (HCN) current (Ih) when compared to NEC animals (Cain et al. 2015). The Ih current regulates neuronal excitability by promoting the resting membrane potential, in this way, when the cell is hyperpolarised the Ih current activates, resulting in an inward current of cations which begins to slowly depolarise the cell. In thalamic neurons, this would facilitate the activation of T-type calcium channels following hyperpolarisation and thus facilitate the generation of a LTS and subsequent burst firing (McCormick and Bal 1997). Pharmacological block of the Ih current in GAERS reduced tonic and not burst firing of VB TC neurons. This caused significant reduction in spontaneous AS (David et al. 2018), an effect that was repeated also in the GHB model, demonstrating that synchronous tonic TC firing is important for AS. Indeed, there are numerous studies in patients with generalised epilepsy that have found mutations in HCN channels (Tang et al. 2008; DiFrancesco et al. 2011).

Another thalamic alteration is a greater tonic $GABA_A$ current in VB TC neurons, which is found in many genetic models, including the GAERS rats and the Stargazer mouse, is a This is caused by a reduced function of GABA transporter 1 (GAT-1) in local astrocytes which leads to increased ambient GABA concentration. This dysfunction, if emulated using a GAT-1 blocker, is sufficient to produce AS in non-epileptic Wistar rats which are blocked by ETX (Cope et al. 2009). This finding illustrates a role of astrocytic changes in genetic models of AS, as well as explaining why compounds that increase GABA levels exacerbate AS in animal models (Hosford and Wang 1997) and human patients (Perucca et al. 1998; Ettinger et al. 2005).

Multiple alterations in the CTC network lead to the initiation of SWD in the S1 and the acceptance of this cortical initiation theory has led to additional questions, such as how the seizure spreads from an ictogenic sensitive area to the whole brain. Such questions are difficult to explain if only the principal CTC network is considered, due to the specific connectivity between VB and S1. Therefore, to answer this question recent studies have begun to look beyond the principal CTC network.

## 1.6 Higher order thalamic nuclei - Beyond the principal CTC network

Naturally, the principal CTC network is interconnected with many brain regions and is not a stand-alone system. Firstly, direct cortico-cortical connections from S1 are abundant, with connections to the motor, insular, restrospenial and visual cortex, to name some (Zakiewicz et al. 2014). Another form of cortico-cortical communication is trans-thalamic, which involves HO nuclei via strong excitatory cortical inputs. HO nuclei can therefore manipulate information between cortical regions and have diffuse connectivity profiles (D'Souza and Burkhalter, 2017) and project to both primary and higher cortical areas and consequently they are possible candidates for transmitting SWD from the initiation site to the rest of the brain.

The non-specific thalamic HO nuclei differ greatly from FO nuclei in connectivity and function. As briefly introduced in 1.2.1, instead of relaying bottom-up sensory information, the major excitatory, Class 1/driver input to HO nuclei is cortical layer V. In turn, they project not only back to the same cortical region, but to a range of other regions, spanning all cortical layers (Bickford 2016).

Class 1 synapses are often larger in size and generate large EPSPs via ionotropic glutamate receptors that will depress in paired-pulse stimulation protocols (Viaene et al. 2011). These properties often enable inputs to directly affect firing rates of neurons (Sherman and Guillery 1998). Cortical inputs to HO nuclei are class 1, additionally HO neurons form Class 1 synapses at higher-order cortical areas (Viaene et al. 2011).

Class 2 synapses are usually smaller in size and modulatory in nature. Their EPSPs are generated by both ionotropic and metabotropic glutamate receptors that increase in amplitude with repetitive stimulation (Sherman 2014). HO neurons are therefore capable of exerting long-lasting (hundreds of ms) effects, depending upon the type of metabotropic receptors involved, for example group I or group II metabotropic receptors that can generate excitatory or inhibitory effects, respectively. Additionally, synapses between cortical neurons can also fall into these two types, which adds to the complexity. Class 2 synapses are most abundant where HO nuclei synapse to primary cortical regions (Viaene et al. 2011).

The diverse connectivity of HO nuclei is an anatomical advantage when influencing and transmitting information across the entire brain and may enable them to play a

key role in the generalisation of AS. As HO nuclei receive and send axons from and to the cortex, a parallel route of cortico-cortical information is established, the trans-thalamic route (Sherman and Guillery 2011). Whereas cortico-cortical communication is formed of feed-forward glutamatergic connections, the trans-thalamic route provides a point of modulation and gating between cortico-cortical regions.

HO nuclei can be split into intralaminar nuclei (IL), the posterior thalamic group (PO) and lateral posterior group (LP), each with their own interesting influence in AS. In rodents, all these nuclei are formed primarily of glutamatergic neurons. In 2018, a very small population (2%) of inhibitory neurons was reported in LP (Evangelio et al. 2018) of the C57/BL6 mouse. In the same study, a few inhibitory cells in PO were detected (but their proportion was not quantified). Finally, in the rat IL nuclei, GABA reactive cells were not found (Bentivoglio et al. 1991).

### 1.6.1 Intralaminar nuclei

The IL nuclei group reside between the internal medullary lamina of the thalamus and can be split into a rostral and caudal group. The rostral group consists of the central medial (CM), paracentral (PC) and central lateral (CL) nuclei. The caudal group consists of the parafascicular (PF) and in higher mammals and primates there is also the centromedian/centre median nuclei just lateral to, and forming a complex with, PF (n.b. this is different to rostral CM nuclei) (Groenewegen and Berendse 1994; Van der Werf et al. 2002).

These nuclei all project preferentially but not exclusively to the frontal-parietal cortex and the ventral striatum, the region of the basal ganglia most sensitive to pharmacological interventions of AS (Deransart et al. 2000), although the weightings of these connections vary across different IL nuclei. Some topography is present, the rostral IL group receive sensory and to a lesser degree, motor information (Groenewegen and Berendse 1994). A commonality of the whole IL complex is their involvement in global brain state and arousal. IL nuclei receive input from the brain stem and have relatively non-specific efferents, in this way they can have a global effect on cortical excitability and thus, cortical responsiveness to incoming sensory stimuli (Van der Werf et al. 2002). The ability of IL to manipulate excitability of the whole cortex has already been shown sufficient to generate AS (Meeren et al. 2005) but since, studies on specific IL nuclei have been undertaken.

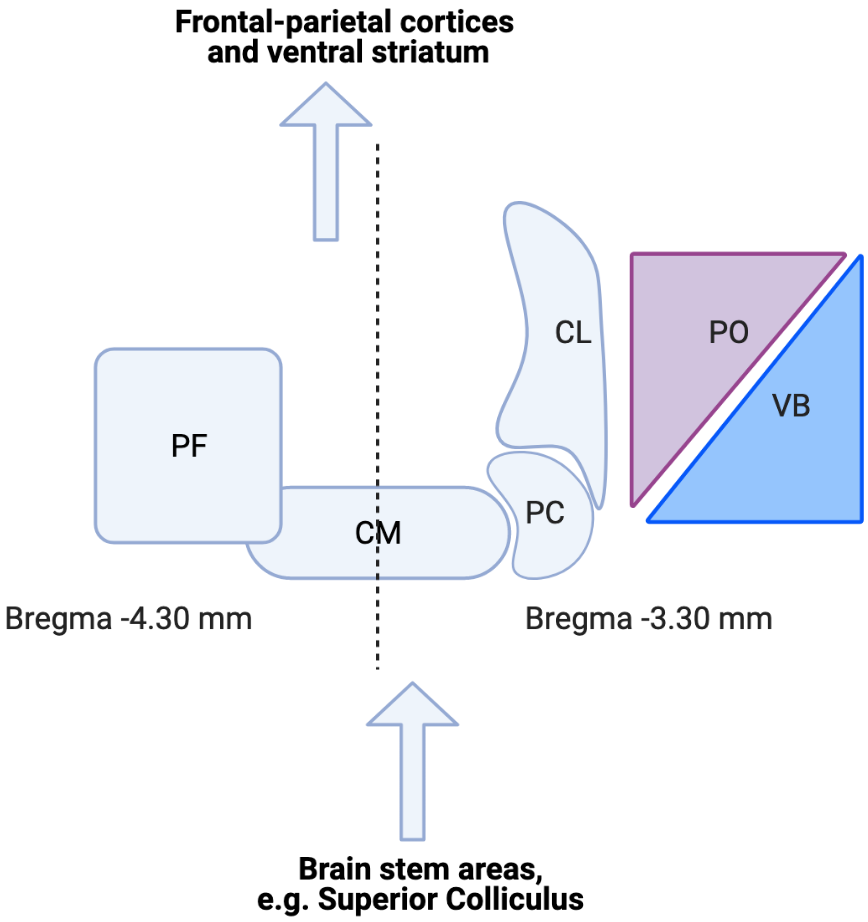


***Figure 1.9. Schematic of the rat IL nuclei group.***

*Left hand side shows bregma at AP -4.30 mm and the location of caudal IL group, i.e. parafasicular (PF) nuclei. To the right of the midline (vertical dashed line) is a schematic at bregma -3.30 mm showing the rostral group, containing the paracentral (PC) and centrolateral (CL) intralaminar nuclei which are medial to the posterior thalamic group (PO) and ventrobasal thalamus (VB). The central media (CM) nuclei, part of the rostral group, spans the midline and can be viewed at both -4.30 mm and -3.3 mm in the rat brain. The major projections and inputs are shown by arrows above and below the IL nuclei, respectively. Figure created with BioRender.com*

#### *1.6.1.1 The IL in AS*

Basal and ictal activity of IL vary across nuclei. Intracellular and extracellular recordings of CL and PC neurons revealed a suppression of activity during the spike of a SWC which gave rise to some post-inhibition rebound activity during the wave component (Inoue et al. 1993; Gorji et al. 2011). However, it remains unknown whether IL burst firing during the wave impacts the ongoing seizure. This contrasts with the activity in FO neurons which fire during the SWC spike.

Recently, the involvement of the CM, a nuclei in the rostral group, was investigated (Jonas Terlau and Annika Luttjohann 2020). The rationale for targeting this nucleus was based on previous studies showing involvement of the centromedian nucleus in human generalised epilepsies (Velasco et al. 1997; Tyvaert et al. 2009) and sensorimotor function (Ilyas et al. 2019). The centromedian nucleus that these papers regard is just lateral to the PF and is not found in rodents (Velasco et al. 1997; Ilyas et al. 2019) and thus is different to the CM targeted in the Terlau paper, which is located more medial to the PF location. Nevertheless, this paper contributes novel data regarding the role of CM in AS using pharmacological interventions. Inhibiting the activity of the CM by local injection of DNQX, an AMPA receptor blocker, had no effect on ongoing SWD in S1 but decreased it in M2. In M2 the SWC spike was reduced in amplitude by 30% (Jonas Terlau and Annika Luttjohann 2020), representing a reduction of cortical synchronisation caused directly and/or indirectly by the CM.

These works demonstrate a potential involvement of the IL in the generalisation of AS. However, research in the area is limited and with many small nuclei in proximity it is difficult to know exactly which nuclei to target experimentally.

### 1.6.2 The lateral posterior group

The LP is located lateral of the IL nuclei and ventral of the hippocampus. It receives input from the superior colliculus and the visual cortex and thus forms the paralemniscal pathway of the visual system. The LP has diffuse projections to various regions of the occipital, post-parietal and temporal lobes and the striatum (Kamishina et al. 2009). The LP can be subdivided into three divisions, the lateral, rostromedial and caudomedial portions. The former two target the upper and middle layers of the primary and secondary visual cortex *(Figure 1.10)*, whereas the latter targets temporal

association areas (Nakamura et al. 2015). Some LP projections to S1 have been reported (Massé et al. 2019), although, this is not reciprocal (Zakiewicz et al. 2014). However, LP is indirectly connected to the AS initiation site via the NRT (Nakamura et al. 2015) and two other inhibtiors of the higher-order thalamus, i.e. the zona incerta (ZI) and the anterior pre-tectal nucleus (APT) (Bokor et al. 2005), that all of which receive inputs from S1 (Zakiewicz et al. 2014). In this way, it could aid the initial spread of SWD to brain regions far from the initiation site.

Single unit data has been collected from LP in genetic models of AS (Sorokin et al. 2020). However, this paper focused on PO and grouped together cells of LP and PO. As a group, these LP+PO neurons had a transient reduction in total firing just before seizure onset, before sharply returning to baseline firing at the time of seizure onset. There is currently no data that has directly assessed the role of LP in AS. However, inhibition of the superior colliculus, a major input to LP, temporally supressed SWD in GAERS (Nail-Boucherie et al. 2005). Neither of these studies provide a detailed view on the functionality of LP in AS.

### 1.6.3 The posterior thalamic group

In felines and humans there are distinctive regions of the posterior thalamus that form the lateral, intermediate and medial subdivisions. Of these 3, the medial subdivision is associated with the somatosensory system. In rodents a more homogenous structure, the posterior thalamic group (PO), is present which is analogous to this medial subdivision (Jones 1985; Ohno et al. 2012). The PO can further be categorised in the rostral (POm) and caudal/triangular sections (POc/ POt) as proposed by Diamond (1992). However, in many papers the terms PO and POm are used interchangeably, here the term PO will be used.

Following the definition of HO thalamic nuclei (Sherman and Guillery 1998), class 1 input to PO comes from layer V cortical neurons. Additionally, it receives topographical input from the spinal trigeminal nucleus (Diamond et al. 1992) and also input from cerebellar nuclei (Schäfer and Hoebeek 2018; Dumas et al. 2019). The PO responds roughly equally to 5-6 whiskers in its barrel field, unlike VB neurons that responds strongly to the central whisker of its similarly sized receptive field (Diamond et al. 1992), strongly indicating its role as a general modulator rather than a specific relay.

Anatomical and physiological differences occur along the rostral-caudal axis of PO, as revealed by viral tracing analysis of single neurons. Rostral PO neurons project mainly to layer V of S1 and often have collaterals to M1 (Ohno et al. 2012), with the synapses terminating on regions representing the same body part, e.g. neurons will terminate in the upper lip region of S1 and M1 (C. Porrero, SfN abstract: 221.09, 2019). The caudal neurons of PO have projections predominantly to layer 1 of S1, but also to the striatum. Although these are the main connections, PO neurons exist that project to S2, M2, insular, auditory, and visual cortices (Charbonneau et al. 2012; Ohno et al. 2012).

Glutamatergic TC neurons of PO project predominantly to layer Va and I/II of S1 (Casas-Torremocha et al. 2019). One study reported that all layer V S1 neurons receive PO input, with large amplitude responses evoked in pyramidal cells and PV interneurons (Audette et al. 2018). PO projections to S1 have a modulatory role by activating group 1 metabotropic glutamate receptors that depolarises the membrane potential for hundreds of milliseconds (Viaene et al. 2011). However, some studies have reported S1 EPSPs with depressing responses to paired-pulse stimulation (Audette et al. 2018; Casas-Torremocha et al. 2019), indication a mix of Class 1 and Class 2 synapses in S1. PO neurons also project to S2, where Class 1 synapses are dominant (Viaene et al. 2011), and in addition a trans-thalamic S1-PO-M1 pathway has been shown (Mo and Sherman 2019a). The layer projection profile for M1 is roughly inverse of S1, with most varicosities occurring in superficial layers (Casas-Torremocha et al. 2017) *(Figure 1.10).*

Reciprocal PO connectivity with S1 makes this HO nucleus an interesting candidate to modulate networks at the transition period to ictal states and will be discussed later in this section.

#### *1.6.3.1 Inhibition of LP and PO*

In addition to the well-known inhibition from NRT, LP and PO also receive feedforward inhibition via the extrathalamic ZI and APT *(Figure 1.10)* (Halassa and Acsády 2016). Unlike the NRT, the ZI and APT do not receive any projections from the thalamus and project only to HO nuclei. The ZI and APT are intimately related to the sensory system as they both receive direct input from vibrissae and S1 (Lavallee 2005; Aronoff et al. 2010; Zakiewicz et al. 2014).

There are also additional connections between these inhibitory nuclei. The APT connects to ZI (Giber et al. 2008) and the ZI connects to the NRT (Çavdar et al. 2006), although the latter was not found in all ZI connectivity studies (Barthó et al. 2002).

These extra-thalamic sources are more abundant and potentially more powerful than that of the NRT, with their terminals being larger in size with multiple release sites (Barthó et al. 2002; Bokor et al. 2005) and the capability of generating tonic and burst firing patterns (Talley et al. 1999; Masri et al. 2009). The ZI fire synchronously to SWC-spikes (Barthó et al. 2007) and its inhibition reduces the occurrence of SWD (Shaw et al. 2013), or if done via closed-loop stimulation, can disrupt an ongoing seizure (Liang et al. 2011). No study has investigated the activity of APT during SWD.

#### *1.6.3.2 The LP and PO in AS*

The importance of LP and PO in AS is initially implied by alterations in their synaptic anatomy in genetic models of AS. In GAERS, there is a significant increase in the number of large terminals containing round vesicles in PO and LP, but not in a third HO nuclei, the mediodorsal nuclei, when compared to Wistar controls (Çavdar et al. 2012). This type of terminal is associated with stronger, high fidelity synapses, such as Class 1 relays (Bickford 2016). An increase in these terminals could result in hyperexcitability of PO neurons by cortical afferents. However, it remains unknown whether this has a significant impact on AS.

The activity of LP and PO during AS was first investigated in the 1980's with a feline model of SWD (Avoli et al. 1983; McLachlan et al. 1984). Single unit recordings from two studies showed that a majority of neurons fire during the SWC spike, like cortical neurons. However, a small population existed that fired during the wave component, this may reflect the two populations of neurons recorded from, i.e. LP and PO, or perhaps different populations within these areas. Aligned with the cortical focus model, it was observed that rhythmic excitation-inhibition sequences occurred in cortical neurons 1-3 cycles before thalamic neurons. Interestingly, this rhythmicity was more likely to happen when thalamic neurons fired before the cortical neurons, which suggested some leading role/bidirectional excitation occurring at the interictal to ictal transition period when thalamic neurons facilitated the synchronicity of cortical neurons.

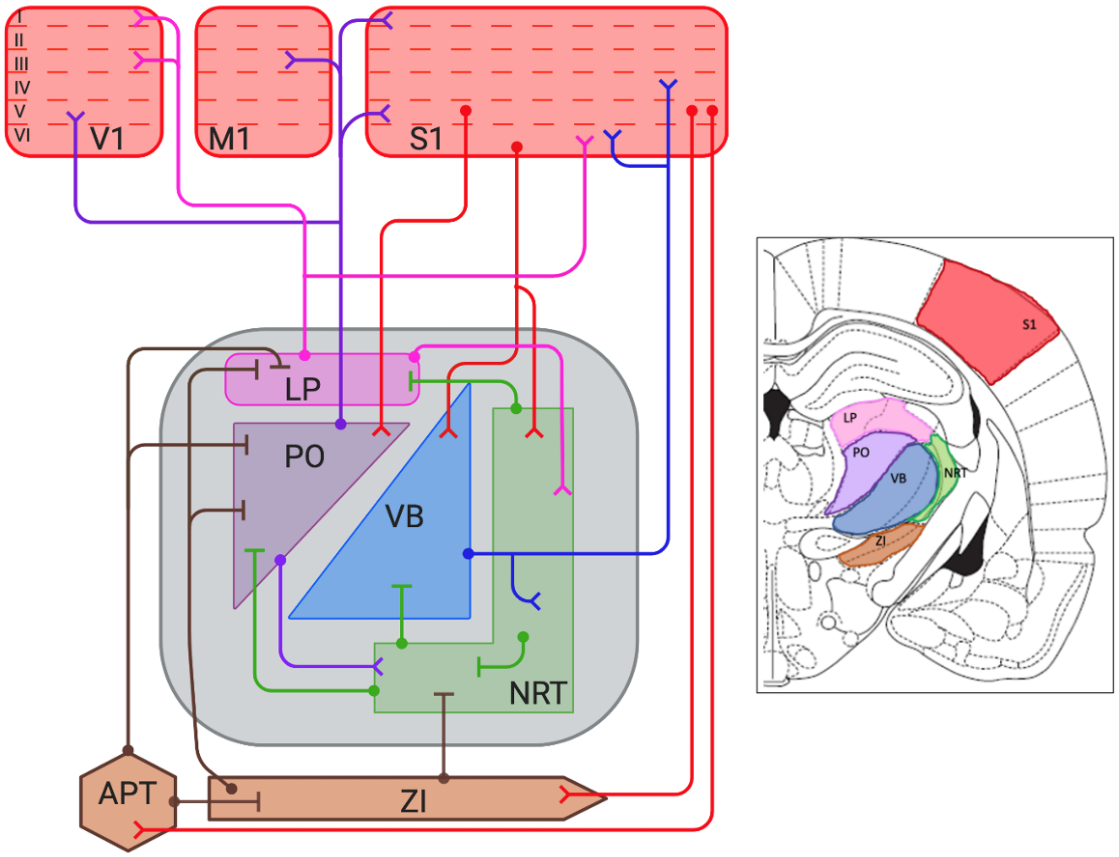


***Figure 1.10. Connectivity of PO and LP to the principal CTC network.***

*The diagram shows connections in the principal CTC network (as seen in Figure 1.3), as well as connections to and from LP and PO, both intra-thalamic and to primary cortical areas. Diagram is accurate at the layer level but cortico-cortical connections are emitted for simplicity. Excitatory inputs and inhibitory synapses are indicated by lines terminating in a '>' and a '|', respectively. Figure created with BioRender.com Figure inset highlights these regions in anatomical space with the regions highlighted over a diagram of a brain slice at -36mm from bregma, taken from Paxinos and Watson (1988).*

.

Interest in PO in relation to AS has increased in recent years. Non-linear association analysis demonstrated that bidirectional communication between S1 and PO increases from 1.25s prior to seizure onset (Lüttjohann and van Luijtelaar 2012). Importantly, this bidirectional coupling was maintained for the first 500ms of a seizure *(Figure 1.11)*, and therefore providing important feedback to the initiation site. This is the first thalamic nuclei tested to have this relationship with S1 (Lüttjohann and Pape 2019).

Upon termination, although the cortex continues to drive PO, the feedback from PO ceases (Lüttjohann and van Luijtelaar 2015), suggesting that PO response to cortical input changes at SWD termination. This infers that the bidirectional nature of cortico-PO communication is important for the maintenance of SWD. Unfortunately, the effect of PO on the spread of the seizure across cortical regions cannot be inferred because only one cortical region was recorded from.

LP and PO connectivity and activity during SWD demonstrate a potential involvement in the initiation of AS and their generalisation, particularly to regions far from the cortical initiation site. To assess the involvement of HO nuclei in cortical spread of SWD, recordings in the freely moving animal with multiple electrodes in different cortical areas is required.

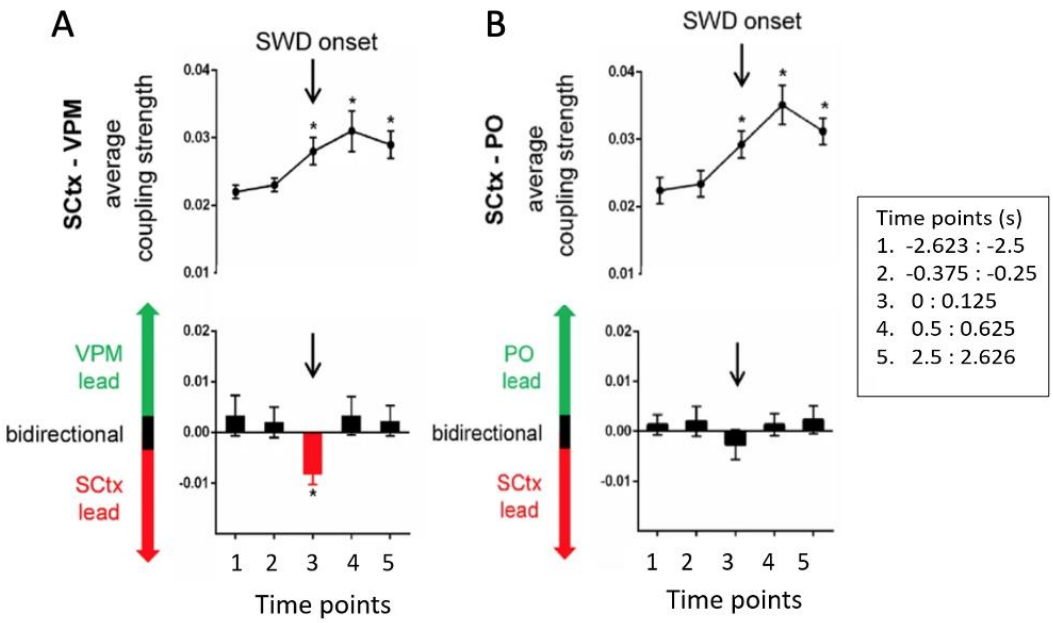


***Figure 1.11. Coupling strength and direction of FO and HO nuclei with the somatosensory cortex at the interictal-ictal transition period.***

*Top panels show the average coupling strength based on cross-correlations between unit recording in S1 (SCtx) and either VB (VPM -**A**) or PO (**B**). Asterisks show when coupling was significantly increased compared to time point 1 (see legend). Bottom panel shows data on directionality of the coupling where negative values represent cortical lead and positive represent thalamic lead. Note: the VB is led by the cortex during the beginning of the seizure (time point 3), whereas PO remains in bidirectional communication with S1 during this period (**B**). [Taken from Lüttjohann and Pape, 2019].*

## 1.7 Aims of thesis

Multiple studies have shown that AS commence in a cortical initiation network (Meeren et al. 2002; Polack et al. 2007), that in GAERS is located in S1 (Polack et al. 2007). What remains to be investigated is how SWD propagate to other regions of the brain. This research will define propagation of SWD by measuring the time between onset in S1 and a region far from the cortical initiation network, i.e. V1.

Looking beyond the CTC network there are some potential nuclei that could be facilitating this process. This work will focus on HO nuclei in the role of AS generalisation as they provide a different, parallel route of cortico-cortical communication (Sherman and Guillery 2011) and thus, propagation of SWD. There is some solid evidence indicating changes in S1-PO communication at the onset of AS (Lüttjohann and van Luijtelaar 2015): therefore, PO was selected as one HO nuclei of interest. As the generalisation of SWD will be defined by investigating it in S1 and V1, LP was also selected for investigation as it is the HO nucleus that is directly connected and functionally related to the visual cortex (Kamishina et al. 2009; Allen et al. 2016).

The role of PO and LP nuclei will be evaluated using various electrophysiological and pharmacological techniques in freely moving GAERS rats.

In particular,

1. the relationships between HO nuclei and cortex will be explored based on amplitude and phase information of their local field potentials (LFP);
2. the relevance of these relationships with SWD will be tested by inhibiting the HO nuclei individually via local injection of the $GABA_A$ agonist muscimol;
3. The temporal firing dynamics of single units in PO will be evaluated to reveal important changes at interictal-ictal and ictal-interictal transitions.

# Chapter 2: Methods

## 2.1 Implantations and data acquisition

### 2.1.1 Animals and ethical statement

Experiments on male GAERS were undertaken in two establishments, the School of Biosciences, Neuroscience Division, Cardiff University, UK and the Department of Physiology, University of Szeged, Hungary. In both institutions the GAERS were bred in-house and all rats had access to food and water *ad libitum.* Both locations had a 12:12 hour light:dark cycle and controlled temperature 19-21℃ and humidity (45-65%). All experiments were conducted on rats aged 4-8 months with approval of the local ethical committees and under the regulations of either the UK Home Office or EU directives.

### 2.1.2 Basic surgical procedures

#### *2.1.2.1 Anaesthesia and analgesia*

All surgical procedures took place under volatile isoflurane anaesthesia, induced via an induction box at 4% in 2L oxygen / minute and maintained at 2% isoflurane via a mask. Isoflurane concentration could often be reduced over time to a concentration of 1.5%. Depth of anaesthesia was regularly assessed by observing breathing rate and testing hind leg withdrawal reflex and tail pinch reflex (Flecknell 2009)**.** Body temperature of the animals was continually monitored and maintained at 37°C using a homeothermic heat blanket (Harvard Appartus, US). Analgesia was achieved by administration of 2 mg/kg meloxicam (Metacam, Boehringer Ingelheim, UK) subcutaneously at the beginning of surgery. Saline was injected at 2.5ml/kg every hour of procedure to ensure good hydration throughout.

#### *2.1.2.2 Skull preparation*

Hair was removed from the head using a standard hair trimmer or hair removal cream. Eyes were protected with a paraffin based eye lubricant (Lacrilube, Allergan Inc, USA). Lidocaine gel (Teva Pharmaceuticals, UK) was applied before disinfection with 3 applications of betadine and ethanol. The skull was exposed with a sterilised scalpel and cleaned of connective tissue with light physical scraping and careful application

of 3% $H_20_2$ which was washed away with cold saline. Any persistent bleeds were terminated with cold saline and pressure, or as a last resort, a cauteriser.

The angle of the head of the animal was moved so that bregma and lambda were in the same plane before bregma coordinates, and subsequent craniotomies, were taken. Common to all experiments, three craniotomies were made over three cortical areas *(Table 2.1)*. The coordinates to target the thalamus varied between experiments and are detailed in the relevant sections.

#### *2.1.2.3 Post-operative care*

Immediately after the procedure, animals were placed into a cage with clean surgical bedding instead of standard sawdust mixture to reduce risk of infection from dirty bedding contacting the wound. The animals usually woke up within 10 minutes and were kept in an 30°C incubator for at least 30 minutes.

For the first 5 days after surgery, every 300ml of drinking water contained 0.6ml of 25 mg/mL Baytril to provide analgesia. At least once a day they were checked for signs of distress and pain. Any additional actions were taken under direction of a veterinarian.

### 2.1.3 Local Field Potential recordings in GAERS.

LFP recordings were made in multiple cortical sites in addition to LP and PO to gauge the involvement of HO nuclei in absence seizures.

#### *2.1.3.1 Electrodes*

Four separate LFP electrode doublets were created to record from M1, S1, V1 and LP/PO. The electrodes were built by placing two 50µM ∅ tungsten wires through a 29G (inner ∅ 0.178mm, outer ∅ 0.33mm) stainless steel tubing (Coopers Needle Works, UK) *(Figure 2.1A)*. The tips of the two electrodes were separated by 0.5mm for S1, M1 and V1 electrodes, so the electrode with the best signal could be selected and by 1mm in the LP/PO electrode, to have one electrode in each area.

The tungsten wires were fixed by applying small amounts of superglue at the non-recording end of the tube, allowing it to flow inside the tube, to ensure a secure fixture. Then, the non-recording end of the tungsten wires were deinsulated with a scalpel

and each tip was threaded through separate holes of a 2*1 pin row header (RS components, UK) that had its pins removed *(Figure 2.1B)*. The pins were then placed back *(Figure 2.1C)* into the pin row header which formed a secure mechanical and therefore electrical connection from tip of the electrode to the pins. The tube electrode structure was then fixed to the plastic pin row header with small amounts of dental cement.

A holder was made with a 3*1 pin row header with 2 pins removed *(Figure 2.2)*. A long metal rod was fixed onto the remaining pin. This enabled the electrodes to be fitted and removed easily to this holder, facilitating implantations.

Gold plated screws (Dentorama, Sweden) with copper wire attached were used for ground and reference electrodes and 2mm M1 stainless-steel screws (Accu Limited, UK) were used for various implant anchor points.

#### *2.1.3.2 Data Acquisition*

Animals were habituated to the experimenter and recording plexiglass boxes (30*30*30 cm) in the two days prior to the experiment. To acquire the data, the female PCB connector on the head of the animal was connected, via a custom-made cable, to two preamplifiers (4 channels per amplifier) (SuperTech, HU). Here a high-pass 0.08 Hz filter was applied before it passed through an amplifier that applied a gain of 1000 and a 500 Hz low pass filter. Data was digitised at 1 kHz by a 1401 interface (CED, UK) and acquired with Spike2 software (CED, UK). Data was acquired for 1 – 2 hours, until a sample of at least 40 seizures was obtained.

#### *2.1.3.3 LFP recordings in the dark*

LFP recording revealed temporary lapses of SWD, particularly in V1, while ongoing in S1. This phenomenon, termed SWD-breaks (detailed in 3.3.5) could be induced by brief light stimulations. Therefore, to ensure that these SWD-breaks were not being caused by transient changes in ambient light, animals were habituated to the dark before being recorded the following day. Comparisons were made between SWD-break duration and rate between the light and dark condition.

| Area/Axis | AP | ML |
|---|---|---|
| **S1** | 0 | 5.5 |
| **M1** | 2 | 2.5 |
| **V1** | -7.5 | 3 |

***Table 2.1. Co-ordinates for cortical targets used throughout the project in the anterior-posterior (AP) and mediolateral (ML) axis***

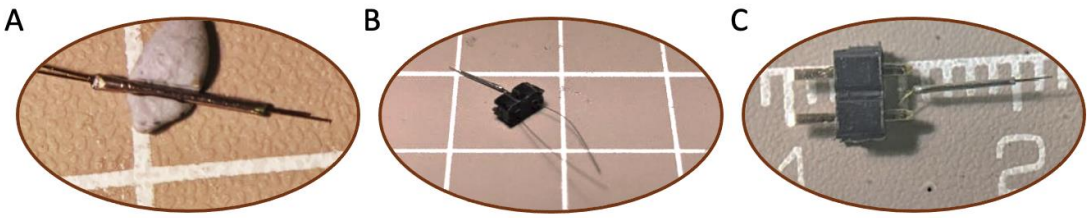


***Figure 2.1. Electrode Manufacture for LFP recordings in vivo.***

*Firstly, two tungsten wires were threaded through steel tubings (**A**) secondly, after being deinsulated, they are threaded through an empty pin row header (**B**). The pins are then placed back into the header ensuring a tight mechanical fit (**C**).*

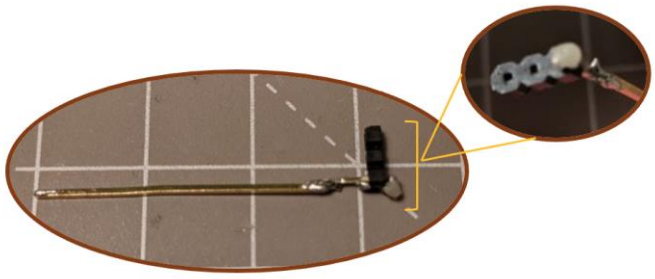

***Figure 2.2. Electrode holder to facilitate implantation of electrodes***

*An electrode holder was made that can easily and quickly fit electrodes, details of how the holders are made is in the text. The long gold pin fits into the stereotactic frame and the empty holes, as shown in insert, fit to electrode pins.*

## 2.1.4 Seizure perturbation with visual stimulus

A set of experiments was carried out on the previous set of animals to demonstrate how a brief visual stimulus could disrupt ongoing SWD in V1.

### *2.1.4.1 Visual stimuli and protocol*

Phase reversal gratings *(Figure 2.3)* were produced using the PsychToolBox 3 (Psychtoolbox.org) via MATLAB running on Windows 10. The background holding screen was grey, set to half maximal brightness. Grating stimuli split the screen equally into black and white bars and should have the same brightness as the grey screen. Therefore, the only acting stimuli on the rat visual system should be reversal gratings, rather than fluctuations in brightness.

Four stimuli were presented to the animal;

1. Control grey screen, same as baseline screen, 500ms
2. Control phase grating stimuli of 0.05 degrees, 500ms
3. Test phase reversal grating of 10 degrees, 500ms
4. Test phase reversal grating of 10 degrees, 1000ms

The second control screen should not elicit a response as Wistar rats have a visual acuity of 0.5 cycles/degree (Prusky et al. 2002) and therefore should only perceive grating of 2 degrees and larger.

The screen was placed 57cm (where 1 degree = 1 cm) from 5cm in from the back of the plexiglass cage, the preferred resting spot of the animals. As the animals are freely moving the true degree of stimulus 2 ranges between 0.05 and 0.08 degrees, and stimuli 3 and 4 range from 9.2 and 17.81 degrees.

### *2.1.4.2 Data Acquisition*

Data was recorded with the same system and parameters as *2.1.3.2.* The animals were first habituated to the background grey screen on the day before experiment, and on the experiment day for 20 minutes. When SWD in V1 reached an amplitude threshold (~75% of max) and maintained this way for approximately 500ms, a stimulus (randomly chosen by software) was manually prompted by a press of the space bar.

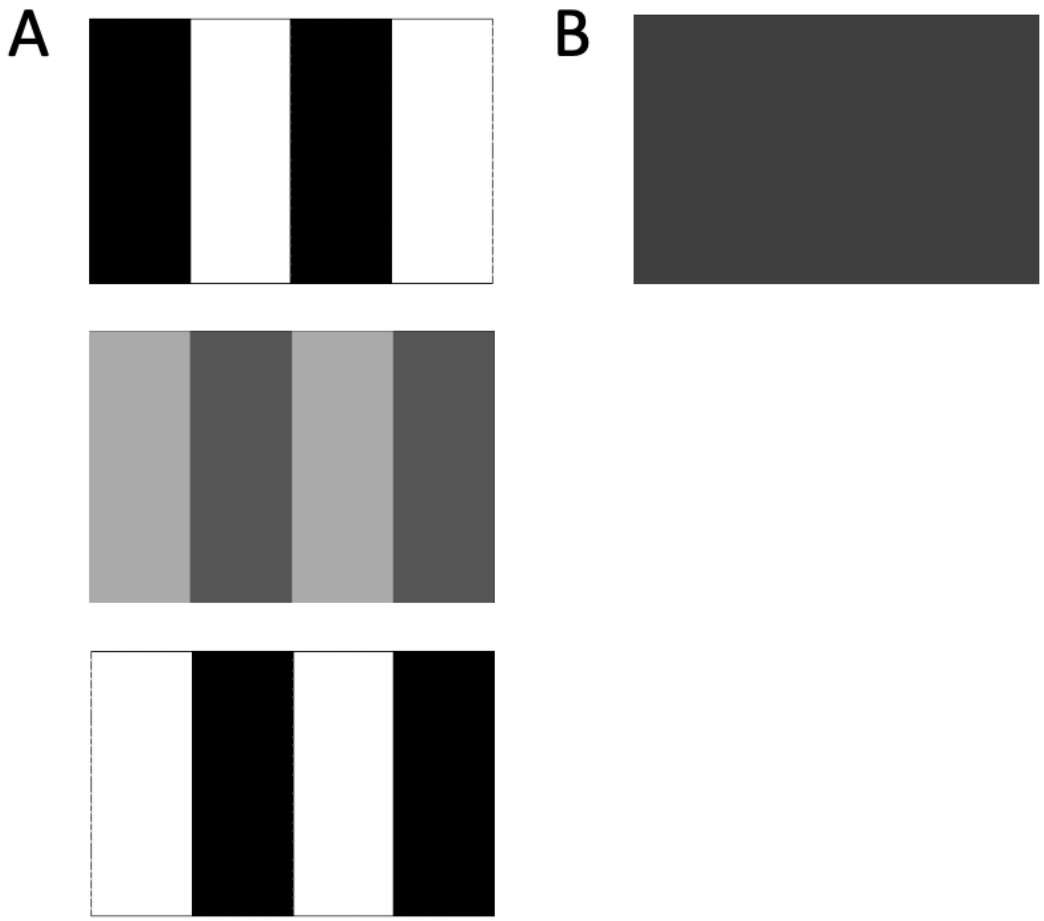


***Figure 2.3. Representation of presented phase reversal gratings.***

*Two types of phase reversal gratings were presented to GAERS, a wide (**A**) and a narrow (**B**). Plot **A** shows how the phase grating stimuli evolved with time, i.e. bars on the screen cycle between black and white across frames, with adjacent bars starting as opposite colours. In **B** the bars are thin, so that just a grey screen is perceived by the animal.*

A direct TTL pulse from the MATLAB script to the data aquisition hardware was not possible, so synchronisation of the stimuli to the electrophysiology data was initially done in 3 ways.

1. Manually marked using keyboard marker on recording computer, pressed by experimenter simultaneously to space bar being pressed on visual stimuli computer.
2. GetSecs from Psychtoolbox 3 was used so that the timing of each stimuli, relative to the first, was known. Just the first stimuli needed to be marked using method 1.
3. Tic toc functions on MATLAB to know the duration of time elapsed between each stimulus. Just the first stimuli needed to be marked using method 1.

The stimulus times extracted from these methods varied by just 0.001s, and therefore were deemed accurate. The chosen method was to mark the first stimulation manually and use GetSecs function from the Psychtoolbox3 for subsequent stimuli as this was the most automatic and required the least computation.

#### *2.1.4.3 Histology*

To assess the location of electrodes, electrolytic lesions were performed using a DS3 Isolated Current Stimulator (Digitimer, USA) at the end of experiments. A total of 20μA was administered at a rate of 1μA / second. This was completed on the deeper tip of all cortical electrodes and both LP and PO electrodes. The animals were sacrificed via a 200mg/kg pentobaribital (Dolethal, Vetoquinol, FR) injection 24-48 hours later and the brains stored in 4% PFA for 24 hours.

The brains were sectioned into 80μM slices using a vibratome (Leica, DE) and their membranes were permeabilised with 0.1% PBS Triton X (Invitrogen, USA) solution for 15 minutes while on a shaker. After being washed with a 1X PBS solution the brain sections were mounted onto glass slides (ThermoFisher Scientific, USA) and 22*50mm coverslips fixed using a hard-set mounted medium with DAPI (Heatshield, ThermoFisher Scientific, USA). The slides were viewed with 10x objective of a fluorescent confocal microscope (Zeiss LSM-880, DE) and tile scan images were taken of the ultraviolet light excitation channels using ZEN black software (Zeiss, DE).

## 2.1.5 Microinjection into HO thalamic nucleus and LFP recordings in GAERS

### *2.1.5.1 Electrodes and Cannulae*

Electrodes were made exactly as described in 2.1.3.1. 11mm Cannulae (P1 technologies, VA, USA) were purchased ready for implantation.

### *2.1.5.2 Surgery*

Following steps outlined in section 2.1.2**,** craniotomies for S1, M1 and V1 were made at the co-ordinates outlined in Table 2.1. Craniotomies for LP/PO were made at AP: -3.6mm, ML: +/-3.2mm.

An anchor screw was placed between M1/S1, next to each Cannula site and next to the V1 craniotomy. Using two stereotactic arms, two cannulas were lowered slowly to 1mm above LP (DV: -3mm) at an angle of 15° and fixed with superbond (Sun Medical, JP). An angle was necessary to increase the distance between the two cannulae so internal cannulae and tubing could be fixed during experiment. A dummy internal cannula (<11mm) was fitted before full fixation with additional acrylic cement (Unifast, GC, JP).

Each electrode structure was then lowered and fixed with acrylic cement (GC America INC, USA) before removing the holder. The gold screws for the ground and reference were implanted. A pre-prepared 5*2 PCB connector with copper wires attached were then soldered to each of the electrodes with the aid of phosphoric acid, ground and reference screws were then connected to the PCB connector. Acrylic cement was then used to cover the whole structure to form one smooth implant. Finally, the animals were sutured (Cole Parmer, UK) had a minimum of five days recovery period with the post-surgical care outlined in section 2.1.2.3.

### *2.1.5.3 Habituation and training*

Animals were habituated to the experimenter and recording environment in the three days prior to the first microinjection. The first day consisted of introduction of the animal to the experimenter with basic handling and some gentle restrictions with a towel. On the second day, animals were again restricted with a towel. The method of restriction was to grab the animal from behind the shoulders with the right hand and gently place them on their back legs in a comfortable seated position. Then, with the left hand, the towel was wrapped around the front of the animal and a firm grip with

the left hand maintained this restriction, leaving the right hand free. Animals were also placed in the plexiglass box with cable attached for 20 minutes. Day three of habituation mimicked the protocol on the test day, therefore a recording of one hour was made, in addition to being placed in the injection cage (another plexiglass box) for 10 minutes and then back to the recording box. If animals were habituated for more days than this, problems occurred with the animal often falling asleep during recording, therefore, this short but intense schedule was the most appropriate.

#### *2.1.5.4 Microinjections*

500nL of artificial cerebrospinal fluid (aCSF) (Bilaney, UK), which contained the following (in mM): Na+ 150; K+ 3.0; Ca2+ 1.4; Mg2+ 0.8; P 1.0; Cl- 155), was injected with or without 15ng (0.0002 mg/ml) of Muscimol (Tocris, UK) into LP, or PO, via an internal cannulae (Bilaney, UK) with a 1mm or 2mm projection, respectively.

To this end, an internal guide cannula was attached to cannula tubing (P1 technologies, VA, USA), which was flushed with distilled $H_20$ to clean the tubing and ensure it was free from blockages. Then, a 10μL Hamilton syringe filled with distilled $H_20$ was attached and the plunger fully pressed, to ensure free flow of liquid through the tubing and out of the internal guide cannula.

Following this, the Hamilton plunger was retracted to create a 2μL air bubble at the cannula end. The cannula was then submerged in the drug or aCSF solution to intake 0.5 μL. Finally, another air bubble of 0.5μL was created which kept the solution safely between two air spaces. This ensured no leakage of excess amount was injected into the region of interest. This completed for a second internal guide cannula and the Hamilton syringes were placed into a pump (CMA 400 Syringe pump, CMA Microdialysis AB, USA) which was used to automatically administer the solution. The experiment was counter-balanced so that half the animals first received injection into LP, followed by PO, while the other half received injections in the reverse order.

#### *2.1.5.5 Data Acquisition*

Following a baseline recording of one hour, the animals were disconnected and internal cannulae were fitted. While in a separate plexiglass box, the animals were injected at a rate of 0.25μL/minute. Animals were injected one at a time so the experimenter could ensure injection tubing did not get tangled and a gentle downward slope was maintained from pump to animal. Injections were done in a separate

plexiglass box as the pump induced electrical noise in the recordings. Animals were kept in the injection box for 4 minutes after injection and then returned and reconnected to the recording system for a further 2 hours.

#### *2.1.5.6 Histology*

0.5μL of 10% DiI (ThermoFisher Scientific, USA) was injected with the above method after the last recording was made. The animals were then sacrificed with pentobarbital injection and the brains were dissected and stored in 4% PFA for 24 hours. The brains were sectioned into 80uM slices using a vibratome (Leica, DE) and mounted onto glass slides (ThermoFisher Scientifica, USA) and 22*50mm coverslips fixed using a hard-set mounted medium (Heatshield, ThermoFisher Scientific, USA). The slides were viewed with 10x objective of a fluorescent confocal microscope (Zeiss LSM-880, DE) and tile scan images were taken of the transmitted light and green light excitation channels using ZEN black software (Zeiss, DE).

### 2.1.6 Single unit extracellular recording of HO thalamic neurons in freely moving GAERS

#### *2.1.6.1 Electrodes and Microdrive*

Thalamic units were detected with 4-Shank, 32 site *Buzsaki* style silicon probes (NeuroNexus, Texas, US). The original ground and reference wires were replaced with more flexible microwires. The probe was then fixed to a custom-made microdrive, adapted from Vandecasteele et al (2012). Briefly, a 2 row pin header was adapted so that the plastic bridge of the pin row header moved up and down a 00-90 screw, fixed between two brass plates. This allowed for probe movement in 272 μm steps for every screw turn.

To record LFP, three 50μm tungsten wires were passed through hypodermic tubing with each wire tip separated by 400 μm, creating an LFP triplet. The tungsten wires were passed through an electrode interface board (EIB) and fixed with gold pins, 3 microwires were soldered to electrically connected points on the EIB board. Finally, the microwires were soldered to a standard PCB connecter.

Implantation was facilitated by attaching electrodes to holders. For the LFP electrodes, 2 gold pins were glued either side of the hypodermic tubing, a long gold pin from a 3cm pin row header was bent at 90° two times and then soldered to the

gold pins. Following implantation, a soldering iron was used to remove the holder long gold pin.

To hold the Neuronexus board, pins were removed from a double row, 3cm, pin row header. The board is placed inside and secured with dental cement. Single holder pins are then soldered on and replaced after implantation.

#### *2.1.6.2 Surgery*

Following steps outlined in 2.1.2**,** craniotomies were made for the 3 electrode triplets according to Table 2.1, in addition to a craniotomy for the silicon probe at (AP: -3.6, ML: 2.4, DV: 3.6) to target LP and PO. The co-ordinate is deliberately 1mm above the region of interest so that it can be moved into clean tissue for the recording.

Muscles attached to the temporal bone were carefully resected and held back with suture to increase cement to skull contact and a reduction of movement artefacts, both necessary for chronic implants.

The craniotomy for the probe was made by drilling a small square and removing the central bone flap, which kept the dura intact. Ground and reference screws were implanted over the cerebellum and multiple anchor screws were implanted, all were secured with a fixative, either Esterecem II (Tokuyama Dental, JP) or super-bond (Sun Medical, JP).

More cement was placed around the perimeter of the skull to form a raised ring which provided the foundation for the faraday cage. A square piece of copper mesh with an oval piece removed from its centre, to fit the cement ring, was attached to the ridge with more cement.

M1 and S1 electrode triplets were implanted and secured with cement. The dura of the probe craniotomy was carefully cut with a hook from a bent needle, avoiding blood vessels visible under the microscope. The probe was dipped in DiI dye for future histological processing and then implanted using a stereotactic frame. Lastly, the V1 electrode triplet was implanted.

The PCB connectors of each electrode triplet was then inserted into a single, larger, female PCB connector which was wired to an Omnetics connector before surgery.

This allowed for all channels to be recorded by one cable and connector on the animals' head, which is necessary in freely moving recordings.

The ground and reference cables from this Omnetics connector and that of the silicon probe, were attached to the ground and reference screws of the implanted in the animal. Finally, the faraday cage was built and covered in cement and epoxy for rigidity.

#### *2.1.6.3 Data Acquisition*

After 5 days recovery period, the animals were placed daily into a plexiglass box to be recorded. HS3 headstages (Amplipex, HU) were attached to the 2 Omnetics connectors (LFPs and silicon probe), which digitised the signal at 20kHz and amplified it by 200X. The signal then passed to a KJE-1001 amplifier (Amplipex, HU) which amplified the signal a further 400X. AmpliRec (Amplipex, HU) software acquired and stored the data as a .dat file.

At the end of each recording session the probe was moved down the dorsal ventral axis by approximately 34μM, i.e. an $1/8^{th}$ of a screw turn, via the microdrive. Data was collected every day until the end of the region of interest was reached.

#### *2.1.6.4 Histology*

Before implantation, the probe was carefully submerged into a 2% DiI (ThermoFisher Scientific, USA) to ethanol solution. At the end of the experiment, animals were perfused with 10mM PBS, followed by 4% PFA solutions and the brains were stored for 24 hours in 4% PFA solution. The brains were sliced, mounted and imaged as in section 2.1.5.6.

## 2.2 Analysis

All analysis was completed using custom MATLAB scripts and all statistics were completed using custom R scripts. Unless stated otherwise, all scripts were written by the author.

### 2.2.1 Seizure extraction

Recordings were visualized in Spike2 (CED, Cambridge, UK) and the times of SWCs were obtained using in-built Spike2 function to detect peaks/troughs over a threshold.

Seizures were then extracted automatically based on SWCs occurring at the right frequency (i.e. 6-8 SWCs in one second) and duration (i.e. at least 1 second) using a custom MATLAB script. Seizures were extracted for all recorded channels and were checked manually and refined if necessary. As non-generalised events were often short and lower in amplitude, these were extracted manually.

### 2.2.2 Common seizure parameters

Seizure number, duration and time spent in seizure was based on S1 SWD. The onset and offset times of SWD from other channels provided information on onset delays (i.e. time from S1 to any other channel) and offset differences (i.e. time difference at seizure offset). SWD-breaks, briefly introduced in section 2.1.3.3, and detailed in 3.3.2 were defined as an ictal period of >0.6s during which SWCs were not observed in a channel, while SWD were ongoing in S1. Their rate and duration were measured. Any further parameters were specific to each experiment and thus detailed in relevant sections.

### 2.2.3 LFP analysis

Not all seizures were kept for analysis due to problems with noise contaminating signals, therefore, only seizures with clear signal (i.e. with no large artifacts or instances with high noise, as detected by increase in baseline amplitude and presence of 50Hz noise oscillation) from 5 seconds prior to onset to 5s post offset, were kept for analysis.

#### *2.2.3.1 Power analyses*

Basic spectrograms to illustrate shifts in frequency power at seizure onset were made using the *spectrogram* function in MATLAB with windows of 600 samples, or 0.6s. To explore correlations in amplitude, ictal signals first were squared to include fluctuations in the negative amplitudes. Then an amplitude envelope of the squared signal underwent cross-correlations. The *crosscoeff* function was used which normalises and removes the mean from the signal before the cross correlation.

#### *2.2.3.2 SWC-spike lags*

SWC-spike lags in M1, V1, LP and PO were calculated relative to S1 SWC-spikes. For each S1 SWC-spike, the time difference to all SWC-spikes in another region within ±200ms were calculated to generate a time frequency histogram with a resolution of 1ms. Means were calculated by multiplying the time bin by the frequency

of events and dividing by the total events. This was completed on time bins -50 – +50ms around trigger to reduce pull from duplicates locked to neighbouring S1 SWC-spikes.

#### *2.2.3.3 Effect from light stimulations*

For each channel, signals from -1 to +3 seconds of each stimulation were extracted. This signal was squared and normalised before an amplitude envelope was fitted. The amplitude envelopes for each stimulation were averaged. Light stimulation did not affect amplitude of S1 or M1. For each channel that was affected by the light stimulation, i.e. V1, LP and PO, the amplitude at 6 time points were extracted, relative to stimuli presentation. These were 0, 0.25, 0.5, 0.75, 1 and 1.25s. Differences were explored against the control grey screen stimulus using a linear mixed model via the *lmer* package in R.

$$Model = amplitude \sim Time * Stimulation + (1|Animal)$$

Post hoc multiple comparison analysis with a Tukey correction via the *lsmeans* package in R revealed any differences in the effect of each stimulation at each time point.

#### *2.2.3.4 Pairwise phase consistency analysis*

The consistency of phase differences between two different signals can suggest synchronicity or lack thereof, between channels, such that as consistency increases, as does the communication between the two brain areas. The concept of PPC is that if phase angle differences are consistent, there will be small angular distances between phase angle differences, and thus indicate increase an in coherence.

To extract phase, signals were first filtered at consecutive 3 Hz ranges from 1-42Hz and from 75-90Hz using the *bandpass* function *(Figure 2.4B).* This function uses a finite response filter which does not cause phase shifts. The filter was checked before applying running the analysis. This was done with visual checks on a few test signals, alike in Figure 2.4. Additionally, the spectrograms of raw vs filtered signals were checked to ensure that the energy in each frequency band was not changed by the filter. The instantaneous phase was extracted following a Hilbert transform *(Figure 2.4C),* which generates a complex number where the complex component represents the phase in radians.

Other methods for phase extraction are available, such as waveform convolution and cross-spectral density analysis. It has been reported that phase extraction via the Hilbert transformation and complex Morlet waveform convolution yield equivalent connectivity statistics, whereas the spectral density measure can lead to spurious results (Le Van Quyen et al. 2001). The Hilbert transform was chosen due to its ease of implantation in MATLAB.

The phase difference between signals can be derived directly from the instantaneous phase information, by taking the phase at the same time point across two different channels and finding the difference between the two complex numbers. For PPC, at every seizure, the phase differences between signals are paired, creating a maximum number of unique pairs of observations *(Figure 2.5).*

$$p = N * 0.5 * (N - 1)$$

Where
P = total number of paired observations
N = number of observations

The angular distance between pairs of observations was computed. This was done by converting all phase differences to 0 – 360° and finding the minimal angle between the two observations. Finally, the cosine of these angular distances was calculated, the average of which generates the PPC value. The smaller the angular distances between pairs of observations, the more consistent phase lag differences are, which generates a higher cosine and therefore, PPC value *(Figure 2.5A).* The larger the angular distance, the closer to zero cosine will be with angular distances of > 90° being negative. Therefore, inconsistent phase lag differences results in lower PPC value *(Figure 2.5B).*

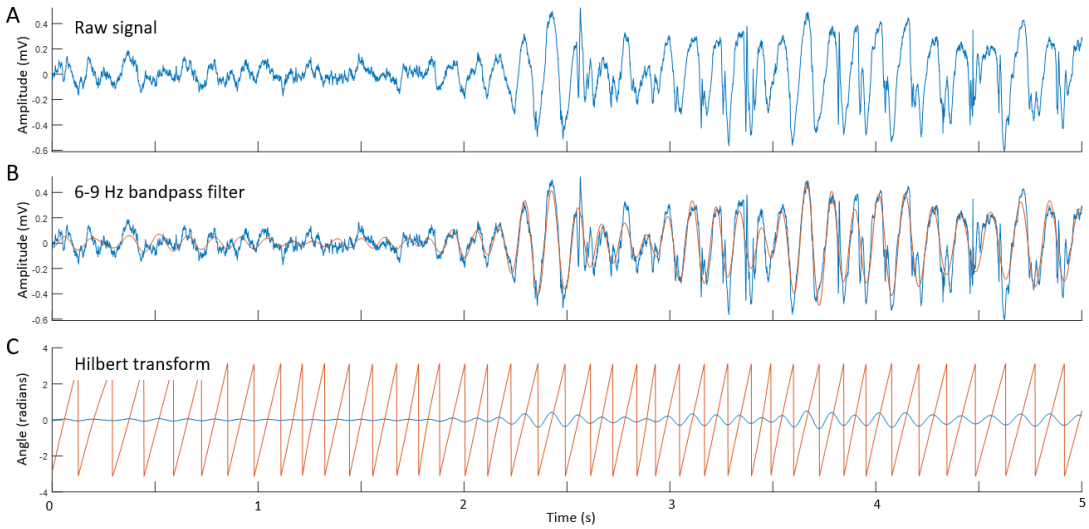


***Figure 2.4. Phase extraction process***

*Raw signals (**A**) first have a band pass filter applied (**B**) before a Hilbert transform is completed (**C**) to extract the phase information at every time point for that specific frequency band.*

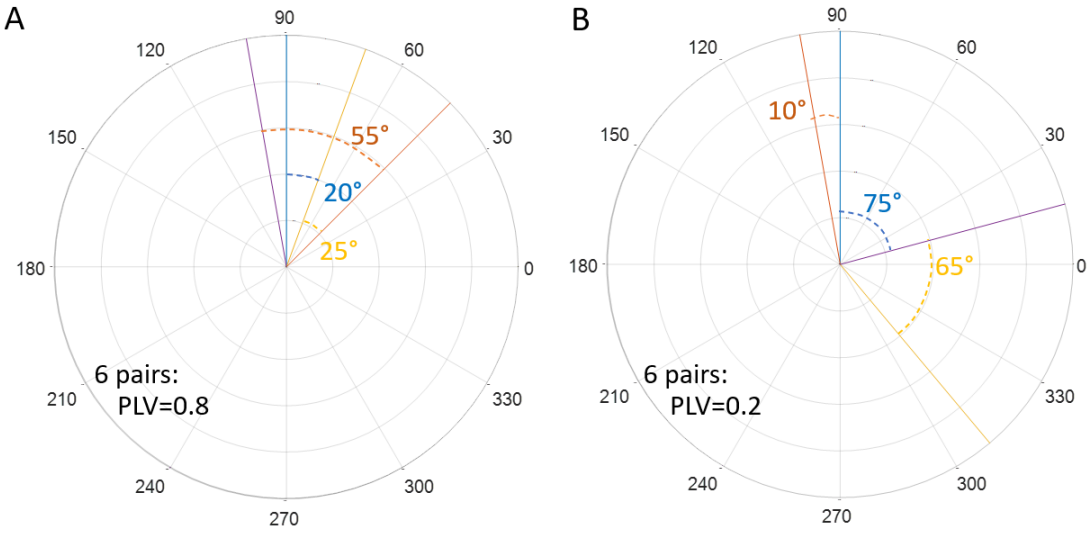


***Figure 2.5. Graphical description of PPC analysis with a high and low synchronised scenario.***

*Every solid line on the polar plot represents a phase lag difference between two filtered signals at a single time point. All observations are paired and the angular distances between these pairs are calculated. Here there are 4 observations and therefore 6 unique pairs, note just 3 angular distances are shown to avoid overcrowding of figure. If phase lags are consistent, angular distances between pairs are small, generating a high cosine value (**A**). The average cosine value across pairs generates the PPC value. If phase lags are not consistent then angular distances become large and cosine values approach zero, resulting in a low PPC value (**B**).*

#### *2.2.3.5 Statistics*

All statistics were completed using R software. Regional differences in each seizure parameter were completed using a one-way ANOVA due to there being more than two groups to compare, e.g. the five brain regions recorded.

To assess PPC data, the values at particular time points (detailed in the relevant results section) were extracted for statistical analysis. PPC data were not normally distributed and therefore a Freidman's test with a post hoc Wilcoxon signed rank test and Bonferroni correction was computed for each channel combination at each frequency range.

Light stimulation experiments were analysed using a linear mixed model which included multiple time points (detailed in results section) and the amplitude change after each stimulation with a random effect of animal. Post hoc tests were completed using the lsmeans function and tukey multiple comparison correction. Including all data allowed comparison across time points for each stimulus in the same model.

### 2.2.4 Analysis of muscimol injections

The test period after drug injection (120min) was split into 30-minute intervals. These intervals were all statistically compared to seizure activity during the 60-minute pre-injection period. The parameters affected by time bin duration, i.e. number of seizures, time spent in seizures and number of non-generalised events where normalised to the bin duration (i.e. halving values collected in pre-drug period).

#### *2.2.4.1 Measured seizure parameters*

As well as those outlined in section 2.2.2, the parameter 'SWC-Failure' was used, which brought together multiple parameters in the following equation:

$$\boldsymbol{SWC-F} = \left( \frac{V1\ delay + V1\ offset\ difference\ + \sum V1\ break}{S1\ seizure\ duration} \right) * 100$$

where,

*V1 delay* is the time between the onset of SWD in S1 and V1, *V1 offset difference* is the time between offset of SWD in S1 and V1,

$\sum V1\ break$ is the sum of all time periods when V1 does not express SWC during ongoing SWD in S1, *S1 seizure duration* is the duration of SWD in S1.

The same equation was used to assess changes in M1 by changing all V1 parameters to measurements made in the M1 channel.

#### *2.2.4.2 Seizure frequency and power*

Power was analysed by extracting a finite sample of 2s at the beginning of the seizure, based on SWD times of V1 to ensure all channels were expressing SWCs during this epoch. Any samples that included a seizure break in either M1 or V1 were removed. The percentage change from the baseline was then calculated to generate a mean percentage change at each interval.

#### *2.2.4.3 Statistics*

The main interest in the microinjection experiment was the effect of muscimol vs aCSF in the two regions, LP and PO. The aCSF injection in both LP and PO was pooled to form the aCSF dataset. This was because of the lack of difference between the two in any parameter, including the key parameters of delay duration and SWC-failure *(Figure 2.6)*. More aCSF injections occurred in PO (n=5) vs LP (n=2). This was because before the decision was made to do two injections per animal, some animals had already been implanted with bilateral cannula targeting only PO.

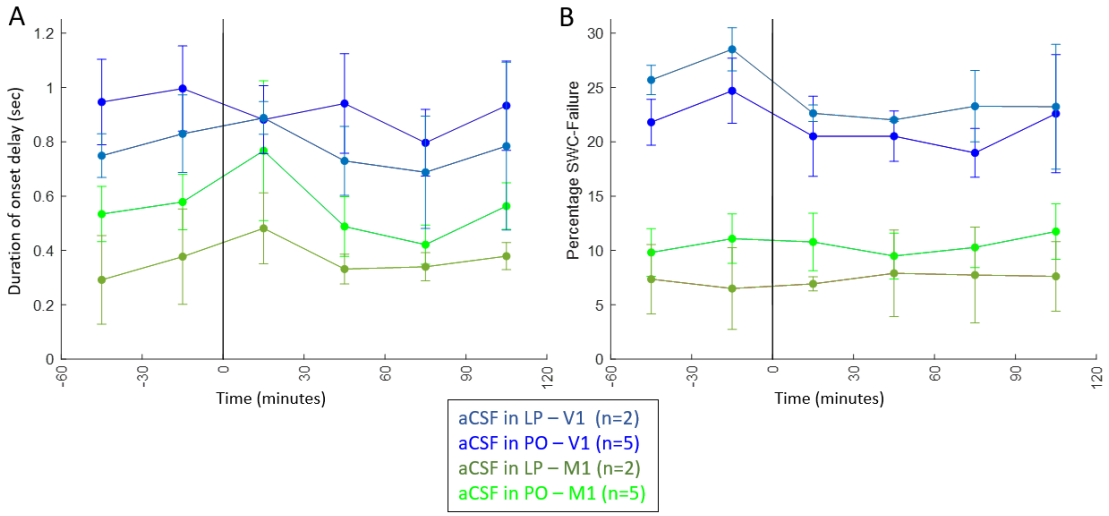


***Figure 2.6. Injections of aCSF in LP or PO had the same effect on SWD.***

*GAERS were injected with aCSF in either LP or PO and the effects were measured in M1 and V1, as in the colour code in figure legend. The effect of muscimol on M1 and V1 SWD onset delay (**A**) and percentage of SWC-Failure (**B**) were the same, therefore these data were pooled to form the control dataset.*

For intra-seizure parameters; duration, delay duration, offset difference, SWC-Failure, break rate and break duration and power, the lmer function, from the lme4 package was used to produce a linear mixed effect model with the formula:

$$Model = dependent\ variable \sim TimeBin * Drug\ Condition * Cortical\ Region + (1|Injection\ order) + (1|Animal)$$

TimeBin and Drug Condition (i.e. aCSF injection vs muscimol in LP vs. muscimol in PO) were the fixed factors of interest. This allowed many effects to be assessed, across and within condition groups within a single model.

Although a fully cross over design of the injection order of muscimol between regions was intended, not all data could be used from all animals. This was due to problems including drug administration on one experiment session or signal issues post injection. Ultimately, this created an imbalance in the number of animals in each injection order group. Therefore, this variance is not implicitly accounted for so linear mixed effect model was the most appropriate.

The experimental design had crossed over random effects, i.e. multiple animals received 2 injections, which is denoted in the formula by ' + (1|x) '. The 1 indicated the random intercept and slope of each variable.

Data for individual seizures were included in the model, rather than an average of each animal at each time point. This greatly improved homoscedasticity of residuals, which were qualitatively checked using residual vs fitted plots, in addition to box plots at different time / condition levels. A gaussian distribution of residuals and linearity of predictor variables were also assessed via histograms of residuals and a plot of residuals vs observed values, respectively, ensuring that assumptions for linear mixed models were met. Interaction effects were tested with a Tukey adjustment of the p values for the multiple comparisons.

The seizure parameters number, time spent in seizure and number of non-generalised events yield one value per animal per time bin, but were analysed the same as above. One animal had an issue with M1 electrode after LP injection and therefore it was removed for the analysis of M1 onset delay, offset difference, M1 SWD-break rate and duration, as well as number of S1-only and S1+M1-only events.

One animal was removed from analysis of seizure number and time spent in seizure due to unusually low number of seizures in first 30 minutes of recording.

## 2.2.5 Analysis of single unit data

### *2.2.5.1 Spike Sorting*

Silicon probes have multiple recording sites that are close together which enables a unit waveform to be detected in multiple channels *(Figure 2.7A)*. The representation of this waveform and the channels it occupies is dependent on many features such as distance and orientation of the neuron relative to the probe recording site. This results in multiple units having a unique pattern of waveforms on distinct channels, enabling them to be sorted.

Kilosort 2 (Pachitariu et al. 2016) was used to sort extracellular spikes. Kilosort2 is an algorithm ran on MATLAB that begins by removing channels that have no spiking activity. A 150Hz high pass filter is then applied and the data then 'whitened', which removed high-frequency correlations between neighboring channels to eliminate noise generated from far away spiking neurons and improve signal to noise ratio of sortable spikes.

A novel step in Kilosort2 compared to other available spike sorting packages is the drift correction which can track a waveform over time even if changes in morphology, which can occur due to electrode or tissue drift. To this end, the data from all channels is broken down into 2s batches and reordered as one signal, such that similar batches with similar signals and waveforms are adjacent. This makes it easier to track changes in waveform due to drift correction. Effectively, this reorders time and often is organized in order of probe location as close by sites will have similar signals.

The data was then analysed in the new order computed in the above step. First, templates of waveforms were made, that can be slightly altered in each step, accounting for variation due to electrode drift. Once all the spikes that fit the template were isolated, the spike at each time stamp is removed from the data *(Figure 2.7B)*. The residual data can then be assessed again and more templates made if necessary until no more spikes are detected to generate a new template. The output of this algorithm was visualised using phy2 package in python. The graphical user interface allowed manual refinement of automatically sorted spike clusters.

#### *2.2.5.2 Waveform extraction*

A high pass 150Hz filter was applied to the best channel of each single unit. The timestamp was located and a 60 sample, +/- 1.5ms was extracted and averaged to create an average waveform of the spike.

#### *2.2.5.3 Width at half amplitude and trough-to-peak of extracellular spikes*

A MATLAB script was formed to mark various points of the average unit waveform; the start, peak and end of the spike and the point of half-amplitude on the descending and ascending phase *(Figure 2.8).* The beginning of the spike was defined when the trace deflects beyond baseline, which was defined as 10% the max amplitude. The peak of the spike is known from the time stamp detected by the spike sorting algorithm. The end of the spike was marked when the trace after the peak switches from moving in a positive direction to a negative direction which detects when the rising phase of the extracellular spike ends.

The sample of the signal that intersects the amplitude between points 1 and 2 is subtracted from the sample of intersection between 2 and 3. This width was converted to real time by dividing the sampling rate. The trough-to-peak time was duration between the peak and the end of the rising phase of a spike. These parameters were used to classify units in Chapter 5, the details of which will be explained in results section 5.3.1.

#### *2.2.5.4 Classification of spikes*

Neuronal firing was classified into total, tonic and burst firing. Total firing was simply all spikes that occur. Tonic firing was defined as spikes that are separated from neighbouring spikes by at least 7ms. A burst was defined as 2 or more spikes with an inter-spike interval of less than 7ms that was preceded by at least 100ms of neuronal silence. Spikes that occurred before and after events of interest, e.g. SWD onset or V1 SWD-onset were extracted and normalised to the event time. The exact peri-event duration varied between events and is detailed in the relevant results section. The firing rate was determined with a 100ms epoch that slides by 10ms. The average firing rate was determined for each cell individually and then an average across cells was calculated for the population average. This was completed using custom made MATLAB code.

#### *2.2.5.5 Burst profile*

Bursts were assessed to aid the classification of cells (5.3.1). To this end, bursts were extracted and separated based on the number of spikes within them. As the burst profile of TC and NRT neurons have already being characterised (1.3.2), this is a useful tool for future neuronal classification. The burst properties are represented graphically when their inter-spike-interval is plotted against the intra-burst spike number *(Figure 2.9),* which reveals a decelerando and accelerando-decelerando pattern, for TC and NRT neurons, respectively.

#### *2.2.5.6 Auto and cross-correlation analysis*

Spike times were converted into binary spike trains where each bin represented 1ms and a 1 represented a spike. Autocorrelation and cross correlations were then computed with the *crosscoeff* function of MATLAB. Autocorrelations were checked for all units and cross-correlograms were computed for all simultaneously recorded units.

#### *2.2.5.7 SWC-spike triggered unit spike average*

The relation of unit firing to the ongoing SWC-spikes in S1 and V1 was assessed. SWC-spikes were extracted in spike2 software by an amplitude threshold and minimum step of 0.07s. Unit spikes were first classified into tonic, burst or total firing. Then all unit spikes surrounding each SWC were extracted and time differences between the two were calculated and converted to a histogram. Only the first spike (i.e. the spike closest to zero) in each firing type was considered to understand when PO neurons were first or last activated following or preceding the SWC-spike, respectively.

#### *2.2.5.8 Events per SWC*

First, all spikes were classified into total, tonic and burst spikes. Then, the number and type of events between every SWC was assessed. This gave a measure of percentage of SWCs that contained bursts, tonic spikes or no activity. This was done for the first ictal second and then the whole ictal period.

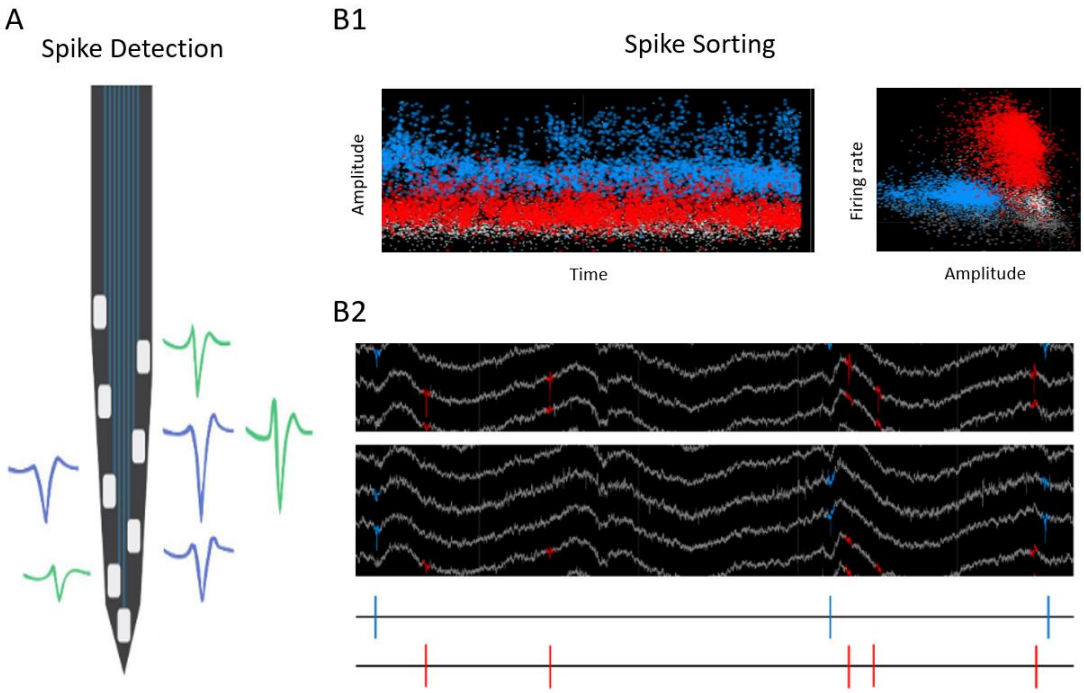


***Figure 2.7. Example of LFP traces with spikes of two different units***

*An action potential from multiple units can be detected on a selection of channels, combined to form a unique waveform representation of a cell (**A**). All spikes that fit a specific waveform template were grouped into clusters. Different clusters can be viewed in space by plotting particular features of each spike, for e.g. amplitude and firing rate, as the two units shown in **B1**. Raw LFP traces show many spikes in two clusters, highlighted in red and blue (**B2**). A vector of time stamps for each cell was then extracted for input into analysis of neural dynamics (**B2**, lower panel).*

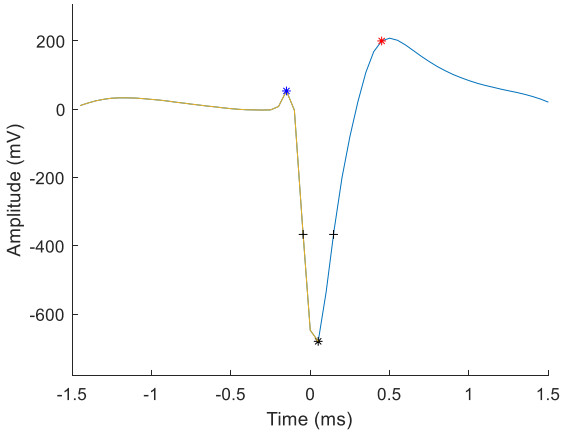


***Figure 2.8. Example of waveform and identified points to calculate width at half-amplitude and trough-to-peak time.***

*Various points of the spike waveform were extracted, i.e. the start, peak and end of the spike (asterisks). The half amplitude of the ascending and descending phase was then extracted (crosses). The width at half-amplitude was the distance between those two crosses and the trough-to-peak time was the end of the spike (red asterisk) minus the peak of the spike (black asterisk).*

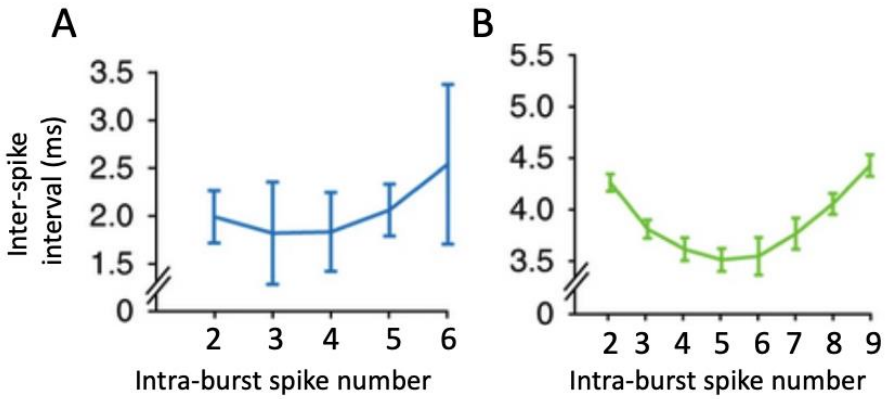


***Figure 2.9. Burst profile of thalamic neurons***

*The burst profile of TC (**A**) and NRT (**B**) neurons, showing the characteristic decelerando and accelerando-decelerando pattern, respectively [Taken from (McCafferty et al. 2018)]*

#### *2.2.5.9 Firing rate changes and statistics*

The total tonic and burst firing rates were aligned to a time point of interest, i.e. SWD onset or offset, V1 SWD-break onset or onset of S1-only and S1+M1-only SWD. Firing rates were plotted using MATLAB and the *shadedErrorBar* function (Rob Campell, Github: raacampbell). The rate at particular time points was extracted (detailed in relevant results section) for statistical analysis. Unless stated otherwise, a repeated measures ANOVA was completed on each firing type separately using *anova* function in R. A pairwise post-hoc comparison Tukey test was completed to explore differences within groups, across time, and between unit groups at different time points. This was completed after the assumptions of normality and homoscedasticity were confirmed. If the assumptions were violated, which was the case in some analysis of burst firing, the data was transformed to its log to remedy the violation.

# Chapter 3: Novel features of SWD in the cortex and higher-order thalamic nuclei

## 3.1 Introduction

The spread of SWD from S1 to other cortical areas was measured with electrodes placed on the dura in WAG/Rjj rats (Meeren et al. 2002). Delays on the millisecond scale were observed, with an average of 10ms from the upper lip region of S1 to M1 (distance: 6.3mm). The observed signal speed (average: 1.4 m/s) equals that of intra-cortical propagation (Castro-Alamancos and Connors 1996), and thus this process was concluded to underlie SWD propagation (Meeren et al. 2002).

However, similar experiments completed in the GAERS model (Polack et al., 2007) using electrodes in deep layers of S1 and M1, showed delays of around 1s. This demonstrated a potential time-window for TC interactions and trans-thalamic communication to occur. Such TC interactions were identified by Lüttjohann and van Luijtelaar (2012), who showed increased cortical-PO bidirectional interactions from 1.25s prior to the initiation of AS, as measured by electrodes in each area.

By building on this knowledge, this chapter aims to answer the following questions:

1. what are the delays from S1 to distal cortical areas, for example, V1?
2. can LFP amplitude and phase information reveal HO thalamo-cortical relationships?

## 3.2 Methods

The methods used in this chapter are detailed in section 2.1.3. Briefly, LFP were obtained from electrodes positioned in S1, M1, V1, LP and PO of freely moving GAERS to explore various parameters of SWD including amplitude-correlations and phase-coherence during ictal-interictal transitions.

### 3.2.1 Histology

The histology protocol is detailed in section 2.1.4.3. Briefly, electrolytic lesions at electrode locations were visualised using DAPI *(Figure 3.1).* One animal was removed from data analysis because the LP and PO electrode location could not be confirmed.

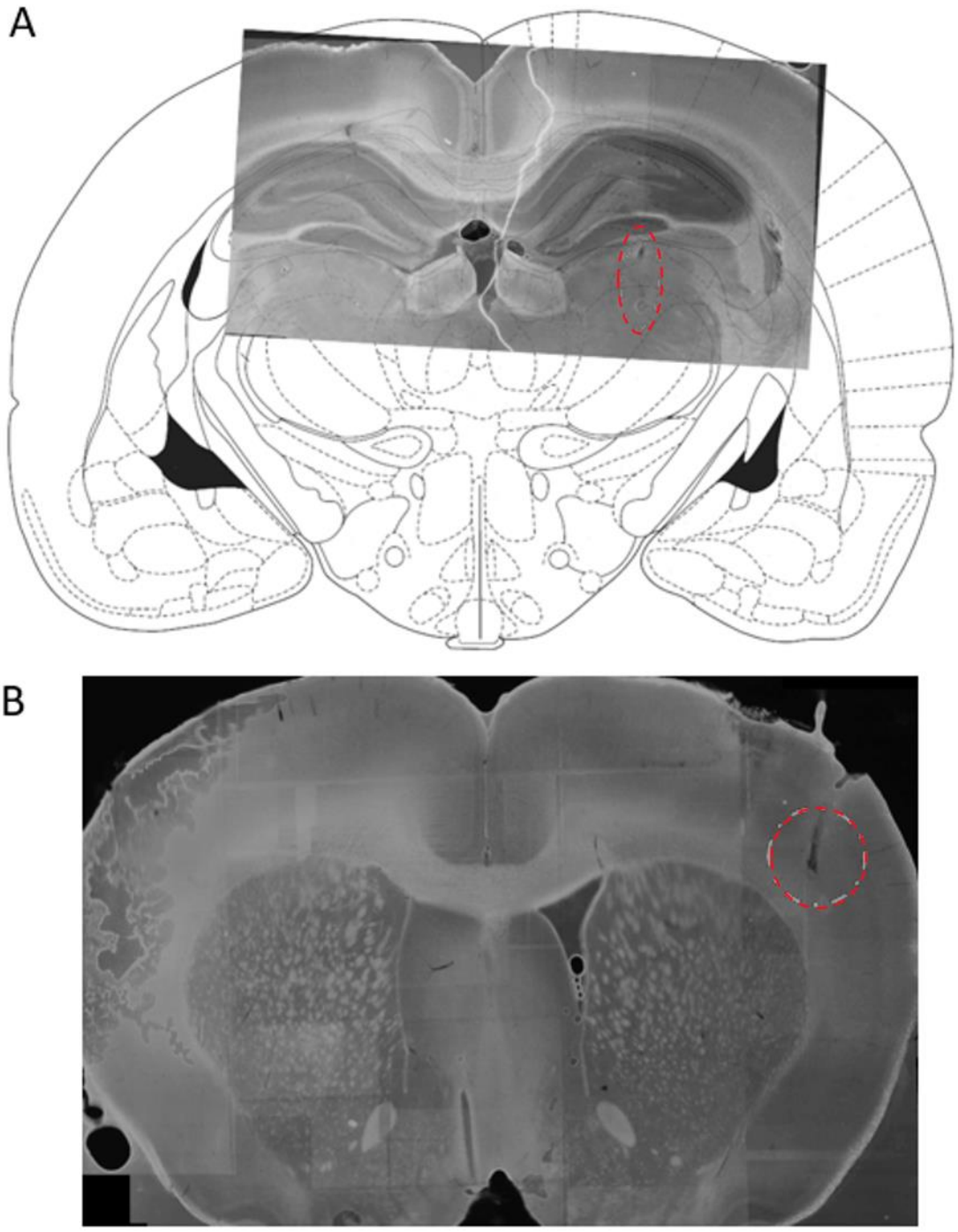


***Figure 3.1. Histology of lesion in LP, PO and S1.***

*Example brain sections showing location of LP and PO electrodes (**A**) and S1 electrode (**B**) where red dashed circles highlight lesion location. The brain section in **A** is overlaid on stereotactic map from Paxinos and Watson (1998) since the entire brain section could not be retrieved because of technical issues with microscope.*

## 3.3 Results

### 3.3.1 General parameters of SWD

In 7 GAERS, an average of 30 ±4 SWD were analysed (total=209), following criteria outlined in section 2.2.3. SWD had an average duration of 25.3 ±3.1s and an average frequency of 7.2 ±0.3 Hz. These features are similar to those previously observed, from multiple groups (Depaulis et al. 2016; McCafferty et al. 2018)

### 3.3.2 Different delays of SWD onset in various brain regions

SWD began in S1, before spreading to other cortical and thalamic regions. This is a well-known phenomenon of AS (Meeren et al. 2002; Polack et al. 2007) and could be observed on both the raw traces and the corresponding increase in power at 7 Hz (and harmonics) in spectrograms *(Figure 3.2).* The time of SWD onset, defined as the first detectable SWC-spike in each area (which was over a threshold of at least 2 times the amplitude of background wake activity) was significantly different between the recorded brain regions (F=97.9, Probability (Pr) (>F) <0.0001) (*Figure 3.2 and Figure 3.3).* V1 had a significantly longer onset delay than all other channels (V1: 0.9 ±0.1sec vs. M1: 0.4 ±0.05sec, p<0.0001; or LP: 0.5 ±0.08sec, p= <0.0001; or PO: 0.5± 0.08 p<0.0001).

### 3.3.3 Brief SWD occur that do not generalise

SWD were observed that occurred only in S1 (hereafter referred to as S1-only SWD), in S1 and M1 (S1+M1-only SWD) (Figure 3.4*)*, whereas no similar events occurred in S1 and V1 only, or in S1 and thalamus only. Every hour, 2.4 ±0.8 S1-only (total:18) and 1.2 ±0.5 S1+M1-only SWD (total:9) occurred, these rates were not significantly different to each other *(Figure 3.5A).* S1-only SWD were 1.0 ±0.04s in duration. In S1+M1-only SWD, S1 expressed SWD for 1.2 ±0.4s whereas the M1 component was significantly shorter (0.5 ±0.08s, p=0.003) (*Figure 3.5B)*.

### 3.3.4 SWC-spikes consistently lagged behind S1

The times of SWCs were extracted from all recorded channels of 5 GAERS and relative to S1, SWC-spike lags were measured *(Figure 3.6)*. There was a significant effect of channel combination on the SWC-spike delay (F=12.8, Pr(F) < 0.001) and all recorded channels lagged the S1, with M1 having the smallest delay (3.9 ±1.4s), followed by LP (4.3 ±1.8s), PO (8.7 ±2.1s) and V1 (12.2 ±2.0s). The V1 delay was significantly longer than M1 (p=0.002) and LP (p=0.003*) (Figure 3.6B).*

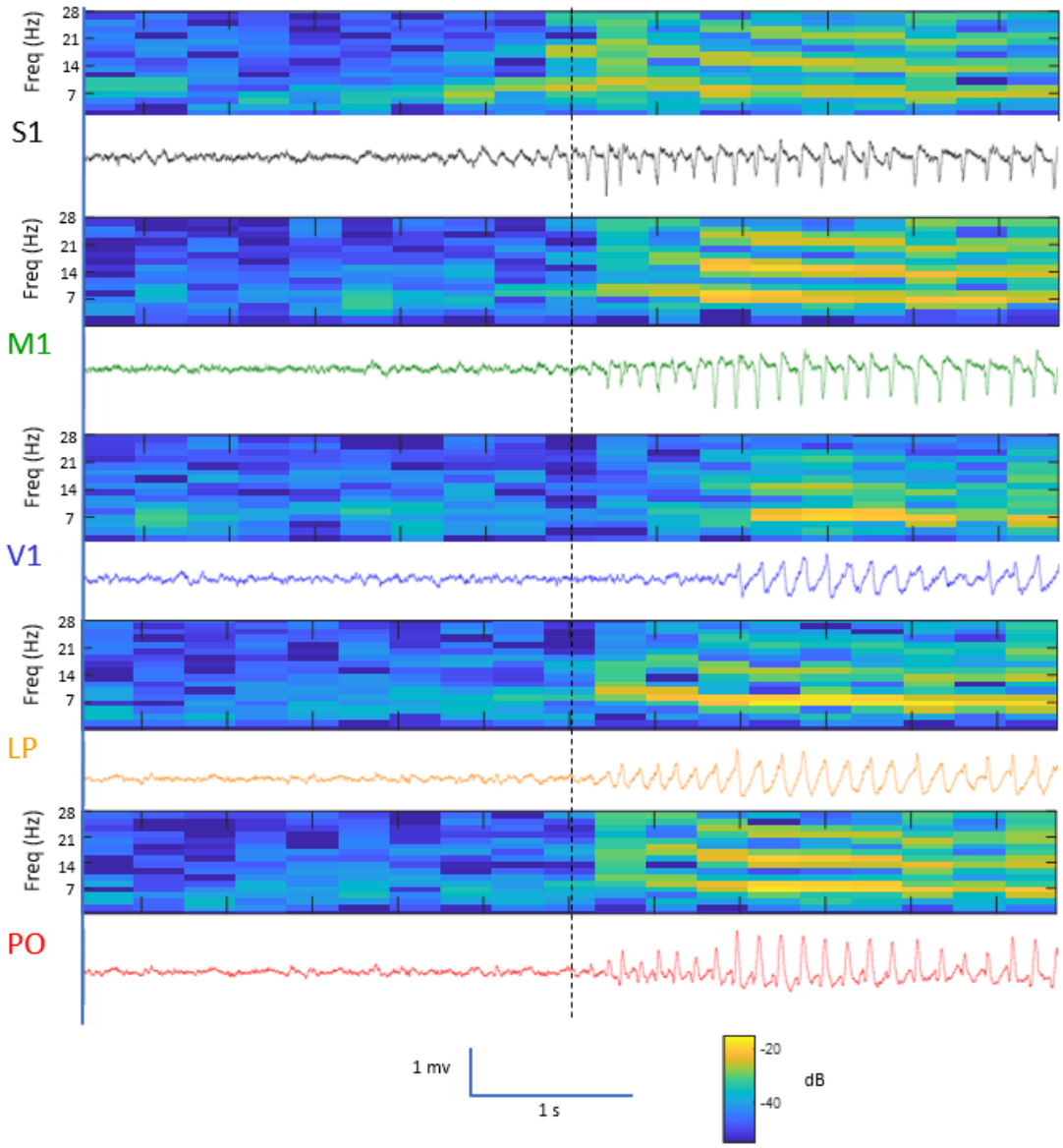


***Figure 3.2. Spectrogram and raw traces of SWD in different brain areas.***

*Spectrograms (calculated in 600ms bins) and raw traces are shown for S1, M1, V1, LP and PO. Spectrograms demonstrate the increase in power of 6-9 Hz activity and its harmonics in all locations, at the time of SWD onset in S1, as denoted by the vertical dashed black line.*

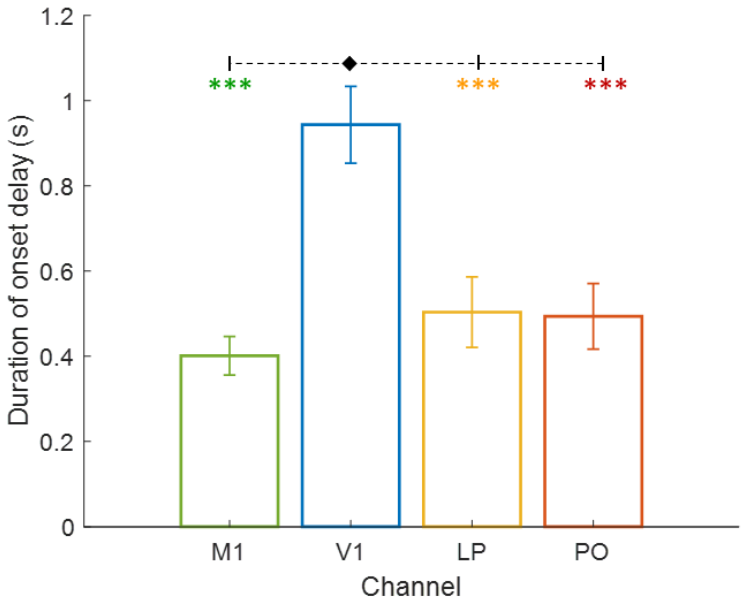


***Figure 3.3. Onset delay was different between recorded brain regions.***

*Onset delay, as defined by the time difference from the onset of SWD in S1, was assessed in M1, V1, LP and PO. Significance is shown with respect to V1 channel as denoted with a diamond. *** p <0.001*

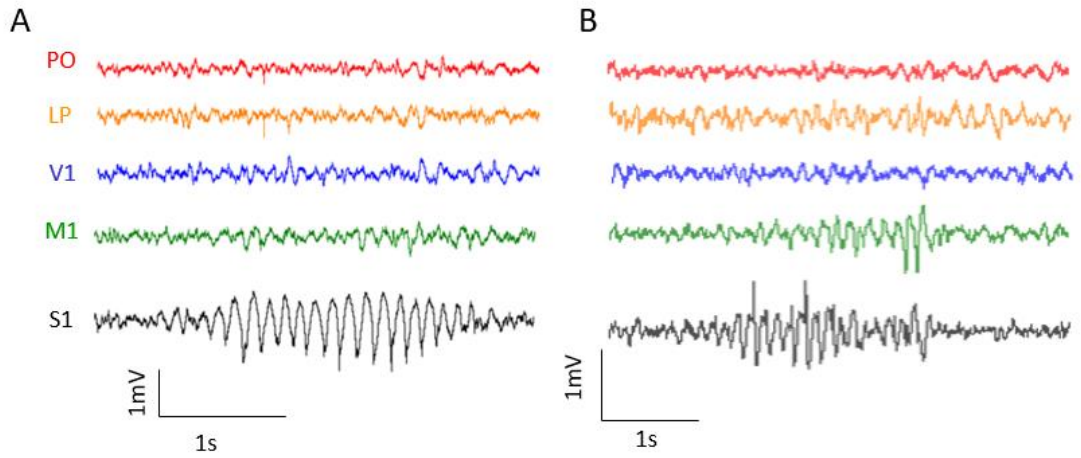


***Figure 3.4. S1-only and S1+M1 only events.***

*LFP activity in S1, M1, V1, LP and PO with a typical example of a S1-only SWD (**A**) and S1+M1-only SWD (**B**).*

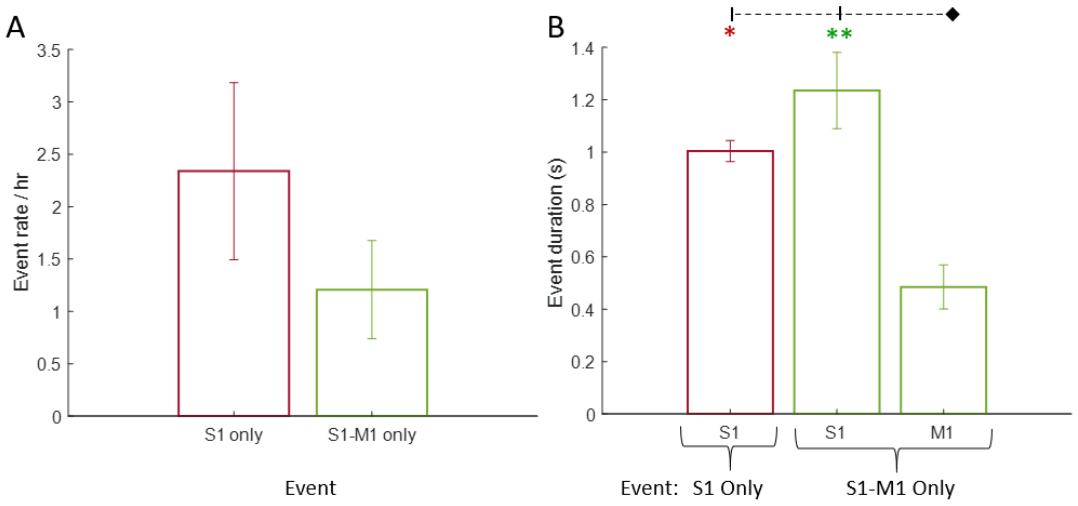


***Figure 3.5. Quantification of non-generalised events.***

*The plots show the occurrence (**A**) and the duration (**B**) of S1-only and S1+M1-only SWD. Statistical significance is indicated with respect to M1 (marked by a diamond). *p <0.05, **p< 0.01.*

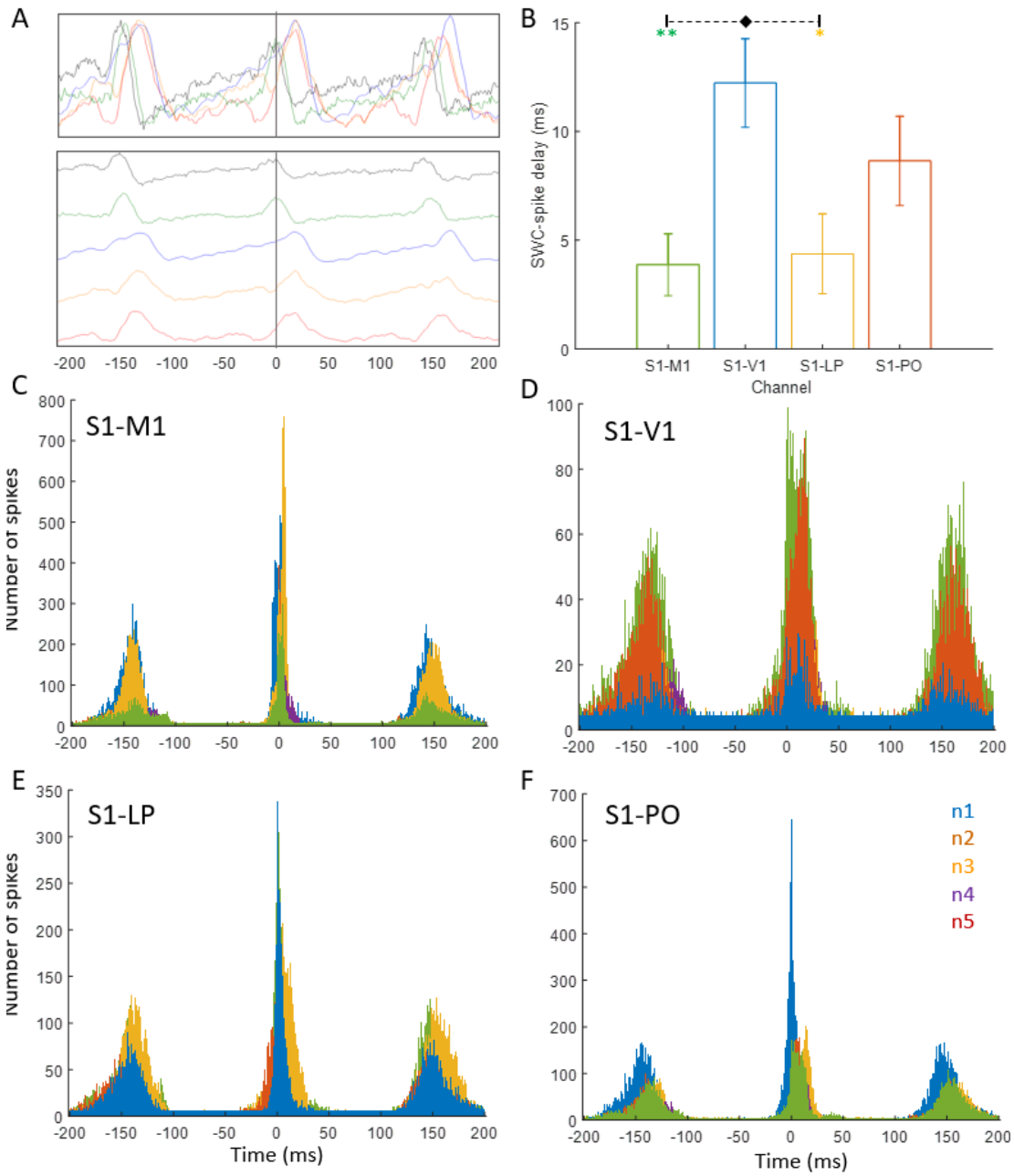


***Figure 3.6. SWC-spike lags from S1 to other recorded channels.***

*The plots show a raw trace (**A**) of S1 (black), M1 (green), V1 (blue), LP (yellow) and PO (orange) centred at the peak of a SWC-spike in S1 (black line), either overlaid (top panel) or in parallel (bottom panel). SWC-lags were quantified relative to S1 (**B**), according to SWC-spike triggered time histograms (**C-F**), where each colour represents a different animal.*

### 3.3.5 V1 and M1 did not continually express SWCs during S1 SWD

The duration of AS was defined by continuous presence SWD in S1 and the lack of locomotion as S1 is the initiation site. Multi-site LFP recordings revealed instances of brief interruptions in SWD (hereafter referred to as SWD-breaks) in M1, V1, LP and PO, but never in S1 *(Figure 3.7)*, as disruption in S1 would signify the end of the SWD rather than a SWD-break. The rate at which the SWD-breaks occurred (measured as the number of SWD-breaks per ictal second) was significantly higher in V1 (0.05 ±0.07 Hz) than in M1 (0.004 ±0.002 Hz, p=0.002). SWD-break rate was more varied in thalamic than cortical channels (LP: 0.03 ±0.01 Hz, PO: 0.02 ±0.01 Hz) *(Figure 3.8A).* The duration of SWD-breaks was the same in all recorded channels (M1: 0.8 ±0.04s, V1: 0.8 ±0.03s, LP: 0.9 ±0.07s, PO: 0.8 ±0.03s) (*Figure 3.8B).*

V1 SWD-breaks occurred after a drop in amplitude in V1, and the amplitude fluctuations observed in V1 was correlated to the amplitude changes in LP and PO *(Figure 3.9A).* This relationship was observed in the raw traces and was more noticeable when signals were squared, which ensured changes in the negative scale were considered *(Figure 3.9B).* This was confirmed numerically by cross-correlating the ictal amplitude envelopes of squared signals *(Figure 3.10).* The correlation coefficient for V1-LP (0.5 ±0.03) and V1-PO (0.6 ±0.03) was significantly higher than any other HO-cortical combination or cortico-cortical combination ($p<0.001$) (*Figure 3.10)*. There was no significant difference between V1-LP and V1-PO. LP-PO showed significantly higher correlation than any other channel combination (0.7 ±0.04, $p<0.001$) which demonstrates how activity in LP and PO is relatively similar, even under normal conditions.

The coherence between channels, as measured by their Pairwise Phase Consistency (PPC) (n=6), was completed to identify changes at times of V1 SWD-breaks. Only V1-SWD-breaks were analysed because M1 SWD-breaks were relatively few, and additionally, due to the aforementioned high amplitude correlation of V1 with LP and PO, the breaks in LP and PO coincided with that of V1, so it would be redundant to analyse these breaks separately. Clear PPC changes were only observed in the 6-9Hz frequency band and harmonics of 7Hz *(Figure 3.11).* At 6-9Hz, M1-V1, PO-M1 and S1-V1 had a significant decrease of PPC at -0.375s, followed by a decrease at -0.25s in PO-V1, and finally, from -0.125s LP-PO also had a significant reduction in PPC *(Figure 3.11B).*

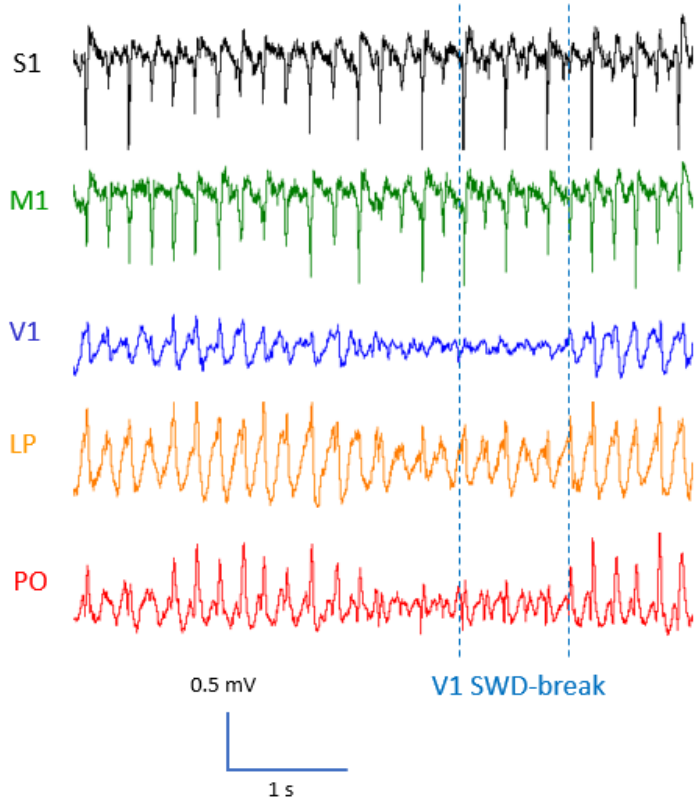


***Figure 3.7 SWD-break in V1.***

*Ictal activity in S1, M1, V1, LP and PO with a typical example of a SWD-break in V1 that is highlighted by the blue dashed lines.*

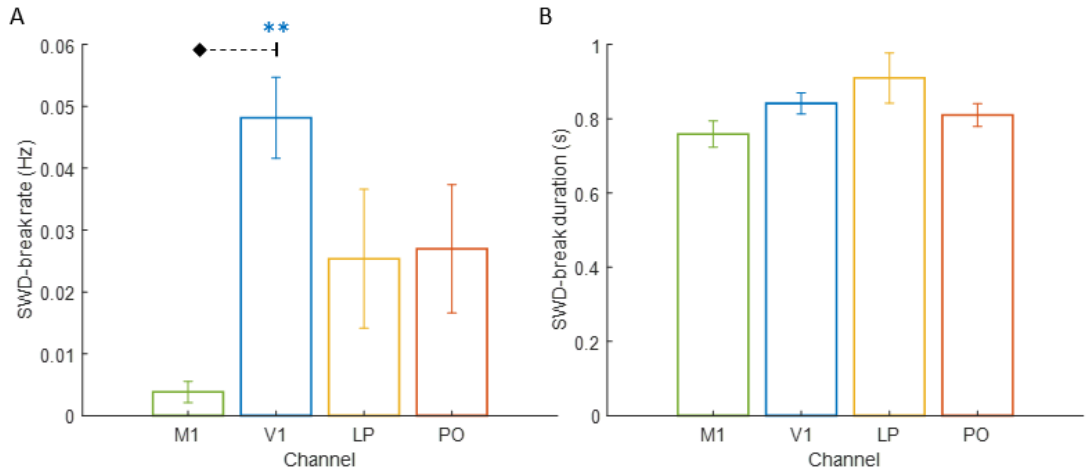


***Figure 3.8 Quantification of SWD-breaks across brain regions***

*The plots show the rate of SWD-breaks (**A**) and their duration (**B**) in M1, V1, LP and PO. Diamond head indicates root comparison of statistics. ** p < 0.001.*

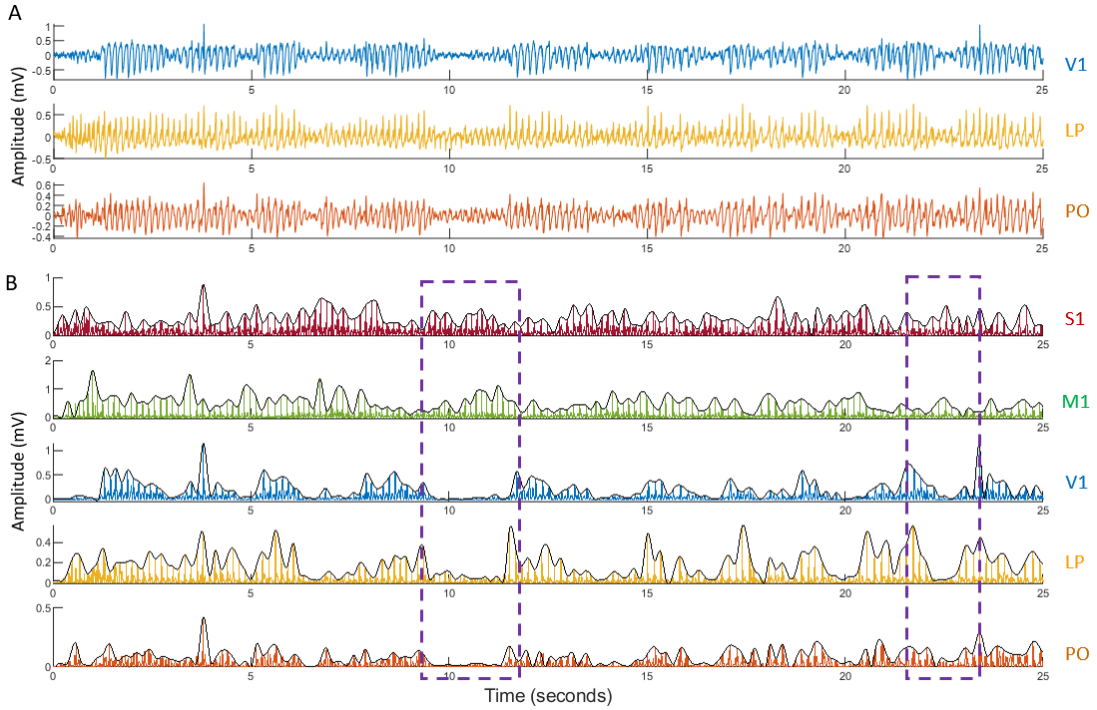


***Figure 3.9. Correlations of amplitude during ictal periods across recorded channels.***

*Example raw trace of V1, LP and PO (**A**) showing amplitude changes within a seizure. The signals were squared to ensure that fluctuations in the negative values were considered, before an amplitude envelope (thin black line) was fitted, as shown in **B.** Purple boxes highlight two periods where reduction in V1 amplitude was temporally correlated to reductions in amplitude of LP and PO but not S1 and M1.*

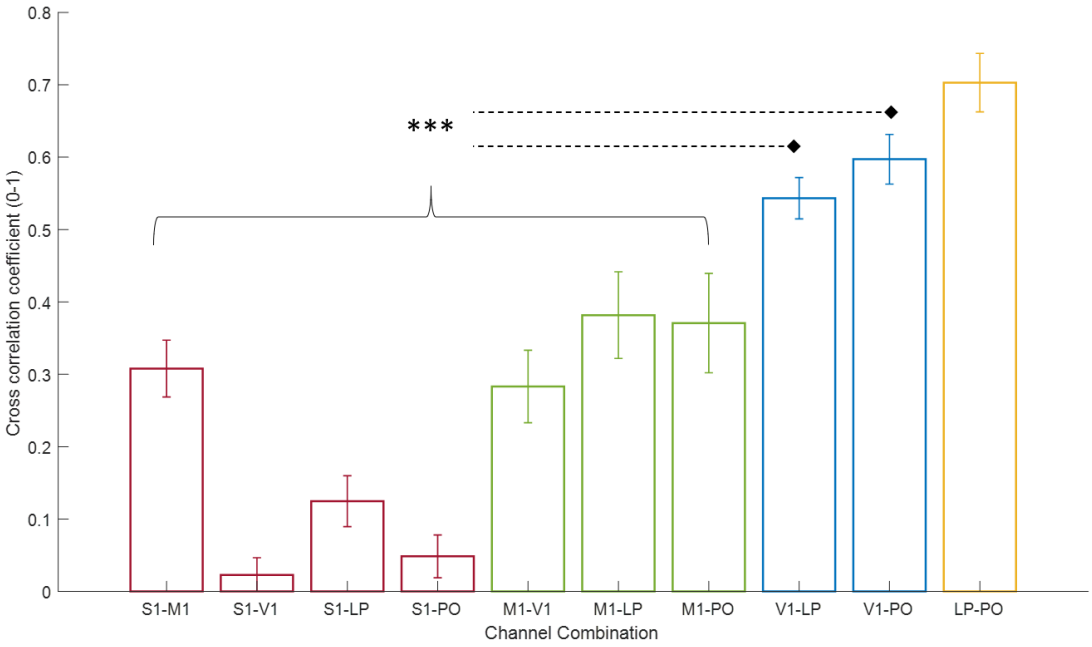


***Figure 3.10. Differences in amplitude correlation between brain regions.***

*Cross-correlations of amplitude envelopes were performed and the cross-correlation coefficient at 0 time lag, where 0 is no correlation and 1 is complete correlation, was compared. V1-LP and V1-PO had significantly higher correlation coefficients compared to all other cortico-cortical and cortico-thalamic combinations. *** $p < 0.0001$.*

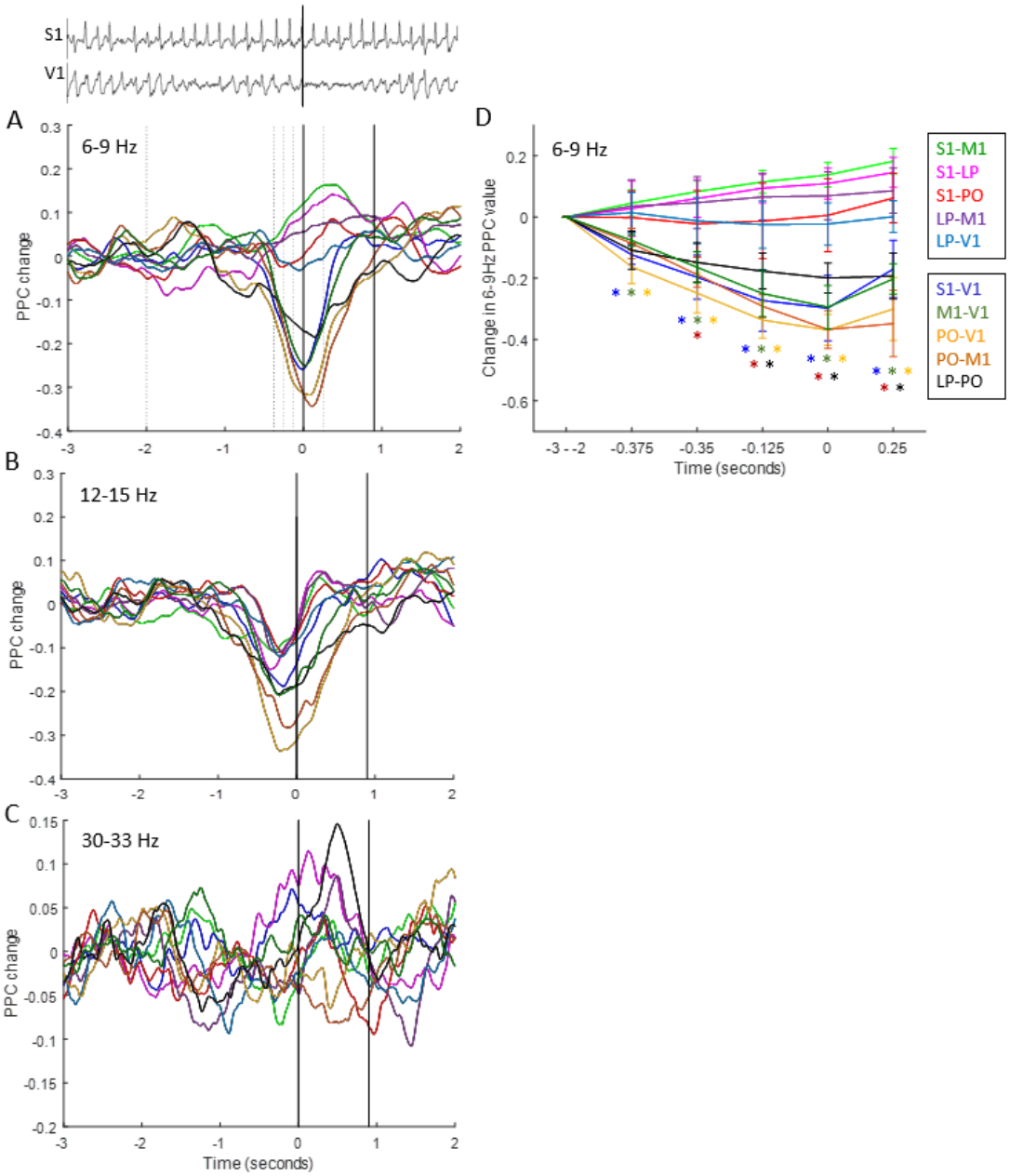


***Figure 3.11. PPC changes at the start of V1 SWD-breaks.***

*PPC analysis at 6-9 Hz (**A**) was performed on all possible channel combinations around V1 SWD-breaks (see example in raw LFP trace in top panel). Values are aligned to V1 SWD-break onset (solid black lines on left and right indicates onset and average duration of the SWD-break, respectively (**A-C**)). Vertical dashed lines in **A** indicate time points used for quantification of PPC changes shown in **D**. (Colour code in **D** applies to all panels). Values are normalised to average PPC in the time period from 3 to 2 sec prior to the start of V1 SWD-breaks. Similar PPC changes were found at 12-15 Hz (**C**), but not in any non-harmonic frequencies (**D**). *p <0.05*

The other channel combinations had no change at 6-9 Hz but showed a slight non-significant decrease in PPC at harmonic frequencies *(Figure 3.11C)*. No clear changes occurred at other frequencies, but fluctuations between -0.1 and 0.1 were usual *(Figure 3.11D)* which reflects normal ongoing variation in phase coherence.

### 3.3.6 SWD-breaks in V1 could be induced by brief light stimulation

During initial recordings, it was noticed that brief light stimulations could induce V1 SWD-breaks during on-going SWD. Therefore, some animals were habituated to, and recorded in the dark (n=4), to ensure that the observed SWD-breaks observed were not solely explained by fluctuations in ambient light of the laboratory where experiments were performed. Although there was a reduction in the rate of occurrence of SWD-breaks in V1 under the dark recording condition (light: 0.04 ±0.008 Hz vs. dark: 0.02 ±0.008 Hz), it was not significant. The duration of the SWD-breaks were the same for each experimental condition (light: 0.8 ±0.03s vs. dark: 0.8 ±0.3s).

To demonstrate the observed effect of light on SWD-breaks, an experiment using phase reversal grating stimuli during SWD was performed on 6 GAERS. Four stimuli were used: a control grey screen (500ms), a control narrow grating screen (0.05°, 500ms) and two test stimuli of wider gratings (10°) at 500 and 1000ms. These light stimulations (n=899 during 542 SWD) reduced the amplitude of ongoing SWD in V1, LP and PO *(Figure 3.12C,D)* but not in S1 and M1 *(Figure 3.12A,B).*

The stimuli were presented when V1 amplitude was at its peak. Since V1 amplitude waxed and waned (Figure 3.9) the periods of high/max amplitude were transient and thus stimuli were presented as soon as V1 SWD amplitude reached a peak. This resulted in an amplitude peak occurring before stimuli presentation in V1, which can be seen in *(Figure 3.12).* This pre-stimulus peak was also observed in LP and PO due to the aforementioned amplitude correlations.

The three grating stimuli (n=681) were compared to the control grey screen stimulus (n=218) at 6 time points *(Figure 3.13A,B)*. V1 SWD amplitude was significantly affected by the grating light stimuli ($F = 18.7$, $Pr(>F) = <0.0001$). At 0.5s there was a significantly smaller amplitude after a narrow grating stimulus (0.13 ± 0.019, $p<0.0001$), and both wide gratings (0.1 ±0.02, $p<0.001$ and 0.1± 0.02, $p<0.001$) compared to control (0.2 ±0.03), which was maintained at 0.75s. The 1000ms, wide

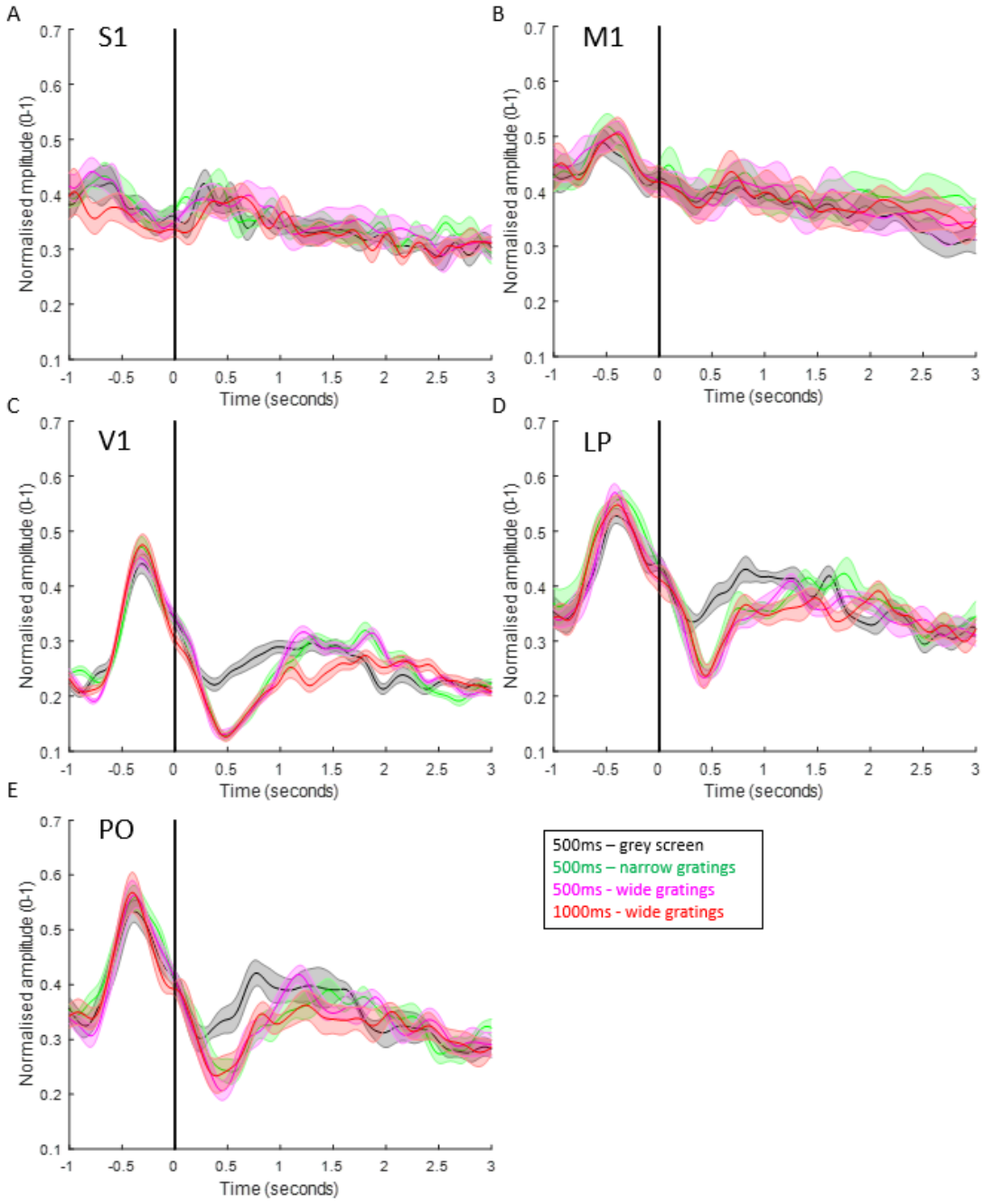


***Figure 3.12. Average amplitude envelopes before and after a brief, light stimulus.***

*The average amplitude envelope decreases in V1 (**C**), LP (**D**) and PO (**E**), but not in S1 (**A**) and M1 (**B**), after 4 brief light stimuli. Stimuli: control grey screen (500ms), control narrow grating screen (500ms) and two test stimuli of wide gratings at 500 and 1000ms. Time 0 indicates the onset of light stimulation.*

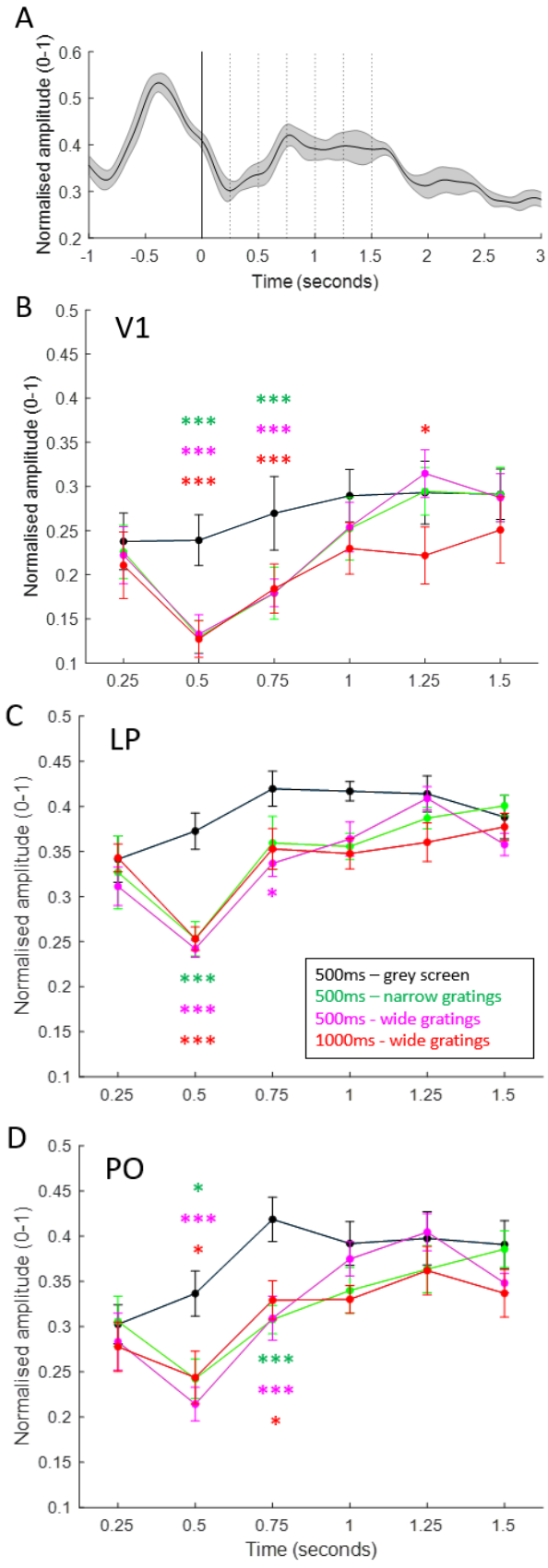


***Figure 3.13. Quantification of SWD amplitude changes in V1, LP and PO after visual stimuli of different gratings.***

*Example of amplitude envelope (**A**), black vertical dashed lines represent the 6 time points extracted for analysis of amplitude changes in V1 (**B**), LP (**C**) and PO (**D**). Colour of '*' indicate which stimuli (onset at time 0) is significantly different to the grey screen stimulus, * p < 0.05, ** < 0.01, *** p< 0.0001.*

grating stimuli resulted in a significantly reduced amplitude also at 1.25s after stimulus presentation (0.3 ±0.04, p=0.01) compared to control (0.3 ±0.03). These results show that various visual stimuli are effective at transiently desynchronising V1, LP and PO activity during SWD without causing termination.

Stimuli also affected SWD amplitude in LP (F = 22.5 Pr(>F) <0.0001) and PO (F=11.9 Pr(F) < 0.0001) (*Figure 3.13C,D)*. The narrow grating stimulus generated a significant reduction in SWD amplitude in LP (Ctrl: 0.4 ±0.02 vs. 0.3 ±0.2, p<0.001) and PO (Ctrl: 0.3 ±0.02 vs. 0.2 ±0.2, p=0.02). The two wide gratings caused a similar reduction in LP (0.2 ±0.009, p<0.0001 and 0.3 ±0.01 p=0.0001) and PO (0.2 ±0.02, p<0.0001 and 0.2 ±0.03 p=0.03), when measured 0.5s after presentation.

At 0.75s after presentation in PO the narrow, wide, and long duration wide grating stimuli had a significant reduction in amplitude (Ctrl: 0.4 ±0.02 vs. 0.3 ±0.01, p<0.0001; 0.3 ±0.02, p=0.0004; and 0.3 ±0.02, p=0.03, respectively). At 0.75s after stimuli presentation in LP, only the 500ms wide grating stimuli had a significant reduction in SWD amplitude compared to control (Ctrl: 0.4 ±0.02 vs 0.3±0.02, p=0.03).

### 3.3.7 Thalamo-cortical phase coherence increased before generalisation

To explore changes in LFP phase coherence at interictal to ictal transitions, and vice-versa, PPC was performed between all channel combinations in the frequency ranges of 1-42 Hz and 75-95 Hz. Most channel combinations had a low interictal PPC values *(Figure 3.15A)* of <0.15, M1-S1 was slightly higher at 0.2 ± 0.05 and LP-PO was significantly higher than M1-S1, with interictal PPC values of 0.5±0.05, p=0.007. In order to make appropriate comparisons between the channel combinations, PPC changes were taken such that each channel was normalised to its own inter-ictal period. Eight time points of interest were chosen to investigate PPC changes around the onset time:

0. Baseline (average between -5 and -3s)
1. 0.5s before SWD onset in S1
2. 0.125s before SWD onset in S1
3. 0s, time of SWD onset in S1
4. 0.5s after S1 SWD onset (the average time at which SWD reached M1 and HO areas)

5. 0.75s after S1 SWD onset
6. 1s after SWD onset (the average time at which SWD reached V1)
7. 2.5s after S1 SWD onset (when SWD are fully established)

At 1-3 Hz no clear changes were observed whereas at 3-6 Hz there was an increase in PPC 1-1.5s after seizure onset, however, none of these changes were statistically significant after Bonferroni correction *(Figure 3.14).* At 6-9 Hz, the main SWD frequency, there was a clear dichotomy in the temporal profile of PPC *(Figure 3.15A,B).* S1-M1, S1-LP, S1-PO, LP-M1 and LP-V1 channel combinations all had a significant increase in PPC from -0.125 sec prior to SWD onset (p=0.02), whereas S1-V1, M1-V1, PO-V1, PO-M1 and LP-PO showed a significant rise in PPC values from 0.75s after SWD onset (p=0.02) (*Figure 3.15C).* The presence of these two groups was maintained when PPC values were aligned to V1 SWD onset *(Figure 3.15A)*.

Many channel combinations expressed a transient increase in PPC activity at 9-12 Hz *(Figure 3.16).* In S1-PO, S1-LP, LP-M1 and LP-V1, this begun at -0.125s before SWD onset. For cortico-cortical connections, this occurred later, at 0.5s after SWD onset. PO-M1 and PO-V1 also increased at 0.5s after SWD onset, however this was sustained. Finally, no significant change in LP-PO connectivity was observed.

LP-PO coherence dropped in many frequency ranges at the time of SWD onset *(Figure 3.17A).* At 18-21 Hz there was a small, but significant transient decrease at time of onset (p=0.02) (*Figure 3.17B),* whereas at higher frequency bands (27-42Hz), the negative change was stronger and sustained *(Figure 3.17B)*. At the gamma frequency range of 75-90 Hz, there was a small but significant reduction in LP-PO from 0s *(Figure 3.17C)*. No other channel expressed a negative PPC change at SWD onset or changes in the gamma frequency band.

SWD harmonics did not replicate the grouping observed at 6-9 Hz: instead, all channels increased at the approximately the same time *(Figure 3.18)*. At 18-21 Hz, this was from 0.5s from SWD onset in all channels (p=0.02). However, at 12-15 and 21-25 Hz, increases in PPC were only observed after 1s or 2.5s, that is after SWD were already established in S1. Non-harmonic frequency ranges between 15 Hz and 42 Hz showed similar patterns *(Figure 3.18D).* In general, at increasingly higher frequency ranges the changes in PPC became smaller.

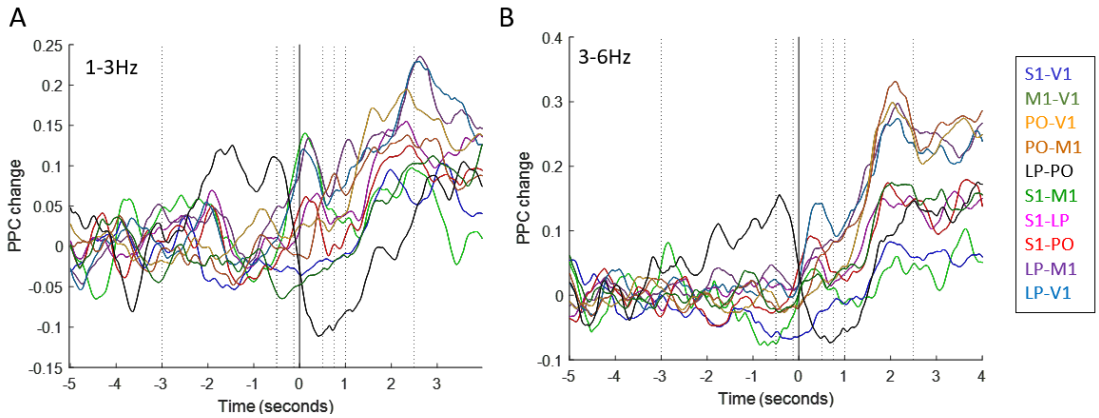


***Figure 3.14. PPC changes at SWD onset at 1-6Hz.***

*Plots show the PPC changes at 1-3Hz (**A**) and 3-6Hz (**B**) at time of SWD onset in S1 (vertical solid line). Vertical dashed lines show time points extracted for statistical analysis, but there were no significant differences compared to baseline (-5 to -3s prior to SWD onset).*

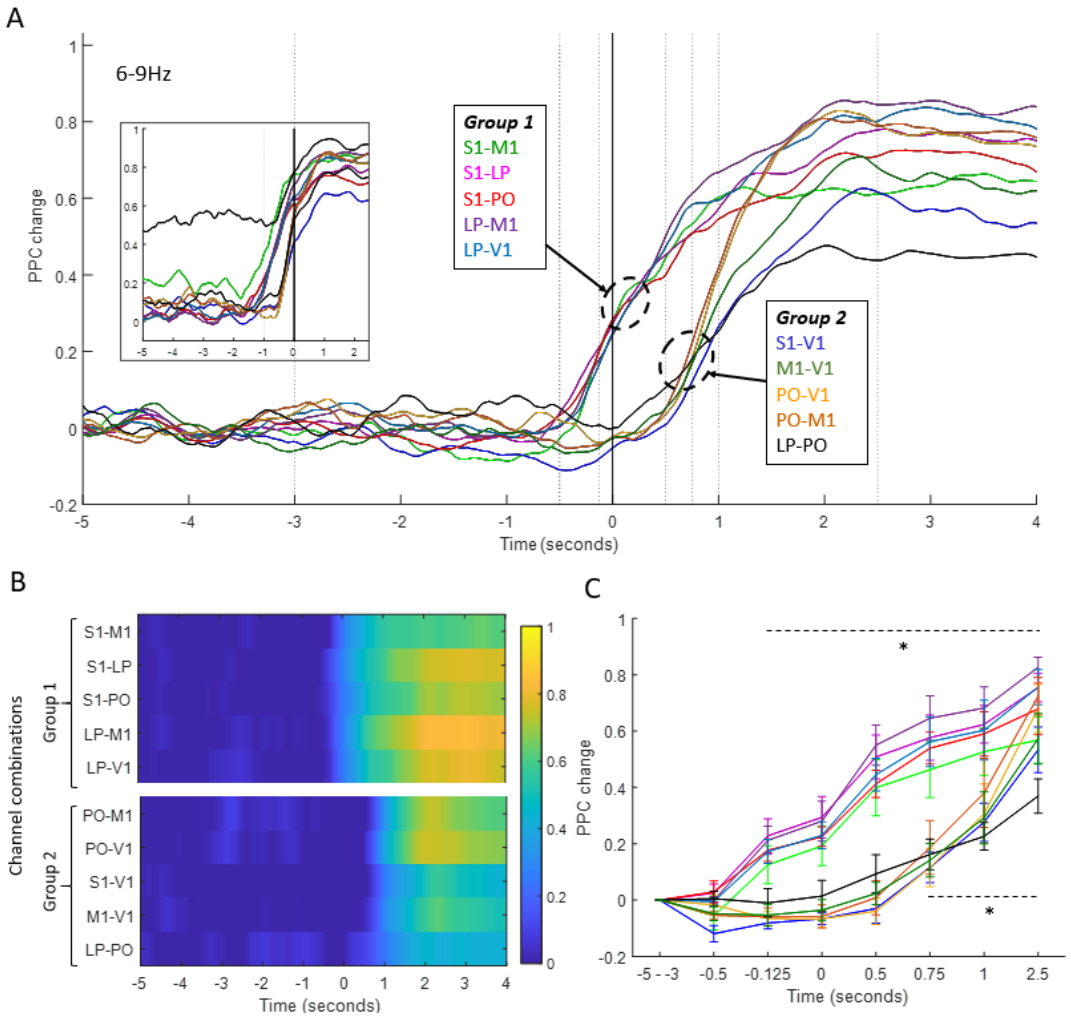


***Figure 3.15. PPC changes in 6-9 Hz at SWD onset.***

*PPC changes at SWD onset (**A**) (vertical solid line) shows the existence of two clearly defined groups. Insert in **A** shows raw PPC values that are aligned to V1 SWD onset (time=0). All time points used of the analysis shown in **C** are denoted by vertical black dotted and solid lines. Same data in **A** are expressed as colour plot (**B**) and quantitative analysis of PPC (**C**) shows the different times at which Group 1 and 2 reached statistical significance. Dashed line in (**C**) indicates all time points with a significant increase in PPC for group 1 (top) and group 2 (bottom) relative to baseline, * p <0.05.*

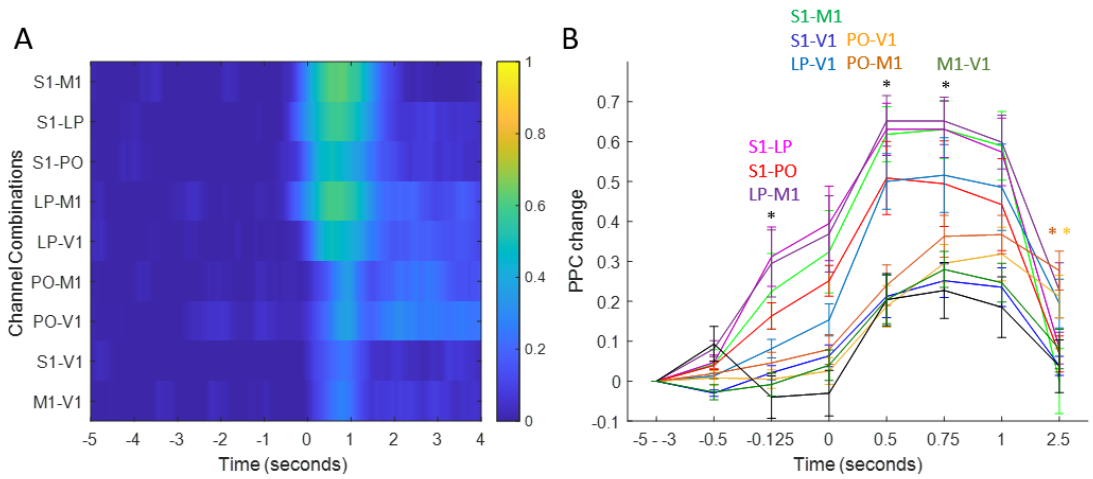


***Figure 3.16. PPC changes at 9-12 Hz.***

*Colour map of PPC changes for all channel combinations at 9-12Hz (**A**) and their quantification (**B**). * show time points when PPC first showed significant increases in the illustrated channels. All channels remained significant at 1sec, and only PO-V1 and PO-M1 reamined significant at 2.5s, as shown by an additional asterisk. No changes were observed in LP-PO (black line). * $p < 0.05$.*

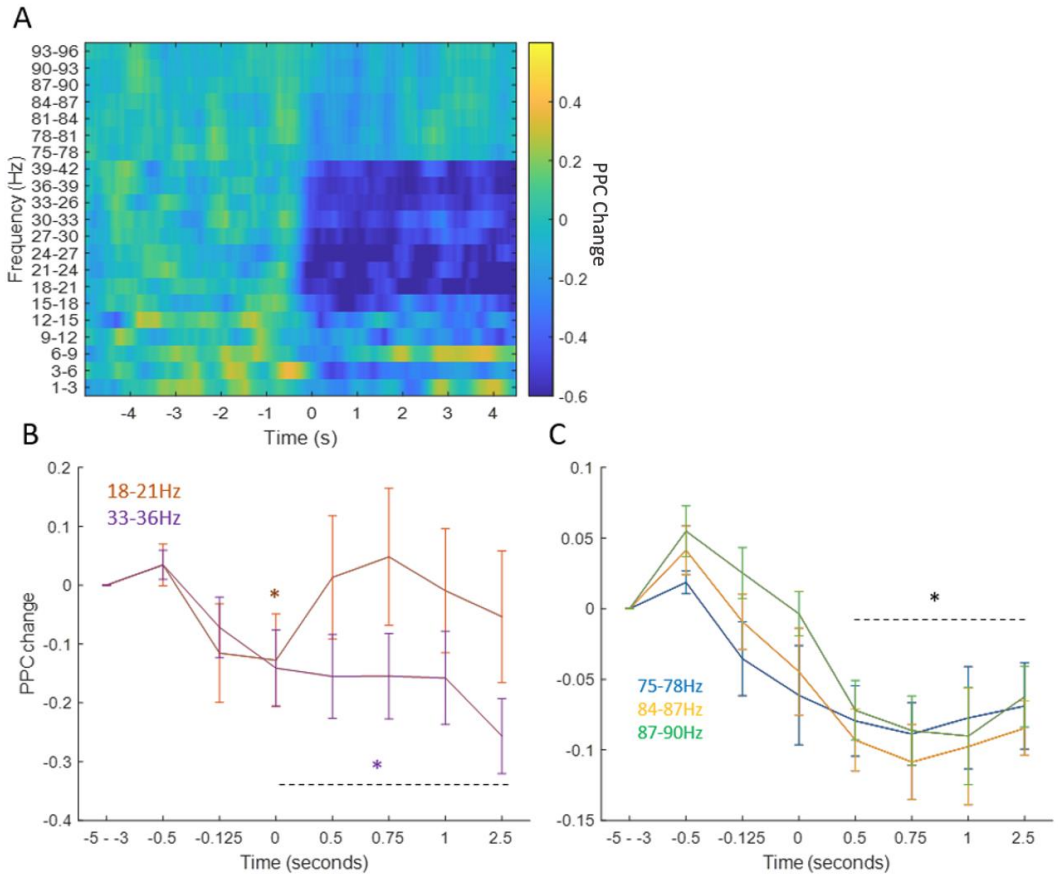


***Figure 3.17. PPC changes in LP-PO in the 1-96 Hz frequency band at S1 SWD onset.***

*Colour map of LP-PO PPC changes across time (**A**) at all analysed frequency ranges. Quantification of 18-2 1Hz and 33-36 Hz changes in PPC are shown in (**B**) and those in the gamma frequency ranges in (**C**). Dashed lines indicate time points with significant reduction in PPC, *p <0.05.*

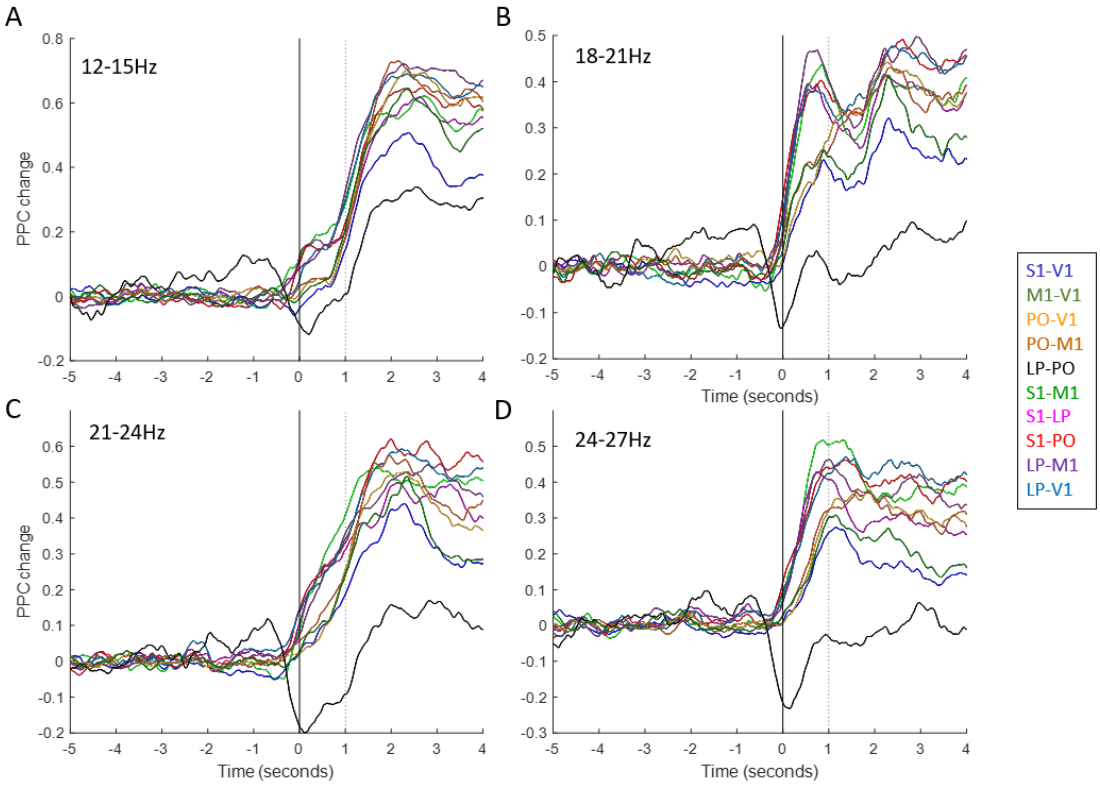


***Figure 3.18. PPC changes for all channel combinations at SWD onset at frequencies between 15 and 27 Hz.***

*PPC value changes at 3 harmonics of the main SWD frequency are shown in **A** (12-15 Hz), **B** (18-21Hz) and **C** (21-24 Hz). An example of a non-harmonic frequency range, 24-27 Hz (**D**) is shown to demonstrate similarity in PPC changes above 24Hz. Plots show time around S1 SWD onset (solid line). Dashed black lines indicate approximate time of SWD appearance in V1.*

At seizure offset, the earliest statistically significant decrease in PPC was observed at -1s in S1-PO, S1-V1, PO-V1 and PO-M1 *(Figure 3.19)*. This was then followed at -0.75s by LP-V1, LP-PO and M1-V1. Finally, at -0.5s there were PPC decreases in the rest of the channel combinations, i.e. S1-M1, S1-LP and LP-M1 *(Figure 3.19)*. PPC reductions were observed at SWD harmonic frequencies, however they occurred at -0.5s and overall were smaller than at 6-9 Hz.

At non-harmonic frequency ranges above 24 Hz, contrary to observations at SWD onsets, there was an increase in LP-PO PPC after offset *(Figure 3.20)*. This was significant for the frequency range 39-42 Hz from 1s after offset (p=0.02). For other channels, at 24-27 Hz, significant PPC reductions were only observed in S1-M1, S1-PO, S1-LP and LP-M1 (p=0.02) *(Figure 3.20A)*. As frequency increased, the PPC reductions decreased, and at 36-39 Hz there were only significant reductions in S1-M1, S1-PO and S1-LP (p=0.02) *(Figure 3.20B)*. There were no PPC changes in the high gamma frequency band.

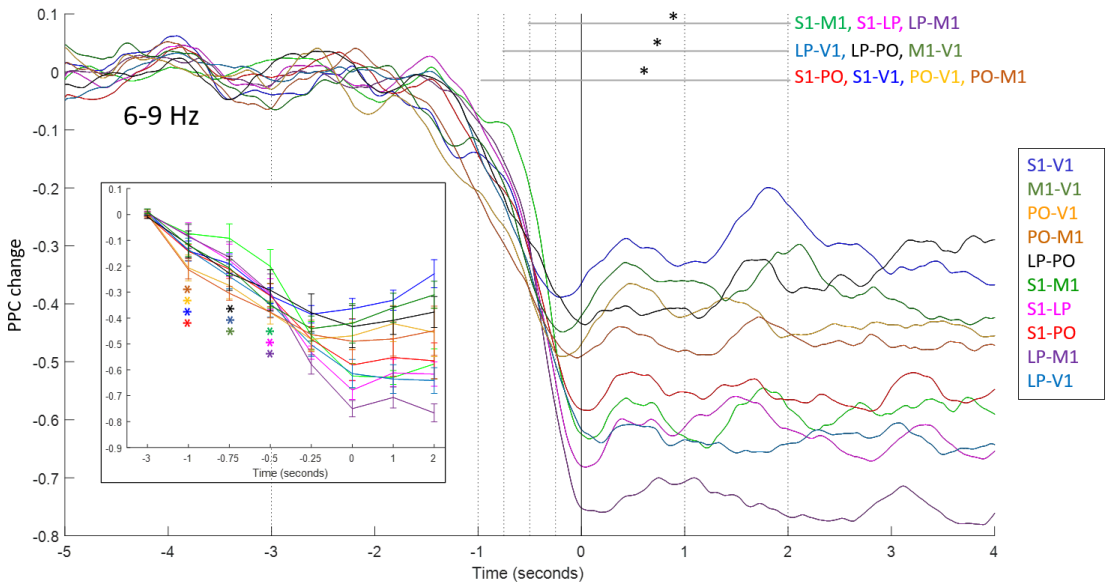


***Figure 3.19. PPC changes at 6-9 Hz around SWD offset.***

*PPC changes in all channel combinations (colour coded as in insert on right) around SWD offset (solid black line). Dashed black lines indicate times where quantitative analysis was carried out, which is shown in insert, where * shows when channel combination was first found to be statistically significant at p <0.05. Horizontal grey lines show the timepoints with a statistically significant decrease in PPC, * p<0.05.*

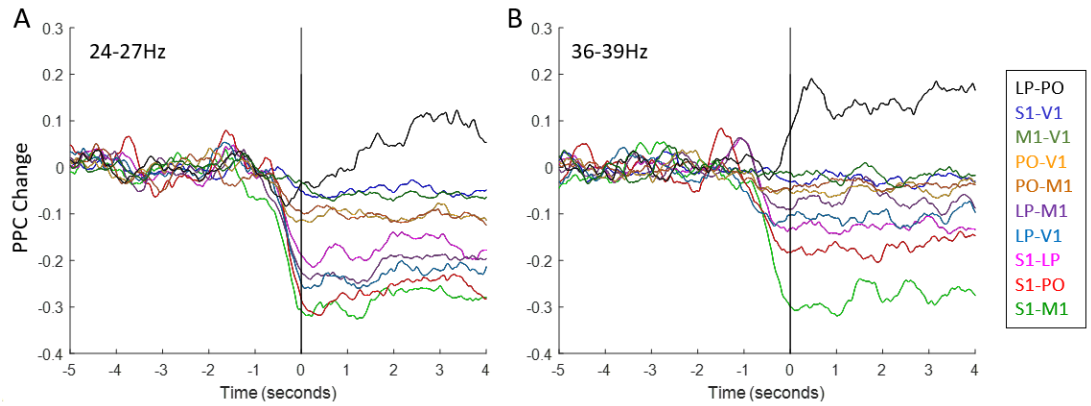


***Figure 3.20. PPC changes at seizure offset at non-harmonic frequencies***

*Plots show PPC changes at 24-27 Hz (**A**) and 36-39 Hz (**B**) for all channel combinations. Vertical line indicated time of S1 SWD onset.*

## 3.4 Discussion

### 3.4.1 Summary of results

The main results described in this chapter are:

1. SWD appeared first in S1, approximately 0.5s later they were visible in M1 and in both thalamic channels and they appeared last in V1 after approximately 1s, a time significantly later than that of M1. During this period, phase coherence between channels increased. S1-M1, S1-LP, S1-PO, LP-M1 and LP-V1 coherence increased first, followed by the rest of the channel combinations almost a second later. At seizure offset, all channels reduced their coherence significantly at similar times for all channels.
2. I report for the first time that SWD-breaks occurred in V1 during ongoing behavioural seizures and continuous SWD in S1. Amplitude fluctuations, including the SWD-breaks, were temporally correlated with both LP and PO, significantly more than any other channel combination. During SWD-breaks in V1, phase coherence significantly decreased in M1-V1, S1-V1, PO-V1, PO-M1 and LP-PO.
3. For the first time, S1-only and S1+M1-only events were confirmed to not spread to other cortical regions and their occurrence and duration were quantified

### 3.4.2 Methodological implications

The accuracy of SWD onset times across brain regions tested was important as much of the analysis was aligned to these time points. SWD in S1 at onset was often smaller and less spiky than during the middle of SWD, therefore detectability and accuracy of onset could have been influenced by factors such as signal quality and electrode depth in S1. Additionally, onset delays within S1 occur (Polack et al. 2007) which highlights the importance of consistent electrode location. In this study the onset delays were consistent between animals which indicates consistent electrode location and extraction of onset time.

Typically, research into AS utilising LFP recordings identifies the time of seizure onset as the time when the SWD occur in both the thalamus and the cortex (Meeren et al. 2002; Lüttjohann and van Luijtelaar 2015). However, as this thesis was focused on what neural changes occur during the initial SWD propagation, the onset time was

taken as SWD appearance in S1 only. The clear time-locked PPC changes observed at SWD onset in S1 indicate the physiological relevance of this time point in AS.

The time delay between SWD onset in S1 and that in V1 was taken as the time period of SWD propagation: although this cannot be an exact measure of AS generalisation, it is considered a suitable proxy due to V1 being one of the farthest cortical region from S1. When PPC changes were aligned to V1 onset instead of S1 onset, the same changes were observed *(see insert in Figure 3.15A)*, albeit shifted in time, which again indicated that the onset times were extracted appropriately.

As the rate of S1-only and S1+M1-only events were very low, longer recordings would need to be made to increase the number of these events thus, reducing the variability in enable application of PPC analysis. It is possible that the detectability of S1-only and S1+M1-only events was influenced by small changes in electrode location in the DV axis, as they may be most detectable in a specific layer, such deep layers of the cortical initiation network. In this work the electrodes were targeted to layers V and VI but the true depth of the electrode in each animal is not available, but these would be assessed in future experiments.

Only 5 animals could be used to assess SWC-spike lags between regions. This was because in some animals the morphology of the SWC-spike was not clear and therefore accurate SWC-spike times could not be extracted. More animals here could help reduce the variability observed in LP and PO SWC-spike lags, perhaps leading to a significant difference that appeared as a trend in Figure 3.6B. Although the PPC measure is a good tool to measure phase coherence, it does not provide information on directionality of the coherence. Therefore, we cannot know whether early S1-HO increases are driven from S1, HO nuclei, or a bidirectional partnership.

The three phase reversal grating stimuli were chosen for the light stimulation experiments, one of which was supposed to act as a control due to the narrow gratings being undetectable by Wistar rats (Prusky et al. 2002). However, this stimulus resulted in a reduction of the LFP amplitude in V1, LP and PO, alike the test stimuli. This may have been due to high contrasting edges between the vertical black and white gratings that have been shown to alter visual response (Roth et al. 2018). If repeated, this would be rectified by fitting a gaussian distribution from white to black and vice versa, as opposed to binary distribution.

### 3.4.3 Implications for AS

This work is the first to show that short breaks in SWD occur in V1 during ongoing behavioural seizures. However, Meeren et al., (2020) did observe thalamic SWD-breaks when recording LFP in thalamus simultaneous to electrodes on the dura: “thalamic SWDs could transiently disappear during the course of a cortical train of SWDs”. However, data of those events were not shown and they were not analysed in any way.

SWD-breaks are of interest here because examining network differences during this period can provide insight into what contributes or is necessary for AS maintenance and could reveal some properties of the network that are susceptible to being perturbed. The short S1-only and S1+M1-only SWD, which have been previously observed (Polack et al, 2007 and 2009) provide a similar insight as they represent unsuccessful generalisation of AS.

#### *3.4.3.1 Synchrony of HO and V1 neurons are temporally related.*

Synaptic activity is the main contributor to the LFP signal and when many synchronised synaptic events occur, the amplitude of the LFP increases and this can be measured as an increase in power (Buzsáki et al. 2012). The power of SWD is known to wax and wane *(Figure 3.9)*, which represent fluctuations in underlying synchrony of the cortico-thalamic network. Here, we observed that this property in V1 was temporally correlated with amplitude changes in LP and PO *(Figure 3.10).* Therefore, the level of synchrony of V1 activity was related to that of HO activity.

The SWC-spike, which represents synchronous firing of cortical pyramidal neurons (Steriade et al. 1998), occurred 12 ±2ms (Figure 3.6) later in V1 than LP. A similar delay of 8-10ms occurred between LP or PO stimulation and monosynaptic activation of EPSP peaks in extrastriate visual areas (Fuentealba et al., 2004) or S1 (Viaene et al. 2011; Audette et al. 2018a). The overlap in these delays suggests that LP could be directly influencing the synchrony in V1 via monosynaptic connections.

Furthermore, LP and PO TC neurons monosynaptically excite inhibitory interneurons in V1 (Zhou et al. 2018) and S1 (Audette 2018), respectively. Notably, at least in layer Va of S1, pyramidal cell EPSPs were recorded with delayed IPSPs. The onset of the IPSP was consistently ~3ms after EPSP onset, which coincided with the timing of PO driven PV EPSPs. This suggested that PO stimulation resulted in disynaptic inhibition

of pyramidal neurons via PV interneurons (Audette, 2018). This type of activity is ideal for entraining neurons as it tightly limits the duration in which the cortical neurons can fire, therefore promoting synchronous activity.

Synapses between HO TC and cortical neurons can be classified as Class 1 or Class 2, as introduced in section 1.6. The former generates large amplitude EPSPs driven by only ionotropic glutamate receptors and the latter typically has a longer lasting effect by also activating metabotropic receptors.

The general view is that HO TC synapses in primary cortical areas are of the Class 2 type (Sherman 2014). However, studies have indicated, using paired-pulse stimulations, the existence of Class 1 LP-V1 (Zhou et al., 2018) and PO-S1 (Audette et al. 2018) synapses with depressing EPSPs. However, these studies did not focus on the distinction between Class 1 or 2 and therefore did not test other Class 1 features, such as the absence of a metabotropic glutamate receptor component. This is in contrast to other studies of the PO-S1 layer V synapse that found exclusively Class 2 synapses with paired-pulse facilitation as well as the presence of metabotropic components (Viaene et al. 2011; Casas-Torremocha et al. 2019).

Previous research shows that stimulation of PO neurons activates group 1 mGluRs in the cortex, generating a long lasting (350ms) membrane depolarisation (Viane 2011). Due to the similarities between HO nuclei, this is likely the case at LP-V1 synapses too, and reviews on the subject generalise this finding to all HO nuclei (Sherman 2014). The modulation of membrane potential could be useful during AS as it would increase the excitability of V1 neurons by enhancing the efficacy of incoming cortico-cortical inputs.

The simple classification of Class 1 and Class 2 synapses enables us to make assumptions on network properties but in reality, it is more complex. Not only have Class 1 TC-V1 synapses been found, despite the general view that only class 2 synapses occur in primary cortical areas. But also, beyond TC synapses there are also intracortical neurons with similar heterogeneity (Sherman 2014) that need to be considered. Moving forward, it would be essential to characterise what class of synapse occurs at HO TC synapses in GAERS as their properties may be different to other rats. In fact, anatomical differences reported in the HO nuclei of GAERS suggests that both LP and PO have a higher number of CT driver synapses than Wistar rats (Cavdar 2012).

The LP-V1 amplitude relationship observed, potentially a result of direct connectivity, were not observed between PO-M1 or PO-S1, which are directly connected. This suggests that HO influence may be different in V1 than S1. S1 is the initiator site of SWD with different electrophysiological properties, e.g. hyperexcitable neurons (Polack et al. 2007), compared to other cortical regions. Additionally, ictal V1 activity has been little studied, with reports of ictal desynchronisation (Meyer et al. 2018). Due to these cortical differences, we cannot assume that PO neuronal activity has the same effect in S1, as LP neurons in V1. Regarding M1, there are contradictory results on whether M1 projecting PO neurons, or S1 projecting PO neurons are more active following S1 stimulation (Mo and Sherman 2019a; Guo et al. 2020), but this may be due to the differential focus of the experiments as each study focused on cells either in S1 (Kinnischtzke et al. 2016), or M1 (Mo and Sherman 2019a). Additionally, due to the very strong feedforward S1-M1 excitation (Petrof et al. 2015), it may be more difficult for PO to influence M1 activity than for LP to influence V1 activity.

On the other hand, amplitude correlations between LP-PO and PO-V1 occurred. This was less expected because PO primarily contacts S1, S2 and M1 (Viaene et al. 2011; Ohno et al. 2012; Casas-Torremocha et al. 2019; Rodriguez-Moreno et al. 2020), although there are reports of moderate V1 connections following viral tracer injections into the rostromedial portion of PO (Ohno et al. 2012). PO neurons are heavily studied in sensory-motor functions and the lack of reports of PO effect on V1 may simply be due to a lack of focus on the function of this potentially smaller group of neurons. Notwithstanding, it cannot be ruled out that V1 projecting PO neurons have an influence of V1 synchrony during AS.

Ultimately, although this work shows an amplitude correlation between these areas, the data does not allow the identification of the mechanisms involved, although some directionality between LP and V1 is inferred as the SWC-spike delay matches previously reported monosynaptic LP to visual cortex delays. Due to the similarity of amplitude in both LP and PO, it is likely that there is a common modulator that is simultaneously affecting the amplitude of both of these HO nuclei. Whether either or both LP and PO have a causal effect on V1 is unknown at this stage.

#### *3.4.3.2 Brief light stimulation affects V1 synchrony*

Recently, it was shown that both humans and genetic models of AS can process visual and tactile stimuli, respectively, during SWD, as demonstrated by the presence of a visual evoked potential (VEP) (Genç et al. 2005) or sensory evoked potential in

S1 (Chipaux et al. 2013), respectively. Therefore, the phase reversal stimulations in my experiments, which generates VEPs in awake rats (Boyes and Dyer 1983), should have been processed by the GAERS visual system during SWD.

The light stimulation here was successful at temporally disrupting V1 SWD amplitude. No effect was seen in M1 and S1 which suggests that there are local synchronising mechanisms and that cortico-cortical communication during SWD is kept unidirectional from the initiator site (Meeren et al. 2002).

LP can transmit sensory information to all areas of the visual cortex (Lyon et al. 2010; Scholl et al. 2020), and sub-groups occur within LP that differentially process visual information (Foik et al. 2020). On the contrary, PO is primarily researched in relation to the somatosensory and motor system (Casas-Torremocha et al. 2017; Mo and Sherman 2019), despite this, PO was just as affected by the light stimulation as V1 and LP. This indicates that there is some cross-talk between the visual system and PO. This is not the first case of functional overlap between the two nuclei, when whisker responses were assessed (Petty et al. 2020), surprisingly both LP and PO tracked whisking equally well. Additionally, PO neurons have been shown to respond to simple visual stimuli (Allen et al. 2016) despite the same group not detecting any direct connections from melanopsin-expressing retinal ganglion cells. Finally, there are reports of small populations in both PO and LP that project to V1 (Ohno et al. 2012) and S1 (Massé et al. 2019) respectively, providing a potential trans-thalamic route for sensory-visual integration. However, it must be noted that not all groups have detected LP-S1 connections (Nakamura et al. 2015).

#### *3.4.3.3 HO-cortical networks are recruited before the generalisation of AS*

The duration of AS generalisation was taken as the delay between SWD onset in S1 and SWD onset in V1, which was on average 0.8s. Cortico-cortical delays of this magnitude were shown by raw LFP traces in Polack et al. (2007), although these were not quantified.

Signal coherence between brain regions represents a form of network communication (Fries, 2015). This was measured here, via PPC, to reveal changes in connectivity during at SWD onset. During this period of SWD propagation, PPC analysis showed a large increase in coherence in the seizure frequency band of 6-9 Hz. Additionally, ictal coherence between 9-42 Hz was much larger than interictal periods. At higher frequencies (from 10 to 42 Hz), the PPC changes became progressively smaller. A

similar broadband increase in coherence has previously been observed during SWD between the frontal-parietal cortices of human patients with SWD (Benedek et al. 2016; Lee et al. 2017).

Luttjohann et al. (2013) reported a significant increase between 6-48 Hz in S1-PO coherence at onset of SWD in S1 and thalamus in the WAG/Rjj model. In my work, significant increases were observed slightly earlier at the time of onset in S1 only. This discrepancy could be due to different statistical methods and animal models, but ultimately, the two studies agree that there are early increases in coherence between S1 and PO.

The recorded sites in this work differed to that of Luttjohann et al. (2013), allowing for PPC analysis of various cortical regions in addition to two HO nuclei. This revealed two distinct groups of connections that became more synchronous at different times *(Figure 3.16)*. At 0.125s prior to SWD onset, there was an increase in S1-M1 connectivity and S1-HO connectivity. The early increase in S1-M1 connectivity is not surprising due to their proximity and driving capabilities of S1 to M1 (Petrof et al. 2015), which was also reflected by a slightly higher interictal PPC value *(Figure 3.16)* than other cortico-cortical combinations.

S1 has efferents to PO, but not LP, therefore the simultaneous increase in phase consistency between S1 and both HO nuclei suggests that there is perhaps a separate nucleus that enables S1 activity to simultaneously affect LP and PO. The assumption that S1 is affecting LP and PO, rather than vice versa is made on the basis of two findings: 1. it is accepted that SWD are generated in S1, and 2. S1 SWC-spikes occur before all other regions.

If S1 was simultaneously affecting LP and PO via indirect connections, LP-PO coherence should increase as soon as S1-HO, but this was not the case. However, this can be explained by the high LP-PO coherence observed during interictal periods, which in fact begins to increase as soon at S1-HO PPC reaches baseline PPC levels of LP-PO. S1 has Class 1 inputs to PO so it is likely that these are also having a significant impact on PO activity, especially as the number of round large terminals, associated with driver synapses, are significantly increased in PO (and LP) nuclei of GAERS (Çavdar et al. 2012). However, as neuronal communication occurs both linearly and non-linearly, it is possible that the linear approach applied here is unable to detect PO and LP differences. Regardless of the exact mechanism, early linear

coherence between S1 and HO nuclei was detected, well before AS generalisation, suggesting their involvement during this period.

Interestingly, LP-V1 and LP-M1 connectivity were among the first to exhibit increases in PPC, whereas PO-V1 and PO-M1 coherence increased alongside S1-V1 coherence, just before AS generalisation. The fact that LP-V1 PPC increased significantly before the onset of SWD in V1 indicates that linear LP-V1 communication is not sufficient to generate SWCs in V1. However, this does not rule out a facilitatory role of LP: additionally, non-linear methods, such as those used to by Luttjohann and van Luijtelaar (2012) to detect early S1-PO bidirectional communication, could show different results. It is expected that most brain regions have an increase in coherence during AS, regardless of connectivity, due to the 7Hz entrainment. Therefore, some of the differences observed later, such as that of PO-V1, may be a biproduct of the generalisation.

#### *3.4.3.4 Reduction in intra-HO thalamic network coherence at SWD onset*

The LP-PO channel combination was the only one to show significant decreases in PPC activity at seizure onset with a transient decrease in the beta frequency range (18–12 Hz), sustained decrease in low gamma range (30–42 Hz) and a small decrease in high gamma (75–90 Hz). Beta oscillations (15–29 Hz) have been shown to be coherent across the cortical-thalamic-basal ganglia axis in various species that is higher in power when animals are stationary (Engel and Fries 2010; Brittain et al. 2014), which was generally the case during my recordings as animals had previously explored and became habituated to the recording environment. The transient reduction of LP-PO beta coherence could therefore indicate a decoupling from the basal network in this frequency range at seizure onset. Synchronisation of faster oscillations (30–40 Hz) has been demonstrated in intra-thalamic and thalamocortical networks under various conditions and behavioural states (Steriade et al. 1996) and the reduction observed between LP-PO could be due to a shift from physiological to pathological oscillations.

In all other channel combinations there was an increase in PPC coherence, which were strong in the beta frequencies. Coherent beta band oscillations between LP-pulvinar complex and V1 in cats have been shown to occur during spatial discrimination tasks, when multiple cortical domains need to actively communicate (Wróbel et al. 2007). Therefore, the increase in HO-cortical beta coherence could be facilitating cortical communication during AS.

#### *3.4.3.5 V1 SWD-breaks occurred concurrent to cortico-cortical decoupling.*

PPC analysis was again utilised to reveal changes in connectivity during V1 SWD-breaks. Before the onset of V1 SWD-breaks, 6-9Hz network coherence was disrupted between V1 and both of the other cortical regions tested, i.e. S1 and M1, whereas each HO nuclei remained coherent with its associated cortical region (i.e. LP with V1 and PO with S1). This suggests that brief interruptions are not caused by a reduction in coherence of HO-cortical networks. However, as neuronal communication occurs both linearly and non-linearly, it is possible that the linear approach applied here is unable to detect meaningful changes in HO-cortical networks. Alternatively, a combination of both cortico-cortical and HO-cortical networks may be necessary for the ongoing maintenance of SWD.

In addition to cortico-cortical connections, PPC value decreased between LP-PO, PO-V1 and PO-M1. PO neurons have axonal collaterals to both S1 and M1 and therefore it seems unusual that PPC would be disrupted selectively for PO-M1 and not PO-S1. One possible explanation is that PO is not involved in the SWD between these areas as S1 to M1 communication is already very strong, with monosynaptic 'driver' like inputs from S1 to M1 (Petrof et al. 2015). During interictal period, LP-PO PPC is high which indicates a nucleus or nuclei is influencing the activity of both regions simultaneously. Therefore, a reduction in LP-PO PPC during V1 SWD-breaks may indicate disrupted activity in this modulator nucleus.

The selective disruption of PO-V1 may be an indication that the smaller portion of V1-projecting PO neurons are active during SWD. Ultimately, the interpretation of these results is complex and alike in the amplitude correlations, some findings are better explained if a common modulator nucleus projecting to both LP and PO is considered. Potential candidates of a common modulator will be discussed in Chapter 6:.

#### *3.4.3.6 HO-cortical network coherence at seizure offset*

In my work, a reduced PPC is observed 1s before offset, defined as the termination of SWD in S1. At offset, all channel combinations reduced their PPC activity within a 0.5s window and returned to interictal PPC levels within 0.25s of one another. Although channel combinations did significantly decrease at different time points, a clear grouping, alike at onset, was not observed here. The differences in PPC reductions may have been influenced by errors, of which there was large overlap between different channel combinations *(Figure 3.19).* The two channel combinations that visually, and statistically, reduced before the others was PO-V1 and PO-M1,

which could be an indication that PO influences on V1 have a functional impact. All reductions in coherence occurred before seizure offset, which indicate that non-linear dynamics may be maintaining the SWD for during this period. Indeed, non-linear, bidirectional communication between S1 and PO still occurred until 1.5s after the last cortico-thalamic SWC (Lüttjohann and van Luijtelaar 2015).

#### *3.4.3.7 Summary*

The main conclusions of this chapter are:

1. For the first time, the presence of V1 SWD-breaks was shown. These events represent moments of unsynchronised activity in V1, which, due amplitude correlations with LP and PO, may be generated by a disruption of HO nuclei activity.
2. For the first time S1-only and S1+M1-only events were quantified and shown to not occur in cortical regions far from S1.
3. The hypothesis that LP and PO are involved in the initial propagation was put forward as S1-LP and S1-PO networks are recruited before generalisation of SWD.
4. Despite the different dominant anatomical projections between LP and PO to V1 and S1, respectively, PO communications with V1 may be active during the initial period and throughout SWD.
5. Potentially, there is a common modulator of both LP and PO contributing to the observed similarities in phase changes, enabling S1 activity to influence both HO nuclei.

# Chapter 4: Inhibition of LP and PO increases the onset delay of SWD and reduces the power of SWD in V1

## 4.1 Introduction

In the previous Chapter, I showed that the generalisation of an AS can take approximately 1s, with SWD first reaching M1 and thalamic regions, and finally the distal cortical area of V1. Additionally, generalisation of SWD are not always successful, as demonstrated by the occurrence of S1-only SWD. Although HO nuclei have a tight temporal amplitude correlation with V1 and increased connectivity with this region before the appearance of SWD in V1, it remains unknown whether there is a causal relationship.

This chapter aims to answer the following questions:

1. Does inhibition of HO nuclei affect SWD generalisation?
2. Does inhibition of HO nuclei affect the occurrence of S1-only and S1+M1-only events?
3. Are these effects limited to V1?

## 4.2 Methods

The methods used in the experiments described in this chapter are detailed in section 2.1.4. Briefly, to assess the effect of HO nuclei on AS, GAERS were implanted with 3 unilateral electrodes to record LFP in S1, M1 and V1 and bilateral guide cannula in LP or PO to inject muscimol, a $GABA_A$ receptor agonist.

### 4.2.1 Data analysis

The parameters that were used to analyse the data are summarised in *Figure 4.1*. They are onset delay, offset difference, SWD-break rate and SWD-break duration and are detailed in section 2.2.2. These features combine to form SWC-Failure, as shown in the equation in *Figure 4.1* and detailed in section 2.2.4.1.

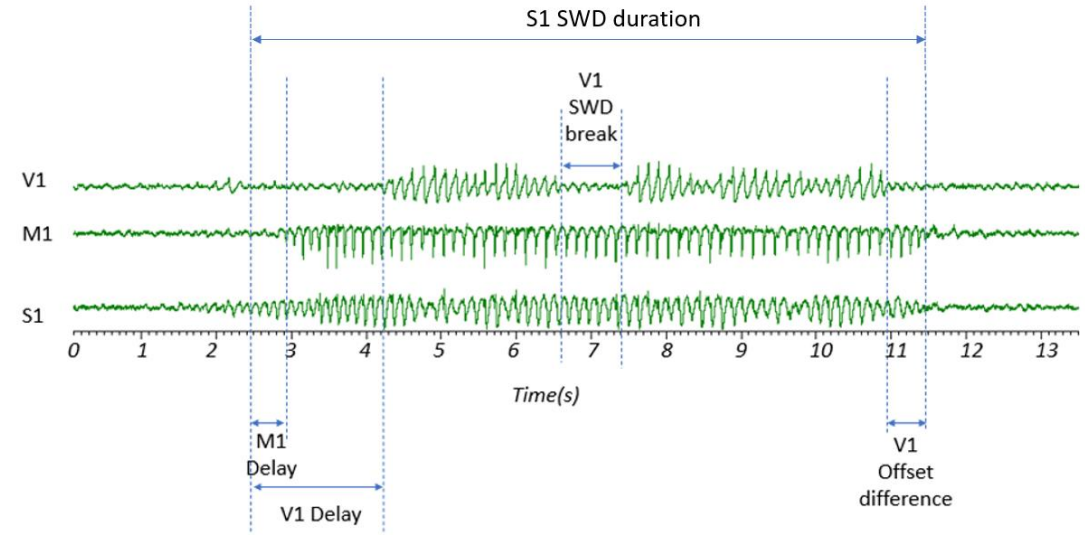


$$SWC - Failure = \left( \frac{V1\ delay + V1\ offset\ difference\ + \sum V1\ break}{S1\ SWD\ duration} \right) \text{x } 100$$

***Figure 4.1. Summary of parameters measured within seizures.***

*Typical raw traces illustrating the typical SWD waveform profile in S1, M1 and V1 which has an onset delay in V1 compared to S1, a SWD-break in V1 and a time difference at SWD offset in V1. These features combine to form SWC-Failure, as per the equation at the bottom of the figure. Note that, although not observed for this seizure, SWD delays, breaks and offset differences also occur in M1.*

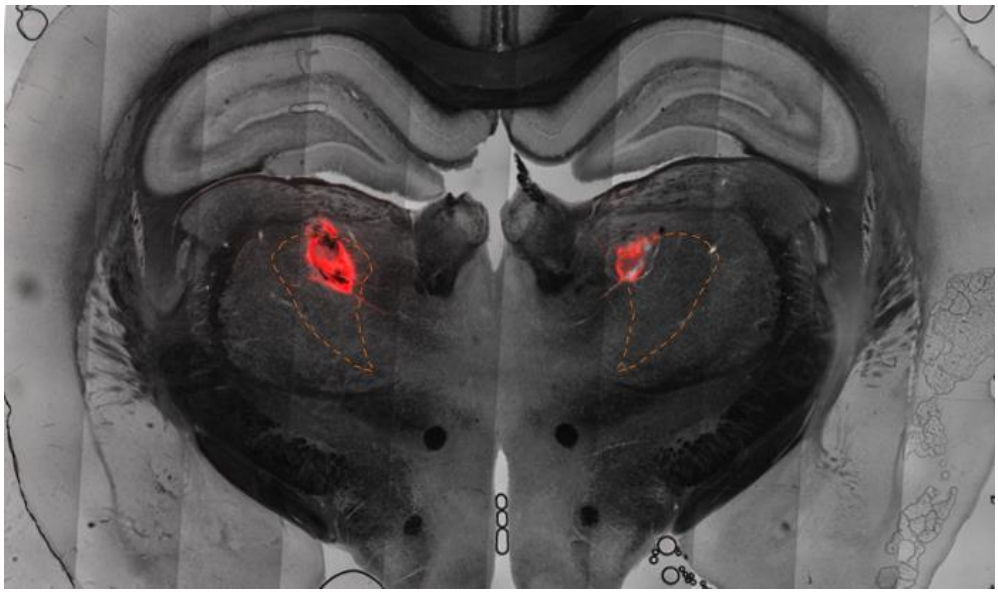

***Figure 4.2. Histology of an injected animal.***

*Typical brain section from a GAERS injected into PO with DiI (red staining) and imaged with a confocal microscope. Orange dashed area shows outline of PO made by tracing an overlayed stereotactic map from Paxinos and Watson (1998).*

### 4.2.2 Histology

The position of the guide cannulae and the potential spread of the injections were checked in all animals by injecting 0.5µL DiI into PO at the end of the last recording session. Briefly, relevant brain sections were histologically processed and then imaged with a confocal microscope *(Figure 4.2),* as detailed in section 2.1.5.6. Animals in which the position of the cannulae was not in the appropriate location were not considered for further analysis.

## 4.3 Results

### 4.3.1 Inhibition of LP and PO with muscimol microinjections did not reduce occurrence of SWD

Muscimol injection in PO (n = 6) or LP (n = 6) did not significantly alter seizure number, duration or total time spent in seizure, when compared to aCSF injection (aCSF in LP=2 and PO n=4) *(Figure 4.3)*. A reduction in time spent in seizure was observed following muscimol injection in LP and PO (37.5 ±12.7% and 55.57 ±20.53%, respectively at 0-30 mins), however this was not significantly different to aCSF injection (23 ±21.8% at 0-30 mins vs LP p=0.5 or PO p=0.4). There was also a reduction in seizure duration immediately after PO injection (51.66 ±10.1%), however, this was not significantly different from aCSF (22.4 ±13.5%, p=0.2). No differences in seizure numbers were observed between the groups.

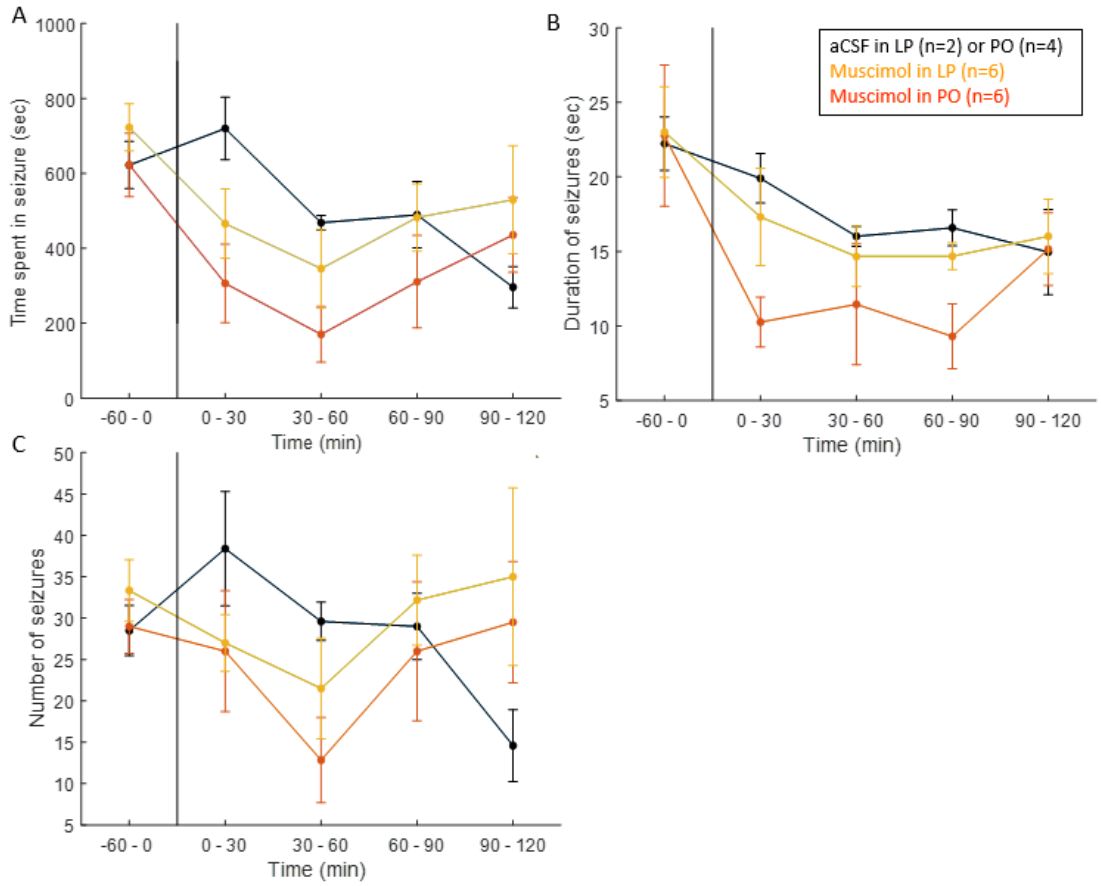


***Figure 4.3. Inhibition of HO thalamic nuclei did not significantly impact basic seizure parameters.***

*The total time spent in seizure (**A**), duration of seizures (**B**) and total number of seizures (**C**) were assessed after aCSF (black) or muscimol injection in LP (yellow) and PO (orange) at time 0 (vertical black line).*

### 4.3.2 Muscimol increased the number of S1-only SWD.

As described in chapter 3, under normal conditions some SWD occurred only in S1 or in S1 and M1 (full analysis of these events is in section 3.3.3). There was a significant effect of muscimol on the occurrence of S1-only SWD (F=8.95, Pr(>F) = 0.003) (*Figure 4.4*). Muscimol injection in PO (n=6) and LP (n=5) resulted in a significant increase in S1-only SWD during the first 30 minutes post-injection (aCSF: 0.7 ±0.8 vs PO: 7.3 ±1.5, p=0.015, and LP: 6.90 +/- 2.06, p=0.048). There was also a significant effect of muscimol on S1+M1-only events (F= 5.4, Pr(>F) 0.02), however, there were no differences at the interaction level due to large variation. S1+V1-only SWD were rare (total: 27 vs. total S1-only: 292, vs. total S1+M1-only: 170) and no difference was found between aCSF and muscimol injection.

### 4.3.3 Inhibition of LP and PO increased onset delay and ongoing expression of SWCs in V1 during SWD

Muscimol had a significant effect on SWC-Failure in V1 and M1 during AS (F=13.8, Pr (>F) = 0.0005). Muscimol injection in LP and PO resulted in a significant increase in SWC-Failure in V1 (*Figure 4.5),* relative to aCSF (comprehensive details of means and sample sizes can be found in Table 4.1). This occurred within 30 minutes after injection (aCSF: -3.2 ±2.1, LP: 16.5 ±3.2, PO: 27.2 ±4.9%, both p <0.0001) and was sustained until 90 minutes after injection (aCSF: -5 ±2.1, LP: 9.3 ± 4.1, PO: 12.1 ± 5.1%, both p <0.0001).

Only muscimol in PO resulted in a significant increase in SWC-Failure of M1 during AS at 30 minutes post-injection (aCSF: 0.3 ±1, PO: 13.6 ±3.8%, p=0.004) *(Figure 4.5B)*. The effect of muscimol on SWC-Failure was significantly greater in V1 than M1 during the first 30 minutes after injection in PO (V1: 27.2 ± 4.9, M1: 13.6 ±3.8%, p <0.0001) and LP (V1: 16.5 ±3.2, M1: 6.3 ±3.1%, p=0.0001) (*Figure 4.5*). There were no significant differences in the effect of muscimol injection between LP and PO at any time point.

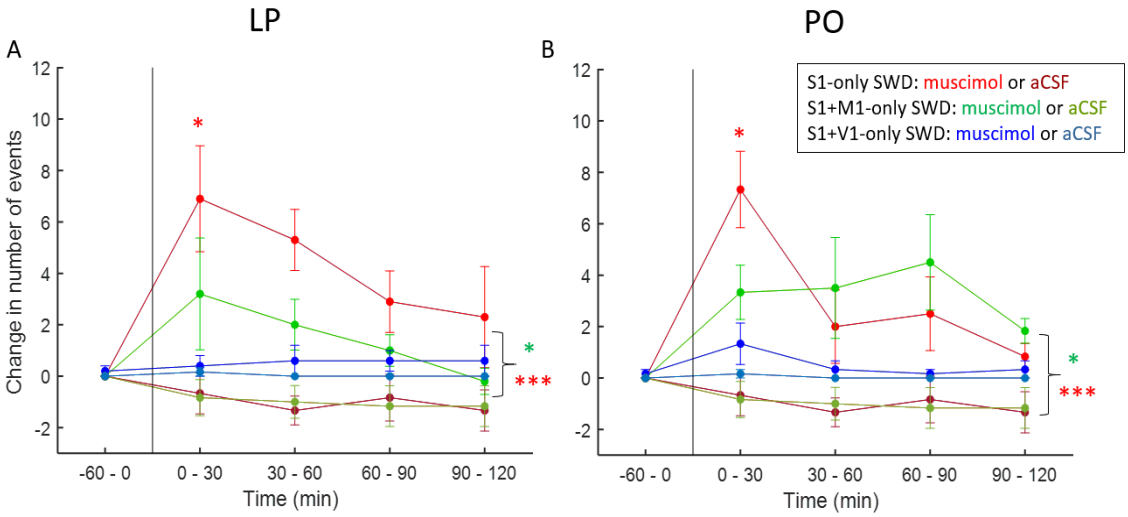


***Figure 4.4. S1-only SWD increased after muscimol injection in LP and PO.*** *Number of S1-only, S1+M1-only and S1+V1-only SWD after muscimol (bright red, green and blue lines, respectively) or aCSF (dark red, green, and blue lines, respectively) injection (time indicated by the vertical black line) in LP (**A**) and PO (**B**) are plotted with respect to the 1-hour pre-injection period. Colour of * indicate the type of event significantly different to control. Black bracket and '*' indicate a significant F-statistic of drug treatment for each type of event. * p < 0.05, *** p < 0.0001.*

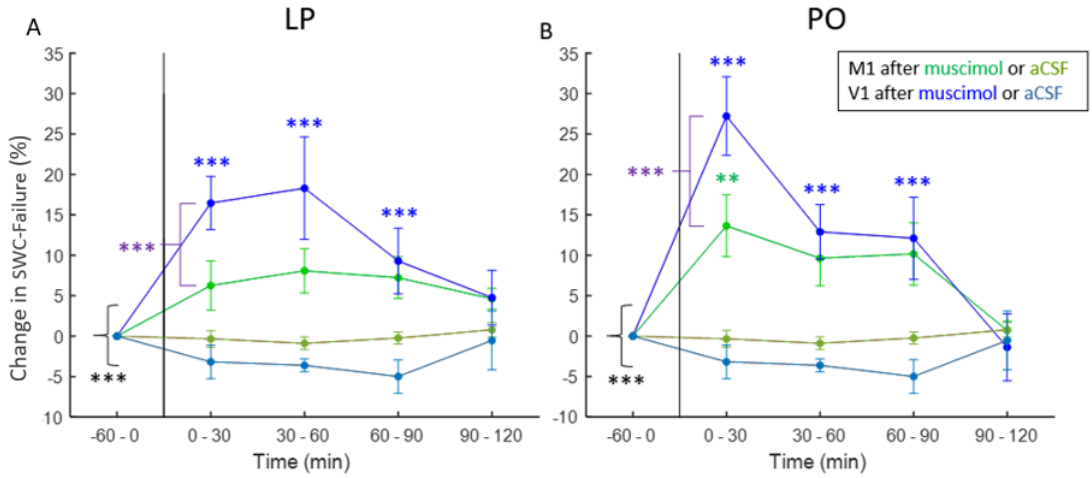


***Figure 4.5. SWC-Failure increased following muscimol injection in LP and PO.*** *Change in the percentage of SWC-Failure in V1 or M1 following muscimol (bright blue and green lines, respectively) or aCSF (dull blue and green lines, respectively) injection in LP (**A**) and PO (**B**). Colour of * indicate the region significantly different to control, the purple and black * indicate differences between V1 and M1 and significant F statistics of drug treatment, respectively. ** p <0.01 *** p < 0.0001.*

| **Injection site** | **Cortical area** | **Time post injection** | **SWC-Failure aCSF** (animal n, seizure n) | **SWC-Failure Muscimol** (animal n, seizure n) | **p-value** |
|---|---|---|---|---|---|
| LP | M1 | 0 – 30 | -0.34 ± 1.02 (6, 218) | 6.26 ± 3.05 (5, 145) | n.s |
| | M1 | 30 – 60 | -0.86 ± 0.80 (6,177) | 8.08 ± 2.75 (5,126) | n.s |
| | M1 | 60 – 90 | -0.22 ± 0.75 (6,197) | 7.22 ± 2.60 (5,183) | n.s |
| | V1 | 0 – 30 | -3.18 ± 2.09 (6,218) | 16.46 ± 3.29 (6,162) | <0.0001 |
| | V1 | 30 – 60 | -3.54 ± 0.82 (6,177) | 18.30± 6.33(6,128) | <0.0001 |
| | V1 | 60 – 90 | -5.00 ± 2.08 (6,197) | 9.29 ±4.06 (6,193) | <0.0001 |
| PO | M1 | 0 – 30 | -0.34 ± 1.02 (6,128) | 13.64± 3.84 (6,156) | 0.0783 |
| | M1 | 30 – 60 | -0.86 ± 0.80 (6,77) | 9.63 ± 3.44(6,77) | n.s |
| | M1 | 60 – 90 | -0.22 ± 0.75 (6,197) | 10.16 ± 3.86(6,156) | n.s |
| | V1 | 0 – 30 | -3.18 ± 2.09 (6,128) | 27.22 ± 4.85 (6,156) | <0.0001 |
| | V1 | 30 – 60 | -3.54 ± 0.82 (6,177) | 12.89 ± 3.36(6,77) | <0.0001 |
| | V1 | 60 – 90 | -5.00 ± 2.08 (6,197) | 12.11 ± 5.09 (6,156) | <0.0001 |

***Table 4.1. SWC-Failure in M1 and V1 in aCSF and muscimol injected animals.***

To investigate the underlying cause of the increase in SWC-Failure of M1 or V1 during an AS, the contributing factors, e.g. onset delay and number of SWD-breaks, were analysed. Muscimol had a significant effect on onset delay ($F=4.6$, $Pr(>F) = 0.028$) (*Figure 4.6)* and SWD-break rate ($F=13.4$, $Pr(>F) = 0.01$) (*Figure 4.7).*

An increase in onset delay in V1 was observed in both LP and PO injected animals *(Figure 4.6A,B)* at 0-30 minutes post injection (aCSF: -0.05 ±0.07, LP: 0.4 ±0.09, $p<0.0001$; PO: 0.4 ±0.2, $p=0.003$). For LP injected animals, this increase was sustained until 60 minutes post-injection (aCSF: -0.10 ± 0.061, LP: 0.2 ±0.2, $p=0.02$). Differences at offsets were not significantly affected by muscimol *(Figure 4.6C,D)*. There was a significant increase in the rate of occurrence of V1 SWD-breaks *(Figure 4.7A,B)* following muscimol injection in PO until 30 minutes post injection (aCSF: -0.01 ±0.02, PO: 0.1 ±0.02, $p = 0.03$) and after LP injection at 30-60 minutes (aCSF: -0.01 ±0.02, LP: 0.1± 0.06, $p= 0.03$). Break duration was not significantly affected by muscimol but V1 offsets became more variable following muscimol injection in PO (*Figure 4.7C,D)*.

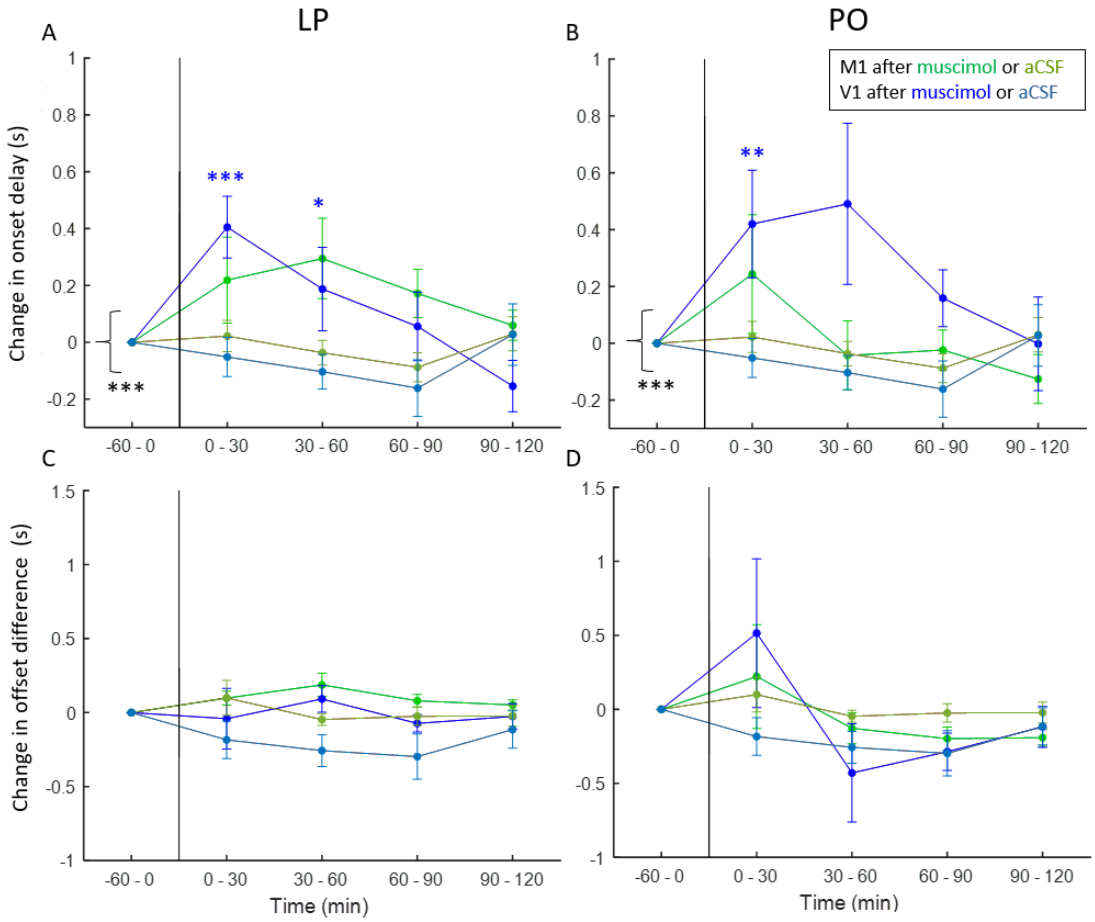


***Figure 4.6. Muscimol injection in LP and PO increased the onset delay between S1 and V1.***

*Analysis of the intra-seizure changes of onset delay (**A,B**) and offset differences (**C,D**), measured in M1 (green lines) and V1 (blue lines) after muscimol injection in LP (**A,C**) and PO (**B,D**). Colour of * indicate the region significantly different to aCSF injections, either blue (V1) or green (M1). Black * indicate significant drug treatment F statistic. * $p < 0.05$, ** $p < 0.01$, *** $p < 0.0001$.*

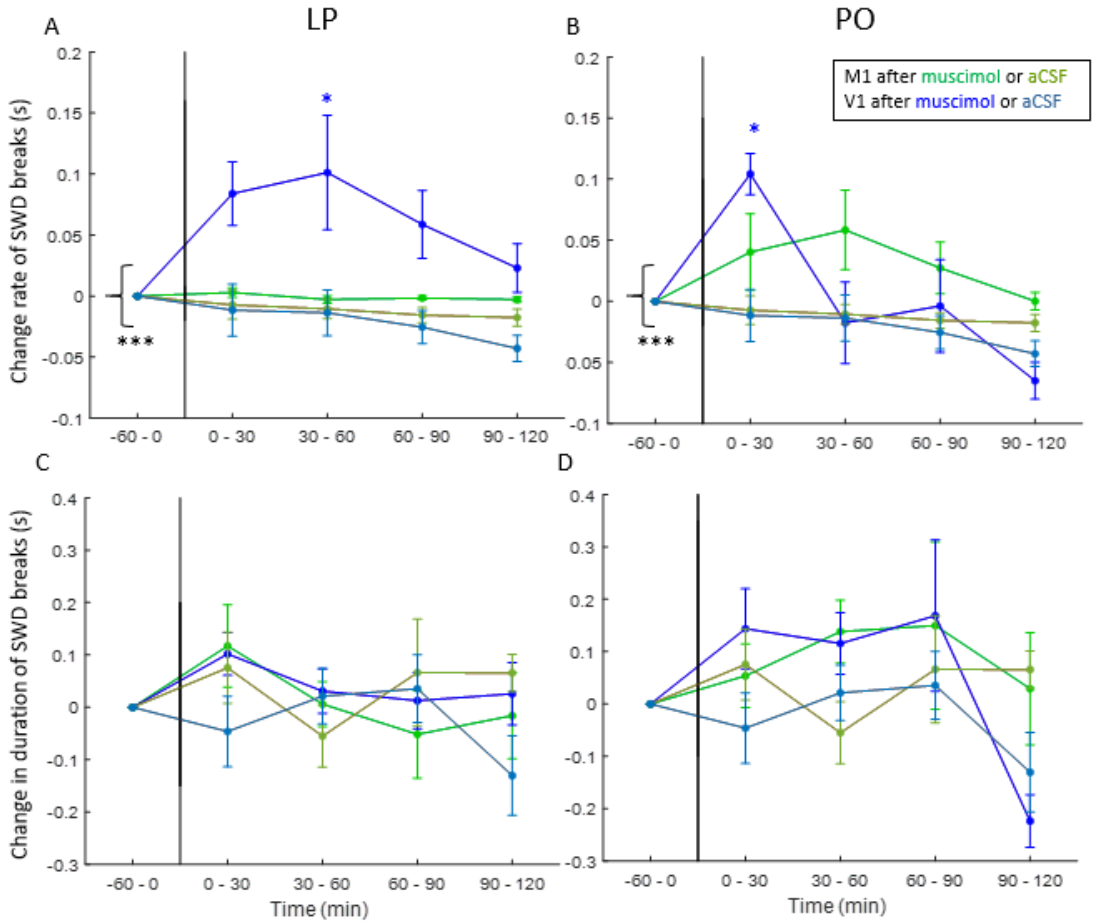


***Figure 4.7. Muscimol injections in LP and PO increased the rate of V1 SWD-breaks.***

*Analysis of the intra-seizure changes of SWD-breaks (**A,B**) and duration of SWD-breaks (**C,D**), measured in M1 (green lines) and V1 (blue lines) after muscimol injection in LP (**A,C**) and PO (**B,D**). Colour of * indicate the region significantly different to aCSF injections, either blue (V1) or green (M1). Black * indicate significant drug treatment F statistic. * $p < 0.05$, ** $p < 0.01$, *** $p < 0.0001$.*

### 4.3.4 Inhibition of LP and PO reduced the amplitude of SWD in cortical regions

Muscimol injection on LP and PO significantly affected the power of SWD ($F=13.52$, (Pr) $>F = 0.0006$) (*Figure 4.8).* Muscimol injections into LP and PO greatly reduced the SWD power in V1 (animal and seizure n = LP: 6 and 626; PO: 6 and 451), when compared to aCSF injection (animal and seizure n = 6 and 668). The peak reduction occurred at 0-30 minutes post injection (aCSF: 11.2 ±3.4%, vs. LP: 52.7 ±5.2%, $p<0.0001$, and PO: 55.7 ±8%, $p<0.0001$) and lasted until 30-60 minutes post injection (aCSF: 10.8 ±3.5% vs. LP: 52.3 ±7.8%, $p<0.0001$, and PO: 58.5 ±10.4%, $p<0.0001$). After this, power began to increase again, but still at 90-120 minutes post-injection there was a significant decrease in power (aCSF: 14.4 ±2.8 vs. LP: 28.7 ±10 $p<0.0001$, and PO: 29.4 ±7.3% $p=0.002$).

Muscimol in PO resulted in a decrease in M1 SWD power (animal and seizure n: 5 and 403) (*Figure 4.8).* This effect developed more gradually than in V1 and was significantly different to aCSF at 30-60 minutes after injection (aCSF: 1.9 ±3.7 vs. PO: -49.8 ±13.9%, $p=0.004$). This change was maintained until 90 minutes (aCSF: 3.3 ± 4.4% vs. PO: -31.4 ±12.8%, $p=0.004$).The power of seizures in S1 was also affected by muscimol injection in PO, however, due to the higher variability across animals it was not significantly different from aCSF injections.

Muscimol injection in LP had a greater effect on the power of V1 SWD than M1 or S1 SWD ($p<0.001$ at all time points). Muscimol in PO only had a greater effect on V1 power than M1 and S1 power 0-30mins after injection ($p<0.001$).

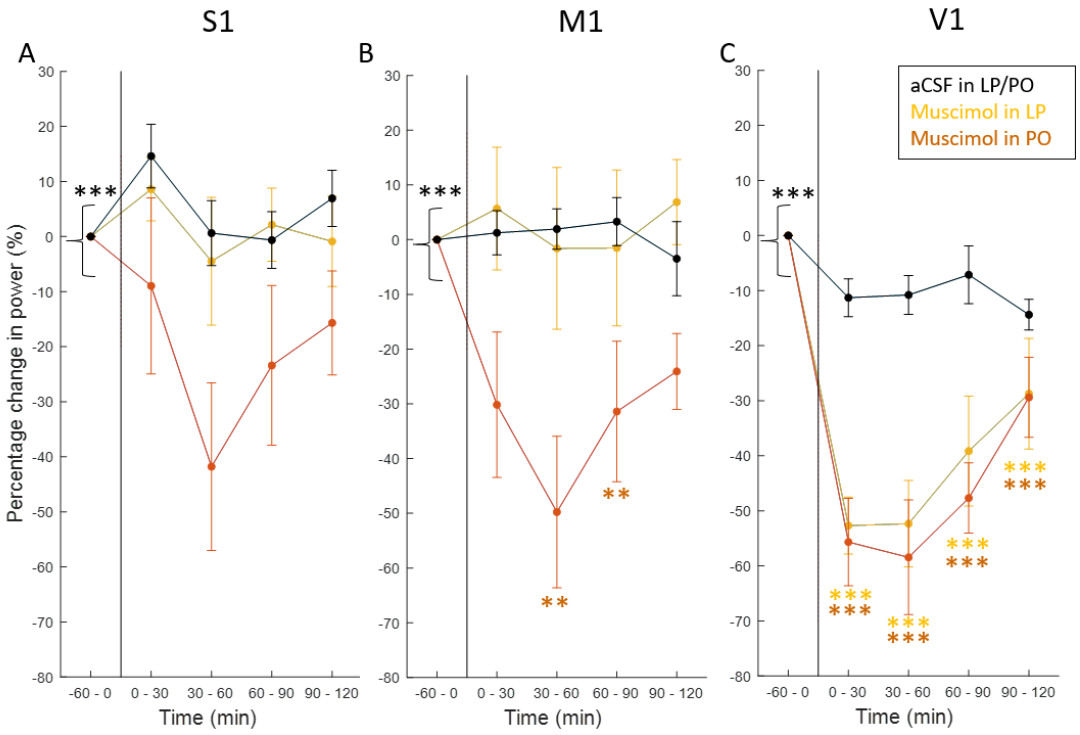


***Figure 4.8 Muscimol in HO thalamic nuclei affects the power of SWD in cortical regions***

*Percentage changes in power of SWD in S1 (**A**) M1 (**B**) and V1 (**C**) were assessed following muscimol injection in LP (yellow) and PO (orange) or aCSF injection in LP or PO (black). Colour of * indicate region of injected that resulted in significant power change. Black bracket and associated * indicate significant F statistic. * p < 0.05, ** p < 0.01, *** p < 0.0001.*

## 4.4 Discussion

### 4.4.1 Summary of key findings

Pharmacological inhibition of LP and PO with the $GABA_A$ agonist muscimol resulted in an increase of SWD onset delay to V1. Together with an increase in the rate of occurrence of V1 SWD-breaks, these contributed to a significant increase in SWC-Failure in V1 during SWD. Injections into PO also significantly increased the SWC-Failure in M1 during SWD, an effect that was not seen following LP injections.

Muscimol injections in both LP and PO increased the number of S1-only SWD events, which was significant for up to 30 minutes post injection. Lastly, muscimol injections in LP and PO greatly reduced V1 SWD power, and PO injections also decreased M1 SWD power.

### 4.4.2 Methodological and analytical considerations

The PO is located immediately ventral to LP, which was convenient as the same animal could be injected into both regions using a needle that projected either 1mm or 2mm from the guide cannula, respectively. However, it did mean that there was the possibility that muscimol might spread from LP to PO and vice versa, reducing the likelihood of detecting differences between LP and PO injected animals. Indeed, even when effects were seen from PO but not LP injections, when compared to control, there was no significant difference between the PO and LP group.

Fluorophore-conjugated muscimol was used in two GAERS to accurately determine the spread, however, although a functional effect was observed, no fluorescence was detected by the microscope. A previous study has administered the same compound at the same flow rate and detected a spread of 0.5-1mm radius (Allen et al. 2008), although the amount injected in that study (0.25-0.5µg) was much higher than here (0.0015µg). Along with this, the DiI injections used to determine electrode location was also an indication that muscimol spread stayed relatively well in nuclei boundaries but due to proximity of injections, some of the neuronal population in the neighbouring nuclei was likely affected.

Although the injection site targeting PO could have been more ventral, this could have led to the problem of muscimol leaking to neighbouring FO thalamic nuclei, something

that is less likely in the wider, more dorsal portion that was targetted in this study. This was considered a greater potential confound than leakage into another HO thalamic nuclei. In addition to the benefit of a reduced number of animals required for a powered study, the method of injecting both regions with 1mm separation was considered the best experimental approach for this study.

A SWD-break was defined as an ictal period (defined by the ongoing SWD in S1) of more than 0.6s without a detectable SWC. The large reduction of power in V1 SWD following muscimol complicated the detection of SWCs as their amplitude reduced to below background amplitude levels (defined as amplitude of wake interictal period). This could have contributed to the observed increase in the SWD-break rate and duration. To confront this, the amplitude threshold for SWCs was reduced and the 0.6s duration was an increase from an original 0.5s duration. Finally, the increase in breaks was something visually noticeable. Consequently, it was thought to be unlikely that this analytical complication alone can explain the observed large increase in SWC-Failure.

Experimental evidence also suggests a true effect of muscimol as power reductions occurred for at least 90 minutes post injection, whereas the maximal SWC-Failure was only 30 minutes in PO injected animals. This shows that the two measured parameters were not temporally correlated. Furthermore, the increase in SWD-breaks was not the only parameter that contributed to the increase in SWC-Failure. Finally, the fact the muscimol injections reduced SWD power, which directly measures synchrony of neuronal activity, indicates a physiological effect on AS from the inhibition of LP and PO.

### 4.4.3 Implication of findings for AS

Muscimol injections to HO nuclei would reduce their excitability by acting on $GABA_AR$ in LP and PO (Bokor et al. 2005), and thus reducing their influence on the regions they project to, i.e. cortical areas and NRT. The findings in this chapter supports the claim made in the previous chapter that trans-thalamic cortico-cortical communication, via LP and PO, facilitates the generalisation and maintenance of SWD.

#### *4.4.3.1 LP and PO activity facilitates AS generalisation*

SWD were not completely abolished by LP and PO inhibition which indicates that these HO nuclei are not necessary for the establishment of SWD, at least for the concentration used in this study. However, there was evidence that HO nuclei at least have a facilitatory role in AS generalisation. The extended V1 onset delay I observed indicates that HO-cortical communication were involved in the early entrainment of neurons to the ongoing SWD. It seems that this initial period of SWD propagation is important to establish 'full blown' AS as there were a greater number of unsuccessful, non-generalised SWD following LP and PO inhibition. These data suggest that while cortico-cortical communication is sufficient to generalise SWD, HO have a facilitatory role and not only speeds up the process but contributes to its success. However, this may only be the case for brain regions that are far from the initiation site (i.e.V1) as M1 onset delay was not affected. Alternatively, SWD propagation to M1 specifically may not be affected because of the strong sensorimotor networks present in rats where S1 has Class 1 inputs to M1.

Despite having different connectivity profiles, the effects from LP and PO inhibition on V1 were not significantly different. The idea put forward is that the facilitation of AS establishment by HO nuclei may occur via multiple mechanisms, where LP facilitates the establishment of SWD within V1 and PO effects the establishment in S1, both impacting the generalisation of AS.

Early bidirectional S1-PO communication has been proven via non-linear association methods (Lüttjohann and van Luijtelaar 2012) to occur during SWD and should be disrupted following muscimol injection to PO. The network pathway of this communication is not known, but the strong Class 1 synapses from the cortex to PO, that are higher in number in GAERS (Çavdar et al. 2012), are likely having an impact here. Alternatively, S1 can affect PO activity via NRT (Pinault 2004) or ZI (Barthó et al. 2002; Barthó et al. 2007). The bidirectional communication was proposed to have a to facilitate the periodic production of SWCs in S1 (Lüttjohann and van Luijtelaar 2015) and this theory can be extended to other cortical areas if the PO neurons involved in this process are multi-areal projecting matrix cells (Clascá 2012) as the early changes that occur in S1 could begin to be transmitted to other brain regions early on. Although the exact cellular mechanism of this communication is unknown, removing this activity, such as via muscimol as done here, would likely increase the time taken to entrain larger numbers of neurons that is needed for then synchronise other cortical regions.

In contrast, LP inhibition should not impact this early mechanism and therefore the initial generation of SWCs should occur as normal within S1. Inhibition in LP would affect trans-thalamic cortico-cortical communication, which from work in the previous chapter, is postulated to affect the synchrony of V1 neurons. The increase in V1 onset delay possibly reflects the fact that cortico-cortical communication alone is not as effective compared with combining the trans-thalamic route.

In addition to muscimol affecting the aforementioned CTC processes, intrathalamic mechanisms will also be affected. Both LP and PO have reciprocal connections to the NRT and therefore activity of the NRT is likely to be indirectly modulated by the pharmacological manipulation of LP and PO. As this thesis has not recorded from the NRT, it is hard to know what effect these connections have. However, pre-ictal changes in the NRT have been observed via PPC analysis, including a decoupling from PO and S1 (Lüttjohann et al. 2013), therefore such connections are not thought to play a big role in the AS generalisation.

#### *4.4.3.2 LP and PO activity influences the synchronicity of V1 neurons during AS*

The idea that HO affect synchrony of V1 neurons during SWD was introduced in the discussion of the previous chapter. This concept is reinforced by the results of this chapter since inhibition of both LP and PO drastically reduced the power and therefore the synchrony of V1 during SWD. When the synchrony of V1 SWD was very low, V1 SWD-breaks occurred, and such breaks were more frequent in the absence of HO activity. These data support the notion that HO-V1 connections are important in the ongoing, regular stimulation of the V1 neuronal population during AS.

The effect on V1 SWD power was the same following LP and PO muscimol injections. The similarity of LP and PO effects on V1 has been observed consistently. With direct LP to V1 connections (Kamishina et al. 2009) it is feasible that the reduction in power is generated because of the lack of V1 modulation and excitation from LP. However, it remains unclear why the same effect occurs after PO inhibition with much fewer direct connections with V1. One simple explanation could be that muscimol leaked into LP after PO injection, but if this were the case, there should be a smaller effect after PO injection as fewer LP neurons would be affected by the muscimol. However, if only a small proportion of LP neurons are required to generate a reduction in power than even a small diffusion into LP from a PO injection could achieve the effect observed. Alternatively, V1 projecting PO neurons, which have not been studied

functionally, may be active and sufficient to generate a large reduction of power. More specific inhibitions, for example by using opto- or chemo-genetic inhibition of LP and PO separately, is required to answer this fully.

### 4.4.4 Summary

In conclusion, the data in this chapter provided strong evidence of a causal relationship between LP and PO activity with the initial propagation of SWD to V1 and ongoing V1 synchrony during SWD. This chapter therefore supports the notions that the trans-thalamic pathway is active and relevant for SWD generalisation.

# Chapter 5: PO neurons switch from tonic to burst firing before SWD generalisation

## 5.1 Introduction

In the previous chapter, I demonstrated that inhibition of PO and LP increases V1 onset delay and decreases the synchrony of neuronal activity within V1, as demonstrated by a decrease in power following muscimol injections. As these data show LP and PO activity impact SWD generalisation, multi-unit recordings of PO neurons were obtained to investigate their temporal firing dynamics during SWD.

Polack et al., (2009) were the first to investigate the firing of single PO cells in GAERS under neurolept anaesthesia while recording SWD in S1 and M1. They showed that PO units were inactive during very short seizures of less than 2s, but active during the establishments of longer SWD that were present in both S1 and M1. However, as no electrodes were implanted far away from the initiation site of S1, it is difficult to know if the short SWD observed were fully generalised or not. Nevertheless, this demonstrates a potential influence of PO activity on the success or failure of the generation of SWD.

More recently, silicon probes were implanted into the Scn8a-/- genetic mouse model of AS, which detected units from the cortical-hippocampal-thalamic axis (Sorokin et al., 2020). These authors showed a sharp increase in PO unit activity at the time of seizure onset that decreased shortly after. This can indicate an involvement of PO units at the very beginning of the seizure, i.e. during the time of generalisation. However, as in the work of Polack et al. (2009), the lack of multiple cortical electrodes in this study makes it difficult to draw solid conclusions on the role for PO in the generalisation of AS.

This chapter aims to answer the following questions:

1. what are the temporal firing dynamics of PO neurons during the transition from local to global SWD?
2. are the temporal firing dynamics of PO neurons different between generalised and non-generalised SWD?

3. what are the temporal firing dynamics of PO neurons during the SWD-break in V1?

These questions are focused on PO as these experiments were completed before the decision to explore a second HO thalamic nucleus, i.e. the LP.

## 5.2 Methods

The experimental and analytical methods used are detailed in section 2.1.6 and 2.2.5, respectively. Briefly silicon probes in freely moving GAERS recorded PO single units while simultaneously recording LFPs in S1, M1 and V1.

### 5.2.1 Histology

Details of histological processing can be found in section 2.1.6.4. Briefly, silicon probes were coated in DiI before implantation and electrolytic lesions were made to visualise probe tracks and final depth, respectively *(Figure 5.1).*

## 5.3 Results

### 5.3.1 Classification of units

A total of 36 units from 3 GAERS were successfully sorted from the raw data. Of these, 5 units were removed after visual inspection of their burst firing profile, i.e. the ISI of spikes within a burst did not match any of the known burst firing profiles of excitatory or inhibitory thalamic neurons (Tscherter et al. 2011)

Previous work has shown that action potentials originating from excitatory and inhibitory neurons can be differentiated on the basis of the width of their waveform and trough-to-peak time, such that wider waveforms are associated with excitatory cells and narrower waveforms are characteristic of inhibitory cells (Senzai et al., 2019). Although generally true, spike waveform durations occur on a wide spectrum and McCafferty et al. (2018) demonstrated that TC cells have a varied width at half-amplitude. Therefore, to discriminate TC and NRT neurons, they also used the burst acceleration index (AI), i.e. the ratio of the duration of the first ISI in a burst divided by the duration of the shortest ISI. Since TC and NRT neurons have different T-type calcium channel subtypes (Talley et al., 1999), they have different burst profiles and AI values.

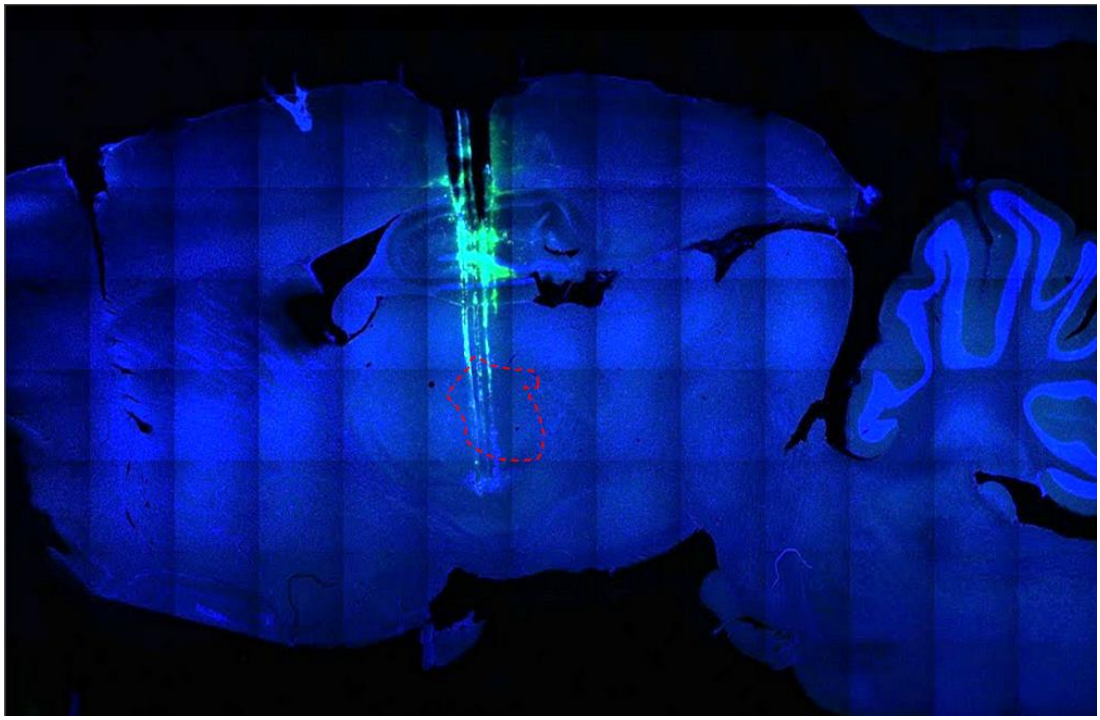

***Figure 5.1. Silicon probe location in a GAERS rat.***

*The picture shows a typical sagittal brain section from a GAERS implanted with DiI coated silicon probe and an electrolytic lesion at the most ventral recording site, imaged with a confocal microscope. Red dashed line shows outline of PO by tracing an overlayed stereotactic map from Paxinos and Watson (1998). Silicon probes were advanced in the dorso-ventral axis via a microdrive and were moved below PO to record units from other nuclei, hence the electrolytic lesions being more ventral than PO in this image.*

Thus, combining the spike width at half-amplitude, the trough-to-peak time and the burst AI, the 31 units that passed the spike sorting criteria could be differentiated in putative excitatory (n=27) and putative inhibitory neurons (n=4) *(Figure 5.2)*. Units with a width at half-amplitude >0.25ms, a trough to peak time <0.45ms and an AI <1.1 were classified as putative excitatory neurons, whereas units with a width at half-amplitude of <0.25ms, a trough to peak time of <0.4ms and an AI of > 1.3 were classified as inhibitory neurons *(Figure 5.2A).*

Two units did not fit all three criteria (filled blue and red circles in *Figure 5.2A).* The highlighted blue unit had a high AI and a narrower waveform relative to other excitatory units and was therefore removed from further analysis. The red unit had a narrow waveform, indicative of an inhibitory unit, but it did not fulfil the AI criterion as only one burst was recorded. Since silicone probes can detect spikes from axon fibres, as shown with simultaneous probe and juxtacellular recordings (Bartho et al 2014), it is possible that the inhibitory units were from fibers originating from the GABAergic ZI, APT and NRT nuclei, in addition to inhibitory PO neurons, although very few of these cells have been reported (Evangelio et al. 2018). As burst firing is not a known property of all these inhibitory sources (McCafferty 2018, Shaw, 2013), the red unit was kept in the dataset.

#### *5.3.1.1 Excitatory units*

All excitatory units expressed a decelerando burst pattern *(Figure 5.3),* where the ISI increases with subsequent spikes within a burst. This is characteristic of neurons containing $Ca_v3.1$ T-type calcium channels (Tscherter et al., 2011), which includes the FO TC neurons (McCafferty et al., 2018).

Ictal changes in burst firing were quantified using the following ratio: peak firing rate (i.e. maximum firing rate between 0 and 0.5s) *(t2 in Figure 5.4A)* over the average firing rate at 4-5s after onset *(t3 in Figure 5.4A)*. This ratio was plotted against the interictal – ictal firing rate change. This was calculated from the interictal period (i.e. from 5 to 4s prior to seizure onset *(t1 in Figure 5.4A)* over the firing at onset as previously described *(Figure 5.4B).* This led to the identification of three groups of units *(Figure 5.4):* units with a transient ictal increase in burst firing at the start of a seizure (n=10), units with a persistent ictal increase in burst firing (n=15), and units with relatively little burst firing (n=3).

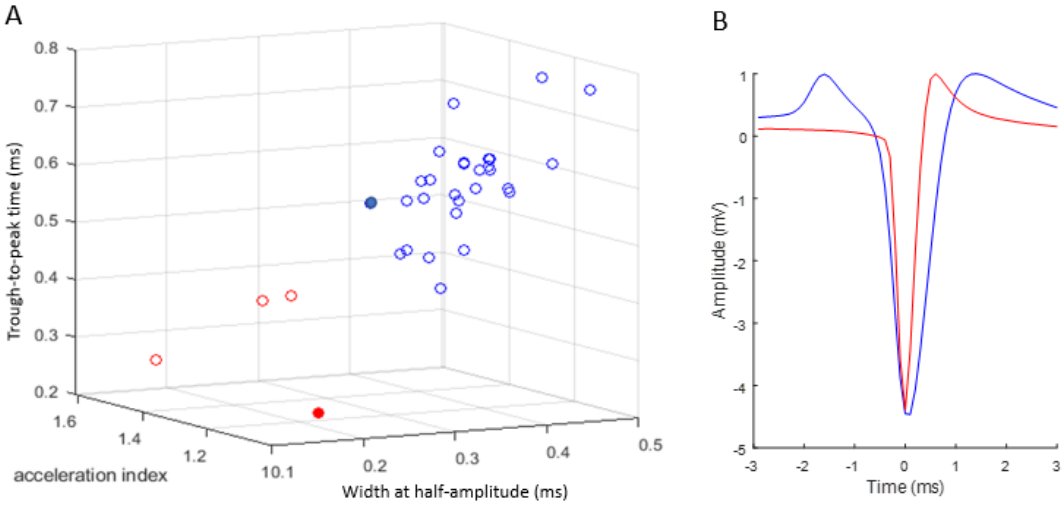


***Figure 5.2. Classification of sorted units into putative excitatory and inhibitory PO neurons.***

*A 3-D plot showing width at half-amplitude, trough-to-peak time, and burst acceleration index of the 31 sorted single units (**A**). The units were split into putative excitatory (blue) and putative inhibitory (red) units based on these parameters. The unit identified by the filled circles in **A** did not fit the criteria of their respective group (see text for further details). Examples of the typical waveform of a putative excitatory (blue) and putative inhibitory (red) neurons are illustrated in **B**.*

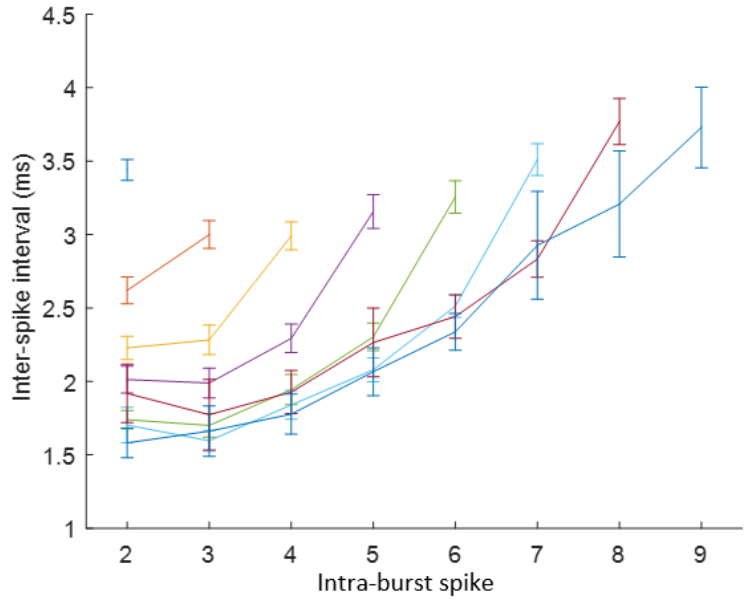


***Figure 5.3. Burst profile of excitatory units.***

*The interspike interval between consecutive spikes for bursts of various lengths are plotted to demonstrate the decelerando burst pattern observed in single units classified as excitatory.*

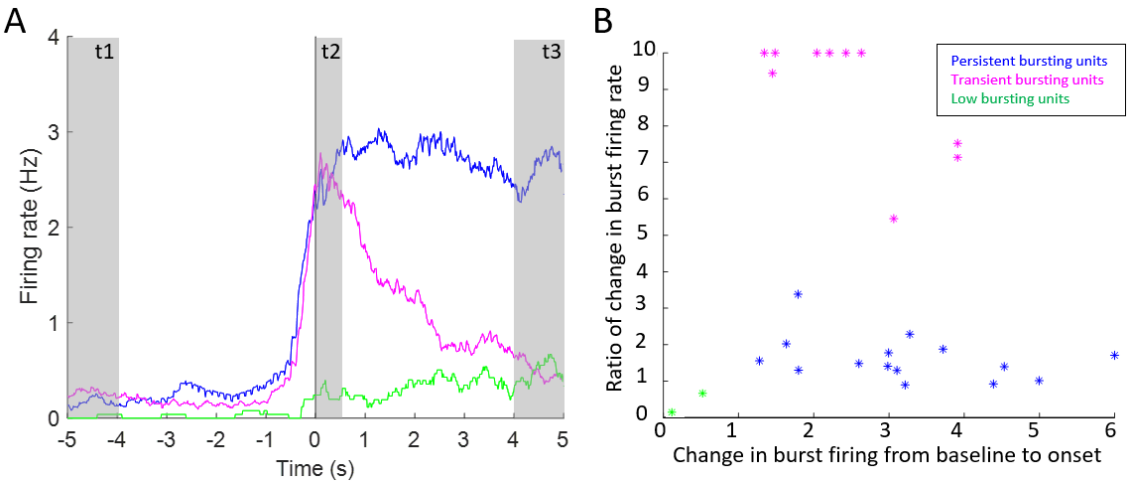


***Figure 5.4. Different temporal patterns of burst firing during SWD***

*Analysis of the burst firing dynamics revealed three types of excitatory neurons (**A**). There were 15 units that had a persistent ictal increase in burst firing (blue), 10 units that had a transient ictal increase in burst firing only at the start of the seizure (magenta) and 2 units that had a relatively low ictal burst rate (green) (**B**).*

Note that transient increases in burst firing would yield higher peak firing:ictal firing ratios, which were capped at 10 *(Figure 5.4B)* because excessively large numbers were obtained when burst rates changes fell below 0.1 during the seizure in the TB excitatory neuron group. All groups were kept separate in further analysis and will be referred to as transient bursting (TB), persistent bursting (PB) or low bursting (LB) excitatory neurons, respectively.

All three types of excitatory neurons had a decelerando bursting pattern *(Figure 5.5)*, with an average intraburst frequency for PB, TB and LB units of 367 ±6 Hz, 422 ±10 Hz, and 404 ±18 Hz. PB burst frequency was significantly lower TB units ($p<0.001$). None of the 3 groups of putative excitatory neurons showed a preferential location within PO *(Figure 5.6)*.

#### *5.3.1.2 Inhibitory units*

The 4 putative inhibitory neurons showed different burst profiles *(*Figure 5.7*).* One unit had an accelerando-decelerando pattern *(Figure 5.7C),* i.e., an initial decrease in the ISI, followed by progressively increasing ISI between subsequent spikes within the burst (Tscherter 2011). The other two units had a slight decrease in the ISI between the first and second spike in the burst *(Figure 5.7A,B)*, but was less pronounced. One unit only had one doublet throughout the recording period, so it had no burst pattern. Of these 4 putative inhibitory units, two came from one GAERS in which no other units were successfully sorted which could suggest something was wrong with the implantation or data acquisition of this animal. Additionally, it may be the case that these units were located just outside of PO as their post-hoc location was found to be at the border of the nucleus *(Figure 5.6)*. The other two units were in the middle of PO and therefore it can be claimed confidently that these units were recorded in PO. Finally, as aforementioned, these inhibitory units could have been recorded from fibers from NRT, ZI and APT.

#### *5.3.1.3 Summary of single unit classification*

In summary, different groups of neurons could be identified in the dataset based on waveforms and burst profile as well as the peri-ictal temporal dynamics of burst firing:

1. Putative excitatory units (PB, TB and LB units)
2. Putative inhibitory units

Further analysis of their neural dynamics was carried out on each of these groups separately.

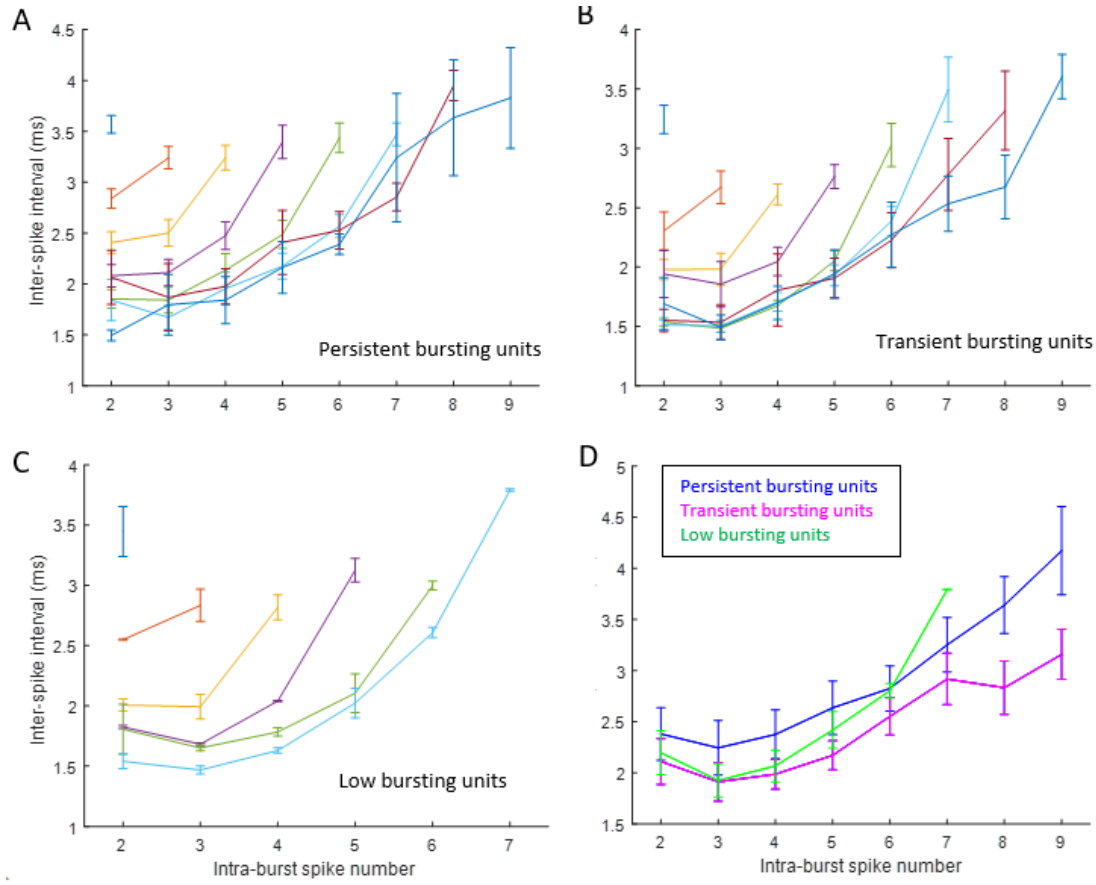


***Figure 5.5. The burst pattern of the three types of excitatory units.***

*The interspike intervals between consecutive spikes for bursts of various lengths are plotted for each type of putative excitatory unit: persistent bursting (**A**), transient bursting (**B**) and low bursting (**C**) units. Plot **D** is the overall burst profile for all 3 types of units, colour coded as insert in **D**.*

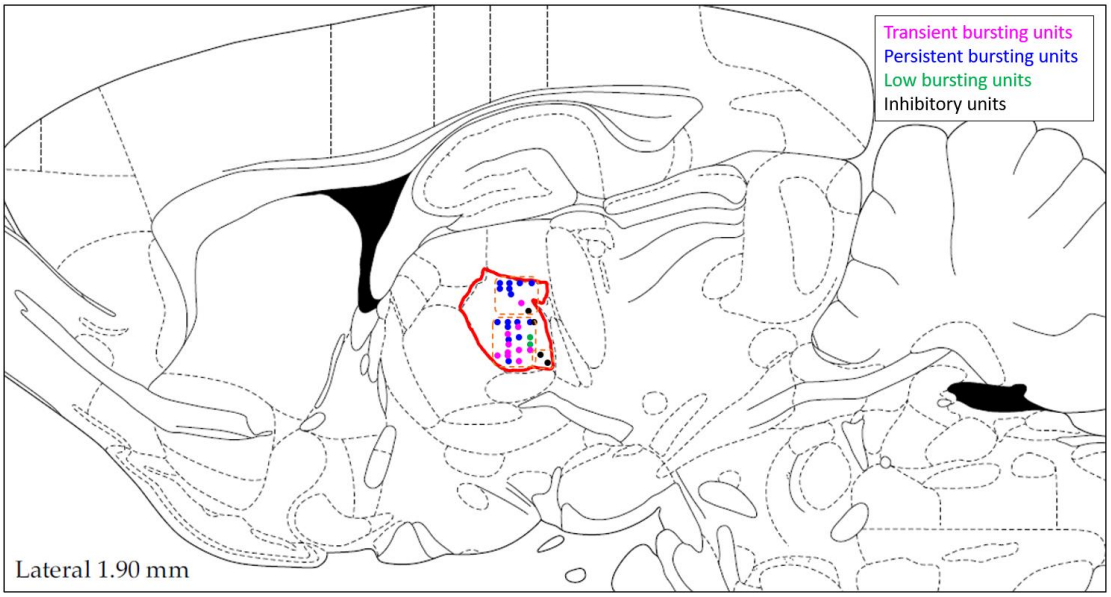


***Figure 5.6. Location of all recorded units in PO.***

*The location of of putative excitatory and inhibitory units as colour coded in insert. Units are depicted as dots over a stereotactic map (Paxinos and Watson, 1998) of a sagittal brain slice (ML: 1.9mm), the plane in which the silicon probes were implanted. Red line highlights the border of PO. Orange dashed lines highlight which units belong to the three different GAERS that form this data set.*

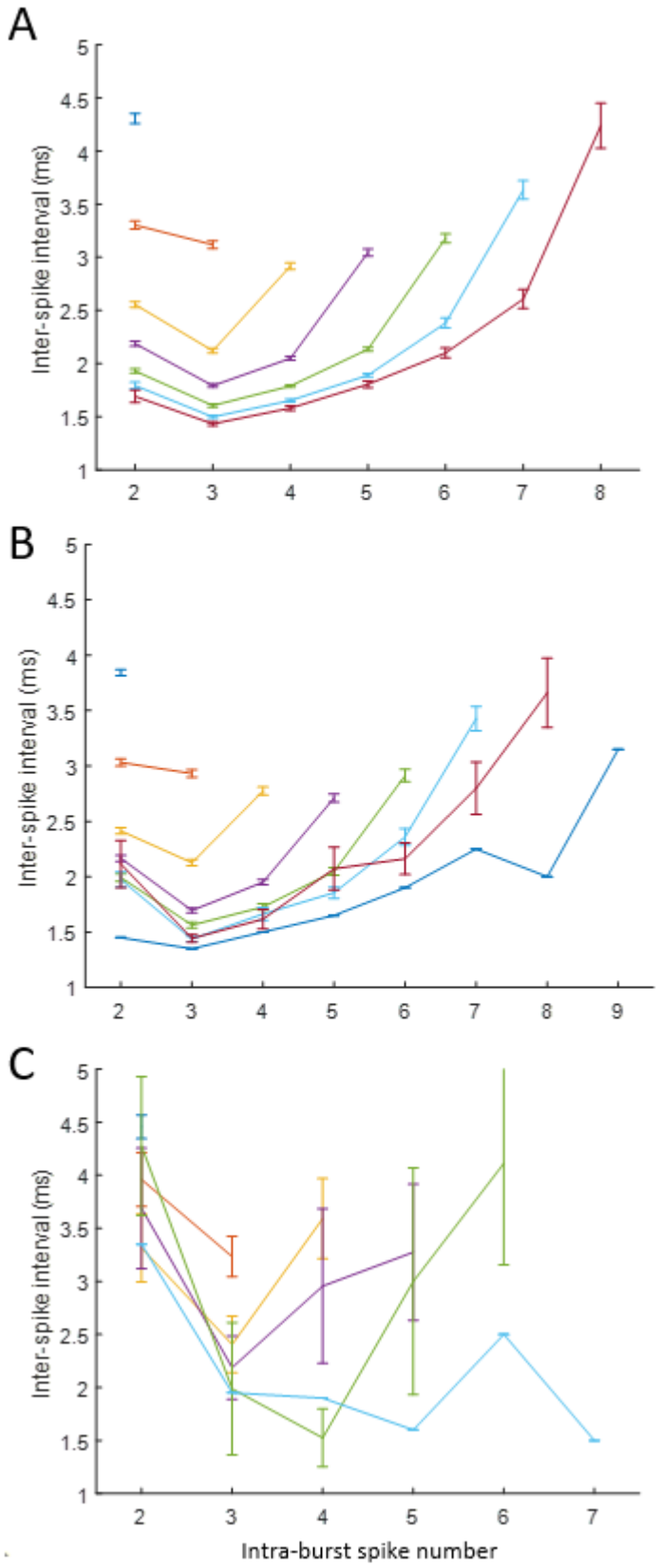


***Figure 5.7. Burst profile of inhibitory units.***

*The interspike interval between consecutive spikes for bursts of various lengths are plotted to demonstrate the burst pattern observed in each inhibitory unit (**A**-**C**). Only 3 of the 4 putative inhibitory units exhibited bursts and therefore only 3 are plotted.*

### 5.3.2 Excitatory units increased burst firing at SWD onset

The neural dynamics of the 15 PB units (during 281 SWD), the 10 TB units (during 182 SWD) and the 2 LB units (during 49 SWD) were aligned to the time of onset and offset of SWD in S1. Relative to S1, there was a SWD onset delay of 0.3 ±0.05s in M1, 0.3 ±0.04s in PO and 0.7 ±0.05s in V1 (similar to those in the dataset described in Chapter 3). The latter time was taken to indicate the full generalisation of AS. Seven time points were selected to evaluate changes in total, tonic and burst firing:

1. Baseline (BL) at 3 sec prior to S1-SWD onset (taken as inter-ictal firing)
2. 0.25s prior to S1-SWD onset, which was the 50% rise time of the transient change in burst firing of TB units at the interictal to ictal transition
3. S1 SWD onset
4. 0.7s after S1-SWD onset, i.e. the average onset delay in V1
5. 3s after SWD onset, when SWD is fully established
6. S1-SWD offset
7. 3s after S1-SWD offset, as the interictal period.

For the entire putative excitatory dataset, the total firing rate significantly decreased ictally (F: 7.6, Pr(F) <0.0001) (*Figure 5.8A)*. Tonic and burst firing also changed significantly over time (F:27.2, Pr(F) <0.0001 and F:40.7 Pr(F) <0.0001, respectively) *(Figure 5.8B,C),* showing a clear switch from tonic to burst firing during AS.

As far as changes of firing within individual unit groups are concerned, the total firing of PB units showed a transient statistically significant reduction from the interictal rate (17.7 ±2 Hz) at 0.25s prior to SWD onset (11.3 ±1.6 Hz, p=0.007) (*Figure 5.9A)*. Total firing rate begun to reduce at -1.7s, initially, the decline was gradual but there was an increase in the rate of change from -0.6s. The minimum total firing rate occurred at -0.4s. After this, there was a sharp small increase with the total firing rate returning to baseline levels by SWD onset. There was a further increase in total firing from 0.5s prior to offset, which reached a slightly elevated level at 0.25s post offset (22.13 ±1.7 Hz), but there was no significant difference between interictal periods before and after the seizure *(Figure 5.9A)*.

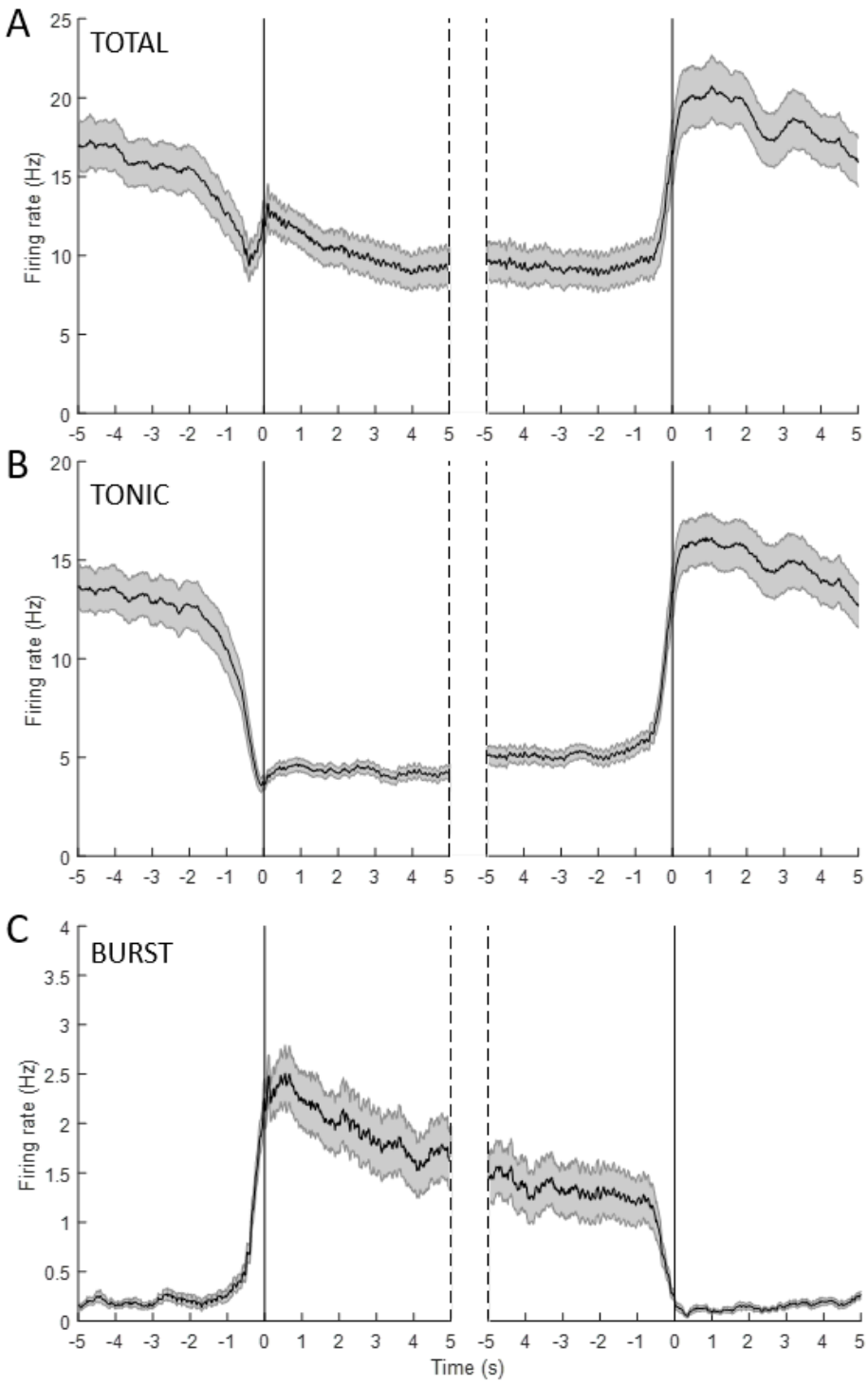


***Figure 5.8. Firing rate changes at SWD onset and offset for all excitatory PO units.***

*Firing rates of all putative excitatory neurons are plotted over time for total (A), tonic (**B**) and burst (**C**) firing. Onset and offset of SWD in S1 are marked by the vertical solid black lines and indicated on the X axis by the left and right 0s. Data are mean (solid line) ± SEM (shadows).*

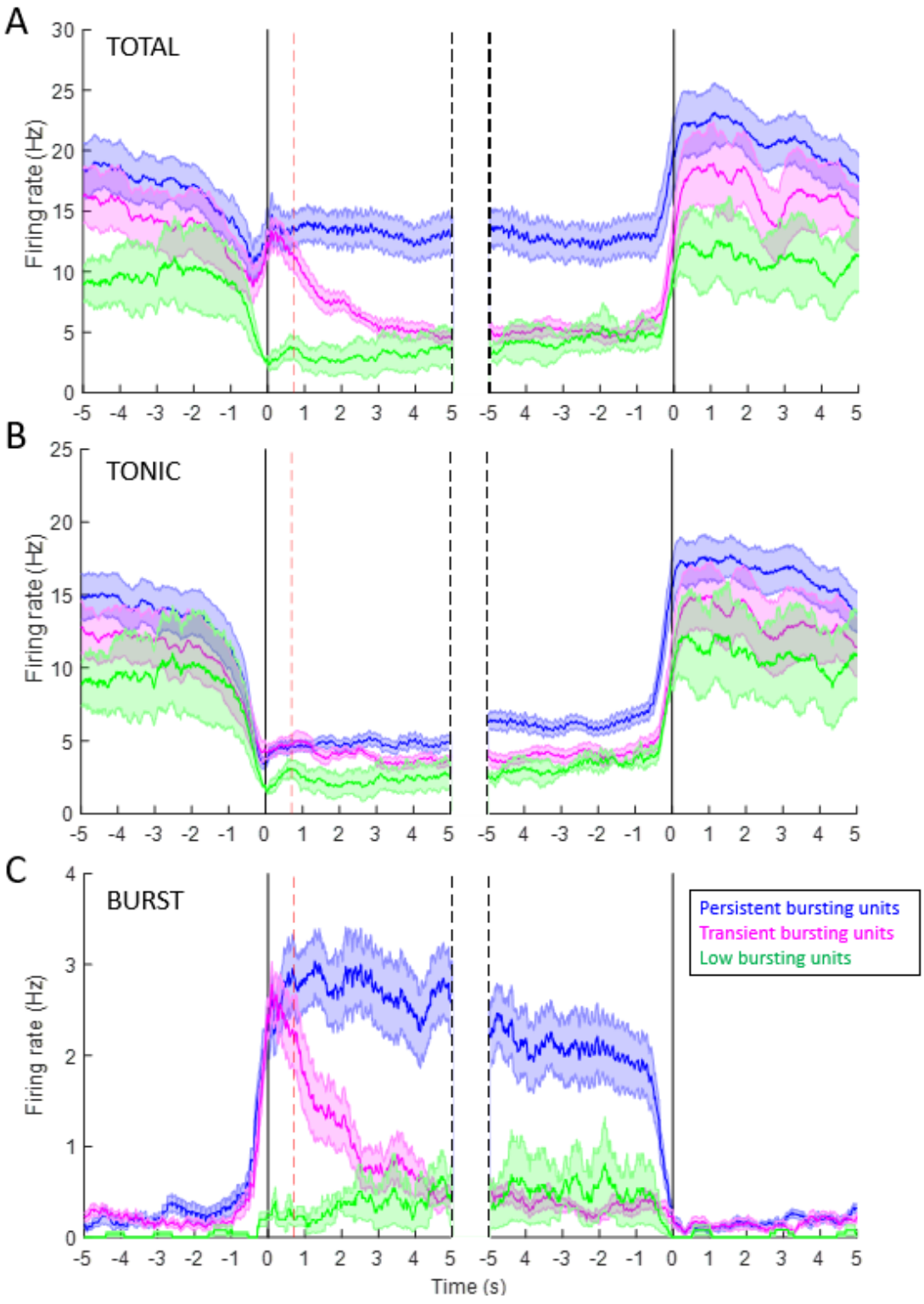


***Figure 5.9. Firing rate changes at SWD onset and offset.***

*Firing rates of excitatory units (colour coded as in inset in (**C**)) are plotted over time for total (**A**), tonic (**B**) and burst (**C**) firing. Onset and offset of SWD in S1 are marked by the vertical solid black lines and indicated on the X axis by the left and right 0s. Red dashed line indicates average V1 onset delay. Data are mean (solid line) ± SEM (shadows).*

On a similar time scale as PB units, there was also a transient reduction in total firing of TB units (*Figure 5.9A)*. There was a gradual reduction from -1.2s with a minimum at -0.4s. After this time, there was a sharp increase in total firing which peaked at 0.08s after SWD onset. The total firing rate then declined again and ictal rate was lower than interictal periods (BL: 14.3 ±2.0 vs 3s: 5.6 ±0.5 Hz, p=0.001). Total firing of TB units quickly returned to BL rates at SWD offset, beginning approximately 0.5s prior to SWD offset and being complete by 0.4s post offset.

The reduction in total firing of LB units begun at -0.6s and reached a minimum at SWD onset (*Figure 5.9A*). This reduction was not transient like the other two neuronal groups. Instead, total firing of LB remained lower than interictal rates (9.6 ±3.5 Hz) throughout the SWD (3s: 2.7 ±2 Hz). From 0.5s prior to SWD offset, the total firing rate quickly returned to baseline levels by 0.2s post offset (*Figure 5.9A).*

The linear mixed model used for statistical analysis did not show any ictal difference between the total firing of the three groups, however, an ANOVA including the firing rate of each group only at 3s after SWD onset showed that PB unit total firing was significantly higher than the other two groups (PB: 13.4 ±1.5 vs TB: 5.6 ±0.5, p=0.002, and LB: 2.7 ±2 Hz, p=0.02).

During the initial reductions in total firing aforementioned, there was a switch from tonic to burst firing in all 3 excitatory populations *(Figure 5.9B,C)*. Regarding PB units, tonic firing started to gradually reduce from -1.5s, and the rate of change increased at -1s and then again at -0.5s, reaching the minimum at -0.08s. The reduction from interictal tonic firing rate (14.4 ±1.5 Hz) was significant at 0.25s prior to onset (5.9 ±10.2 Hz, p<0.0001), an effect that was sustained throughout the SWD (5.05 ±0.5 Hz, p<0.0001) until offset. Tonic firing started to return to baseline at 0.5s prior to offset, which stabilised at 0.2s post offset. The interictal tonic firing after SWD offset (14.1 ±1.6 Hz) was not significantly different to baseline.

The tonic temporal dynamics of TB units were similar to PB units (*Figure 5.9B)*. TB units had a reduction in tonic firing from -1.3s which steadily decreased until 0.1s prior to SWD onset. This reduction was sustained throughout the seizure (interictal: 12.0 ±1.5 vs -0.25s: 5.6 ±1.1 Hz, p=0.001; vs 3s: 3.9 ±0.2 Hz, p<0.0001). At 0.4s prior to offset the tonic firing begun to increase again, and by offset there was no significant difference in tonic firing rate from baseline (12.2 ±2.3 Hz). Post ictal tonic firing

stabilised from 0.4s. Interictal tonic firing after SWD (8.01 ±0.6 Hz) was not significantly different to baseline *(Figure 5.9B)*.

LB units had a reduction of tonic firing from -0.8s, which reached a minimum rate at 0.05s after SWD onset (*Figure 5.9B)*. Although ictal firing rate was reduced compared to inter-ictal rates (Interictal: 9.3 ±13.8 vs -0.25s: 4.5 ±1.8, vs 3s: 2.1 ±1.4 Hz), the change was not statistically significant. Tonic rate started to return to baseline levels at -0.4s and stabilised at 0.2s after offset *(Figure 5.9B).*

While tonic firing reduced the burst firing increased during seizures with a different temporal profile between the groups (F:12.9 Pr>F, <0.0001) *(Figure 5.9C).* PB units increased burst firing from interictal rates (0.2 ± 0.06 Hz) from -0.7s which became significant at 0.25sec prior to SWD onset (1.3 ± 0.2, p<0.0001). Peak burst rate occurred at 0.6s after onset (3 ±0.3 Hz), very close to the time of AS generalisation at 0.7s. The elevated burst rate of PB units was sustained throughout the SWD (3s: 2.7 ±0.4 Hz, p<0.0001). Burst firing began to sharply decline 0.5s prior to offset and by SWD offset had returned to baseline levels (0.4 ±0.09 Hz).

TB units initially increased burst firing from -1s, which was significantly different from interictal burst rates (0.1 ±0.02 Hz) at 0.25s prior to SWD onset (0.8 ±0.2Hz, p=0.004) *(Figure 5.9C)*. Peak burst rate occurred 0.1s after SWD onset and was still higher than baseline at 0.7s after onset (2.2 ±0.4 Hz, p<0.00001), i.e. time of AS generalisation. Burst rate declined by 50% and 75% after 1.5s and 2.9s, respectively. Ictal rates (0.7 ±0.2 Hz) were not significantly different to interictal baseline (0.7 ±0.2 Hz). There was a small final reduction in burst firing rate at 0.2s prior to offset.

Burst firing of LB units increased from the interictal period (0.04 ±0.04 Hz) at -0.3s to a stable rate of 0.3 ±0.3 Hz during ictal periods, but this was not significant *(Figure 5.9C)*. Burst firing rate returned to interictal levels from 0.5s prior to SWD offset. Comparison of ictal burst firing rates between the three unit groups showed that it was significantly higher in PB units (2.7 ±0.4 Hz) compared to TB (0.7 ±0.2 Hz, p<0.0001) and LB units (0.3 ±0.3 Hz, p=0.001). Additionally, at S1 SWD onset the burst firing rate was significantly lower in LB units (0.2 ± 0.1 Hz) than PB units (2.0 ±0.2 Hz, p=0.01) and TB units (2.0 ±0.2 Hz, p=0.01), but similar in these two groups.

In summary, prior to S1 SWD onset there was a shift from tonic to burst firing in all 3 types of units. PB units had a significant increase in burst firing and decrease in tonic

firing at SWD onset, which lasted throughout the ictal period. However, TB units only had a transient increase in burst firing that lasted about 2s, with a sustained decrease in tonic firing, this resulted in an overall reduction of total firing. Finally, in LB units there was a visible decrease in tonic firing and increase in burst firing but ictal burst rates was lower relative to other unit types. Significant changes over time in this unit group was not found, likely due to the small sample size.

### 5.3.3 Excitatory units fired more rhythmically during ictal periods.

Firing rhythmicity within and between simultaneously recorded units was assessed with auto- and cross-correlograms. Auto-correlograms of spike trains revealed rhythmic firing at 7 Hz in most units during ictal but not inter-ictal periods *(Figure 5.10).* This feature was evident in all PB units *(Figure 5.10A),* both LB units *(Figure 5.10D)* and most TB units *(Figure 5.10B),* though 3 of 10 TB units had little rhythmicity during ictal periods *(Figure 5.10C)*.

All possible pairs of PB units (n=14) showed clear synchronous activity during ictal periods, as shown by correlation peaks at time 0 *(Figure 5.11A).* However, this was not true for the available TB pairs (n=2) *(Figure 5.11B).* The firing of PB-TB (n=2) and PB-LB (n=2) unit pairs was not strongly correlated *(Figure 5.11C,D),* as was that of the only LB-TB unit pair (n=1) *(Figure 5.11E).*

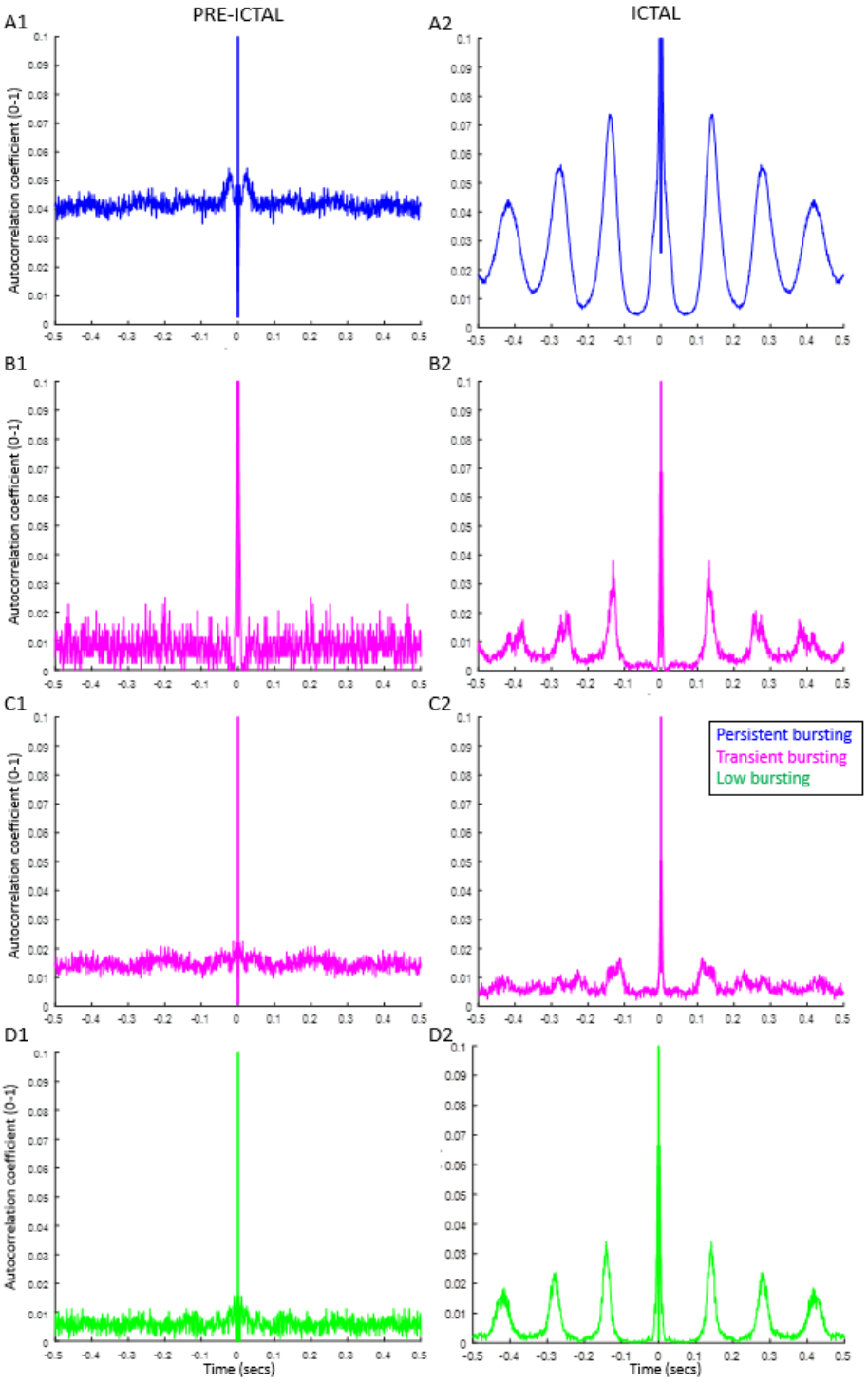


***Figure 5.10. Firing auto-correlation of the three putative excitatory groups during ictal and interictal periods.***

*Auto-correlograms of unit spike times during pre-ictal (left) and ictal (right) periods. Plots show an example of a PB unit (**A**), a TB unit that showed rhythmicity (**B**) and one that did not (**C**) and a LB unit (**D**).*

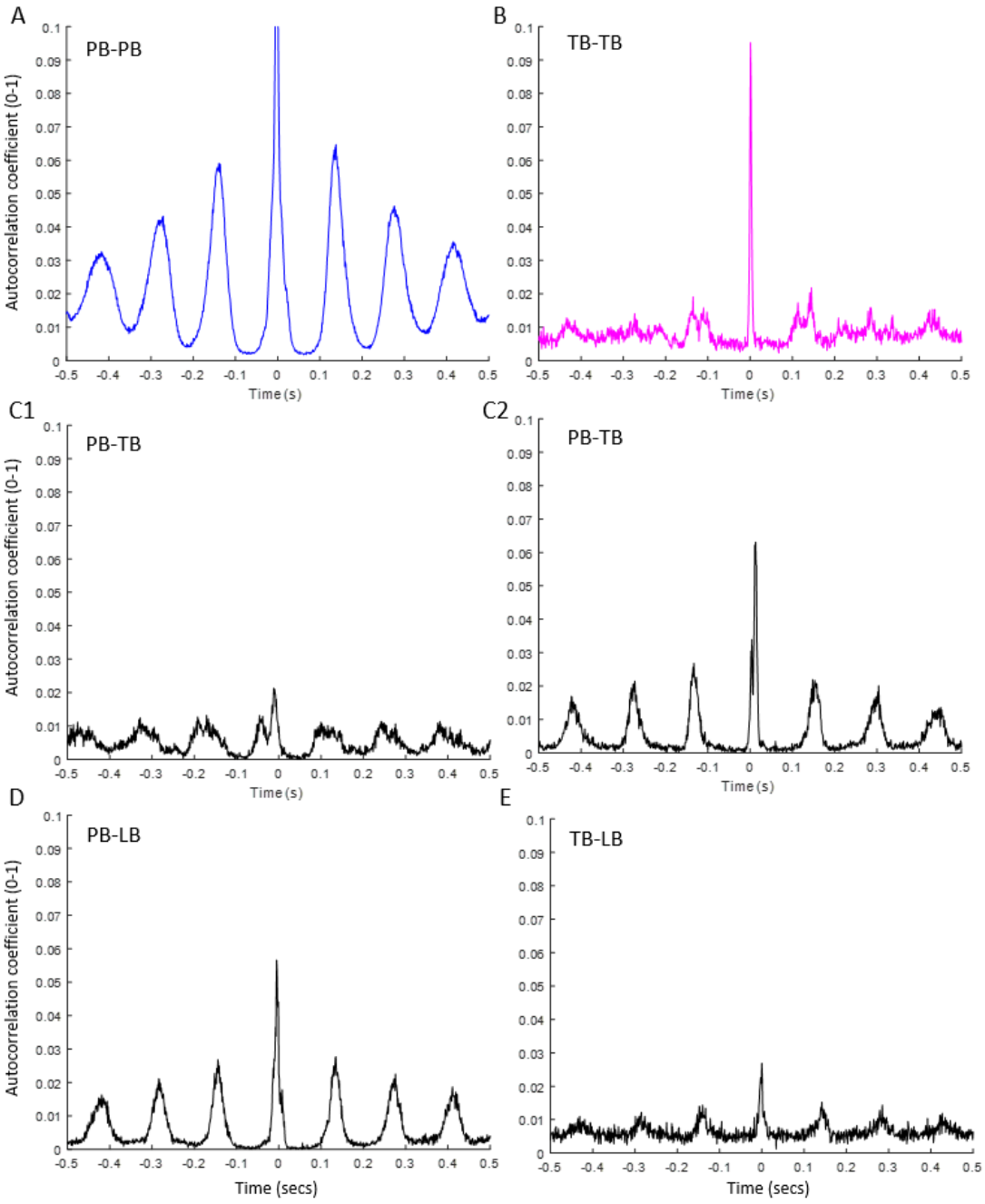


***Figure 5.11. Firing cross-correlations of pairs of PB, TB and LB units during ictal periods.***

*Representative examples of firing cross-correlations between simultaneously recorded PB units (**A**), TB units (**B**), two PB-TB pairs (**C**), a PB and a LB unit (**D**) or a TB-LB unit pair (**E**).*

### 5.3.4 Excitatory units did not fire in every SWC cycle.

To understand how total, tonic and burst firing contributed to each cycle of the SWD, the prevalence of each firing type at the SWC level was calculated. These measurements were made not only during the whole seizure (*Figure 5.12B*) but also during the first second of ictal activity (*Figure 5.12A*) when TB units showed their characteristic transient increase in burst firing.

As a whole population, during the first second of SWD, the prevalence of burst, tonic or action potential silence at each SWC was approximately equal (burst: 33.7 ±3.2, tonic: 36.8 ±2.1, silence: 32.9 ±3.6%) (*Figure 5.12A*). However, throughout the seizure tonic firing became dominant (49.0 ±3.2%), followed by action potential silence (35.8 ±4.4%) then burst activity (20.1 ±3.3%) (*Figure 5.12B*).

During the first second of SWD *(Figure 5.12A)*, approximately 30% of SWCs in PB and TB neurons had no associated spikes (PB: 27.4 ±4.5%, TB: 32.8 ±3.5%). The rest of the SWCs contained an almost equal amount of tonic and burst firing in both PB (37.9 ±4.6 and 39.9 ±2.7%, respectively) and TB units (33.3 ±2.6 and 32.8 ±3.50%, respectively). The prevalence of each firing type in LB units was highly variable (tonic: 23 ±7.4%, burst: 4.3 ±3.6%), but these units showed no firing during the vast majority of SWCs (73.74 ±10.0%) *(Figure 5.12A)*.

When analysing the whole seizure *(Figure 5.12B)*, tonic firing of PB units occurred in 53.9 ±4.1% of SWCs, while burst firing only occurred in 30.4 ±4.4%, and the remaining (24.2 ±5.7%) of SWCs had no associated spike. For TB units, burst firing was only present in 8.7 ±1.6% of SWCs, with the remaining SWC containing an approximately equal amount of tonic firing (44.4 ±4.7%) and action potential silence (47.4 ±5.8%). For both LB units, most SWCs (63.4 ±10%) had no spike. There was moderate tonic firing (29.0 ±7.4%) and minimal burst firing (3.1 ±3.6%) *(Figure 5.12B)*.

### 5.3.5 Only PB units burst before S1 SWC-spike

To understand when units fired in relation to the ongoing SWD, S1 SWC-spike triggered time histograms were computed separately for total, tonic and burst firing *(Figure 5.13)*. Only the first spike (i.e. closest to SWC-spike) of each firing type was considered to get a more accurate idea of when PO are first / last activated before / following the SWC-spike, respectively.

The first tonic spike of PB and TB units occurred both before and after the SWC-spike, whereas LB unit tonic spikes occurred after (*Figure 5.13*). First tonic spikes of PB units occurred maximally (0.02 ±0.003 tonic spikes/ms) 1ms before the SWC-spike but the peak was spread across negative and positive time lags with the 50% maximum between -8ms and +9ms with respect to the SWC-spike. TB unit tonic firing had 2 peaks, one larger (0.025 ±0.007 tonic spikes/ms) at 3 – 6ms and a smaller one (0.014 ±0.008 tonic spikes/ms) at 3 – 1ms prior to the SWC-spike. Finally, LB tonic spikes occurred after the SWC-spike with a peak (0.022 ±0.01 tonic spikes/ms) at 4 – 6ms and a 50% maximum at 1 – 10ms after the SWC-spike (*Figure 5.13A*).

Burst firing in PB units occurred before other unit types *(Figure 5.13B)*. PB units had a peak burst rate (0.014 ±0.004 bursts/ms) 6 - 8ms prior to the SWC-spike, with the 50% maximum occurring 13ms prior to SWC-spike (*Figure 5.13B).* In contrast, both TB and LB units had their peak burst rate after the S1 SWC-spike *(Figure 5.13B).* The TB peak (0.005 ±0.001 bursts/ms) occurred between 2 - 3 ms after the SWC-spike, with a 50% maximum at 1.5ms prior to it. LB had a maximum (0.01 ±0.008 bursts/ms) at 5ms after the SWD-spike, with a 50% peak 1.5ms prior to the SWC-spike. When all spikes were considered, PB cells peak at 0s (0.05 ± 0.01 spikes/ms), with 50% maximum from -4 to 4s. Regarding TB units, there was a peak from 2 – 5ms, (0.03 ±0.015 spikes / ms) and with a 50% maximum from -3 to 9 ms. Finally, LB units peaked at 4 – 6ms (0.04 ±0.02 spikes/ms), with a 50% maximum from 1 – 9.5ms.

As my work was focusing on the role of PO in the generalization of SWD, their firing pattern relative to the V1 SWC-spike was also studied *(Figure 5.14).* Relative to V1 SWC-spike, there was a peak burst rate of PB units at -24 – -18ms (0.007 ±0.002 bursts/ms) with a 50% peak from -36 – 4ms. PB peak tonic rate occurred at -10ms (0.009 ±0.0005 spikes/ms) with a 50% maximum at -25 – 7ms. Both TB and LB units had a peak burst rate at -11ms and a peak tonic rate at -13ms.

To summarise, the burst firing of all excitatory units showed a higher time-locking to the SWC than tonic firing, as indicated by their narrower peaks. PB units fired bursts before the S1 SWC-spike, whereas TB and LB units fired after the S1 SWC-spike. Firing rates were also checked relative to V1 SWCs, which shifted times by 12ms, consistent the 12±2ms V1 to S1 SWC-spike delay described in section 3.3.4. Spike rates relative to V1 occurred less precisely than to S1, as indicated by their wider peaks.

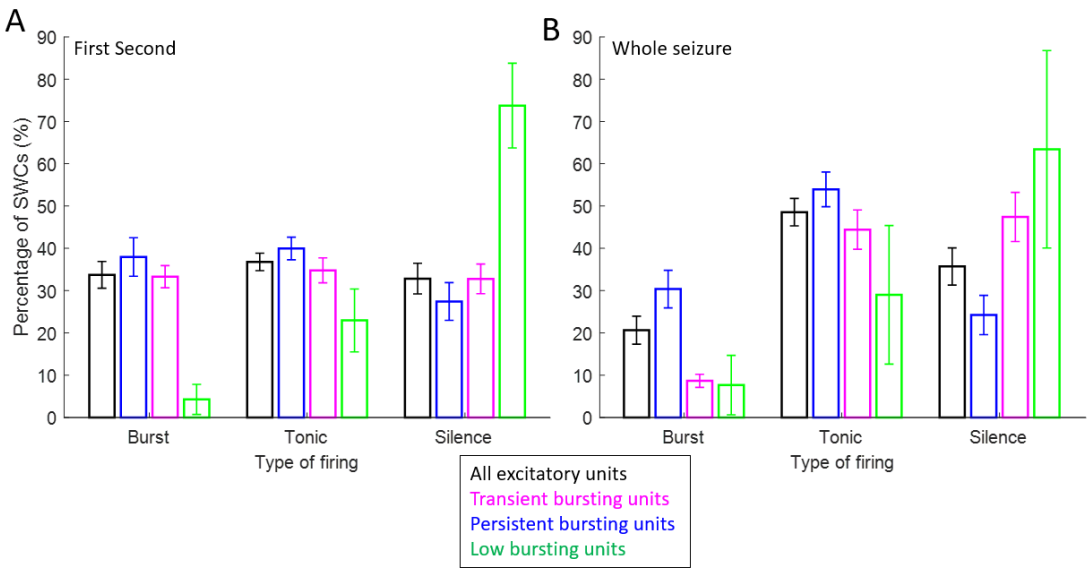


***Figure 5.12. Prevalence of tonic and burst firing and action potential silence in individual SWCs.***

*The percentage of SWCs that were associated with tonic firing, burst firing, or action potential silence of excitatory units (colour coded as in inset) was calculated for all SWCs within the first second of SWD (**A**), or for the whole SWD (**B**).*

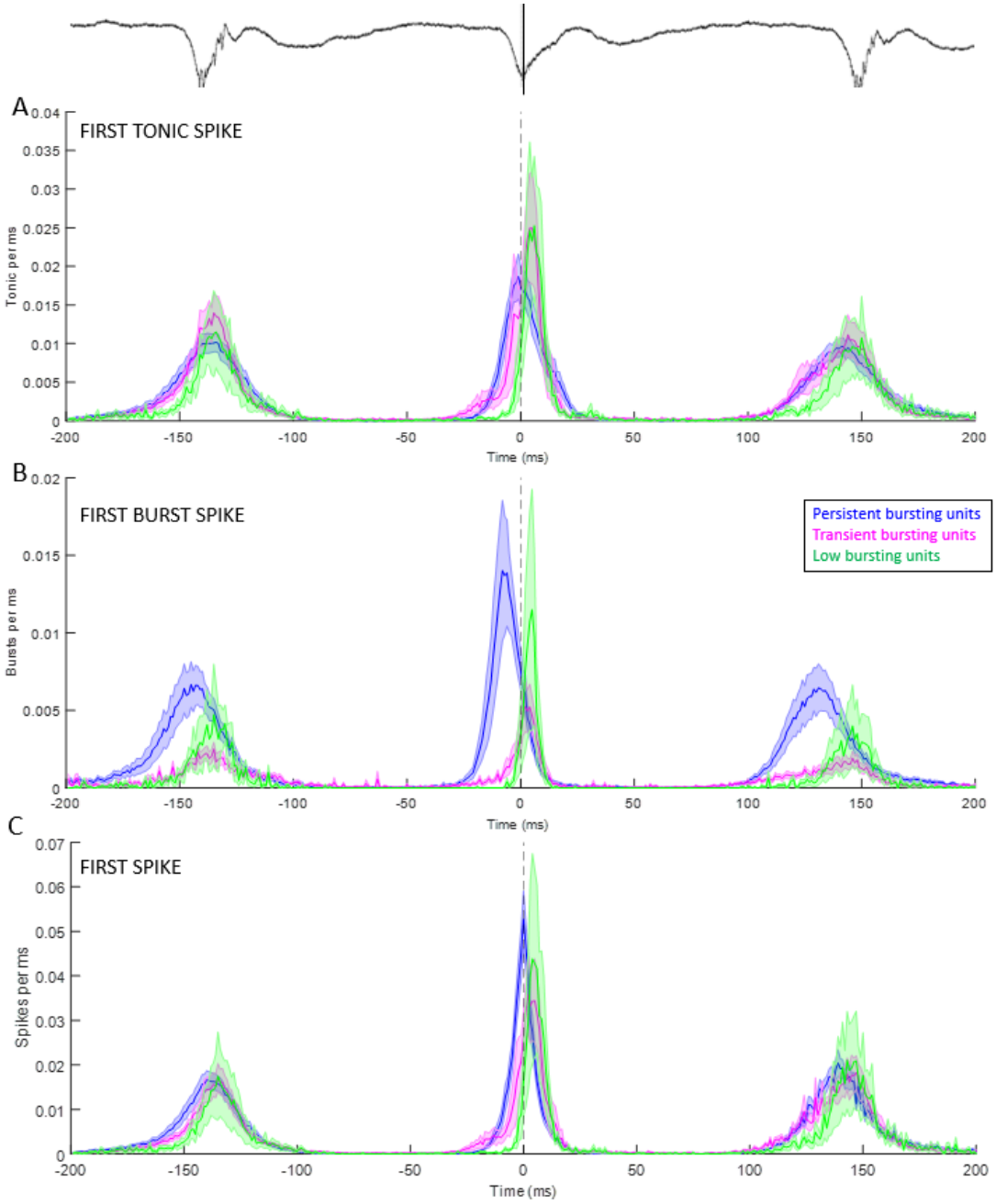


***Figure 5.13. S1 SWC-spike triggered time histogram of unit spikes to S1 SWC-spikes.***

*Plots show S1 SWC-spike triggered time histogram of the first spike of the tonic (**A**), burst (**B**) or total firing (**C**) relative to the peak of the SWC-spike in S1 (time 0, vertical dashed lines in plots and S1 LFP trace at top) for excitatory units (colour coded as in the inset in (**B**)). Lines show the mean firing per ms (solid lines) ± SEM (shadows)*

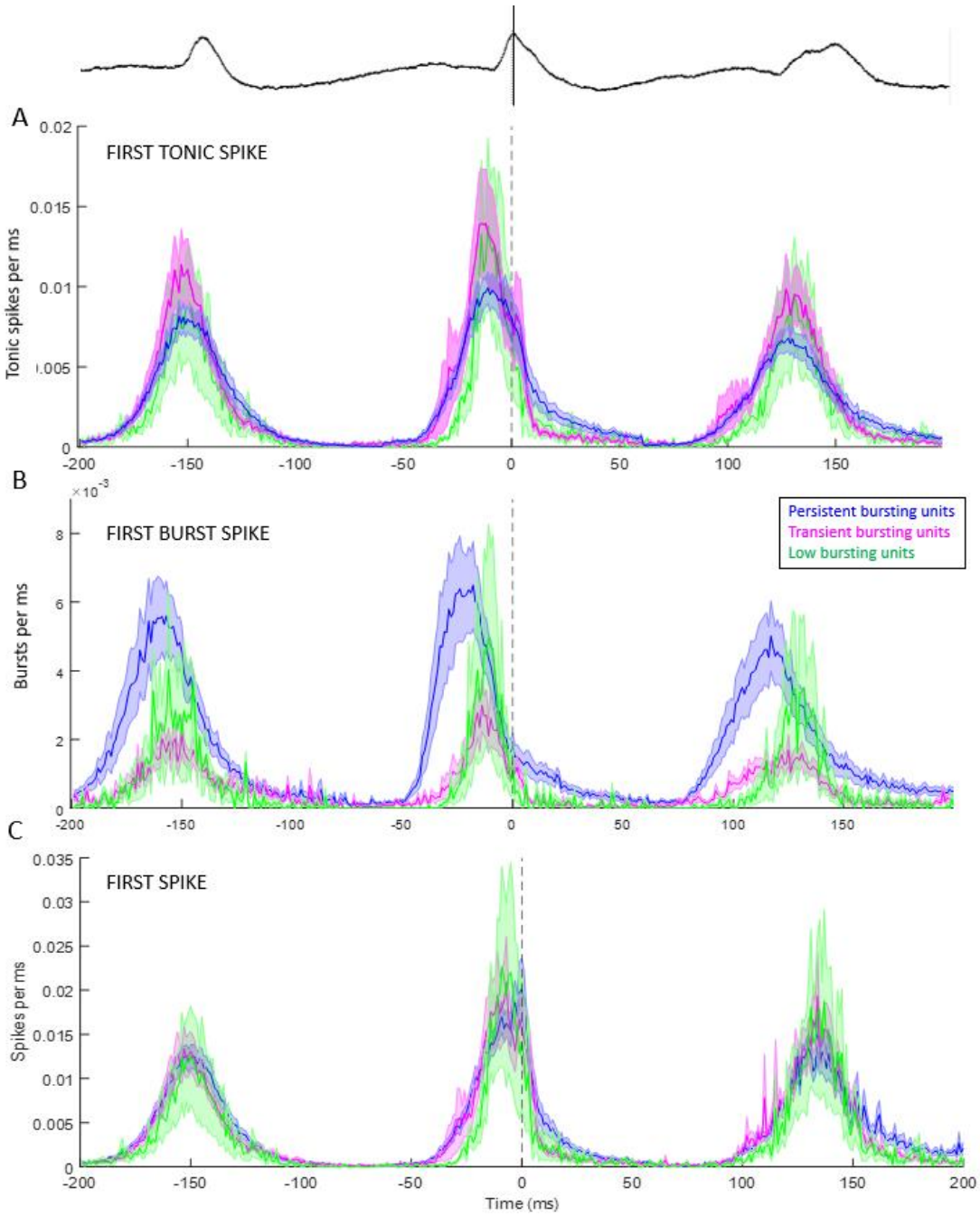


***Figure 5.14. V1 SWC-spike triggered time histogram of PO excitatory unit firing.*** *Plots show V1 SWC-spike triggered time histogram of the first spike of tonic (**A**), burst (**B**) or total firing (**C**) relative to the peak of the SWC-spike in V1 (time 0, vertical dashed lines in plots and V1 LFP trace at top) for excitatory units (colour coded as in the inset in (**B**)). Lines show the mean firing per ms (solid lines) ± SEM (shadows)*

### 5.3.6 Decreased burst firing and increased tonic firing in PB neurons during SWD-breaks in V1

V1 SWD-breaks occurred at a rate of 0.3 ±0.01 events/ictal second and had an average duration of 0.8 ±0.04s, similar to those reported in Chapter 3. V1 SWD-breaks were included for analysis if they were separate from other events by at least 3s, instead of the usual 5s to maintain a good sample size. Since V1 SWD-breaks occurred on average every 3s, having a 5s peri-SWD-break period would result in many samples being excluded from the analysis. This criterion was fulfilled by 182, 89 and 22 V1 SWD-breaks for 10 PB, 9 TB and 2 LB units, respectively. To investigate the firing dynamics of these neurons during V1 SWD-breaks the following time points were used:

1. BL: 2s prior to the onset of V1 SWD-breaks
2. 0.25s prior to onset
3. onset
4. 0.8s (average duration of a V1 SWD-break).

As shown in Figure 5.15, changes in firing during SWD-breaks in V1 were only observed in PB neurons, which were then analysed with a repeated measures ANOVA. The burst firing rate of PB units begun to decrease from 1s before the SWD-break onset. This reduction was significant before onset (BL: 2.3 ±0.3 vs 0.25s: 1.4 ±0.2 Hz, p=0.03) and reached a maximum reduction at -0.08s (1.2 ±0.2 Hz) *(Figure 5.15C)*. The burst rate at onset was significantly lower than baseline (1.3 ±0.2 Hz, p=0.01). The burst rate returned to ictal levels 0.8s after onset (2 ±0.4 Hz), i.e. the average duration of V1 SWD-breaks.

As burst firing decreased, tonic firing simultaneously increased in PB units. The increase begun at -0.9s and peaked exactly at the time of V1 SWD-break onset, by which time the change was significant (BL: 5.0 ±0.7 vs onset: 7.2 ±1.1Hz, p=0.03) *(Figure 5.15B)*. Tonic firing had returned to baseline rates at 0.6s after onset (5.3 ± 0.6 Hz), slightly before the end of V1 SWD-breaks. As the changes in burst and tonic firing of PB units occurred simultaneously, no changes were observed in the total firing rate of PB units during V1 SWD-breaks *(Figure 5.15A)*.

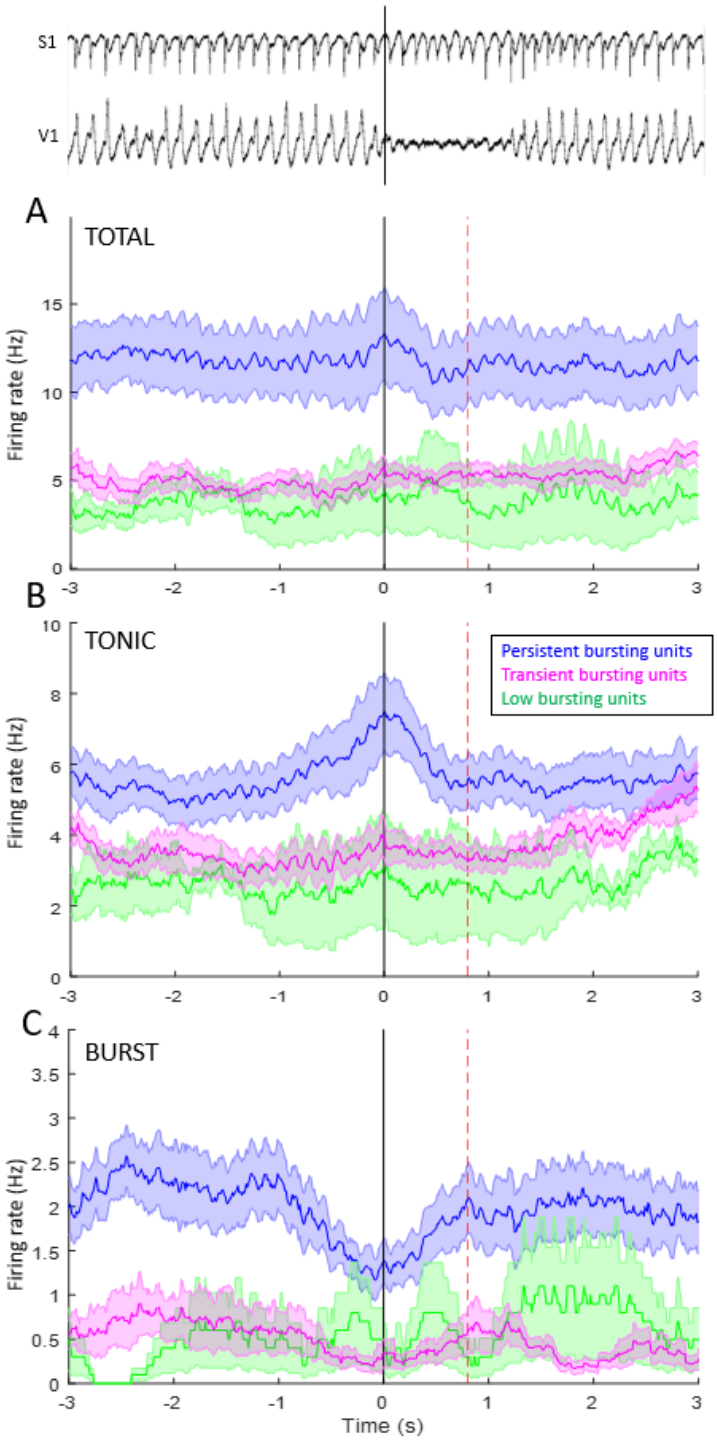


***Figure 5.15. PB units were the only excitatory neurons to show firing rate changes during V1 SWD-breaks.***

*Firing rates are plotted over time for total (**A**), tonic (**B**) and burst (**C**) firing for the three groups of putative excitatory PO units (colour coded as in the inset in (**B**)), at V1 SWD-breaks (see representative LFP in S1 and V1 at the top of the panels), as denoted by the vertical black line. Red dashed line indicates the average duration of a V1 SWD-break. Firing rates are plotted as mean (solid line) ±SEM (shadows).*

### 5.3.7 Firing rate changes during S1-only and S1+M1-only SWD

S1-only SWD and S1+M1-only SWD occurred in 10 of 27 recordings sessions at a rate of 1.7 ±0.4 and 1.1 ±0.4/hour, respectively, with an average duration of 1.6 ±0.3 and 1.5 ±0.2s, respectively. Five PB units were recorded during 29 events, 5 TB units during 40 events and 2 LB units during 10 events. Firing activity at the following time points was extracted for quantitative analysis:

1. BL: 2s prior to onset
2. onset
3. 1s after onset
4. 1.5s after onset (average duration of the events)

PB units had two peaks of burst firing, one (2.2 ± 0.7Hz) at onset and another one (2.0 ±1.0Hz) 0.5 s after onset, whereas TB units had a singular peak (1.7 ±0.6Hz) at onset *(Figure 5.16C).* However, these rates were not significantly different to those of the respective baseline (PB: 0.3 ±0.2Hz, TB: 0Hz). No burst firing was observed in LB units during S1-only and S1+M1-only events.

At time of onset, there was a significant decrease in tonic firing only in the PB units (baseline: 14.4 ±1.8; onset: 4 ± 0.6Hz, p=0.01) *(Figure 5.16B).* There was indication of a decrease of tonic firing in TB and LB units at the onset of S1-only SWD and S1+M1-only SWD (TB: 4.1 ±0.9, LB: 4.1 ±2.1Hz), but these changes did not differ significantly from the baseline activity (TB: 10.4 ±1.3, LB: 12.16 ±5.8Hz) *(Figure 5.16B).* No changes in total firing were observed in any unit group *(Figure 5.16A)*.

To explore the differences between successful and non-successful generalisation of SWD, the firing rate of all excitatory units at SWD onset was superimposed onto firing rates at the onset of S1-only and S1+M1-only events *(Figure 5.17).* Total firing rate was less stable during interictal period of S1-only and S1+M1-only events compared to SWD onset, as shown by its greater fluctuations *(Figure 5.17A).* Despite this, there was indication that the maximum reduction occurred later in S1-only and S1+M1-only events (-0.25s) than at SWD onset (-0.5s). The increase in burst firing and decrease in tonic firing occurred at the same time for both events *(Figure 5.17B,C)*.

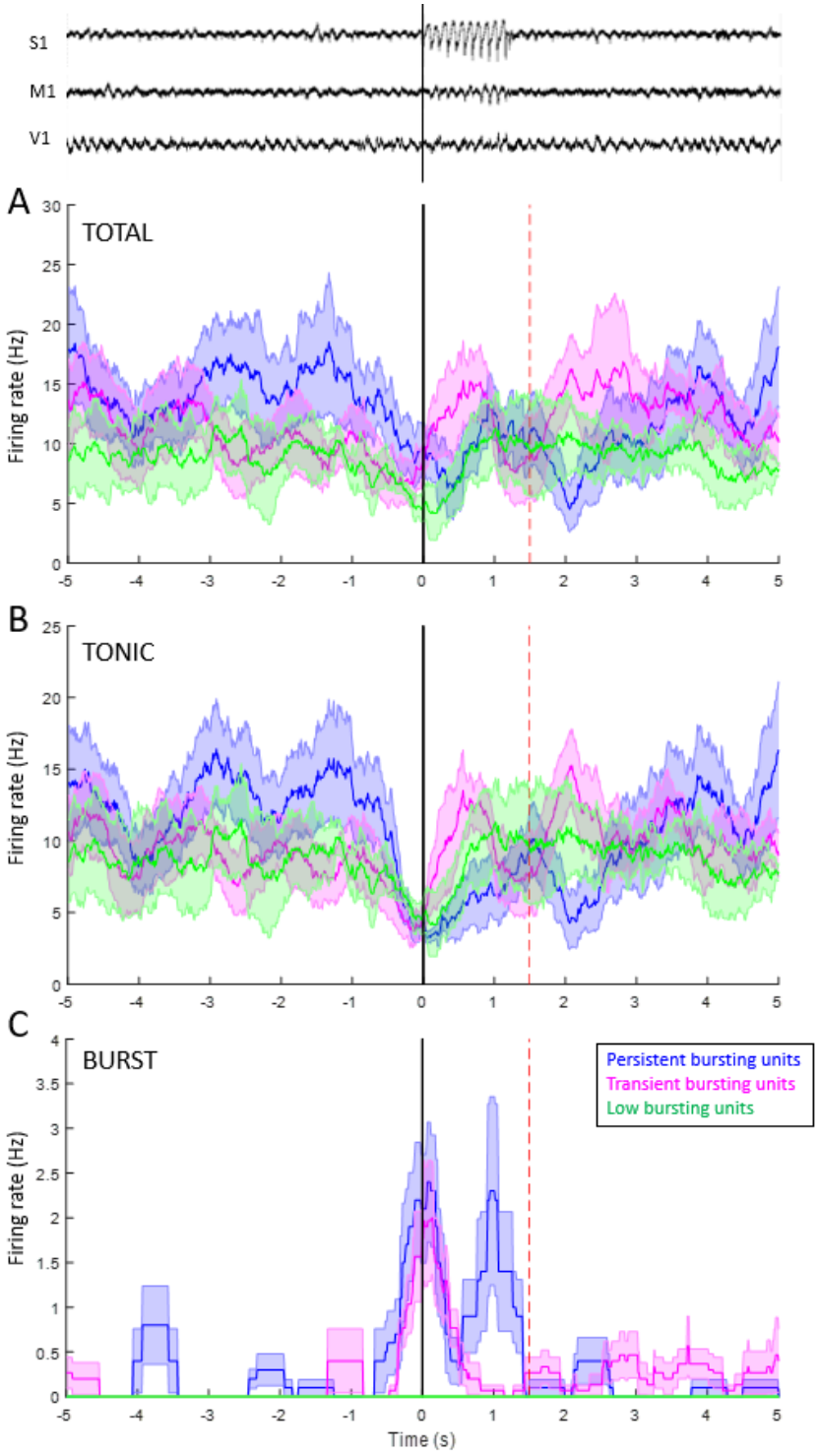


***Figure 5.16. Firing rate changes during S1-only and S1+M1-only SWD.***

*Firing rates are plotted over time for total (**A**), tonic (**B**) and burst (**C**) firing for the three groups of putative excitatory PO units (colour coded as in the inset in (**B**)) during S1-only and S1+M1-only SWD (see representative LFP traces at the top of the panels). Onset of event is denoted by vertical solid black line. Red dashed line indicates the average duration of these events. Firing rates are plotted as mean (solid line) ±SEM (shadows).*

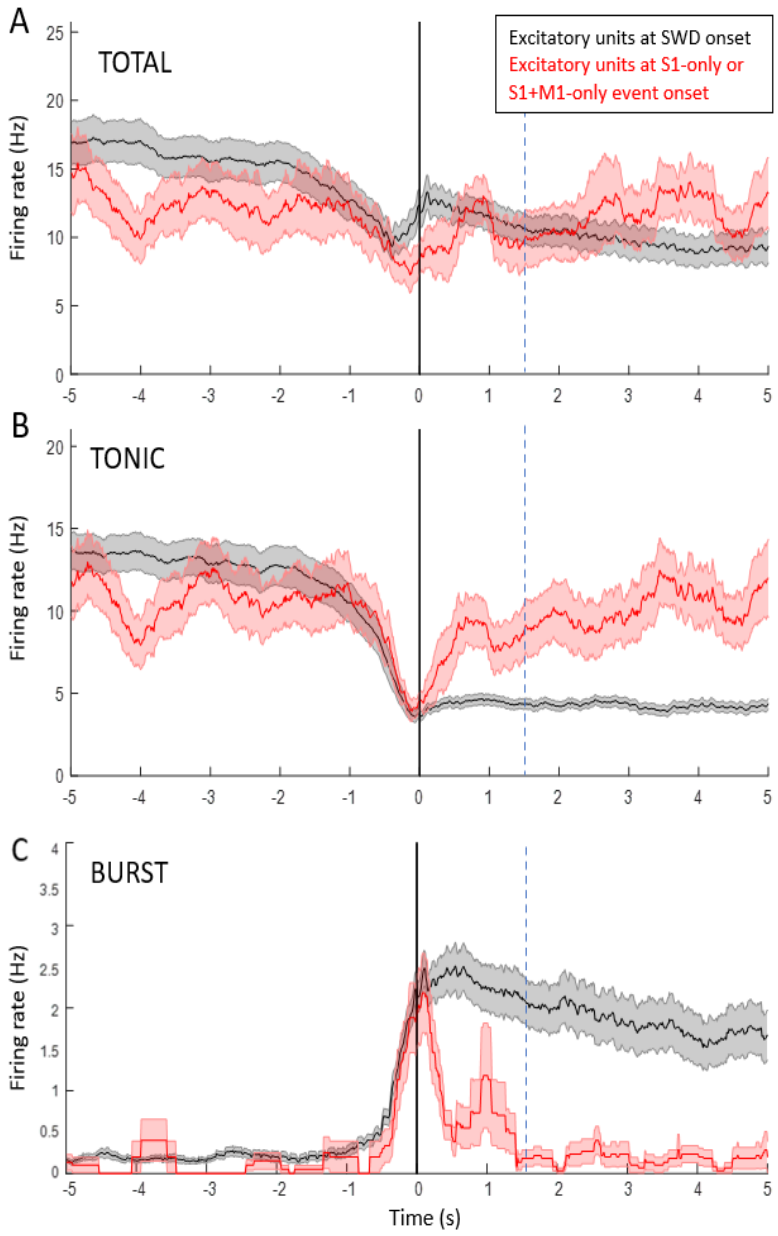


***Figure 5.17. Firing rate changes at onset of generalized SWD compared to S1-only and S1+M1-only SWD.***

*Firing rates are plotted over time for total (**A**), tonic (**B**) and burst (**C**) firing all putative excitatory neurons at the onset of S1-only and S1+M1-only SWD (red) or SWD onset (black), as denoted by vertical solid black line. Blue dashed line indicates the average duration of these events. Firing rates are plotted as mean (solid line) ±SEM (shadows).*

When individual groups were analysed separately, differences of total firing for PB and TB units were hard to distinguish due to unstable baseline during S1-only and S1+M1-only events *(Figure 5.18A1,B1).* Despite this, for PB units there was indication of a later maximum reduction in total firing in S1-only and S1+M1-only events (+0.5s) than at SWD onset (-0.5s) *(Figure 5.18A1).* LB units had a similar interictal total firing rate in both scenarios where the maximal reduction occurred at the same time *(Figure 5.18C1)*. At onset of S1-only and S1+M1-only SWD, total firing was slightly higher (4.7 ±0.9 Hz) than at SWD onset (2.8 ±0.2 Hz).

The tonic and burst firing dynamics of PB and TB units were similar between the two scenarios (*Figure 5.18A2,A3,B2,B3*). In these cases, the maximum change occurred at the same time. In TB units the burst peak was slightly lower at S1-only and S1+M1-only SWD onset (2.0±0.6 Hz) compared to SWD onset (2.8 ±0.3 Hz) (Figure 5.18B3), but this was not significant. For LB units only the tonic firing change was temporally matched between SWD onset and S1-only and S1+M1-only SWD onset (Figure 5.18C1). On the other hand, LB burst activity, which increased during SWD onset, was completely absent during S1-only and S1+M1-only events (Figure 5.18C).

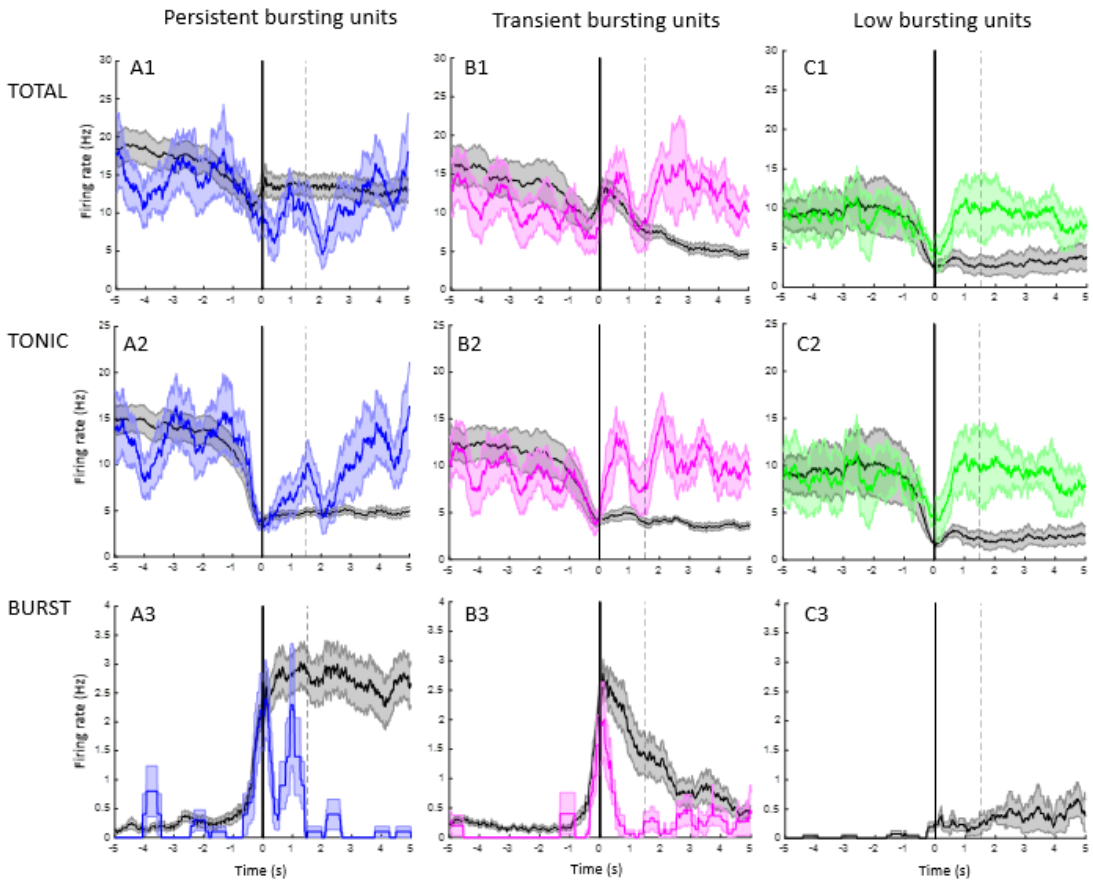


***Figure 5.18. Firing rate changes at seizure onset for generalized SWD compared to S1-only and S1+M1-only SWD for different groups of putative excitatory units.***

*Firing rates (total, tonic and burst **1-3**) are plotted over time for the three groups of putative excitatory PO units (columns labelled at the top, **A-C**). Firing rates are aligned to SWD onset (black) or S1-only and S1+M1-only SWD onset (colours), as denoted by vertical solid black line. Black dashed line indicates the average duration of S1-only and S1+M1-only events. Firing rates are plotted as mean (solid line) ±SEM (shadows).*

### 5.3.8 Inhibitory units had varied activity during SWD

Four inhibitory units were classified based on waveforms and burst profiles and in theory can be from PO inhibitory units of from incoming fibres from NRT, ZI or APT (details in 5.4.2). Two of the four putative neurons were presented together as they behaved similarly while the remaining two units are illustrated individually as their firing dynamics were different. The two cells (total 16 SWD) *(blue line in Figure 5.19)* that were grouped together exhibited a switch from tonic to burst firing at seizure onset. Tonic firing reduced from 13.6 ±2.5 Hz to 5.2 ±1.1 Hz and burst firing increased from 0.4 ±0.1 Hz to 2.13 ±0.6 Hz (values taken at -3 and 3s relative to onset). This change was sustained throughout the seizure with no net change in total firing.

One unit *(green line in Figure 5.19)* had a transient peak in tonic (14.7 ±2.1 Hz) and total (14.4 ± 3 Hz) firing at 0.5s after onset (SWD=8) and relatively little total ictal firing (1.8 ±0.5 Hz). The remaining unit *(red line in Figure 5.19)* had a gradual decrease in tonic and total firing from interictal levels (total: 32.3 ±2.5, tonic 26.3 ±2.6 Hz) that started 3s before SWD onset (SWD=8). The maximum reduction was at -0.2s (total: 16 ±1.1, tonic: 15 ±0.8 Hz) and just after onset, the rate returned to interictal levels. Both the red- and green-coloured units expressed negligible burst activity throughout.

During V1 SWD-breaks, one unit (*green line in Figure 5.19),* like at SWD onset, had a transient increase in total (9.5 ± 1.4 Hz) and tonic (9.7 ± 1.8 Hz) firing 0.1s after the onset of V1 SWD-breaks (SWD-breaks=41), with negligible burst firing throughout. For the units that exhibit bursts, burst firing decreased at onset of V1 SWD-breaks (pre-break max: 4.8 ±1.6, min: 0.8 ±0.5 Hz) (n=12) *(blue line in Figure 5.20).* Finally, the cell with no net change in total firing during seizure did not exhibit any alterations in firing rate during V1 SWD-breaks (SWD-breaks=32) *(red line in Figure 5.20)*.

S1-only and S1+M1-only events occurred while 3 of the 4 units were recorded. The two cells that had negligible bursts during seizures also did not burst during these events *(green and red lines in Figure 5.21)*. One of these cells had a minimum total and tonic firing rate at 1.4s after S1-only and S1+M1-only SWD (total min: 4.7 ±0.5 Hz) (events=7), which is the average duration of these events. In contrast, the other unit began to increase its total and tonic firing after event onset (events =3) (total max: 12.65 ±4.8 Hz) and returned to baseline (4 ±2.1 Hz) at +4.5s *(green line in Figure 5.21)*. The remaining cell had a peak burst firing rate at the time of event onset (5 ±2.1 Hz) (n=1), while tonic firing rate was low (4.1 ±0.5 Hz) *(blue line in Figure 5.21)*.

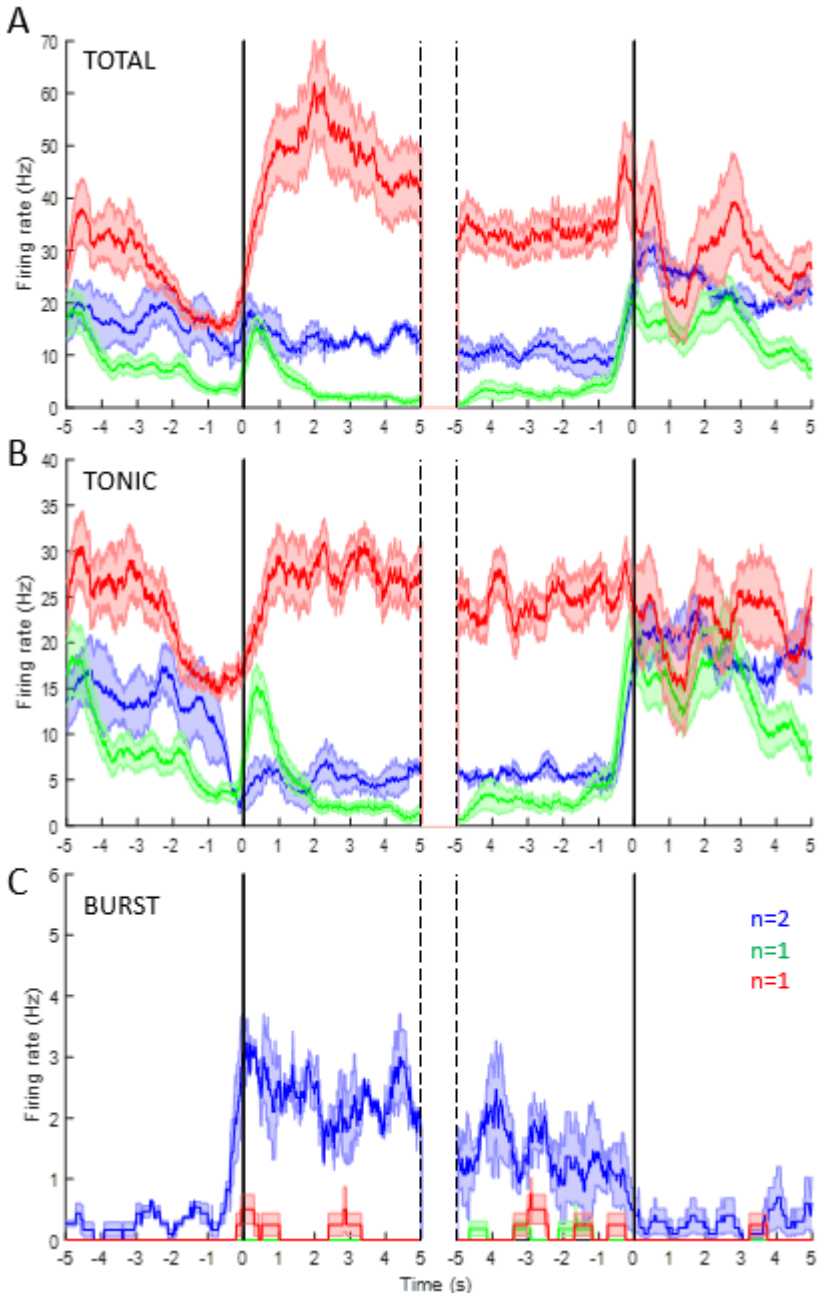


***Figure 5.19. Firing activity of putative inhibitory units at SWD onset and offset.*** *Firing rates are plotted over time for total (**A**), tonic (**B**) and burst (**C**) firing for the four putative inhibitory units (data for two of them that showed similar changes are illustrated by a single blue line). Onset and offset of SWD in S1 are marked by the vertical solid black lines and indicated on the X axis by the left and right 0s. Data shown are mean (solid line) ± SEM (shadows).*

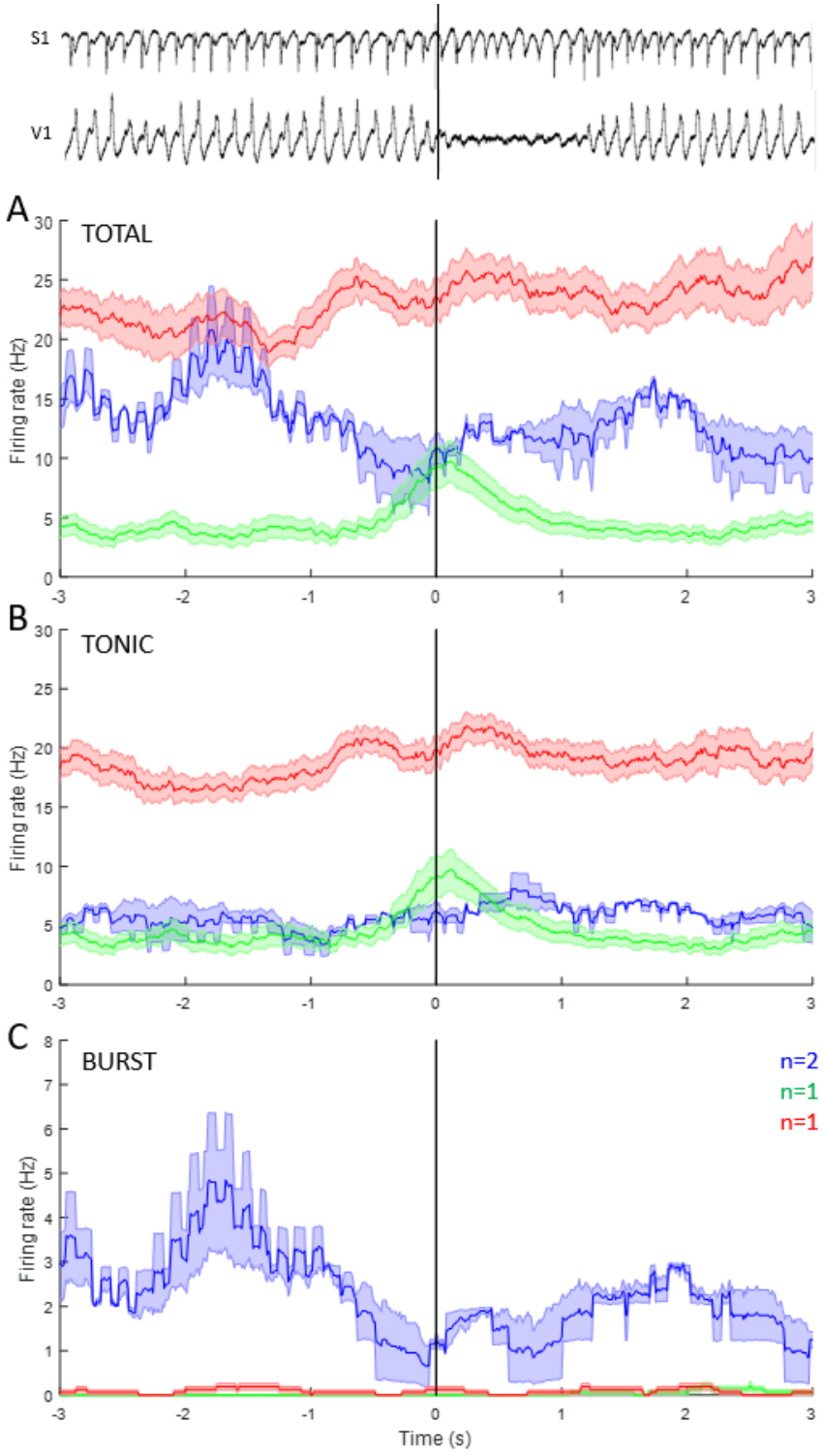


***Figure 5.20. Firing activity of inhibitory units during V1 SWD-breaks***

*Firing rates are plotted over time for total (**A**), tonic (**B**) and burst (**C**) firing for the four putative inhibitory units (data for two of them that showed similar changes are illustrated by a single blue line) during V1 SWD-breaks (see representative LFP in S1 and V1 at the top of the panels) as denoted by vertical black line. Firing rates are plotted as mean (solid line) ±SEM (shadows).*

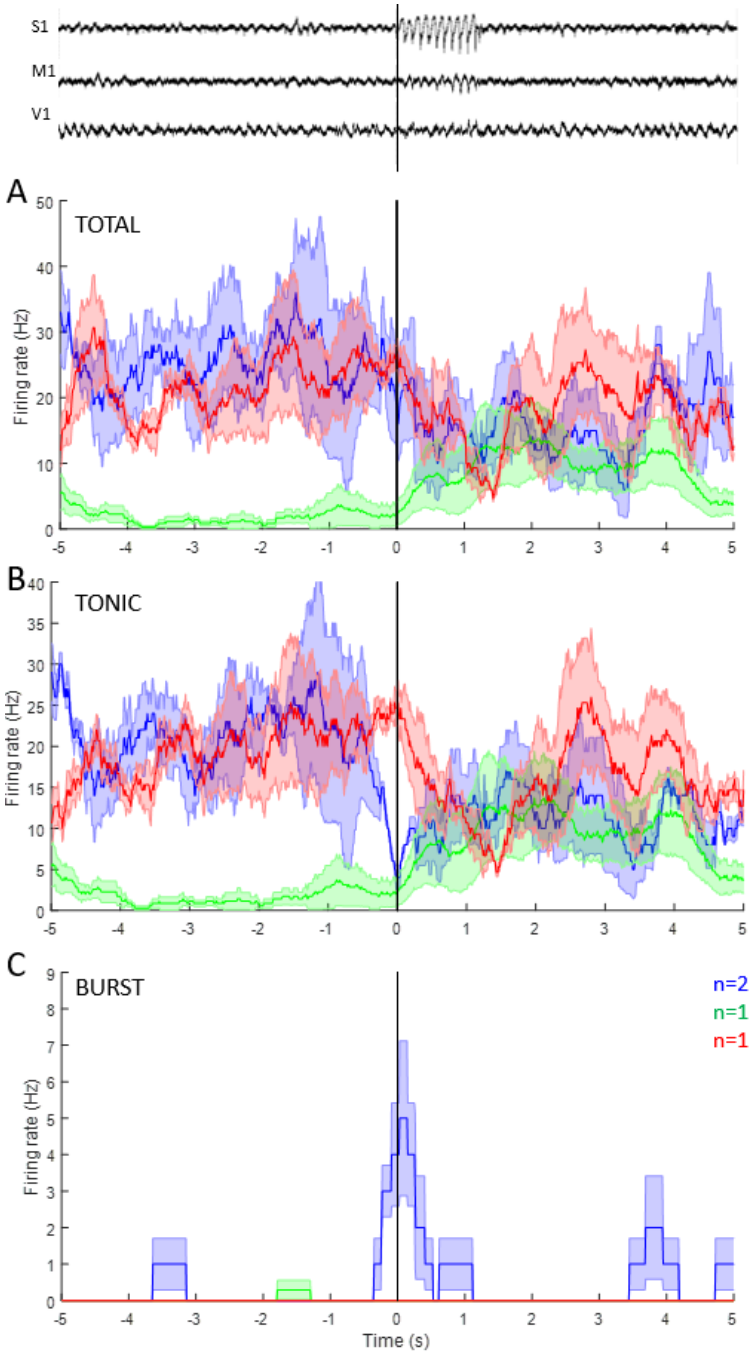


***Figure 5.21. Firing activity of inhibitory units during S1-only and S1+M1-only events.***

*Firing rates are plotted over time for total (**A**), tonic (**B**) and burst (**C**) firing for the four putative inhibitory units (data for two of them that showed similar changes are illustrated by a single blue line) during S1-only and S1+M1-only events (top LFP traces). The onset of which is denoted by vertical black line. Firing rates are plotted as mean (solid line) ±SEM (shadows).*

## 5.4 Discussion

### 5.4.1 Summary of results

All putative excitatory PO neurons had a switch from tonic to burst firing before the onset of SWD. There were different temporal dynamics of burst firing which led to the classification of these units into 3 groups: PB units that had elevated burst firing throughout the seizure, TB units that had a peak in burst activity at SWD onset, followed by a rapid decrease just after SWD generalisation, and LB units that had a much smaller and persistent ictal increase in burst firing than PB units.

The tonic to burst firing switch also occurred in PB and TB neurons during S1-only and S1+M1-events but it did not occur in LB units. The tonic to burst switch during these events was very brief and inter-ictal rates resumed before the end of the event. LB units that increased burst firing rate at SWD onset did not exhibit any bursts during these events.

During ictal periods, burst rates were high and tonic rates were low, relative to inter-ictal periods, despite this, tonic firing was the most prevalent firing type during SWD. Before V1 SWD-breaks, there was a shift back toward inter-ictal levels, i.e. a reduction in burst firing simultaneous to an increase in tonic firing. This occurred only in PB units and the change begun 1s before the onset of a V1 SWD-break.

All excitatory units, except a few of the TB type, fired more rhythmically during SWD than inter-ictal periods and hence, were time-locked to the ongoing SWCs. The burst firing of PB units occurred before the S1 SWC-spike (peak at -8ms), whereas TB and LB units both fired bursts afterwards. Tonic firing was less time-locked and fired both before and after the S1 SWC-spike. Similar activity was observed relative to V1 SWC-spikes but shifted by -12ms, and with wider peaks representing a reduction of time-locked behaviour.

The activity of the inhibitory units was varied. Two units had an increase in burst firing and decrease in tonic firing which lasted throughout the SWD. The remaining two units, which were analysed separately had negligible bursting activity. One of these cells had a transient increase in tonic activity that was time-locked to seizure onset while the other had decreases in tonic firing before SWD onset.

### 5.4.2 Methodological issues

The main bottleneck between data collection and final analysis was the spike sorting process. Isolating spikes can be difficult during SWD as the high-amplitude synchronous oscillations can generate population spikes large enough to warp or mask the unit waveforms (Anderson 1971). This makes it difficult for the spike-sorting algorithm to accurately group spikes during this period.

Therefore, an extra step to check the burst profile of all individual units was taken to ensure that spike sorting was completed accurately. The burst profiles were then compared to the profiles of thalamic neurons (Tscherter 2011) and any sorted units with abnormal burst profiles were removed from the analysis. This bottleneck can lead to a selection bias of what neurons are included into the dataset, for e.g. units that fire at the time of the SWC-spike will be hard to distinguish due to overlap of population and unit spike. This would make such cells unlikely to be successfully isolated and therefore not considered as part of the PO population.

The only way to avoid completely these spike sorting issues is to record units in a head-restrained or anaesthetised preparation. In these circumstances glass electrodes can be used which detect very few units with one dominant unit that can be easily sorted online or offline with an amplitude threshold. However, these conditions have their own disadvantages and as new cell types are being explored here it felt crucial to use animals only in the freely-moving condition where we can be confident that the cellular counterpart of SWD, i.e. the action potentials of individual neurons, is not confounded by anaesthetics or physical restriction. Notably, I attempted to record the firing dynamics of PO neurons in 2 head-restrained GAERS but the results were confounded by the limited recording period (10 min per cell), the long SWD (29.4 ±4s) and the extremely short interictal periods (3.7 ±3.4s).

The classification of units into excitatory and inhibitory was based predominantly on the extracellular recorded waveform of their spikes and the burst features, which need to be confirmed by more conclusive immunohistochemical identification of labelled units. Here, I have classified PO units under the assumption that their spike waveform and burst parameters are similar to FO neurons, which have been shown previously (Bartho et al., 2014). Based on this classification, four inhibitory units identified There are no detailed studies on GABAergic neurons in the rat PO. A study that focused on GABAergic neurons in LP identified a few GABA-positive cells in PO, but this was not

quantified (Evangelio, 2018). In addition, as aforementioned, the inhibitory units recorded here could be from fibres originating from ZI, APT and NRT nuclei and without experiments focused on these inhibitory sources it will remain unknown where the inhibitory units originated from. This issue, together with the very low sample size and the variability of the firing dynamics, greatly limits the conclusions that can be made from the putative inhibitory neuron data.

### 5.4.3 Implications for AS

This is the first work to record from single PO units in freely moving GAERS to reveal the firing dynamics and patterns at SWD onset and offset, as well as during V1 SWD-breaks and S1-only and S1+M1-only SWD.

#### *5.4.3.1 A tonic to burst shift occurs before the AS generalisation.*

Evaluating the firing rate of units over time revealed a change in activity patterns occurring up to 1.4s prior to the detection of SWD in S1. Many network changes on a similar time scale have been reported (Luttjohann 2013) showing that seizure onset is a gradual process.

During the pre-ictal period, tonic firing reduced and burst firing increased, this was true for all putative excitatory units. While this switch was happening, there was a transient reduction in total firing, which has been observed previously in PO units from $Scn8a^{+/-}$ mice (Sorokin et al, 2020), another genetic model of AS. However, not all findings in Sorokin et al. (2020) were replicated in this study. For example, the authors observed a gradual increase in total firing during the seconds prior to the transient decrease aforementioned. The increase they report was slight, but significant, however, the standard deviation was higher during this period and only one of the two raw examples shown have this 'ramp up' of firing. This suggests that the ramp up in firing is not ubiquitous feature of PO neurons which could explain the discrepancy observed.

Intracellular PO recordings (Polack et al 2009) showed little interictal firing and an increase during SWD that lacked rhythmicity. This does not align with the findings here, since I observed no change or a decrease in total firing (also observed by Sorokin et al., 2020) as well as ictal rhythmic firing. Additionally, this intracellular method did not show any changes of firing prior to SWD onset, alike what was observed via silicon probe recordings. The most likely explanation for this discrepancy

was the different experimental conditions (neurolept anaesthesia in Polack et al, 2009 vs freely-moving in my study). Notably, the axons that form excitatory synapses on HO nuclei are collaterals of cortical layer V neurons that also form synapses on motor output centres such as the brain stem (Sherman and Guillery 2011). The HO input therefore contains motor commands, which are likely to be vastly different between freely-moving and anaesthetised conditions. As cortical-PO synapses are class 1 inputs, any change in the activity will likely impact the firing rate of PO neurons, this highlights the need to use animals that move freely to make inferences on mechanisms of AS.

The tonic to burst switch was ubiquitous in recorded PO neurons and therefore may be key in the role of this HO nucleus in facilitating the generalisation and maintenance of SWD, as I reported in previous chapters. In order for a neuron to begin firing bursts of action potentials T-type calcium channels must be deinactivated, which occurs when cell membranes are hyperpolarised. During SWD, TC (Pinault 1998), cortical (Charpier 1999) and PO (Polack 2009) neurons experience a tonic hyperpolarisation of the membrane that lasts throughout the discharge which would facilitate the burst firing type as rhythmic depolarisations occur on top of this envelope. This is one of the first changes to occur across the whole circuit and has been observed before the first detectable EEG spike (Pinault 1998). This hyperpolarising envelope could therefore be playing a key role in the ability of PO neurons to fire bursts during SWD.

There is evidence that the hyperpolarising envelope observed in TC cells is driven by metabotropic $GABA_B$ receptors, and the secondary activation of K+ channels. This requires an active inhibition which may be reflected in by the transient reduction in total firing that peaks 0.4s prior to SWD onset, just after burst onset. In the case of PO (and other HO) neurons, this inhibition could originate from NRT, ZI or APT. Some inhibitory neurons were recorded here but in none of these was there an increase in activity observed before the onset of PO burst activity, i.e. 0.7s prior to SWD onset.

NRT neurons during ictal transitions have already been characterised (McCafferty et al. 2018) and no unit here had similar dynamics to those previously reported. However, neurons of the NRT are not homogenous in their burst firing capabilities, with ‘edge’ NRT cells (as opposed to ‘central’ NRT cells) often failing to burst. These edge cells formed reciprocal loops with PO (Martinez-Garcia et al. 2020) and therefore are the type to be detected in this study. Indeed, one unit here hinted to be of NRT origin as it had an accelerando-decelerando burst pattern *(Figure 5.7C)*.

Additionally, inter-ictal tonic spikes (the rate of which were the same for edge and central NRT cells, as shown by Martinez-Garcia et al. 2020) occurred at the same rate in this unit (25 - 30 Hz) (*red line in Figure 5.19)* as VB projecting NRT neurons (25 Hz). Furthermore, pre-ictal reductions 2.5s prior to onset was observed in this unit and from NRT units of McCafferty et al., (2018). Therefore, as the difference between this unit and previously reported NRT neurons was only the lack of burst firing, which can be explained by NRT heterogeneity, this unit could represent a PO-projecting NRT neuron.

Of the remaining inhibitory neurons, one had a transient increase in total and tonic firing time locked to S1 onset, but as the tonic to burst switch of putative excitatory units occurs before this time, this unit type is unlikely to be facilitating this change. Finally, two putative inhibitory neurons had a tonic to burst switch temporally matching those in excitatory cells, which could have a functional impact.

To summarise, there is a clear shift from tonic to burst firing that occurs before the onset of SWD in all recorded putative excitatory PO neurons and therefore there must be an active inhibition occurring at SWD onset. Although inhibitory units were also detected, due to the limitations of this dataset (as discussed in section 5.4.2), no solid conclusion can be made on the nature of ictal inhibitory effects to PO. However, it is a clear point of future research to gain a greater understanding of the mechanisms behind the neural dynamics observed in PO neurons.

#### *5.4.3.2 PO activity influences the maintenance of V1 SWD.*

In previous chapters the argument of HO activity maintaining SWD in V1 was put forward based on the temporal amplitude correlations of SWD between V1 and HO nuclei in addition to a reduction in V1 SWD power following muscimol injection in LP and PO. Further evidence of the influence of HO nuclei on V1 synchrony is that PB neurons change their activity up to 1s prior to a V1 SWD-break. This suggests that ictal neuronal firing pattern of PB neurons is actively facilitating cortical synchrony. No changes were observed in TB or LB units which reinforces the concept of a heterogenous PO population.

Overall, PO neurons were more active than VB neurons during SWD. Burst and tonic activity occurred in a greater number of SWCs for PO neurons (33% and 50%, respectively), compared to VB neurons (17% and 30%, respectively) (McCafferty et

al., 2018). However, this doesn't necessary correlate with a greater functional impact as FO and HO neurons have differential influences on cortical activity.

Relative to the S1 SWC-spike, burst activity occurred just 8ms prior, which relates to time of monosynaptic excitation from PO TC neurons (Audette et al. 2018a). So, although this synapse may be modulatory (i.e. Class 2) in nature, ionotropic components are present, which with burst activity would generate large EPSPs due to temporal summation (Kim and McCormick 1998) and increase vesicular release as the initial release probability is lower for Class 2 synapses (Dobrunz and Stevens 1997).

Firing of PO neurons was less time-locked to the V1 SWC-spike than the S1 SWC-spike. This indicates that PO neurons are more related to S1 activity, than V1 activity. Similar analysis would need to be done on the firing of LP neurons to identify evidence of monosynaptic influence on V1 neurons.

#### *5.4.3.3 The contribution of PO activity to the success of AS generalisation*

Comparing the onset of generalised SWD to the onset of SWD that occurred only in S1 and in S1+M1 drew meaningful differences between successful and non-successful AS. The main difference observed in this chapter was the complete absence of burst firing of LB neurons during S1-only and S1+M1-only events but not during SWD onset. This could be an indication that burst firing of LB units contribute to the initial propagation of SWD.

All three excitatory unit types had the same burst profile which indicates that they express the same T-type calcium channels. Therefore, the differences in ictal firing may derive from synaptic and connectivity differences. Both focal and multi-areal matrix cells exist in PO (Clascá 2012), which may explain some of the heterogeneity observed in this study, for e.g. multi-areal PO neurons may be utilised more as diffuse connectivity would be an anatomical advantage to SWD propagation. Previous research has hinted to a heterogenous connection profile of PO neurons as one study has found stronger S1-PO-M1 (Mo and Sherman 2019) connections whereas another study found stronger S1-PO-S1 CTC loops (Guo et al. 2020). PO neurons predominantly synapse on layer 5A in S1, and S1 layer 5B neurons are the corticothalamic projections to PO. However, there are active PO-S1 synapses in layer 5B. Perhaps these layer VB projecting PO neurons are a functionally different neuronal PO population, capable of forming a disynaptic reciprocal loop with S1 and

thus can more easily generate bidirectional excitation. It is necessary to identify connectivity differences between the excitatory neuronal groups found in this chapter to understand their influence of the CTC network and thus, SWD.

#### *5.4.3.4 Summary*

In conclusion, this chapter revealed the neural dynamics of multiple groups of PO excitatory neurons that all have a burst to tonic firing switch during the SWD, likely driven by an inhibitory common modulator. This switch is thought to be functionally relevant and facilitate AS generation, via LB burst activity, and ongoing maintenance in V1, via PB burst activity.

# Chapter 6: Discussion

## 6.1 Summary of key findings

This thesis combined various electrophysiological and pharmacological methods to reveal how HO nuclei and the trans-thalamic pathway contribute to the generation and maintenance of AS. The key findings of this thesis, that are discussed further in this chapter are that LP and PO activity contributes to the ictal synchronisation of V1 neurons and the SWD propagation from S1 to V1. Single unit recordings showed that a switch from burst to tonic firing is a ubiquitous feature of PO neurons during SWD and that these neurons are not homogeneous, with varying impacts on AS initiation and maintenance.

## 6.2 LP and PO contribution to initial SWD propagation

Following the initiation of SWCs in S1, the ictal activity must successfully propagate to and entrain neurons in other cortical regions. There are two main ways action potentials, and thus the SWD can propagate across the cortex. One is via glutamatergic cortico-cortical neurons (Roland et al. 2014), and the other, which is relatively understudied, is the parallel trans-thalamic pathway (Sherman and Guillery 2011). There are multiple findings in this thesis that converge on the conclusion that trans-thalamic communication is recruited during the initial SWD propagation.

This thesis has focused on an early, detectable change, the onset of SWD in S1, to identify CTC-HO nuclei network changes during this time. Inter-ictally, LP and PO communication was reasonably high (PPC = 0.5), whereas signal coherence between other regions was very low (PPC <0.1) (*Figure 6.1A)*. Lack of cortico-cortical associations preceding SWD onset have previously been reported (Meeren et al. 2002), whereas S1-PO communication has been shown to increase from ~1.25s prior to onset (Luttjohann and Luijtelaar 2012).

In my work, changes in neural dynamics were observed from a similar time (~1.5s prior to onset), with the beginning of the shift from tonic to burst firing of all putative excitatory PO neurons. Once this shift had surpassed half the maximal change, there was a coincidental increase in S1-HO nuclei coherence and, in addition, an increase in LP-V1 coherence *(Figure 6.1B),* which could suggest that the burst firing of PO neurons is facilitating the recruitment of HO-cortical networks.

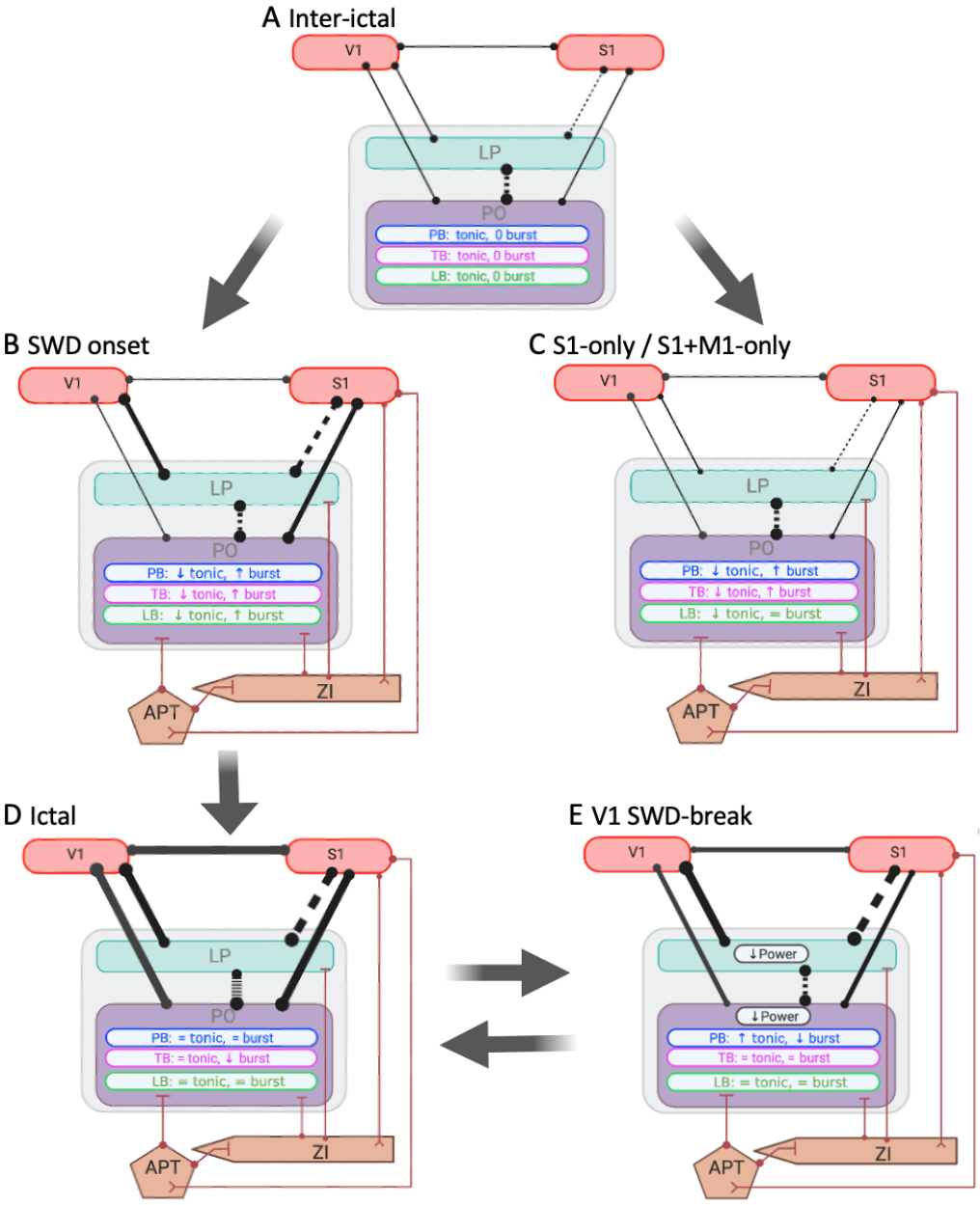


***Figure 6.1. Summary of changes between HO nuclei and cortical connectivity and of HO neural dynamics during different stages of SWD.***

*Schematic of connectivity between LP, PO, S1 and V1 during inter-ictal states (**A**), SWD onsets (**B**), S1/ S1+M1-only events, ictal states (**D**) and V1 SWD-breaks (**E**). Solid and dashed lines demonstrate direct and indirect connections, respectively, and thicker lines represent higher PPC values (note – PPC was not measured at **C**, therefore lines are the same thickness as interictal period). Solid brown lines indicate ZI and APT connections that are the proposed candidates of a common modulator. Labels within LP or PO demonstrate tonic and burst firing changes of persistent, transient and low bursting (PB, TB and LB) neurons in PO, or power changes of the whole nuclei. These changes are reported as relative to the prior network state, as indicated by the arrows between schematics. Figure created with BioRender.com*

The timing of PB unit burst activity relative to S1 SWC-spikes was the same as the duration of monosynaptic activation of S1 EPSPs (Audette et al., 2018), suggesting a functional role of PB unit bursts during initial and ongoing bidirectional excitation with S1. Interestingly, while LB units increased burst firing at SWD onset, they did not exhibit any bursts during non-generalised SWD, i.e. S1-only and S1+M1-only events *(Figure 6.1C).* This reinforces my suggestion that burst firing of PO neurons could be important at the start of an AS.

This work has highlighted a heterogenous PO neuronal population in regard to their firing dynamics and influence on AS, which requires further exploration. Heterogenous populations in both PO and LP have already been reported in vitro (Li et al. 2003; Wei et al. 2011), with one paper identifying two groups of higher-order neurons with different burst propensities in the adult tree shrew (Wei et al. 2011). Neurons with high burst propensity had multiple LTS elicited following current inputs, a feature that could be beneficial for AS generalisation as the rhythmic activity in HO can be spread to other areas. Particularly, these could relate to PB neurons that have a higher burst rate and fires more rhythmically during ictal periods that LB and TB neurons, respectively. A computational model of the data in Wei et al. 2011 suggested that Cav3.2 distal dendrite density could explain different burst propensities and could therefore be a property that is altered in GAERS HO neurons, although this has not yet been investigated. Additionally, multi-areal matrix cells (Clascá 2012) may have an anatomical advantage to facilitate the initial generalisation of SWD and thus, may relate to LB neurons which had different activity during S1-only and S1+M1-only events.

Ultimately, although the cellular mechanisms behind the heterogeneity in this study is unknown, these results could imply that PO bursts at the beginning of a seizure is contributing to S1 synchronous firing and the establishment of the very first SWCs via monosynaptic connections. Indeed, when HO nuclei were inhibited by muscimol, SWCs took longer to develop which either increased the duration of propagation across the whole brain, or even prevented its success, as demonstrated by the increase in S1-only and S1+M1 only SWD.

Coherence increases in the 6-9 Hz frequency band occurred first between S1 and LP or PO, as well as between LP and V1. The latter result has also been shown in the WAG/Rjj model (Lüttjohann et al., 2013). This increase in PPC between S1-LP was surprising as there are no reports of direct connections from S1 to LP (Kamishina et

al. 2009; Zakiewicz et al. 2014). The fact that one group of connections increased significantly earlier than another group was a good indication that the changes observed were not simply a by-product of SWD, which would presumably result in a global increase in PPC values at the same time. The simultaneous increase in PPC of both HO nuclei was the first indication that there may be a common modulator that receives S1 efferents and influences HO nuclei. The existence of this common modulator, likely of an inhibitory nature, would also aid the shift from tonic to burst firing of PO neurons.

Some candidates of this common modulator might be the ZI, APT and/or NRT as they both receive direct connections from S1 and project to both LP and PO (Pinault 2004; Bokor et al. 2005). However, previous research into NRT connectivity and neural dynamics suggests that the NRT is not involved in pre-ictal PO inhibition for two main reasons. Firstly, PPC analysis has revealed a pre-ictal reduction in coherence in the beta frequency between NRT and PO prior to seizure onset (Lüttjohann et al. 2013). Secondly, NRT neurons have a reduction in total and tonic firing prior to AS onset (McCafferty et al. 2018) which would likely relieve some PO feed-forward inhibition. Although this was shown in NRT neurons that form circuits with FO nuclei (Martinez-Garcia et al. 2020), this could well be the case of NRT – HO circuits, with a potential NRT neuron in this thesis also showing a pre-ictal reduction in total and tonic firing. Therefore, the NRT is not considered a likely prime candidate for the role of a common modulator.

The next proposed candidates is the ZI *(Figure 6.1)*, which receives direct input from S1 cortical layer V and projects to both LP and PO (Barthó et al. 2002). In addition, ZI-NRT projections have been reported (Çavdar et al. 2006) which could be responsible for some the pre-ictal reduction in NRT firing (McCafferty et al., 2018). However the finding of ZI-NRT is not reported in other studies (Barthó et al. 2002), and therefore should be taken with some caution. The role of ZI in SWD is relatively unknown but studies have shown that excitation via closed loop stimulation can cease AS (Liang et al. 2011). Additionally, in Long-Evans rats, S1 SWD spike amplitude was higher while ZI expressed rhythmic activity and ZI lesions reduced SWD power (Shaw et al. 2013), suggesting that ZI, alike LP and PO, influences cortical synchrony. Furthermore, muscimol inhibition reduced SWD number and time spent in seizures. These effects occurred after unilateral and bilateral injections, which shows the contralateral connectivity of ZI (Power and Mitrofanis 2001) is active during SWD. Overall, its connectivity and its influence on SWD make ZI an interesting candidate

for the facilitation of the recruitment of cortico-HO networks shown by the PPC analysis in this study. Finally, although the influence of APT in SWD has not been tested directly, it remains a candidate for the role of modulator due to its direct connectivity with S1 and HO nuclei (Bokor et al. 2005; Giber et al. 2008; Zakiewicz et al. 2014).

## 6.3 LP and PO contribution to the maintenance of global SWD

Between SWD onset and ictal periods (i.e. after AS generalisation), there was an increase in coherence across all cortico-cortical and cortico-HO nuclei networks. PB and LB neurons of PO maintained their burst firing throughout SWD, but TB neurons decreased in burst activity after onset *(Figure 6.1D)*, again demonstrating neuronal heterogeneity within PO.

During SWD there was ongoing influence of LP and PO activity on V1 synchrony. This was first illustrated by a temporal synchronisation of SWD amplitude fluctuations which ultimately reflect underlying neuronal synchrony (Buzsáki et al. 2012). Additionally, LP SWC-spikes occurred 10ms before V1 SWC-spikes, again relating to the duration of monosynaptic connections between LP and V1 (Fuentealba and Steriade 2005). A causal relationship was then demonstrated by the fact that inhibition of LP and PO dramatically reduced V1 SWD power.

The presence of V1 SWD-breaks, which were described for the first time by my work, provided a quantitative period when V1 was not synchronised with the rest of the cortex, as demonstrated by a reduction in cortico-cortical coherence *(Figure 6.1E)*. These events provided a unique insight into the mechanisms that contribute to generalisation on a cycle-to-cycle basis. Single PO unit activity revealed changes in PB units occurring up to 1s prior to the onset of V1 SWD-breaks *(Figure 6.1E)*, which may relate to a causal effect.

Although LP is heavily implicated in the visual system (Kamishina et al. 2009), I repeatedly observed the same effects on V1 SWD amplitude when manipulating PO, additionally, PO-V1 coherence significantly decreased during the breaks *(Figure 6.1E)*. These are the first indications that the small population of V1-projecting PO neurons, which are yet to studied, may be functionally relevant in SWD.

## 6.4 Summary and future direction

This thesis has provided novel results of global features of AS and correlative and causative data supporting two key notions that LP and PO activity not only facilitate SWD generalisation but also their maintenance. The surprising consistency of LP or PO effects on V1 activity led me to propose that a nucleus, projecting to both LP and PO, is mediating effects from S1 to these nuclei. The results in this thesis also led to the identification of key research areas that would unravel the mechanisms behind the effects of LP and PO on AS observed in this study.

1. Exploring synaptic and network differences of the putative groups of excitatory PO neurons is imperative to understand how they differentially impact the CTC network during AS and the importance of sub-groups during either initial propagation of SWD or V1 SWD-breaks. For example, exploring the multi-areal vs focal matrix cells could be achieved via a retrograde virus into layer V where multi-areal cells but not focal matrix cells synapse to (Clascá 2012).
2. Increasing the specificity of LP and PO inhibition, ideally by specific chemo- and opto-genetic methods will provide conclusive evidence on whether there is a functional overlap of these two HO nuclei.
3. Recording from single LP units would give further information of similarities and differences with PO.
4. Classifying HO-S1 and HO-V1 synapses into Class 1 and Class 2 would provide useful insight to the influence of HO TC synapses. Although there are previous data on this, it has not been performed in an animal model of absence epilepsy, where Class 1 and Class 2 ratios may be different.
5. Investigating the role of the ZI via LFP recordings can give an initial insight as to whether it is involved in generalisation of AS. If the hypotheses in this discussion are correct, ZI should show an increase in PPC simultaneous to both HO nuclei and have amplitude correlations with HO nuclei and V1.

# Bibliography


Allen, A.E. et al. 2016. Visual input to the mouse lateral posterior and posterior thalamic nuclei: photoreceptive origins and retinotopic order. *The Journal of Physiology* 594(7), pp. 1911–1929. doi: 10.1113/JP271707.

Allen, T.A. et al. 2008. Imaging the spread of reversible brain inactivations using fluorescent muscimol. *Journal of neuroscience methods* 171(1), pp. 30–38. doi: 10.1016/j.jneumeth.2008.01.033.

Aronoff, R. et al. 2010. Long-range connectivity of mouse primary somatosensory barrel cortex. *European Journal of Neuroscience* 31(12), pp. 2221–2233. doi: https://doi.org/10.1111/j.1460-9568.2010.07264.x.

Audette, N.J. et al. 2018. POm Thalamocortical Input Drives Layer-Specific Microcircuits in Somatosensory Cortex. *Cerebral Cortex* 28(4), pp. 1312–1328. doi: 10.1093/cercor/bhx044.

Avoli et al. 1983. An analysis of penicillin-induced generalized spike and wave discharges using simultaneous recordings of cortical and thalamic single neurons. *Journal of Neurophysiology* 50(4), pp. 819–837. doi: 10.1152/jn.1983.50.4.819.

Avoli, M. and Gloor, P. 1982. Interaction of cortex and thalamus in spike and wave discharges of feline generalized penicillin epilepsy. *Experimental Neurology* 76(1), pp. 196–217. doi: 10.1016/0014-4886(82)90112-1.

Bai, X. et al. 2010. Dynamic time course of typical childhood absence seizures: EEG, behavior, and functional magnetic resonance imaging. *Journal of Neuroscience* 30(17), pp. 5884–5893. doi: 10.1523/JNEUROSCI.5101-09.2010.

Barthó, P. et al. 2002. Selective GABAergic innervation of thalamic nuclei from zona incerta: GABAergic afferents to thalamus from zona incerta. *European Journal of Neuroscience* 16(6), pp. 999–1014. doi: 10.1046/j.1460-9568.2002.02157.x.

Barthó, P. et al. 2007. Cortical Control of Zona Incerta. *Journal of Neuroscience* 27(7), pp. 1670–1681. doi: 10.1523/JNEUROSCI.3768-06.2007.

Bazhenov, M. et al. 2000. Spiking-Bursting Activity in the Thalamic Reticular Nucleus Initiates Sequences of Spindle Oscillations in Thalamic Networks. *Journal of Neurophysiology* 84(2), pp. 1076–1087. doi: 10.1152/jn.2000.84.2.1076.

Benedek, K. et al. 2016. Neocortical gamma oscillations in idiopathic generalized epilepsy. *Epilepsia* 57(5), pp. 796–804. doi: https://doi.org/10.1111/epi.13355.

Bentivoglio, M. et al. 1991. GABAergic interneurons and neuropil of the intralaminar thalamus: an immunohistochemical study in the rat and the cat, with notes in the monkey. *Experimental Brain Research* 87(1). doi: 10.1007/BF00228509.

Benuzzi, F. et al. 2012. Increased cortical BOLD signal anticipates generalized spike and wave discharges in adolescents and adults with idiopathic generalized epilepsies. *Epilepsia* 53(4), pp. 622–630. doi: 10.1111/j.1528-1167.2011.03385.x.

Berg, A.T. et al. 2010. Revised terminology and concepts for organization of seizures and epilepsies: Report of the ILAE Commission on Classification and Terminology, 2005-2009. *Epilepsia* 51(4), pp. 676–685. doi: 10.1111/j.1528-1167.2010.02522.x.

Beyer, B. et al. 2008. Absence seizures in C3H/HeJ and knockout mice caused by mutation of the AMPA receptor subunit Gria4. *Human Molecular Genetics* 17(12), pp. 1738–1749. doi: 10.1093/hmg/ddn064.

Bickford, M.E. 2016. Thalamic Circuit Diversity: Modulation of the Driver/Modulator Framework. *Frontiers in Neural Circuits* 9(1), pp. 1–86. doi: 10.3389/fncir.2015.00086.

de Boer, H.M. et al. 2008. The global burden and stigma of epilepsy. *Epilepsy & Behavior* 12(4), pp. 540–546. doi: 10.1016/j.yebeh.2007.12.019.

Bokor, H. et al. 2005. Selective GABAergic Control of Higher-Order Thalamic Relays. *Neuron* 45(6), pp. 929–940. doi: 10.1016/j.neuron.2005.01.048.

Boyes, W.K. and Dyer, R.S. 1983. Pattern reversal visual evoked potentials in awake rats. *Brain Research Bulletin* 10(6), pp. 817–823. doi: 10.1016/0361-9230(83)90214-9.

Brittain, J.-S. et al. 2014. The highs and lows of beta activity in cortico-basal ganglia loops. *The European Journal of Neuroscience* 39(11), pp. 1951–1959. doi: 10.1111/ejn.12574.

Browne, T.R. et al. 1974. Responsiveness before, during, and after spike-wave paroxysms. *Neurology* 24(7), p. 659. doi: 10.1212/WNL.24.7.659.

Buzsáki, G. et al. 2012. The origin of extracellular fields and currents — EEG, ECoG, LFP and spikes. *Nature reviews. Neuroscience* 13(6), pp. 407–420. doi: 10.1038/nrn3241.

Caddick, S.J. et al. 1999. Excitatory but not inhibitory synaptic transmission is reduced in lethargic (Cacnb4(lh)) and tottering (Cacna1atg) mouse thalami. *Journal of Neurophysiology* 81(5), pp. 2066–2074. doi: 10.1152/jn.1999.81.5.2066.

Cain, S.M. et al. 2015. Thalamocortical neurons display suppressed burst-firing due to an enhanced Ih current in a genetic model of absence epilepsy. *Pflugers Archiv: European Journal of Physiology* 467(6), pp. 1367–1382. doi: 10.1007/s00424-014-1549-4.

Caplan, R. et al. 2005. Depression and Anxiety Disorders in Pediatric Epilepsy. *Epilepsia* 46(5), pp. 720–730. doi: 10.1111/j.1528-1167.2005.43604.x.

Caplan, R. et al. 2008. Childhood absence epilepsy: Behavioral, cognitive, and linguistic comorbidities. *Epilepsia* 49(11), pp. 1838–1846. doi: 10.1111/j.1528-1167.2008.01680.x.

Casas-Torremocha, D. et al. 2017. Posterior Thalamic Nucleus Modulation of Tactile Stimuli Processing in Rat Motor and Primary Somatosensory Cortices. *Frontiers in Neural Circuits* 11, p. 69. doi: 10.3389/fncir.2017.00069.

Casas-Torremocha, D. et al. 2019. Posterior thalamic nucleus axon terminals have different structure and functional impact in the motor and somatosensory vibrissal cortices. *Brain Structure and Function* 224(4), pp. 1627–1645. doi: 10.1007/s00429-019-01862-4.

Casillas-Espinosa, P.M. et al. 2017. Evaluating whole genome sequence data from the Genetic Absence Epilepsy Rat from Strasbourg and its related non-epileptic strain. *PloS One* 12(7), p. e0179924. doi: 10.1371/journal.pone.0179924.

Castro-Alamancos, A. and Connors, W. 1996. Spatiotemporal Properties of Short-Term Plasticity in Sensorimotor Thalamocortical Pathways of the Rat. *Journal of Neuroscience* 16(8), pp. 2767–2779.

Çavdar, S. et al. 2006. Connections of the zona incerta to the reticular nucleus of the thalamus in the rat. *Journal of Anatomy* 209(2), pp. 251–258. doi: 10.1111/j.1469-7580.2006.00600.x.

Çavdar, S. et al. 2012. Do the quantitative relationships of synaptic junctions and terminals in the thalamus of genetic absence epilepsy rats from Strasbourg (GAERS) differ from those in normal control Wistar rats. *Neurological Sciences* 33(2), pp. 251–259. doi: 10.1007/s10072-011-0666-5.

Chang, M.C. et al. 2009. Glutamate Receptor Clusters: Narp, EphB2 Receptor, Stargazin. In: *Encyclopedia of Neuroscience*. Elsevier, pp. 895–899. doi: 10.1016/B978-008045046-9.00363-6.

Charbonneau, V. et al. 2012. Cortical and subcortical projections to primary visual cortex in anophthalmic, enucleated and sighted mice. *European Journal of Neuroscience* 36(7), pp. 2949–2963. doi: https://doi.org/10.1111/j.1460-9568.2012.08215.x.

Chen, J.W. et al. 2019. Cannabidiol: A New Hope for Patients With Dravet or Lennox-Gastaut Syndromes. *Annals of Pharmacotherapy* 53(6), pp. 603–611. doi: 10.1177/1060028018822124.

Chen, Y. et al. 2003. Association between genetic variation ofCACNA1H and childhood absence epilepsy. *Annals of Neurology* 54(2), pp. 239–243. doi: 10.1002/ana.10607.

Chipaux, M. et al. 2013. Persistence of Cortical Sensory Processing during Absence Seizures in Human and an Animal Model: Evidence from EEG and Intracellular Recordings. *PLoS ONE* 8(3). doi: 10.1371/journal.pone.0058180.

Clascá, F. 2012. Unveiling the diversity of thalamocortical neuron subtypes. *European Journal of Neuroscience* 35(10), pp. 1524–1531.

Clemente-Perez, A. et al. 2017. Distinct Thalamic Reticular Cell Types Differentially Modulate Normal and Pathological Cortical Rhythms. *Cell Reports* 19(10), pp. 2130–2142. doi: 10.1016/j.celrep.2017.05.044.

Coenen, A.M.L. and Van Luijtelaar, E.L.J.M. 2003. Genetic animal models for absence epilepsy: a review of the WAG/Rij strain of rats. *Behavior Genetics* 33(6), pp. 635–655. doi: 10.1023/a:1026179013847.

Cope, D.W. et al. 2009. Enhanced tonic GABAA inhibition in typical absence epilepsy. *Nature Medicine* 15(12), pp. 1392–1398. doi: 10.1038/nm.2058.

Crunelli, V. et al. 2018. Dual function of thalamic low-vigilance state oscillations: rhythm-regulation and plasticity. *Nature Reviews. Neuroscience* 19(2), pp. 107–118. doi: 10.1038/nrn.2017.151.

Crunelli, V. and Leresche, N. 2002. Childhood absence epilepsy: Genes, channels, neurons and networks. *Nature Reviews Neuroscience* 3(5), pp. 371–382. doi: 10.1038/nrn811.

Danober, L. et al. 1998. Pathophysiological mechanisms of genetic absence epilepsy in the rat. *Progress in Neurobiology* 55(1), pp. 27–57. doi: 10.1016/S0301-0082(97)00091-9.

D'Antuono, M. et al. 2006. Synaptic hyperexcitability of deep layer neocortical cells in a genetic model of absence seizures. *Genes, Brain and Behavior* 5(1), pp. 73–84. doi: https://doi.org/10.1111/j.1601-183X.2005.00146.x.

David, F. et al. 2018. Suppression of Hyperpolarization-Activated Cyclic Nucleotide-Gated Channel Function in Thalamocortical Neurons Prevents Genetically Determined and Pharmacologically Induced Absence Seizures. *The Journal of Neuroscience* 38(30), pp. 6615–6627. doi: 10.1523/JNEUROSCI.0896-17.2018.

Deleuze, C. and Huguenard, J.R. 2006. Distinct Electrical and Chemical Connectivity Maps in the Thalamic Reticular Nucleus: Potential Roles in Synchronization and Sensation. *Journal of Neuroscience* 26(33), pp. 8633–8645. doi: 10.1523/JNEUROSCI.2333-06.2006.

Depaulis, A. et al. 2016. The genetic absence epilepsy rat from Strasbourg as a model to decipher the neuronal and network mechanisms of generalized idiopathic epilepsies. *Journal of Neuroscience Methods* 260, pp. 159–174. doi: 10.1016/j.jneumeth.2015.05.022.

Deransart, C. et al. 2000. Dopamine in the striatum modulates seizures in a genetic model of absence epilepsy in the rat. *Neuroscience* 100(2), pp. 335–344. doi: 10.1016/S0306-4522(00)00266-9.

Desai, N.V. and Varela, C. 2021. Distinct burst properties contribute to the functional diversity of thalamic nuclei. *Journal of Comparative Neurology* , pp. 1–25. doi: https://doi.org/10.1002/cne.25141.

Deschênes, M. et al. 1998. The organization of corticothalamic projections: reciprocity versus parity. *Brain Research Reviews* 28(3), pp. 286–308. doi: 10.1016/S0165-0173(98)00017-4.

Deschênes and Steriade 1982. Thalamic bursting mechanism: an inward slow current revealed by membrane hyperpolarization - ScienceDirect. *Brain Research* 239(1), pp. 289–293. doi: 10.1016/0006-8993(82)90854-X.

Di Lazzaro, V. et al. 2016. Canonical cortical circuits: current evidence and theoretical implications. *Neuroscience and Neuroeconomics* , p. 1. doi: 10.2147/NAN.S70816.

Diamond, M.E. et al. 1992. Somatic sensory responses in the rostral sector of the posterior group (POm) and in the ventral posterior medial nucleus (VPM) of the rat thalamus. *The Journal of Comparative Neurology* 318(4), pp. 462–476. doi: 10.1002/cne.903180410.

DiFrancesco, J.C. et al. 2011. Recessive Loss-of-Function Mutation in the Pacemaker HCN2 Channel Causing Increased Neuronal Excitability in a Patient with Idiopathic Generalized Epilepsy. *The Journal of Neuroscience* 31(48), pp. 17327–17337. doi: 10.1523/JNEUROSCI.3727-11.2011.

Dobrunz, L.E. and Stevens, C.F. 1997. Heterogeneity of release probability, facilitation, and depletion at central synapses. *Neuron* 18(6), pp. 995–1008. doi: 10.1016/s0896-6273(00)80338-4.

Dravet, C. 2011. The core Dravet syndrome phenotype: Core Dravet Syndrome. *Epilepsia* 52, pp. 3–9. doi: 10.1111/j.1528-1167.2011.02994.x.

Dumas, D.B. et al. 2019. Anatomical development of the cerebellothalamic tract in embryonic mice. *bioRxiv* , p. 731968. doi: 10.1101/731968.

Engel, A.K. and Fries, P. 2010. Beta-band oscillations--signalling the status quo? *Current Opinion in Neurobiology* 20(2), pp. 156–165. doi: 10.1016/j.conb.2010.02.015.

Ettinger et al. 2005. Two Cases of Nonconvulsive Status Epilepticus in Association with Tiagabine Therapy. *Epilepsia* 40(8), pp. 1159–1162. doi: 10.1111/j.1528-1157.1999.tb00835.x.

Evangelio et al. 2018. Different cortical projections from three subdivisions of the rat lateral posterior thalamic nucleus: a single-neuron tracing study with viral vectors. *Frontiers in Neuroanatomy* 12:27, pp. 1–12. doi: 10.1111/ejn.12882.

Fisher, R.S. et al. 2014. ILAE Official Report: A practical clinical definition of epilepsy. *Epilepsia* 55(4), pp. 475–482. doi: 10.1111/epi.12550.

Fisher, R.S. et al. 2017. Operational classification of seizure types by the International League Against Epilepsy: Position Paper of the ILAE Commission for Classification and Terminology. *Epilepsia* 58(4), pp. 522–530. doi: 10.1111/epi.13670.

Flecknell, P. 2009. Laboratory Animal Anesthesia. *Laboratory Animal Anaesthesia*

Foik, A.T. et al. 2020. Visual response characteristics in lateral and medial subdivisions of the rat pulvinar. *bioRxiv* , p. 2020.01.26.920454. doi: 10.1101/2020.01.26.920454.

Fuentealba, P. and Steriade, M. 2005. The reticular nucleus revisited: Intrinsic and network properties of a thalamic pacemaker. *Progress in Neurobiology* 75(2), pp. 125–141. doi: 10.1016/j.pneurobio.2005.01.002.

Genç, B.O. et al. 2005. Pattern-reversal Visual Evoked Potentials in Patients with Newly Diagnosed Epilepsy. *Epilepsia* 46(8), pp. 1219–1223. doi: https://doi.org/10.1111/j.1528-1167.2005.63504.x.

Giber, K. et al. 2008. Heterogeneous output pathways link the anterior pretectal nucleus with the zona incerta and the thalamus in rat. *The Journal of Comparative Neurology* 506(1), pp. 122–140. doi: 10.1002/cne.21545.

Glauser, T.A. et al. 2013. Ethosuximide, valproic acid, and lamotrigine in childhood absence epilepsy: initial monotherapy outcomes at 12 months. *Epilepsia* 54(1), pp. 141–155. doi: 10.1111/epi.12028.

Gloor, P. 1968. Generalized cortico-reticular epilepsies. Some considerations on the pathophysiology of generalized bilaterally synchronous spike and wave discharge. *Epilepsia* 9(3), pp. 249–263. doi: 10.1111/j.1528-1157.1968.tb04624.x.

Goldberg, J.H. et al. 2004. Global dendritic calcium spikes in mouse layer 5 low threshold spiking interneurones: implications for control of pyramidal cell bursting. *The Journal of Physiology* 558(Pt 2), pp. 465–478. doi: 10.1113/jphysiol.2004.064519.

Gorji, A. et al. 2011. Seizure-related activity of intralaminar thalamic neurons in a genetic model of absence epilepsy. *Neurobiology of Disease* 43(1), pp. 266–274. doi: 10.1016/j.nbd.2011.03.019.

Groenewegen, H.J. and Berendse, H.W. 1994. The specificity of the 'nonspecific' midline and intralaminar thalamic nudei. *Trends in Neurosciences* 17(2), p. 6.

Guo, K. et al. 2020. Cortico-Thalamo-Cortical Circuits of Mouse Forelimb S1 Are Organized Primarily as Recurrent Loops. *Journal of Neuroscience* 40(14), pp. 2849–2858. doi: 10.1523/JNEUROSCI.2277-19.2020.

Halassa, M.M. and Acsády, L. 2016. Thalamic Inhibition: Diverse Sources, Diverse Scales. *Trends in Neurosciences* 39(10), pp. 680–693. doi: 10.1016/j.tins.2016.08.001.

Hayut, I. et al. 2011. LTS and FS Inhibitory Interneurons, Short-Term Synaptic Plasticity, and Cortical Circuit Dynamics. Graham, L. J. ed. *PLoS Computational Biology* 7(10), p. e1002248. doi: 10.1371/journal.pcbi.1002248.

Hazrati, L.-N. et al. 1995. The thalamic reticular nucleus does not send commissural projection to the contralateral parafascicular nucleus in the rat. *Brain Research* 679(1), pp. 123–134. doi: 10.1016/0006-8993(95)00223-D.

Heron, S.E. et al. 2004. Genetic variation of CACNA1H in idiopathic generalized epilepsy. *Annals of Neurology* 55(4), pp. 595–596. doi: https://doi.org/10.1002/ana.20028.

van Heukelum, S. et al. 2016. Timing of high-frequency cortical stimulation in a genetic absence model. *Neuroscience* 324, pp. 191–201. doi: 10.1016/j.neuroscience.2016.02.070.

Hosford, D.A. and Wang, Y. 1997. Utility of the Lethargic (lh/lh) Mouse Model of Absence Seizures in Predicting the Effects of Lamotrigine, Vigabatrin, Tiagabine, Gabapentin, and Topiramate Against Human Absence Seizures. *Epilepsia* 38(4), pp. 408–414. doi: https://doi.org/10.1111/j.1528-1157.1997.tb01729.x.

Hou, G. et al. 2016. Lack of Intrinsic GABAergic Connections in the Thalamic Reticular Nucleus of the Mouse. *Journal of Neuroscience* 36(27), pp. 7246–7252. doi: 10.1523/JNEUROSCI.0607-16.2016.

Huang, R.-Q. et al. 2001. Pentylenetetrazole-Induced Inhibition of Recombinant γ- Aminobutyric Acid Type A (GABAA) Receptors: Mechanism and Site of Action. *journal of pharmacology and experimental therapeutics* 298(3), pp. 986–995.

Huguenard, J. 2019. Current Controversy: Spikes, Bursts, and Synchrony in Generalized Absence Epilepsy: Unresolved Questions Regarding Thalamocortical Synchrony in Absence Epilepsy. *Epilepsy Currents* 19(2), pp. 105–111. doi: 10.1177/1535759719835355.

Huguenard, J.R. 1996. Low-threshold calcium currents in central nervous system neurons. *Annual Review of Physiology* 58, pp. 329–348. doi: 10.1146/annurev.ph.58.030196.001553.

Huguenard, J.R. and McCormick, D.A. 2007. Thalamic synchrony and dynamic regulation of global forebrain oscillations. *Trends in Neurosciences* 30(7), pp. 350–356. doi: 10.1016/j.tins.2007.05.007.

Ilyas, A. et al. 2019. The centromedian nucleus: Anatomy, physiology, and clinical implications. *Journal of Clinical Neuroscience* 63, pp. 1–7. doi: 10.1016/j.jocn.2019.01.050.

Inoue, M. et al. 1993. Thalamic multiple-unit activity underlying spike-wave discharges in anesthetized rats. *Brain Research* 612(1–2), pp. 35–40. doi: 10.1016/0006-8993(93)91641-5.

Jahnsen H and Llinás R 1984. Voltage-dependent burst-to-tonic switching of thalamic cell activity: an in vitro study. *Archives Italiennes de biologie* 122(1), pp. 73–82.

Jarre, G. et al. 2017. Building Up Absence Seizures in the Somatosensory Cortex: From Network to Cellular Epileptogenic Processes. *Cerebral Cortex* 27(9), pp. 4607–4623. doi: 10.1093/cercor/bhx174.

Jasper and Droogleever Fortuyn 1947. Experimental studies on the functional anatomy of petit mal epilepsy. *Association for Research in Nervous and Mental Disorders* 26, pp. 272–298.

Jonas Terlau and Annika Luttjohann 2020. Spike-wave discharges in absence epilepsy: Segregation of electrographic components reveals distinct pathways of seizure activity. *The Journal of Physiology* 598(12), pp. 2397–2414. doi: 10.1113/JP279483.

Jones, E.G. 1985. *The Thalamus*. Springer US. doi: 10.1007/978-1-4615-1749-8.

Jouvenceau, A. et al. 2001. Human epilepsy associated with dysfunction of the brain P/Q-type calcium channel. *The Lancet* 358(9284), pp. 801–807. doi: 10.1016/S0140-6736(01)05971-2.

Kamishina, H. et al. 2009. Cortical connections of the rat lateral posterior thalamic nucleus. *Brain Research* 1264, pp. 39–56. doi: 10.1016/j.brainres.2009.01.024.

Karpova, A. et al. 2005. Morphometric Golgi study of cortical locations in WAG/Rij rats: The cortical focus theory. *Neuroscience research* 51, pp. 119–28. doi: 10.1016/j.neures.2004.10.004.

Kennard, J.T.T. et al. 2011. Stargazin and AMPA receptor membrane expression is increased in the somatosensory cortex of Genetic Absence Epilepsy Rats from Strasbourg. *Neurobiology of Disease* 42(1), pp. 48–54. doi: 10.1016/j.nbd.2011.01.003.

Kim et al. 2001. Lack of the Burst Firing of Thalamocortical Relay Neurons and Resistance to Absence Seizures in Mice Lacking α1G T-Type Ca2+ Channels: Neuron.

Kim, U. and McCormick, D.A. 1998. The Functional Influence of Burst and Tonic Firing Mode on Synaptic Interactions in the Thalamus. *The Journal of Neuroscience* 18(22), pp. 9500–9516. doi: 10.1523/JNEUROSCI.18-22-09500.1998.

Kinnischtzke, A.K. et al. 2016. Target-specific M1 inputs to infragranular S1 pyramidal neurons. *Journal of Neurophysiology* 116(3), pp. 1261–1274. doi: 10.1152/jn.01032.2015.

Klioueva, I.A. et al. 2001. PTZ-induced seizures in rats: effects of age and strain. *Physiology & Behavior* 72(3), pp. 421–426. doi: 10.1016/s0031-9384(00)00425-x.

Klöckner, U. et al. 1999. Comparison of the Ca2 + currents induced by expression of three cloned α1 subunits, α1G, α1H and α1I, of low-voltage-activated T-type Ca2 + channels. *European Journal of Neuroscience* 11(12), pp. 4171–4178. doi: https://doi.org/10.1046/j.1460-9568.1999.00849.x.

Lacey, C.J. et al. 2012. Enhanced NMDA Receptor-Dependent Thalamic Excitation and Network Oscillations in Stargazer Mice. *The Journal of Neuroscience* 32(32), pp. 11067–11081. doi: 10.1523/JNEUROSCI.5604-11.2012.

Lavallee, P. 2005. Feedforward Inhibitory Control of Sensory Information in Higher-Order Thalamic Nuclei. *Journal of Neuroscience* 25(33), pp. 7489–7498. doi: 10.1523/JNEUROSCI.2301-05.2005.

Lazaridis, D. et al. 2019. Treatment of Seizures Associated with Lennox-Gastaut and Dravet Syndromes: A Focus on Cannabidiol Oral Solution. *Pharmacy and therapeutics* 44(5), pp. 255–258.

Le Van Quyen, M. et al. 2001. Comparison of Hilbert transform and wavelet methods for the analysis of neuronal synchrony. *Journal of Neuroscience Methods* 111(2), pp. 83–98. doi: 10.1016/S0165-0270(01)00372-7.

Lee, C. et al. 2017. Altered Network Characteristics of Spike-Wave Discharges in Juvenile Myoclonic Epilepsy. *Clinical EEG and Neuroscience* 48(2), pp. 111–117. doi: 10.1177/1550059415621831.

Lee, C.C. and Sherman, S.M. 2008. Synaptic properties of thalamic and intracortical inputs to layer 4 of the first- and higher-order cortical areas in the

auditory and somatosensory systems. *Journal of Neurophysiology* 100(1), pp. 317–326. doi: 10.1152/jn.90391.2008.

Lee, S.-C. et al. 2014. Two Functionally Distinct Networks of Gap Junction-Coupled Inhibitory Neurons in the Thalamic Reticular Nucleus. *Journal of Neuroscience* 34(39), pp. 13170–13182. doi: 10.1523/JNEUROSCI.0562-14.2014.

Letts, V.A. et al. 1998. The mouse stargazer gene encodes a neuronal Ca2+-channel γ subunit. *Nature Genetics* 19(4), pp. 340–347. doi: 10.1038/1228.

Letts, V.A. 2005. Stargazer—A Mouse to Seize! *Epilepsy Currents* 5(5), pp. 161–165. doi: 10.1111/j.1535-7511.2005.00051.x.

Li, J. et al. 2003. Unique firing properties of higher order thalamic relay neurons. *Journal of neurophysiology* 90, pp. 291–9. doi: 10.1152/jn.01163.2002.

Liang, S.-F. et al. 2011. Closed-loop seizure control on epileptic rat models. *Journal of Neural Engineering* 8(4), pp. 1–10. doi: 10.1088/1741-2560/8/4/045001.

Lüttjohann, A. et al. 2013. Peri-ictal network dynamics of spike-wave discharges: Phase and spectral characteristics. *Experimental Neurology* 239, pp. 235–247. doi: 10.1016/j.expneurol.2012.10.021.

Lüttjohann, A. and van Luijtelaar, G. 2012. The dynamics of cortico-thalamo-cortical interactions at the transition from pre-ictal to ictal LFPs in absence epilepsy. *Neurobiology of Disease* 47(1), pp. 49–60. doi: 10.1016/j.nbd.2012.03.023.

Lüttjohann, A. and van Luijtelaar, G. 2015. Dynamics of networks during absence seizure's on- and offset in rodents and man. *Frontiers in Physiology* 6(16), pp. 1–17. doi: 10.3389/fphys.2015.00016.

Lüttjohann, A. and Pape, H.-C. 2019. Regional specificity of cortico-thalamic coupling strength and directionality during waxing and waning of spike and wave discharges. *Scientific Reports* 9(1), p. 2100. doi: 10.1038/s41598-018-37985-7.

Lyon, D.C. et al. 2010. A Disynaptic Relay from Superior Colliculus to Dorsal Stream Visual Cortex in Macaque Monkey. *Neuron* 65(2), pp. 270–279. doi: 10.1016/j.neuron.2010.01.003.

Manning, J.P.A. et al. 2004. Cortical-area specific block of genetically determined absence seizures by ethosuximide. *Neuroscience* 123(1), pp. 5–9. doi: 10.1016/j.neuroscience.2003.09.026.

Marini, C. et al. 2003. Childhood absence epilepsy and febrile seizures: a family with a GABAA receptor mutation. *Brain* 126(1), pp. 230–240. doi: 10.1093/brain/awg018.

Martinez-Garcia, R.I. et al. 2020. Two dynamically distinct circuits driving inhibition in sensory thalamus. *Nature* 583, pp. 813–818. doi: 10.1101/2020.04.16.044487.

Masri, R. et al. 2009. Zona Incerta: A Role in Central Pain. *Journal of Neurophysiology* 102(1), pp. 181–191. doi: 10.1152/jn.00152.2009.

Massé, I.O. et al. 2019. Afferent connections of the primary somatosensory cortex of the mouse for contextual and multisensory processing. *bioRxiv* , p. 514414. doi: 10.1101/514414.

McCafferty, C. et al. 2018. Cortical drive and thalamic feed-forward inhibition control thalamic output synchrony during absence seizures. *Nature Neuroscience* 21(5), pp. 744–756. doi: 10.1038/s41593-018-0130-4.

McCormick, D.A. and Bal, T. 1997. SLEEP AND AROUSAL: Thalamocortical Mechanisms. *Annual Review of Neuroscience* 20(1), pp. 185–215. doi: 10.1146/annurev.neuro.20.1.185.

McLachlan, R.S. et al. 1984. Transition from spindles to generalized spike and wave discharges in the cat: simultaneous single-cell recordings in cortex and thalamus. *Experimental Neurology* 85(2), pp. 413–425. doi: 10.1016/0014-4886(84)90151-1.

Meeren, H. et al. 2005. Evolving Concepts on the Pathophysiology of Absence Seizures: The Cortical Focus Theory. *Archives of Neurology* 62(3), p. 371. doi: 10.1001/archneur.62.3.371.

Meeren, H.K.M. et al. 2002. Cortical focus drives widespread corticothalamic networks during spontaneous absence seizures in rats. *The Journal of Neuroscience: The Official Journal of the Society for Neuroscience* 22(4), pp. 1480–1495.

Meyer, J. et al. 2018. Asynchronous suppression of visual cortex during absence seizures in stargazer mice. *Nature Communications* 9(1), p. 1938. doi: 10.1038/s41467-018-04349-8.

Mirsky, A.F. and Buren, J.M.V. 1965. On the nature of the “absence” in centrencephalic epilepsy: A study of some behavioral, electroencephalographic and autonomic factors. *Electroencephalography and Clinical Neurophysiology* 18(4), pp. 334–348. doi: 10.1016/0013-4694(65)90053-2.

Mo, C. and Sherman, S.M. 2019. A Sensorimotor Pathway via Higher-Order Thalamus. *Journal of Neuroscience* 39(4), pp. 692–704. doi: 10.1523/JNEUROSCI.1467-18.2018.

Murray Sherman, S. 2001. Tonic and burst firing: Dual modes of thalamocortical relay. *Trends in Neurosciences* 24(2), pp. 122–126. doi: 10.1016/S0166-2236(00)01714-8.

Nail-Boucherie, K. et al. 2005. Evidence for a role of the parafascicular nucleus of the thalamus in the control of epileptic seizures by the superior colliculus. *Epilepsia* 46(1), pp. 141–145. doi: 10.1111/j.0013-9580.2005.30304.x.

Nakamura, H. et al. 2015. Different cortical projections from three subdivisions of the rat lateral posterior thalamic nucleus: a single-neuron tracing study with viral vectors. *European Journal of Neuroscience* 41(10), pp. 1294–1310. doi: 10.1111/ejn.12882.

Oberlaender, M, et al. Cortical output is driven by transcolumnar pathways in deep layers. Program No. 392.01/AA3. 2018 Neuroscience Meeting Planner. San Diego, CA: Society for Neuroscience, 2018. Online.

Ohno, S. et al. 2012. A Morphological Analysis of Thalamocortical Axon Fibers of Rat Posterior Thalamic Nuclei: A Single Neuron Tracing Study with Viral Vectors. *Cerebral Cortex* 22(12), pp. 2840–2857. doi: 10.1093/cercor/bhr356.

Ono et al. 1990. Electrocorticographical observation of seizures induced by pentylenetetrazol (PTZ) injection in rats. *Functional Neurology* 5(4), pp. 345–352.

Pachitariu, M. et al. 2016. Kilosort: realtime spike-sorting for extracellular electrophysiology with hundreds of channels. *bioRxiv* , p. 061481. doi: 10.1101/061481.

Panayiotopoulos, C.P. et al. 1989. Differentiation of typical absence seizures in epileptic syndromes. A video EEG study of 224 seizures in 20 patients. *Brain* 112(4), pp. 1039–1056. doi: 10.1093/brain/112.4.1039.

Paz, J.T. et al. 2011. A new mode of corticothalamic transmission revealed in the Gria4(-/-) model of absence epilepsy. *Nature Neuroscience* 14(9), pp. 1167–1173. doi: 10.1038/nn.2896.

Penfield, W. and Jasper, H. 1954. *Epilepsy and the functional anatomy of the human brain*. Oxford, England: Little, Brown & Co., pp. xv, 896.

Perez-Reyes, E. 2003. Molecular Physiology of Low-Voltage-Activated T-type Calcium Channels. *Physiological Reviews* 83(1), pp. 117–161. doi: 10.1152/physrev.00018.2002.

Perucca, E. et al. 1998. Antiepileptic Drugs as a Cause of Worsening Seizures. *Epilepsia* 39(1), pp. 5–17. doi: https://doi.org/10.1111/j.1528-1157.1998.tb01268.x.

Petrof, I. et al. 2015. Properties of the primary somatosensory cortex projection to the primary motor cortex in the mouse. *Journal of Neurophysiology* 113(7), pp. 2400–2407. doi: 10.1152/jn.00949.2014.

Petrou, S. and Reid, C.A. 2012. The GABAAγ2(R43Q) mouse model of human genetic epilepsy. In: Noebels, J. L. et al. eds. *Jasper's Basic Mechanisms of the Epilepsies*. 4th ed. Bethesda (MD): National Center for Biotechnology Information (US)

Petty, G.H. et al. 2020. Effects of arousal and movement on secondary somatosensory and visual thalamus. *bioRxiv* , p. 2020.03.04.977348. doi: 10.1101/2020.03.04.977348.

Pinault, D. et al. 1998. Intracellular recordings in thalamic neurones during spontaneous spike and wave discharges in rats with absence epilepsy. *The Journal of physiology* 509 ( Pt 2), pp. 449–56. doi: 10.1111/j.1469-7793.1998.449bn.x.

Pinault, D. 2004. The thalamic reticular nucleus: structure, function and concept. *Brain Research Reviews* 46(1), pp. 1–31. doi: 10.1016/j.brainresrev.2004.04.008.

Polack et al. 2009. Inactivation of the Somatosensory Cortex Prevents Paroxysmal Oscillations in Cortical and Related Thalamic Neurons in a Genetic Model of Absence Epilepsy. *Cerebral Cortex* 19(9), pp. 2078–2091. doi: 10.1093/cercor/bhn237.

Polack, P.-O. et al. 2007 Deep Layer Somatosensory Cortical Neurons Initiate Spike-and-Wave Discharges in a Genetic Model of Absence Seizures. *Journal of Neuroscience* 27(24), pp. 6590–6599. doi: 10.1523/JNEUROSCI.0753-07.2007.

Porrero, C, et al.. The functional logic of higher-order thalamocortical axons branching to innervate multiple areas. Program No. 221.09/J11. 2019 Neuroscience Meeting Planner. Chicago, IL: Society for Neuroscience, 2019. Online.

Powell, K.L. et al. 2008. Genetic absence epilepsy rats from Strasbourg have increased corticothalamic expression of stargazin. *Neurobiology of Disease* 31(2), pp. 261–265. doi: 10.1016/j.nbd.2008.04.012.

Powell, K.L. et al. 2009. A Cav3.2 T-type calcium channel point mutation has splice-variant-specific effects on function and segregates with seizure expression in a polygenic rat model of absence epilepsy. *The Journal of Neuroscience: The Official Journal of the Society for Neuroscience* 29(2), pp. 371–380. doi: 10.1523/JNEUROSCI.5295-08.2009.

Power, B.D. and Mitrofanis, J. 2001. Zona incerta: Substrate for contralateral interconnectivity in the thalamus of rats. *The Journal of Comparative Neurology* 436(1), pp. 52–63.

Prince and Farrell 1969. Centrencephalic spike wave discharges following parenteral penicillin injection in the cat.

Proft, J. et al. 2017. The Cacna1h mutation in the GAERS model of absence epilepsy enhances T-type Ca2+ currents by altering calnexin-dependent trafficking of Cav3.2 channels. *Scientific Reports* 7(1). doi: 10.1038/s41598-017-11591-5.

Prusky, G.T. et al. 2002. Variation in visual acuity within pigmented, and between pigmented and albino rat strains. *Behavioural Brain Research* 136(2), pp. 339–348. doi: 10.1016/s0166-4328(02)00126-2.

Ramcharan, E.J. et al. 2005. Higher-order thalamic relays burst more than first-order relays. *Proceedings of the National Academy of Sciences* 102(34), pp. 12236–12241. doi: 10.1073/pnas.0502843102.

Rodriguez-Moreno, J. et al. 2020. Area-Specific Synapse Structure in Branched Posterior Nucleus Axons Reveals a New Level of Complexity in Thalamocortical Networks. *The Journal of Neuroscience* 40(13), pp. 2663–2679. doi: 10.1523/JNEUROSCI.2886-19.2020.

Roland, P.E. et al. 2014. Cortico-cortical communication dynamics. *Frontiers in Systems Neuroscience* 8, p. 19:1–11. doi: 10.3389/fnsys.2014.00019.

Roth, Z.N. et al. 2018. Stimulus vignetting and orientation selectivity in human visual cortex. de Lange, F. P. and Kastner, S. eds. *eLife* 7, p. e37241. doi: 10.7554/eLife.37241.

Saalmann, Y.B. and Kastner, S. 2011. Cognitive and Perceptual Functions of the Visual Thalamus. *Neuron* 71(2), pp. 209–223. doi: 10.1016/j.neuron.2011.06.027.

Schäfer, C. and Hoebeek, F. 2018. Convergence of Primary Sensory Cortex and Cerebellar Nuclei Pathways in the Whisker System - ScienceDirect.

Schofield, C.M. et al. 2009. A gain in GABAA receptor synaptic strength in thalamus reduces oscillatory activity and absence seizures. *Proceedings of the National Academy of Sciences* 106(18), pp. 7630–7635. doi: 10.1073/pnas.0811326106.

Scholl, L.R. et al. 2020. Projections between visual cortex and pulvinar nucleus in the rat. *bioRxiv* , p. 2020.01.27.921858. doi: 10.1101/2020.01.27.921858.

Shaw, F.-Z. et al. 2013. The zona incerta modulates spontaneous spike-wave discharges in the rat. *Journal of Neurophysiology* 109(10), pp. 2505–2516. doi: 10.1152/jn.00750.2011.

Sherman, S.M. 2001. Tonic and burst firing: dual modes of thalamocortical relay. *Trends in Neurosciences* 24(2), pp. 122–126. doi: 10.1016/S0166-2236(00)01714-8.

Sherman, S.M. 2014. The Function of Metabotropic Glutamate Receptors in Thalamus and Cortex. *The Neuroscientist : a review journal bringing neurobiology, neurology and psychiatry* 20(2), pp. 136–149. doi: 10.1177/1073858413478490.

Sherman, S.M. and Guillery, R.W. 1998. On the actions that one nerve cell can have on another: Distinguishing 'drivers' from 'modulators'. *Proceedings of the National Academy of Sciences* 95(12), pp. 7121–7126. doi: 10.1073/pnas.95.12.7121.

Sherman, S.M. and Guillery, R.W. 2011. Distinct functions for direct and transthalamic corticocortical connections. *Journal of Neurophysiology* 106(3), pp. 1068–1077. doi: 10.1152/jn.00429.2011.

Shu, Y. and McCormick, D.A. 2002. Inhibitory Interactions Between Ferret Thalamic Reticular Neurons. *Journal of Neurophysiology* 87(5), pp. 2571–2576. doi: 10.1152/jn.00850.2001.

Slaght, S.J. et al. 2002. Activity of Thalamic Reticular Neurons during Spontaneous Genetically Determined Spike and Wave Discharges. *Journal of Neuroscience* 22(6), pp. 2323–2334. doi: 10.1523/JNEUROSCI.22-06-02323.2002.

Sorokin, J.M. et al. 2020. Thalamic activity patterns unfolding over multiple time scales predict seizure onset in absence epilepsy. *bioRxiv* , p. 2020.03.04.976688. doi: 10.1101/2020.03.04.976688.

Steriade, M. et al. 1996. Synchronization of fast (30-40 Hz) spontaneous oscillations in intrathalamic and thalamocortical networks. *The Journal of Neuroscience: The Official Journal of the Society for Neuroscience* 16(8), pp. 2788–2808.

Steriade, M. et al. 1998. Spike-Wave Complexes and Fast Components of Cortically Generated Seizures. II. Extra- and Intracellular Patterns. *Journal of Neurophysiology* 80(3), pp. 1456–1479. doi: 10.1152/jn.1998.80.3.1456.

Steriade, M. 2005. Sleep, epilepsy and thalamic reticular inhibitory neurons. *Trends in Neurosciences* 28(6), pp. 317–324. doi: 10.1016/j.tins.2005.03.007.

Steriade, M. and Contreras, D. 1998. Spike-Wave Complexes and Fast Components of Cortically Generated Seizures. I. Role of Neocortex and Thalamus. *Journal of Neurophysiology* 80(3), pp. 1439–1455. doi: 10.1152/jn.1998.80.3.1439.

Sun, Y.-G. et al. 2012. GABAergic Synaptic Transmission Triggers Action Potentials in Thalamic Reticular Nucleus Neurons. *Journal of Neuroscience* 32(23), pp. 7782–7790. doi: 10.1523/JNEUROSCI.0839-12.2012.

Talley, E.M. et al. 1999. Differential Distribution of Three Members of a Gene Family Encoding Low Voltage-Activated (T-Type) Calcium Channels. *The Journal of Neuroscience* 19(6), pp. 1895–1911. doi: 10.1523/JNEUROSCI.19-06-01895.1999.

Tanaka, M. et al. 2008. Hyperglycosylation and Reduced GABA Currents of Mutated GABRB3 Polypeptide in Remitting Childhood Absence Epilepsy. *The American Journal of Human Genetics* 82(6), pp. 1249–1261. doi: 10.1016/j.ajhg.2008.04.020.

Tancredi, V. et al. 2000. Spindle-like thalamocortical synchronization in a rat brain slice preparation. *Journal of Neurophysiology* 84(2), pp. 1093–1097. doi: 10.1152/jn.2000.84.2.1093.

Tang, B. et al. 2008. Mutation analysis of the hyperpolarization-activated cyclic nucleotide-gated channels HCN1 and HCN2 in idiopathic generalized epilepsy. *Neurobiology of Disease* 29(1), pp. 59–70. doi: 10.1016/j.nbd.2007.08.006.

Tangwiriyasakul, C. et al. 2018. Dynamic brain network states in human generalized spike-wave discharges. *Brain* 141(10), pp. 2981–2994. doi: 10.1093/brain/awy223.

Tenney, J.R. et al. 2013. Focal corticothalamic sources during generalized absence seizures: A MEG study. *Epilepsy Research* 106(1), pp. 113–122. doi: 10.1016/j.eplepsyres.2013.05.006.

Tremblay, R. et al. 2016. GABAergic Interneurons in the Neocortex: From Cellular Properties to Circuits. *Neuron* 91(2), pp. 260–292. doi: 10.1016/j.neuron.2016.06.033.

Trinka, E. et al. 2004. Long-term prognosis for childhood and juvenile absence epilepsy. *Journal of Neurology* 251(10), pp. 1235–1241. doi: 10.1007/s00415-004-0521-1.

Tscherter, A. et al. 2011. Minimal alterations in T-type calcium channel gating markedly modify physiological firing dynamics: Functional consequences of T-type calcium channel gating. *The Journal of Physiology* 589(7), pp. 1707–1724. doi: 10.1113/jphysiol.2010.203836.

Tsoukatos, J. et al. 1997. Patterns of neuronal firing in the human lateral thalamus during sleep and wakefulness. *Experimental Brain Research* 113(2), pp. 273–282. doi: 10.1007/BF02450325.

Tyvaert, L. et al. 2009. Thalamic nuclei activity in idiopathic generalized epilepsy: An EEG-fMRI study. *Neurology* 73(23), pp. 2018–2022. doi: 10.1212/WNL.0b013e3181c55d02.

Uebele, V.N. et al. 2009. T-type calcium channels regulate cortical plasticity in-vivo. *Neuroreport* 20(3), pp. 257–262. doi: 10.1097/WNR.0b013e3283200111.

Van der Werf, Y.D. et al. 2002. The intralaminar and midline nuclei of the thalamus. Anatomical and functional evidence for participation in processes of arousal and awareness. *Brain Research Reviews* 39(2–3), pp. 107–140. doi: 10.1016/S0165-0173(02)00181-9.

Vega, C. et al. 2011. Symptoms of anxiety and depression in childhood absence epilepsy: *Symptoms of Anxiety and Depression*. *Epilepsia* 52(8), pp. e70–e74. doi: 10.1111/j.1528-1167.2011.03119.x.

Velasco, M. et al. 1997. Electrocortical and behavioral responses produced by acute electrical stimulation of the human centromedian thalamic nucleus. *Electroencephalography and Clinical Neurophysiology* 102(6), pp. 461–471. doi: 10.1016/S0013-4694(96)95203-0.

Venzi, M. et al. 2015. A Critical Evaluation of the Gamma-Hydroxybutyrate (GHB) Model of Absence Seizures. *CNS Neuroscience & Therapeutics* 21(2), pp. 123–140. doi: https://doi.org/10.1111/cns.12337.

Vergnes, M. et al. 1986. Ontogeny of spontaneous petit mal-like seizures in Wistar rats. *Developmental Brain Research* 30(1), pp. 85–87. doi: 10.1016/0165-3806(86)90133-1.

Viaene, A.N. et al. 2011. Properties of the thalamic projection from the posterior medial nucleus to primary and secondary somatosensory cortices in the mouse. *Proceedings of the National Academy of Sciences of the United States of America* 108(44), pp. 18156–18161. doi: 10.1073/pnas.1114828108.

Vuilleumier, P. et al. 2000. Distinct Behavioral and EEG Topographic Correlates of Loss of Consciousness in Absences. *Epilepsia* 41(6), pp. 687–693. doi: 10.1111/j.1528-1157.2000.tb00229.x.

Waite, P.M.E. 1973. The responses of cells in the rat thalamus to mechanical movements of the whiskers. *The Journal of Physiology* 228(2), pp. 541–561.

Wallace, R.H. et al. 2001. Mutant GABAA receptor γ2-subunit in childhood absence epilepsy and febrile seizures. *Nature Genetics* 28(1), pp. 49–52. doi: 10.1038/ng0501-49.

Wang, X.J. et al. 1995. Emergent spindle oscillations and intermittent burst firing in a thalamic model: specific neuronal mechanisms. *Proceedings of the National Academy of Sciences* 92(12), pp. 5577–5581. doi: 10.1073/pnas.92.12.5577.

Wei, H. et al. 2011. Thalamic Burst Firing Propensity: A Comparison of the Dorsal Lateral Geniculate and Pulvinar Nuclei in the Tree Shrew. *Journal of*

*Neuroscience* 31(47), pp. 17287–17299. doi: 10.1523/JNEUROSCI.6431-10.2011.

Westmijse, I. et al. 2009. Onset and propagation of spike and slow wave discharges in human absence epilepsy: A MEG study. *Epilepsia* 50(12), pp. 2538–2548. doi: https://doi.org/10.1111/j.1528-1167.2009.02162.x.

Wróbel, A. et al. 2007. Two Streams of Attention-Dependent β Activity in the Striate Recipient Zone of Cat's Lateral Posterior–Pulvinar Complex. *Journal of Neuroscience* 27(9), pp. 2230–2240. doi: 10.1523/JNEUROSCI.4004-06.2007.

Yen, C.T. et al. 1985. The morphology of physiologically identified GABAergic neurons in the somatic sensory part of the thalamic reticular nucleus in the cat. *Journal of Neuroscience* 5(8), pp. 2254–2268. doi: 10.1523/JNEUROSCI.05-08-02254.1985.

Zakiewicz, I.M. et al. 2014. Brain-wide map of efferent projections from rat barrel cortex. *Frontiers in Neuroinformatics* 8, p. 5:1-15. doi: 10.3389/fninf.2014.00005.

Zhang, Y. et al. 2002. Mutations in High-Voltage-Activated Calcium Channel Genes Stimulate Low-Voltage-Activated Currents in Mouse Thalamic Relay Neurons. *The Journal of Neuroscience* 22(15), pp. 6362–6371. doi: 10.1523/JNEUROSCI.22-15-06362.2002.

Zhou, N. et al. 2018. The Mouse Pulvinar Nucleus Links the Lateral Extrastriate Cortex, Striatum, and Amygdala. *The Journal of Neuroscience* 38(2), pp. 347–362. doi: 10.1523/JNEUROSCI.1279-17.2017.